THE UNIVERSITY
of EDINBURGH

Ordering components of the slender to stumpy signalling pathway in *Trypanosoma brucei*

Lindsay McDonald

PhD University of Edinburgh 2016

Declaration

I declare that this thesis was written by me and that all the material presented is my own work, except where specified otherwise, and has not been submitted for any other degree.

Lindsay McDonald

Lay Summary

Trypanosoma brucei, the parasite that causes African sleeping sickness, is transmitted from mammals to tsetse flies during its life cycle. To complete this transmission, the parasites must transform in the mammalian bloodstream from dividing forms, known as slender forms, to non-dividing stumpy forms which are able to survive in the harsh environment of the fly gut. As well as facilitating parasite transmission, this transformation regulates population growth within the mammal. The process involves complex metabolic and shape changes and has long been poorly understood at a molecular level. Many genes involved in the process, known as *pos*ST genes, have recently been identified. However, the interactions between the proteins they express and the order in which they act are yet to be elucidated. Deletion of specific *pos*ST genes in *T. brucei* prevents transformation to stumpy forms. In contrast, excess expression of the same genes enhances stumpy formation. Here, deletion of one *pos*ST gene is combined with enhanced expression of another in various combinations to explore the relationship between different *pos*ST proteins. This is used to order the pathway in which *pos*ST components act. In addition, changes in the phosphorylation of every protein in the cell are analysed in response to the deletion of two *pos*ST components to determine which proteins are affected by their absence. Another protein, TOR4, has been shown to inhibit transformation to stumpy forms and therefore acts antagonistically to the *pos*ST proteins. Expression of TOR4 and different *pos*ST components were simultaneously blocked to determine the effect on stumpy formation. This revealed information about the intersection between the stumpy-promoting *pos*ST pathway and the stumpy-inhibiting pathway. The order in which *pos*ST components act was further explored using drugs capable of artificially triggering the transition to stumpy forms. These drugs were tested on parasites in which expression of various *pos*ST genes had been silenced to determine if this loss of expression would block the pathway through which the drugs activated stumpy formation, thereby generating resistance to the compounds. The results provided further insight into the order of components of the *pos*ST pathway. One drug was tested on a population containing parasites in which expression of every gene was separately silenced, and analysis of those which developed resistance was used to identify novel genes involved in the stumpy transition.

Abstract

In the mammalian bloodstream, the protozoan parasite *Trypanosoma brucei* undergoes differentiation from proliferative slender forms to arrested, transmissible, stumpy forms. This transition is associated with extensive cytological and metabolic changes that promote survival in the tsetse midgut, and also influences infection dynamics within the mammalian host. A number of genes involved in this transformation were recently identified using an RNAi library screen for resistance to pCPTcAMP, a membrane-permeable cyclic AMP analogue that induces differentiation. These molecules, referred to here as *pos*ST (*pos*itive mediators of STumpy formation), were thereafter validated to regulate the slender to stumpy transition, with many of them apparently comprising part of a signal transduction and effector pathway. However, it is unknown how these proteins act in relation to one another or are ordered within the pathway.

To this end, null mutants were created for several *pos*ST components in differentiation-competent pleomorphic trypanosomes and, in this genetic background, other members of the predicted pathway expressed to test their ability to restore stumpy formation. Analysis of distinct combinations has been used to build a preliminary pathway structure model for the signalling events underlying trypanosome quorum sensing. In addition, phosphoproteomic analysis of two null mutants has revealed downstream signalling effects of two *pos*ST kinases, MEKK1 and YAK.

A similar extragenic suppression approach was also applied to explore the interaction between the identified drivers of stumpy formation and the target of rapamycin kinase, TOR4, which has previously been shown to act as a negative regulator of stumpy formation in monomorphs. Dual ablation of TOR4 and *pos*ST components revealed insight into the intersection of stumpy-promoting and stumpy-inhibiting pathways.

Finally, a chemical-genetic approach was used to investigate the *pos*ST pathway using two differentiation-inducing compounds: the previously studied E667, and GKI7, newly identified from a kinase inhibitor set. RNAi lines for different *pos*ST

components were tested for their ability to undergo development in the presence of these compounds. An RNAi library screen using GKI7 identified putative new mediators of stumpy formation.

Acknowledgements

I would like to thank Keith Matthews for giving me the opportunity to take on this project and for his support throughout. I would also like to thank everyone in the Matthews lab for making it such an enjoyable place to work these past years and for readily lending advice or an extra pair of hands whenever I was in need. I am indebted to Binny Mony for all her guidance when I first started and to Julie Wilson for help with animal work. The phosphoproteomic analysis was carried out at the FingerPrints Proteomics Facility at the University of Dundee and subsequent data analysis conducted by Matheiu Cayla. Ion Torrent analysis was carried out at University of Edinburgh Wellcome Trust Clinical Research Facility Genetics Core and subsequent data analysis conducted by Alasdair Ivens. Thanks to GSK for sharing compound sets for phenotypic screening. I am particularly grateful to Ele, Rachel, Eva and Paula for all the support, laughter and generally great company. Lastly, I would like to thank my family and friends for their unwavering support in this endeavour, as in every other.

List of abbreviations

AK	Adenosine Kinase
AMP	adenosine monophosphate
ApoL1	Apoliopoprotein 1
ATP	adenosine triphosphate
BES	Bloodstream Expression Site
bp	base pairs
AMP	Adenosine Monophosphate
cAMP	cyclic AMP
CCA	citrate/cis-aconitate
cDNA	complementary DNA
CNS	Central Nervous System
DSP	Dual Specificity Phosphatase
DAPI	4',6-diamindino- 2-phenylindole
DNA	deoxyribonucleic acid
dox	doxycycline
DSP	Dual Specificity Phosphatase
dsRNA	double stranded RNA
DTT	dithiothreitol
E667	DDD00015314
EF1	Elongation Factor 1
ESB	Expression Site Body
FAZ	Flagellar Attachment Zone
FCS	Foetal Calf Serum
gDNA	genomic DNA
GKI7	GSK Kinase Inhibitor 7
GLM	General Linear Model
GUS	β-glucuronidase
HAT	Human African Trypanosomiasis
HRP	Horseradish Peroxidase
Hyp	hypothetical protein

IFA	Immunofluorescent Analysis
IPTG	isopropyl β-D-1-thiogalactopyranoside
kb	kilobase
kDa	kilodalton
kDNA	kinetoplast DNA
MAPK	Mitogen-Activated Protein Kinase
MEKK1	MAPK/ERK kinase 1
mRNA	messenger RNA
MUG	4-Methylumbelliferyl-β-D-glucopyranosiduronic acid
nLC-MS/MS	nano liquid chromatography tandem mass spectrometry
PAD	Proteins Associated with Differentiation
PBS	Phosphate Buffered Saline
PBS-T	PBS+0.1% Tween 20
pCPTcAMP	8-(4-chlorophenylthio)-cAMP
PCR	Polymerase chain reaction
*pos*ST	positive mediators of STumpy formation
PPP	phosphoprotein phosphatase
qRT-PCR	quantitative Reverse Transcription PCR
RBP	RNA-binding protein
RIT-seq	RNA interference target sequencing
RNA	ribonucleic acid
RNAi	RNA interference
rRNA	ribosomal RNA
SDS	Sodium Dodecyl Sulphate
SIF	Stumpy Induction Factor
SL	Spliced Leader
SSR	Strand Switch Region
TAC	Tripartite Attachment Complex
TDB	Trypanosome Dilution Buffer
tet	tetracycline
TLF	Trypanosome Lytic Factor
TMT	Tandem Mass Tag

TOR4	target of rapamycin kinase 4
RNAi	RNA interference
UTR	untranslated region
VSG	Variant Surface Glycoprotein
v/v	Volume per volume
w/v	Weight per volume
X-gal	5-bromo-4-chloro-3-indolyl-beta-D-galacto-pyranoside
ZFK	Zinc Finger Kinase
ZFP	Zinc Finger Protein

Contents

1 Chapter 1: Introduction

1.1 Trypanosoma brucei

Trypanosoma brucei is a protozoan parasite that is the causative agent of human African trypanosomiasis (HAT), or sleeping sickness, in humans and the ruminant disease nagana. Transmission between mammalian hosts, where they are found extracellularly in the bloodstream, is via the tsetse fly vector, geographically restricting disease to the tsetse belt of sub-Saharan Africa. It is an early-branching eukaryote of the Kinetoplastid order of motile flagellates. Reflecting its divergent evolutionary history, this order is of interest for its many unique features of molecular and cellular biology. These include the unusual mitochondrial DNA network, the kinetoplast, which gives it its name, as well as the large number of important human and veterinary pathogens contained within this order, including *T. brucei*, the Chagas disease parasite *Trypanosoma cruzi* and *Leishmania* species responsible for leishmaniasis. In addition to its significance as a pathogen and its distinctive biology, *T. brucei* has added value as a research tool due to its genetic tractability. The presence of an innate RNA interference (RNAi) system (Ngo et al., 1998) along with the establishment of a tetracycline-regulated expression system by Wirtz *et al*. (1999) means that genetic manipulations such as targeted RNAi silencing, protein overexpression and gene knockouts are commonplace tools in the investigation of this unique and important parasite.

1.2 HAT

HAT is caused by two subspecies of *T. brucei, T. brucei gambiense* and *T. brucei rhodesiense*. Humans are resistant to infection by all other African trypanosome species due to the presence of the innate immune molecule apolipoprotein L1 (ApoL1), which acts as a constituent of two serum complexes, trypanosome lytic factors 1 and 2 (TLF-1 and TLF-2) to lyse trypanosomes (Perez-Morga et al., 2005; Vanhamme et al., 2003). *T. b. gambiense* and *T. b. rhodesiense* differ from each other by geographical distribution, rate of disease progression and mechanism of serum resistance. As shown in Figure 1.1, *T. b. gambiense* is found in West and central Africa and accounts for over 98% of HAT cases (WHO, 2015). It causes a

chronic infection which may remain asymptomatic for months or years. Its resistance to human serum can be primarily attributed to TgsGP, a glycoprotein believed to prevent ApoL1 insertion into endosomal membranes (Uzureau et al., 2013). However, both reduced ApoL1 uptake, via mutation of the surface receptor through which it is endocytosed, and increased ApoL1 degradation, as a result of lowered endosomal pH, also contribute (DeJesus et al., 2013; Kieft et al., 2010; Uzureau et al., 2013).

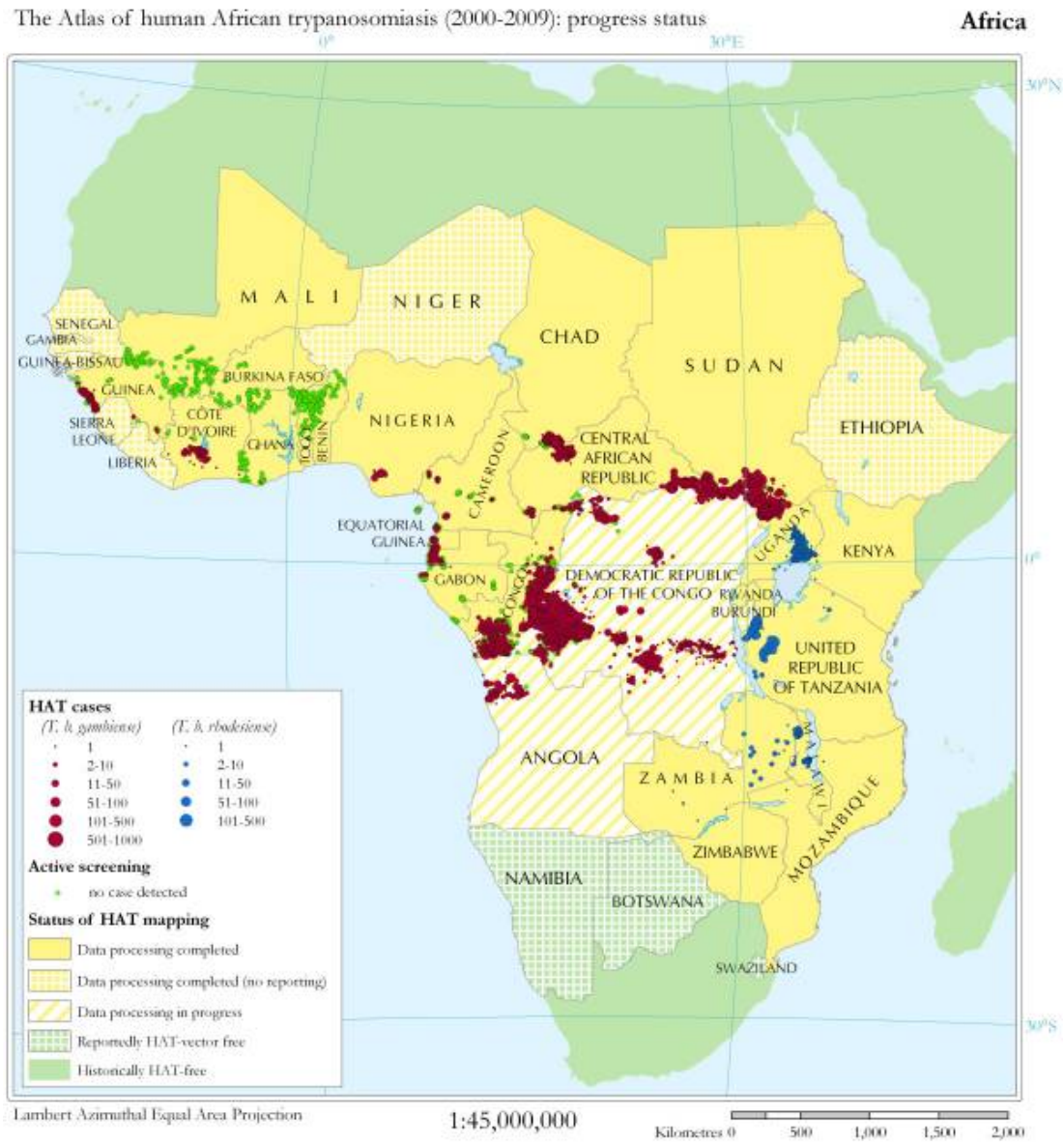

Figure 1.1 Distribution of HAT 2000-2009 (Simarro et al., 2010).

T. b. rhodesiense, which is found in Eastern Africa, causes a more acute infection than *T. b. gambiense,* with symptoms appearing within a few weeks or months. *T. b.*

rhodesiense also infects animals, particularly livestock, which act as a reservoir for the disease (Welburn et al., 2015; Welburn et al., 2001). Serum resistance of *T. b. rhodesiense* is dependent on expression of the serum resistance-associated (SRA) protein, which binds to and inactivates ApoL1 (Vanhamme et al., 2003).

For both rhodesiense and gambiense HAT, the disease can be divided into two stages: an early haemolymphatic stage in which the parasites divide within the blood and lymph, and a late neurological stage in which they penetrate the blood-brain barrier to invade the CNS. This latter stage is invariably fatal if untreated.

There are currently 5 drugs used for treatment of HAT, all of which have significant disadvantages including low therapeutic index and difficulties with complicated administration regimes. Early stage infection is treated with pentamidine for *T. b. gambiense* and suramin for *T. b. rhodesiense*. However, as these compounds cannot cross the blood-brain barrier, melarsoprol or eflornithine must be used for late stage HAT. Melarsoprol is an arsenic-based compound with severe side effects, including reactive encephalopathy, which is fatal in 5-10% of cases. Eflornithine, an irreversible inhibitor of the *T. brucei* ornithine decarboxylase, is better tolerated but is ineffective against *T. b. rhodesiense*. Since 2009, it has been used in combination with the nitroheterocyclic compound nifurtimox, previously used in treatment of Chagas disease (Priotto et al., 2009). This combination therapy allows for a less complex treatment regimen.

HAT occurs in 36 African countries and is considered a neglected disease. It is spread by tsetse flies of the genus *Glossina*. It predominantly affects rural communities with high exposure to these vectors. Disease control primarily involves vector control measures, population screening and chemotherapeutic treatment. Political disruption of surveillance programs in the second half of the 20th century resulted in a resurgence of disease burden. Renewed control efforts led in 2009 to the number of recorded cases dropping below 10,000 for the first time in 50 years. In 2013, 6314 new cases were recorded (WHO, 2015). However, due to the remoteness of the most affected populations, it is likely that this figure underestimates the true disease burden (Odiit et al., 2005).

In addition to the human health consequences of HAT, animal trypanosomiasis, or nagana, has a vast economic impact. Cattle in particular can be infected with *T. b. rhodesiense*, *T. b. brucei* and other *Trypanosoma* species including *Trypanosoma congolense* and *Trypanosoma vivax,* resulting in a lethal wasting disease. This places a huge constraint on livestock farming across vast swathes of the continent, at an estimated economic cost of $1.3 billion dollars per year (Kristjanson et al., 1999).

1.3 Gene expression in trypanosomes

T. brucei is a diploid organism. Its nuclear genome comprises 11 pairs of megabase-sized chromosomes as well as a small number of aneuploid intermediate chromosomes and approximately 100 minichromosomes (Berriman et al., 2005; Melville et al., 1998; Wickstead et al., 2004). The different types of chromosomes are depicted in Figure 1.2.

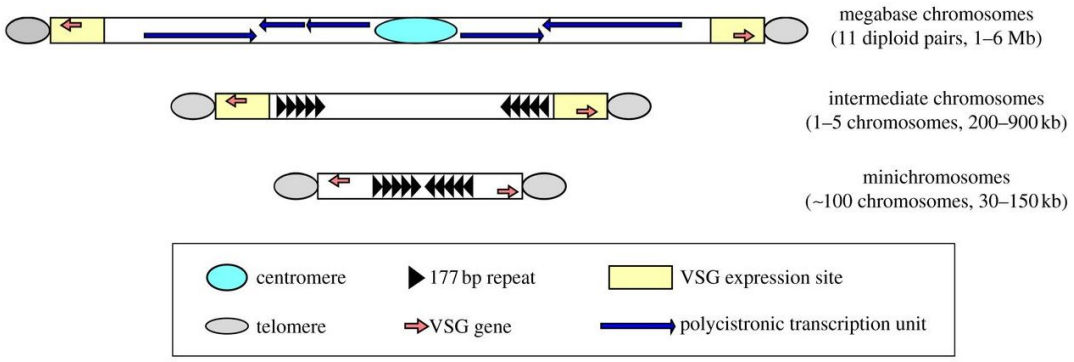

Figure 1.2 Chromosomal complement of *Trypanosoma brucei*. 11 pairs of megabase chromosomes encode almost all protein-coding genes, which are expressed from polycistronic transcription units separated by transcriptional strand-switch regions. Aneuploid intermediate chromosomes and minichromosomes contain 177bp repeat regions and are a source of telomeric VSGs. VSGs are monoallelically expressed from bloodstream expression sites located at the telomeres of megabase and intermediate chromosomes. From Akiyoshi and Gull (2013).

In contrast to other eukaryotes, *T. brucei* RNA polymerase I is responsible for transcribing not only rRNA but protein-coding genes, specifically the major surface proteins of the mammalian bloodstream and insect procyclic forms of the parasite, variant surface glycoprotein (VSG) and procyclin respectively (Gunzl et al., 2003). VSG is monoallelically expressed from an extensive repertoire of VSG genes found in telomeric and subtelomeric regions of the megabase, intermediate and

minichromosomes. The VSG coat protects the parasite from the host immune system by forming a dense physical barrier at the cell surface and undergoing antigenic variation (Cross et al., 2014; Schwede et al., 2011). VSG genes are expressed from telomeric bloodstream expression sites (BESs) located at the ends of the megabase and intermediate chromosomes. Periodic VSG switching occurs principally by either homologous recombination of a new VSG into an active BES or *in situ* switching to a new BES and enables the parasites to evade the humoral immune response (reviewed in (Gunzl et al., 2015; Horn, 2014). Procyclins are expressed from chromosome-internal positions and comprise 2 distinct classes, EP and GPEET, which refer to their respective dipeptide and pentapeptide repeat motifs. GPEET procyclin is expressed transiently in early procyclic forms while EP procyclin expression is maintained (Vassella et al., 2000).

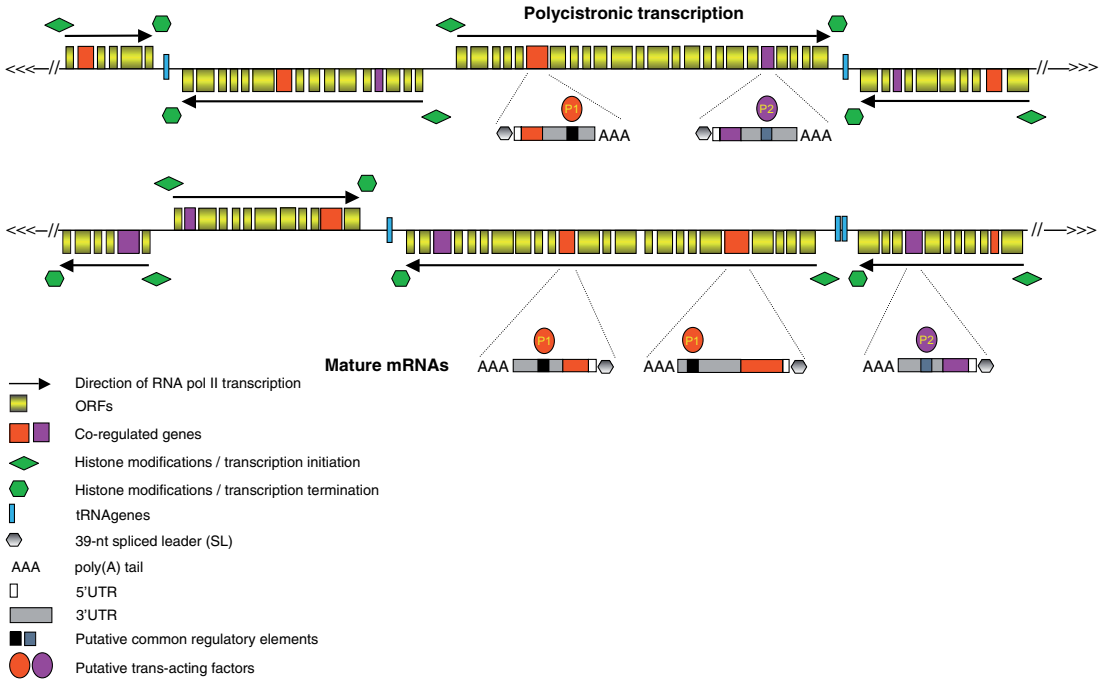

Figure 1.3 Polycistronic transcription of *Trypanosoma brucei* genes by RNA pol II. Genes are arranged in directional polycistrons separated by strand switch regions characterised by modified histones. Mature RNAs are generated from transcribed polycistrons by *trans*-splicing of a 5' spliced leader RNA cap and polyadenylation of the 3'UTR. From Ouellette and Papadopoulou (2009).

Most other protein-coding genes are arranged into long polycistrons separated by strand switch regions (SSRs) on the megabase chromosomes (Berriman et al., 2005; Imboden et al., 1987; Siegel et al., 2009). They are constitutively transcribed by RNA polymerase II and cotranscriptionally processed to monocistronic mRNAs by

trans-splicing of a short spliced leader (SL) RNA to the 5'UTR and polyadenylation of the 3'UTR (Lebowitz et al., 1993; Matthews et al., 1994). With the exception of the SL RNA promoter (Das et al., 2005), no conventional pol II promoter sequences or associated transcription factors have been identified in *T. brucei* but transcription from SSRs appears to be facilitated by an open chromatin state characterised by 4 histone variants (Siegel et al., 2009). This is summarised in Figure 1.3. Constitutive transcription means that regulation of protein expression is apparently exclusively post-transcriptional, in particular at the level of mRNA stability, a property often conferred by sequences within the 3'UTR (Furger et al., 1997; Haanstra et al., 2008a; Siegel et al., 2010).

1.4 The trypanosome cell

The trypanosome cell has an elongated shape maintained by a subpellicular array of microtubules. This cytoskeletal structure determines the defined positions of the numerous single-copy organelles within the cell, as shown in Figure 1.4.

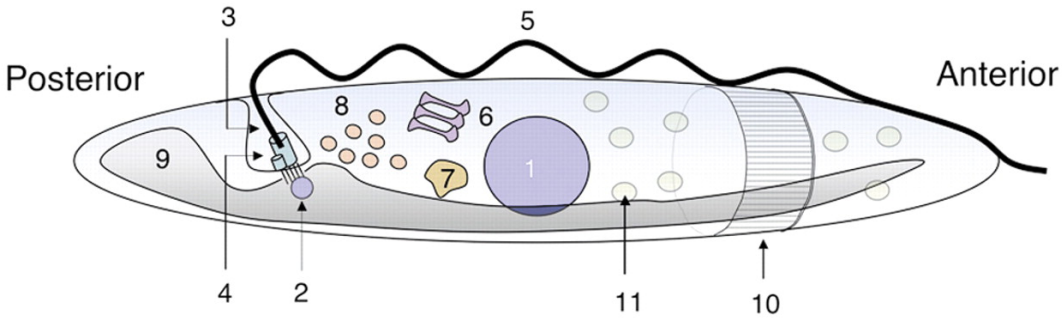

1. Nucleus
2. Kinetoplast
3. Flagellar pocket
4. Basal body and probasal body
5. Axoneme and paraflagellar rod
6. Golgi
7. Lysosome
8. Endosomes
9. Mitochondrion
10. Microtubule cytoskeleton
11. Glycosomes

Figure 1.4 Structure of the trypanosome cell, showing the positions of the principal organelles and cellular features. From Matthews (2005).

The cell is motile by means of a single flagellum, which originates in the basal body and emerges from the flagellar pocket, a membrane invagination at the posterior of the cell. The flagellum is anchored along the length of the cell body via the cytoskeletal flagellar attachment zone (FAZ) before extending from the anterior. Due to the restrictive corset of subpellicular array microtubules adjacent to the plasma membrane, the flagellar pocket is the only site of endocytosis and exocytosis within the cell (Field and Carrington, 2009). This is of particular consequence in the mammalian bloodstream form of the parasite, due to the high expression and rapid turnover of the VSG coat required to form a physical barrier to the host immune system and clear anti-VSG antibodies at low titres (Engstler et al., 2007). The surface coat of $5x10^6$ VSG dimers per cell is completely recycled approximately every 12 minutes, necessitating a phenomonal rate of endo- and exocytosis through an area comprising only 5% of the cell surface area (Engstler et al., 2007; Engstler et al., 2004).

The single trypanosome mitochondrion spans the length of the cell. In bloodstream forms, its structure and activity are diminished, reflecting a minimal role in energy metabolism at this stage, while the elaborated procyclic form contains cristae and has a highly active metabolism involving oxidative phosphorylation via the respiratory chain (Besteiro et al., 2005). Like many higher eukaryotes, various components of the *T. brucei* respiratory chain are mitochondrially encoded. However, the kinetoplast, the mitochondrial genome of the Kinetoplastida, is highly unusual. It comprises a giant network of thousands of concatenated circular DNAs, classed as maxicircles and minicircles (Shlomai, 2004). Maxicircles encode gene products but in many cases these require post-transcriptional processing by addition or deletion of uridines. This complex process, known as RNA editing, uses guide RNAs encoded on minicircles as templates for the production of functional mRNAs (Sturm and Simpson, 1990). The kinetoplast is physically connected to the basal body, and therefore the flagellum, via a filamentous structure known as the tripartite attachment complex (TAC), which enables faithful segregation of the kinetoplast during cell division (Ogbadoyi et al., 2003).

Trypanosomes also feature a number of atypical multicopy organelles. They compertmentalise glycolysis and other key metabolic pathways within peroxisome-like organelles known as glycosomes. This compartmentalisation appears to be essential for the regulation of glycolysis in the absence of allosteric regulation of glycolytic enzymes (Haanstra et al., 2008b; Kessler and Parsons, 2005), and as the enzymatic complement of glycosomes varies between different life stages, potentially provides flexibility for rapid metabolic adaptation to new nutritional environments (Szoor et al., 2014). Acidocalcisomes are acidic organelles in which phosphorus, calcium and other cations are concentrated. They were first named in trypanosomes (Vercesi et al., 1994) but have since been identified in a wide range of organisms (Docampo et al., 2005). Although their precise function remains uncertain, roles have been proposed in intracellular regulation of pH, polyphosphate levels, calcium levels and osmoregulation (Lemercier et al., 2002; Lemercier et al., 2004; Rohloff et al., 2004; Vercesi et al., 1994).

1.5 The trypanosome cell cycle

Cell division in *T. brucei* requires faithful division and segregation of both the nuclear and kinetoplast genomes as well as the various single copy organelles. Therefore, the process is tightly regulated and organelle division proceeds in a precise order. Overall, it follows the typical eukaryotic program of G_0/G_1 phase, followed by DNA replication in S phase, G_2 phase, mitosis and finally cytokinesis. Kinetoplast S phase initiates slightly before that of the nuclear genome. Early in G_2 phase, the first detectable morphological event is the duplication of the basal body from which the new flagellum forms. The connection of the basal body to the kinetoplast via the TAC ensures that this movement also results in segregation of the kDNA, prior to mitosis. This sequence of events allows stages of the cell cycle to be visualised microscopically using a nucleic acid stain such as 4',6-diamidino- 2-phenylindole (DAPI), as cells with a single kinetoplast and nucleus (1K1N) progress first to 2K1N and subsequently to 2K2N during G_2/M phase. Cytokinesis occurs by formation of a cleavage furrow at the anterior of the cell, between the 2 flagella, which ingresses towards the posterior, dividing the newly segregated organelles into

2 new daughter cells. These events are summarised in Figure 1.5. Cell cycle regulation and differentiation are closely linked processes in *T. brucei*, with transmissible stages in both mammalian and insect hosts being cell cycle arrested in G_1/G_0 phase. This allows subsequent differentiation upon entry into a new host to be coordinated with re-entry into the cell cycle.

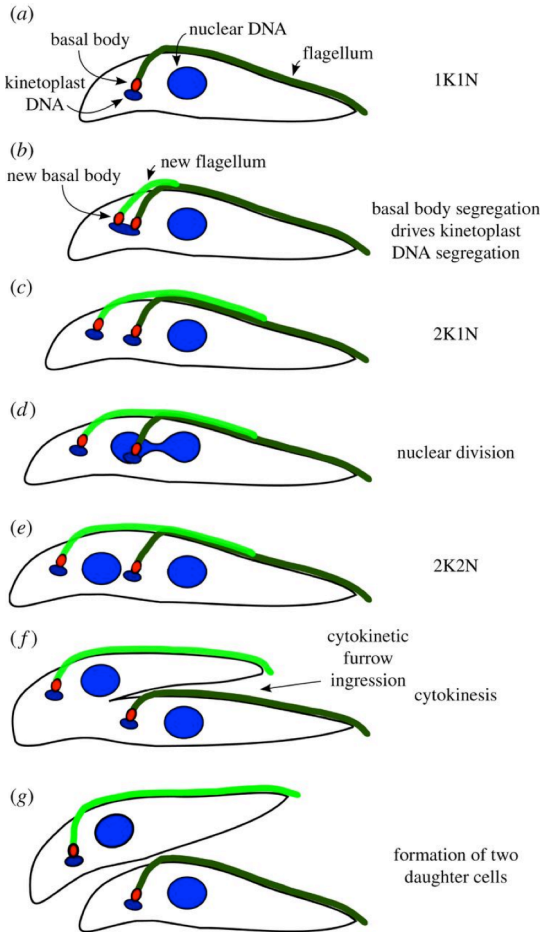

Figure 1.5 Cell cycle events in procyclic *T. brucei*. a) In G_1, cells have a single kinetoplast and nucleus. b) The basal body divides and a second flagellum outgrows. c) Basal body separation leads to segregation of the attached kinetoplast. Cell is now 2K1N. d) Nucleus divides in M phase. e) Completion of mitosis produces 2K2N cell. f) Cytokinesis occurs by furrow ingression from anterior to posterior of cell. g) Cytokinesis completes with formation of 2 daughter cells, each with a single nucleus, kinetoplast and flagellum. From Akiyoshi and Gull (2013).

1.6 The trypanosome life cycle

Trypanosomes encounter metabolically and immunologically diverse environments in the course of their life cycle as they pass from the mammalian bloodstream first to the midgut, then proventriculus and finally salivary glands of the tsetse vector. To adapt to these changes, they undergo a programmed series of differentiation events to distinct life stages, involving changes in morphology, metabolism, gene expression and cell cycle status. This process is depicted in Figure 1.6 and described in detail in sections 1.6.1 and 1.6.2.

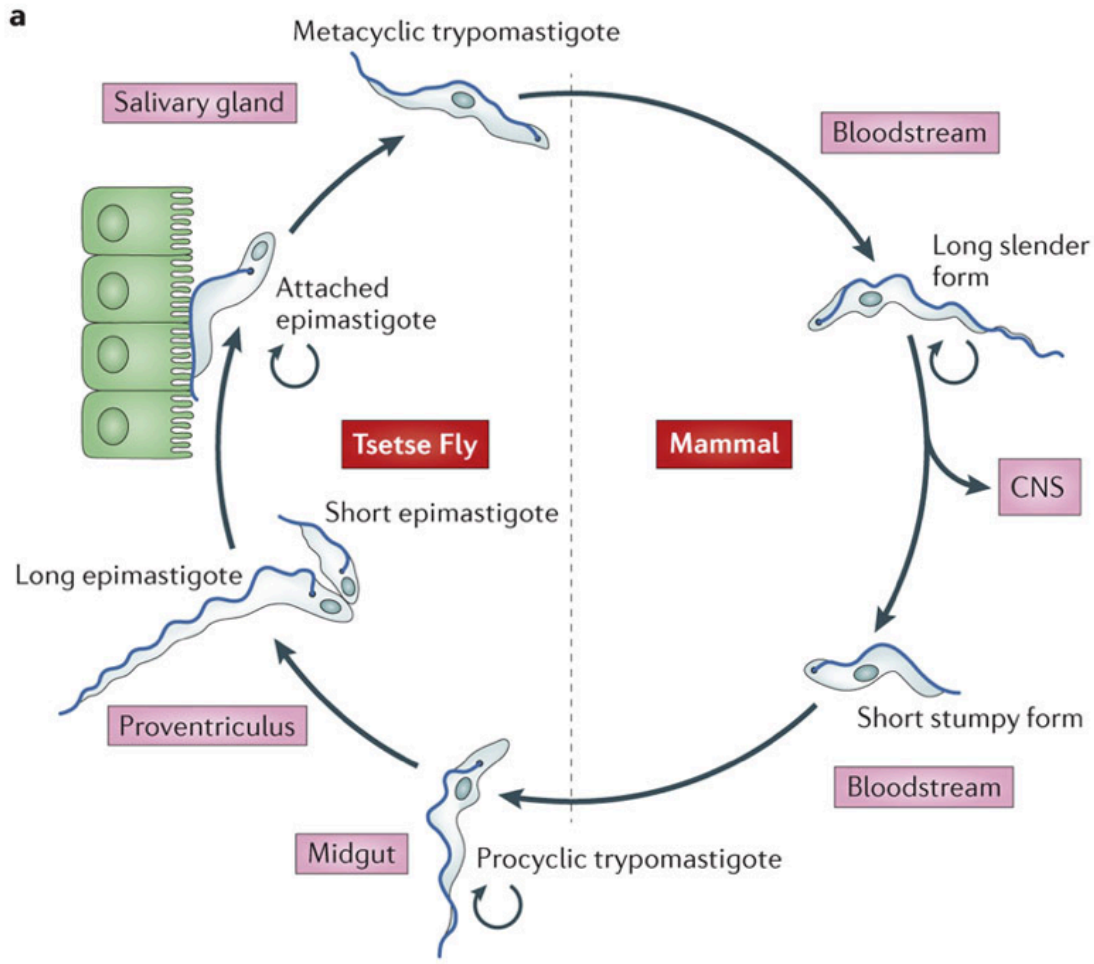

Figure 1.6 Life cycle of *T. brucei*, representing the morphology, location and cell cycle status of each developmental stage. From Langousis *et al*. (2014).

1.6.1 The mammalian stages

Metacyclic trypanosomes enter the dermal connective tissue of the mammalian host via the bite of an infective tsetse fly and pass to the bloodstream via the lymphatic system. These forms already express a VSG coat for immune evasion but metacyclic VSGs represent a distinct, more limited repertoire to those expressed in slender forms (Turner et al., 1988a). Metacyclics transform into long slender forms which proliferate extracellularly in the bloodstream. In this glucose-rich environment, energy is generated by glycolysis and the mitochondrion is relatively repressed. They evade the host's humoral response by VSG switching (see section 1.3) and when present at sufficiently high densities undergo differentiation to cell cycle arrested transmissible stumpy forms which are competent to infect the tsetse fly (Reuner et al., 1997). This transformation is described in detail in section 1.7.

1.6.2 The tsetse stages

Bloodstream trypanosomes taken up in a tsetse blood meal enter the insect midgut where slender forms die and stumpy forms differentiate to procyclic forms (Turner et al., 1988b). This process is described in section 1.8. Procyclic forms are proliferative and have an active mitochondrial metabolism in which ATP is generated via oxidative phosphorylation, for which proline serves as their primary carbon source (Evans and Brown, 1972). They express a surface glycoprotein coat consisting of GPEET and EP procyclins. The former is repressed after 7-9 days while EP expression persists (Vassella et al., 2000). The parasites cross the peritrophic matrix to colonise the ectoperitrophic space and migrate to the proventriculus. Here, cells lengthen and arrest before differentiating to epimastigotes via an asymmetric division which produces one long and one short daughter cell (Sharma et al., 2008). The long cell is believed to die while the short epimastigote moves to the salivary glands and attaches to the epithelium via its flagellum. It is here that they differentiate to proliferative premetacyclics and then arrested metacyclics expressing a VSG coat. Mature metacyclics detach ready for injection into a new mammalian host. The salivary glands are also the site of genetic exchange in the parasite, with meiotic dividers representing a distinct stage of dividing epimastigotes (Peacock et al., 2011).

1.7 Slender to stumpy differentiation

It has long been observed in trypanosome infections that parasitaemia follows a cyclical wave pattern, a phenomenon generally attributed to the battle between the host antibody response and the parasites' subsequent evasion by switching antigenic variant. However, another important contributing factor to this profile is that at high densities, *T. brucei* differentiate to transmissible stumpy forms (Gjini et al., 2010; Reuner et al., 1997; Vickerman, 1985). These forms are cell cycle arrested (Shapiro et al., 1984), which is important for tightly regulated differentiation, causing the subsequent transformation to procyclic form to proceed in a synchronous manner (Ziegelbauer et al., 1990). It also serves as an important mechanism of growth control in the mammalian host, preventing the parasitaemia from overwhelming the host and striking a balance between proliferation and differentiation which enables maximum transmissibility. Indeed, it has been shown using the stumpy-specific marker PAD1 that stumpy forms dominate chronic infections beyond the first wave of parasitaemia (MacGregor et al., 2011).

Differentiation involves significant morphological and metabolic changes which render stumpy forms competent to infect the tsetse fly (Robertson, 1913; Vickerman, 1965). Morphological rearrangements confer the eponymous stumpy appearance and the mitochondrion becomes elaborated in preparation for oxidative phosphorylation in the tsetse fly (Vickerman, 1985). The lysosome relocates anteriorly to the nucleus (Vanhollebeke et al., 2010) and upregulates its activity (Brickman and Balber, 1994). The cells lose mono-allelic control of VSG expression (Amiguet-Vercher et al., 2004) but are able to use hydrodynamic flow to remove surface-bound immunoglobulin more efficiently than slender forms (Engstler et al., 2007) and as a result show greater resistance to antibody-dependent complement-mediated lysis than their slender counterparts (McLintock et al., 1993). They also show increased resistance to acidic and proteolytic stress critical for survival in the tsetse midgut (Nolan et al., 2000). Stumpy forms are also characterised by upregulation of a family of surface carboxylate transporters known as PAD (proteins associated with differentiation), which are responsible for transducing the procyclic differentiation

signal (Dean et al., 2009)(see section 1.8). The stumpy enrichment of PAD1 has made it an invaluable surface marker for this stage (MacGregor et al., 2014; MacGregor et al., 2011; Mony et al., 2014) while PAD2 is upregulated and surface-localised only at low temperatures (Dean et al., 2009). In general, there is a global repression of gene expression in stumpy forms (Brecht and Parsons, 1998). However, a number of recent studies which have analysed global expression changes during differentiation have found selective enrichment of certain transcripts or proteins which are consistent with the changes described above (Capewell et al., 2013; Dejung et al., 2016; Gunasekera et al., 2012; Jensen et al., 2009; Kabani et al., 2009; Nilsson et al., 2010). Among them are numerous mitochondrial transcripts including respiratory complex components and a chloride channel possibly related to elevated lysosomal activity (Kabani et al., 2009). Also upregulated are transcripts required for procyclic differentiation including members of the PAD family, procyclins and the enzyme MSP-B, which is required for VSG cleavage (Capewell et al., 2013; Kabani et al., 2009).

The arrested state of stumpy forms means that the capacity to differentiate is selected against over long periods of continuous passage. As a result, the majority of molecular research on *T. brucei* uses so-called monomorphic strains which have lost the ability to produce stumpy forms, while differentiation-competent strains known as pleomorphs have proved less amenable to culture and genetic manipulation. This has long hindered investigation of differentiation and it was the development of plate-based *in vitro* culture system for pleomorphic trypanosomes by Vassella and Boshart (1996) which enabled the key discoveries that differentiation is density-dependent (Reuner et al., 1997) and triggered by a parasite-derived signal, stumpy induction factor (SIF), in a form of quorum sensing (Vassella et al., 1997). SIF is a low molecular weight factor or factors of unknown identity secreted by the parasites which accumulates extracellularly as the parasites proliferate and induces differentiation beyond a threshold density. Accordingly, pleomorphic trypanosomes can be induced to differentiate by culture in medium conditioned by growth of parasites to a high density. In contrast, monomorphic strains are believed to produce SIF, but have lost the ability to respond to this signal. Thus although media conditioned by dense growth of monomorphic trypanosomes triggers the

differentiation of pleomorphic strains, the converse is not true (Vassella et al., 1997). Although SIF remains unidentified nearly 20 years after these observations were first made, more recent improvements in the culture of pleomorphs and the establishment of a stable and efficient transfection system (MacGregor et al., 2013) are facilitating significant advancement in elucidating the molecular processes governing differentiation.

Another intriguing aspect of the differentiation process is the role of the second messenger cyclic AMP. Vassella et al. (1997) observed that membrane-permeable forms of cAMP could mimic the effects of SIF in triggering differentiation to stumpy forms and that the molecule was upregulated in response to SIF, implicating cAMP as a downstream mediator of SIF. Interestingly, monomorphic parasites can also be induced to differentiate in response to membrane-permeable cAMP (Breidbach et al., 2002), indicating that the factor which confers differential responsiveness to differentiation signals between monomorphic and pleomorphic strains operates somewhere between SIF and cAMP in the pathway. However, the involvement of cAMP is not straightforward. cAMP pathways in trypanosomes are poorly understood and appear to have diverged significantly from their mammalian counterparts (Gould and de Koning, 2011). Its most common substrate, protein kinase A, appears not to be activated by cAMP in this organism (Shalaby et al., 2001). Furthermore, Laxman et al. (2006) subsequently demonstrated that it is not cAMP itself, but its hydrolysis products adenosine and AMP, which are in fact responsible for the effects on differentiation.

1.8 Stumpy to procyclic differentiation

Bloodstream form *T. brucei* enter the tsetse midgut when ingested in the blood meal. Slender forms die while stumpy forms become competent to respond to the differentiation signal citrate/cis-aconitate (CCA) and transform to procyclic forms. At 37°C, the parasites are insensitive to the micromolar concentrations of CCA found in the blood meal (Engstler and Boshart, 2004). However, as mentioned in section 1.7, the cold shock encountered upon entering the fly midgut triggers the

carboxylate transporter PAD2 to be upregulated and relocalised from the flagellar pocket to the cell surface (Dean et al., 2009). This acts as a transporter for CCA and therefore renders the cell sensitive to the differentiation signal. Within the cell, the tyrosine phosphatase *Tb*PTP1 inhibits differentiation (Szoor et al., 2006) by dephosphorylating the DxDxT phosphatase *Tb*PIP39 (Szoor et al., 2010). *Tb*PIP39 in turn activates *Tb*PTP1, thereby reinforcing its own inhibition. CCA abrogates this feedback loop and *Tb*PIP39 is activated and triggers transformation to procyclic forms. Its downstream target is unknown. However, it has been shown that *Tb*PIP39 localises to the glycosomes and that this localization is required for differentiation (Szoor et al., 2010). These events are summarised in Figure 1.7. A number of other triggers have been shown to induce procyclic differentiation (Rolin et al., 1998; Yabu and Takayanagi, 1988). Of these, mild acid treatment has been shown to operate through the *Tb*PTP1 signalling cascade, while protease treatment operates independently of this pathway (Szoor et al., 2013).

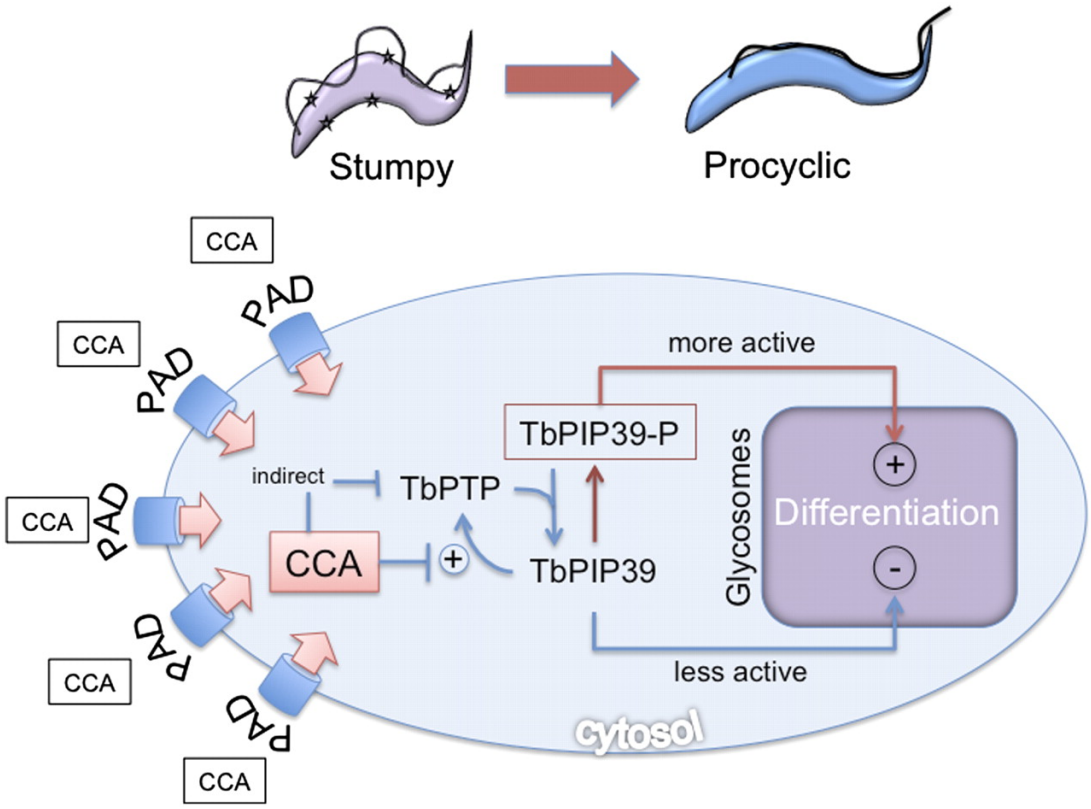

Figure 1.7 Model of the regulation of stumpy to procyclic differentiation. *Tb*PIP39 acts on an unknown glycosomal target to trigger differentiation from stumpy to procyclic form. However, this action is prevented by dephosphorylation and inactivation by *Tb*PTP1. *Tb*PIP39 activates *Tb*PTP1, reinforcing its own inhibition. This feedback loop is abolished by the differentiation signal CCA, which is conveyed to the cell via PAD transporters.

1.9 Molecular components of slender to stumpy differentiation

SIF is believed to initiate stumpy formation via a signalling cascade. However, the molecular identity of SIF remains elusive and that of its downstream effectors have only recently begun to be revealed. A major breakthrough in the identification of such signalling components came from a screen by Mony *et al*. (2014) of a monomorphic RNA interference library. This library takes advantage of the well-established tetracycline-inducible RNA silencing system in *T. brucei* and applies it on a genome-wide scale, so that within a population of cells every gene is separately targeted for RNAi ablation (Morris et al., 2002). Induction of the library under a particular selectional condition or in the presence of a specific compound, followed by sequencing of the RNAi inserts of the surviving population, can therefore be used to identify genes for which silencing confers a selective advantage under those conditions (Glover et al., 2015). This presents a powerful forward genetic screen, which has been used to determine essentiality of genes in different parasite life cycle stages on a genomic scale (Alsford et al., 2011) and to explore diverse aspects of trypanosome biology, including drug action and resistance (Alsford et al., 2012), serum lysis (Lecordier et al., 2014) and RNA regulation (Schumann Burkard et al., 2013).

As discussed in section 1.7, monomorphic trypanosomes are unable to respond to SIF but can be induced to differentiate using membrane-permeable forms of cAMP and AMP (Laxman et al., 2006; Vassella et al., 1997). Therefore, to investigate stumpy formation, the RNAi library was induced in the presence of 8-(4-chlorophenylthio)-cAMP (pCPTcAMP) or 8-pCPT-2'-O-methyl-5'-AMP (Mony et al., 2014). This resulted in the eventual loss of most cells due to differentiation-associated arrest and the outgrowth of a population in which cAMP/AMP response effectors had been silenced. Sequencing of the RNAi loci identified numerous genes implicated in the stumpy signalling pathway. This strategy is depicted in Figure 1.8.

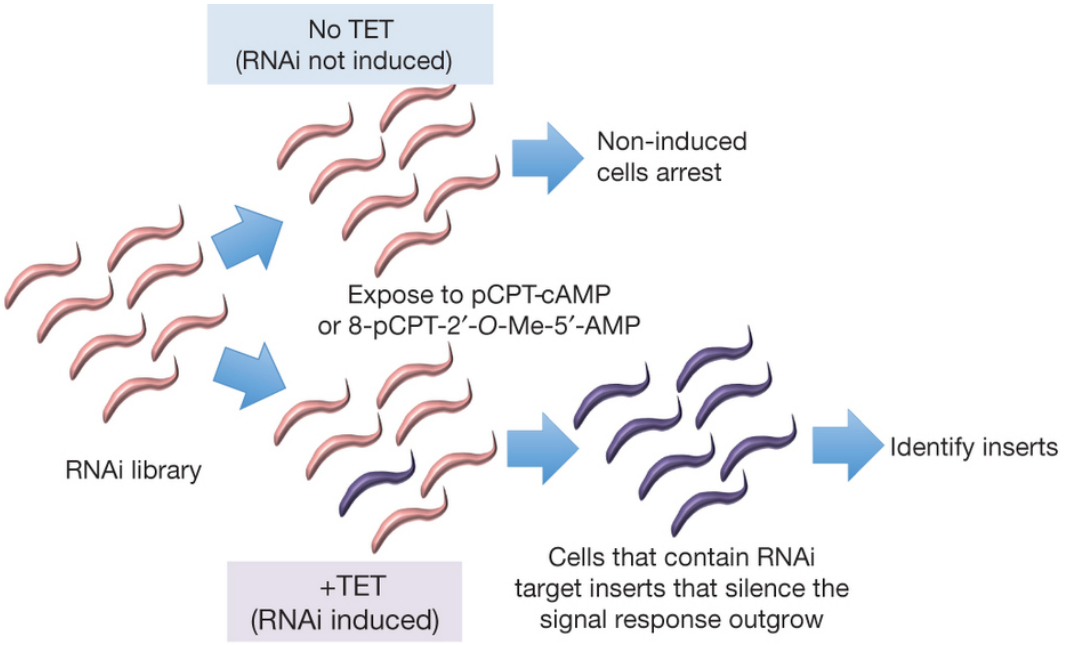

Figure 1.8 RNAi library screen used to identify components of stumpy signalling pathway in Mony *et al.* (2014). Genome-wide RNAi silencing was induced with tetracycline and the cells treated with pCPTcAMP or 8-pCPT-2'-*O*-Me-5'-AMP to trigger differentiation, leading to arrest of the uninduced (tet-) population. Induced (tet+) cells containing RNAi inserts which silence cAMP/AMP response effectors outgrew. The responsible genes were identified by sequencing of RNAi inserts. From Mony *et al.* (2014).

This screen identified numerous components of stumpy formation which are shown in Figure 1.9. Although a number of inhibitors of stumpy formation had previously been characterised (see section 1.9.4), this cohort, referred to here as *pos*ST (*pos*itive mediators of STumpy formation) represented the first known promoters of differentiation. Signal transducers such as kinases and phosphatases as well as regulators of gene expression are represented, but their individual roles and interactions remain to be characterised in order to construct a defined pathway.

1	2	3	4	5	6	7	8
Gene	Screen	Function	Tested	Slow Growth?	SIF Res?	RITSeq[6]	
						DIF	**PCF**
Tb927.2.1810	AMP	ISWI	×	ND	ND	✓	✓
Tb927.2.2720	cAMP	MEK kinase	✓	×	ND	✓	×
Tb927.2.4020	AMP	ubiquitin activating enzyme,	×	1	ND	✓	✓
Tb927.3.4560	cAMP	AMPK SNF1 like family	✓	1	ND	×	×
Tb927.4.670	cAMP	hypothetical conserved	×	ND	ND	×	×
Tb927.4.3620	both	protein phosphatase 1,	✓	2	✓	×	×
Tb927.4.3630	both	protein phosphatase 1,	✓	2	✓	×	×
Tb927.4.3640	both	protein phosphatase 1,	✓	2	✓	×	×
Tb927.4.3650	both	protein phosphatase 1, adjacent gene	×	ND	ND	×	×
Tb927.5.3580	cAMP	phosphoglycerate mutase	×	ND	ND	×	×
Tb927.6.2300	both	adenosine kinase,	✓	3	×	✓	×
Tb927.6.2360	both	adenosine kinase	✓	3	×	✓	×
Tb927.7.2100	cAMP	GMP synthase	✓	3	×	×	×
Tb927.7.7160	cAMP	dual specificity phosphatase	×	4	✓	✓	×
Tb927.8.2860	cAMP	Hypothetical protein	×	×	ND	×	×
Tb927.9.4080	cAMP	hypothetical, conserved (HYP 2)	✓	4	✓	✓	×
Tb927.9.7550	both	ADSL	✓	3	3	✓	✓
Tb927.9.13530	cAMP	hypothetical, conserved	×	ND	ND	✓	×
Tb927.10.5930	cAMP	NEK protein kinase	✓	4	✓	ND	ND
Tb927.10.5940	cAMP	NEK protein kinase	✓	4	✓	×	×
Tb927.10.5950	cAMP	NEK protein kinase	✓	4	✓	×	×
Tb927.10.12100	cAMP	RNA-binding protein	✓	5	✓	✓	×
Tb927.10.15020	both	YAK protein kinase	✓	×	✓		
Tb927.10.16120	cAMP	IMP dehydrogenase	×	ND	ND	✓	×
Tb927.11.290	cAMP	phosphatase and tensin	×	1	ND	✓	✓
Tb927.11.300	cAMP	pre-mRNA-splicing factor CWC26 like C terminus	×	ND	ND	✓	✓
Tb927.11.750	cAMP	DNA repair protein, putative	×	ND	ND	×	×
Tb927.11.760	cAMP	Protein phosphatase 2C	×	ND	ND	✓	✓
Tb927.11.1640	cAMP	Conserved hypothetical	×	ND	ND	×	×
Tb927.11.2250	cAMP	Conserved hypothetical	×	ND	ND	×	×
Tb927.11.3650	both	ADSS	✓	3	3	✓	×
Tb927.11.4610	cAMP	protein kinase A regulatory subunit	×	3	3	✓	×
Tb927.11.6600	both	hypothetical, conserved (hyp1)	✓	×	✓	✓	×
Tb927.11.11470	AMP	Mitochondrial SSU ribosomal protein, putative	×	ND	ND	✓	✓
Tb927.11.11480	AMP	Trichohyalin, putative	×	ND	ND	×	×

Figure 1.9 List of genes identified from RNAi library screen after selection with pCPT-cAMP or 8-pCPT-2'-O-Me-5'-AMP (Mony et al., 2014). Columns indicate: 1) target accession no.; 2) specific screen(s) in which gene was selected; 3) functional prediction where available; 4) whether gene has been tested in independent monomorphic RNAi line; 5) growth characteristics upon RNAi induction (1. No verified RNAi competent lines were isolated from several transfections. 2. Slow growth *in vitro* and, to a lesser extent, *in vivo.* 3. Strong growth inhibition. 4. Weak growth inhibition *in vitro* or *in vivo* 5. Leaky RNAi in all six lines tested.); 6) 'SIF res?' indicates whether RNAi line showed SIF resistance and hence reduced stumpy formation in vivo; 7 and 8) whether a reduced fitness (✓) was observed in differentiating (7) or procyclic (8) in a genome wide RNAi library screen (Alsford et al., 2011). From Mony *et al*. (2014).

1.9.1 Kinases

In eukaryotes, protein phosphorylation is a key mechanism of regulation of diverse cellular functions. Its importance in signal transduction in *T. brucei* is indicated by the large complement of kinases found in the genome (Jones et al., 2014; Parsons et al., 2005) and the widespread changes in phosphorylation between life stages revealed by comparative phosphoproteomics (Urbaniak et al., 2013). In addition, Jones *et al.* (2014) were recently able using a kinome-wide RNAi screen to identify 2 kinases, RDK1 and RDK2 (repression of differentiation kinase), which promote bloodstream to procyclic form differentiation. Of particular significance given the centrality of cell cycle arrest to stumpy formation, a number of kinases have been demonstrated to have roles in the regulation of cell cycle progression (Hammarton et al., 2007; Inoue et al., 2015; Jones et al., 2014; Tu and Wang, 2004; Wei and Li, 2014). Thus, it is unsurprising that the *pos*ST cohort included various protein kinases (Mony et al., 2014). One of these, a regulatory subunit of protein kinase A (PKA-R), was noteworthy for its implication in cellular quiescence in yeast (De Virgilio, 2012). However, lethality of RNAi silencing of PKA-R in *T. brucei* precluded its validation as a mediator of stumpy formation (Mony et al., 2014). Other identified kinases that proved more amenable to validation are described in detail below.

1.9.1.1 MEKK1

MAPK signalling transduction pathways are involved in coordinating gene expression changes in response to external stimuli. These pathways are ubiquitous in eukaryotes and operate in wide-ranging cellular processes and cell types. The pathway comprises a three-tiered cascade: a serine/threonine mitogen-activated protein kinase kinase kinase (MAP3K) or MAPK/ERK (extracellular signal-related kinase) kinase (MEKK) phosphorylates a dual specificity MAP2K/MEK which in turn phosphorylates a serine/threonine MAPK (reviewed in (Chang and Karin, 2001). This process is depicted in Figure 1.10. A putative MEKK, *Tb*MEKK1 (Tb927.2.2720), was identified among the *pos*ST cohort. As depicted in Figure 1.10, it contains a C-terminal MEK kinase catalytic domain as well as 2 predicted N-terminal transmembrane domains. MEKK1 was detected in a comparative phosphoproteomic study by Urbaniak *et al.* (2013) and showed differential

phosphorylation at a number of sites between bloodstream and procyclic forms, supporting the hypothesis that this kinase plays a stage-specific role in signal transduction.

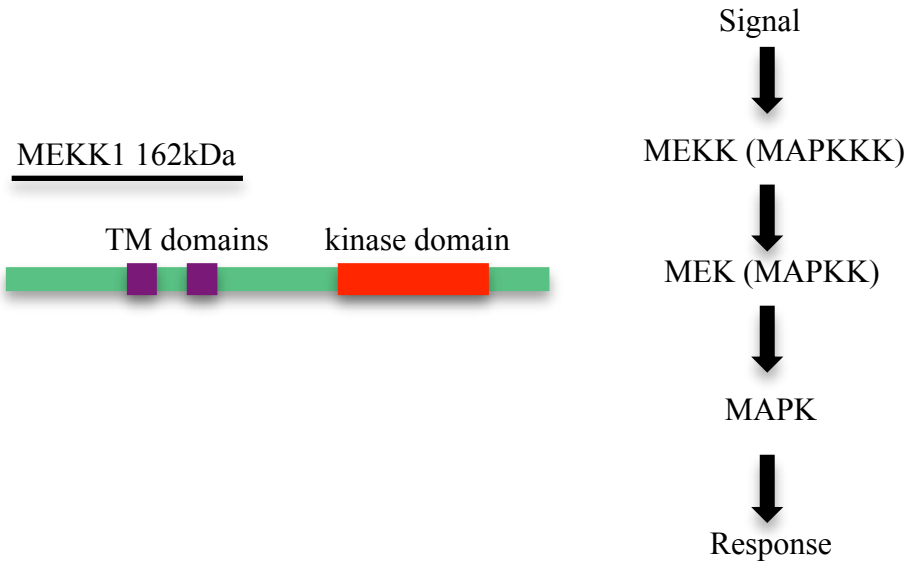

Figure 1.10 Left: Schematic of *Tb*MEKK1 showing predicted N-terminal transmembrane domains and C-terminal kinase domain. Right: Overview of MAPK signalling pathway.

As in other eukaryotes, a number of MAPKs in *T. brucei* have been implicated in growth and differentiation processes. A null mutant of MAPK2 showed delayed differentiation to procyclic forms (Muller et al., 2002) while deletion of MAPK5, conversely, accelerates stumpy formation in mice (Domenicali Pfister et al., 2006). At the second tier, MAP kinase kinase 1 (MKK1) is essential at a different parasite life stage, specifically salivary gland colonisation in the tsetse (Morand et al., 2012). Recently, Jones *et al.* (2014) identified the MEKK-like repressor of differentiation kinase 1 (RDK1) in a kinome-wide RNAi screen as a negative regulator of differentiation to procyclic forms, the only kinase of the uppermost tier of MAPK signalling apart from MEKK1 to be explored in relation to parasite differentiation.

1.9.1.2 NEK

The never in mitosis A (NIMA)-related kinases, or NEKs, represent a family of conserved serine/threonine kinases which function in cell cycle progression (Fry et al., 2012). This family is expanded in *T. brucei* relative to humans (Jones et al., 2014; Parsons et al., 2005). Of those so far studied, NEK12.2/RDK2 (repression of

differentiation kinase 2) has been found to negatively regulate procyclic differentiation (Jones et al., 2014) while NRKA/B exhibits translational upregulation in stumpy forms (Gale et al., 1994) and is involved in the initiation of procyclic differentiation (Domingo-Sananes et al., 2015). NRKC plays a role in basal body separation (Pradel et al., 2006). The *pos*ST cohort includes 3 NEK genes (Tb927.10.5930, Tb927.10.5940, Tb927.10.5950), found in tandem array on chromosome 10 and of near identical sequence, which have been validated in pleomorphs as mediators of stumpy formation (Mony et al., 2014).

1.9.1.3 YAK

Dual-specificity YAK kinases act as suppressors of proliferation in yeast and *Dictyostelium* (Garrett et al., 1991; Souza et al., 1998). In yeast, YAK1 responds to glucose starvation by relocalising to the nucleus where it inhibits cell growth and stimulates the stress response (Lee et al., 2008; Moriya et al., 2001). YakA is involved in the transition from growth to development in *Dictyostelium* (Souza et al., 1998). Correspondingly, silencing of a *T. brucei* YAK kinase identified in the *pos*ST cohort (Tb927.10.15020) resulted in decreased cell cycle arrest and reduced differentiation to stumpy forms (Mony et al., 2014). YAK1 nuclear localisation and consequent activity in yeast is inhibited by phosphorylation by protein kinase A (PKA) (Lee et al., 2011). Interestingly, the *T. brucei* regulatory subunit of PKA, PKA-R, was also idenitified in the RNAi library screen, but could not be validated due to a severe growth phenotype upon RNAi (Mony et al., 2014).

1.9.1.4 Adenosine Kinase

T. brucei lacks a de novo purine synthesis pathway and is therefore dependent on salvage from its hosts (James and Born, 1980). One key purine source, adenosine, is salvaged by one of two pathways: the two step cleavage-dependent pathway, in which it is first cleaved to adenine before phosphoribosylation to adenosine monophosphate, and the cleavage-independent pathway in which it is instead phosphorylated directly (Vodnala et al., 2008). The enzyme responsible for the latter pathway is adenosine kinase (AK) (Luscher et al., 2007; Vodnala et al., 2008). The *T. brucei* genome contains two AK genes (Tb927.6.2300 and Tb927.6.2360). Arising from a gene duplication event, the resulting proteins differ by only 4 amino acids and in previous experimental studies have been treated as a single product (Luscher et al.,

2007). AK was among a number of purine pathway enzymes idenitified in the *pos*ST cohort. Upon further study, many of these showed no role in differentiation, but instead appeared to have been selected due to the ability of the analogues to complement purine salvage defects (Mony et al., 2014). Unlike these enzymes however, it has been previously reported that AK knockdown does not result in any growth defect under normal conditions (Luscher et al., 2007). In addition, a potential role in stumpy formation is supported by the fact that the product of this enzyme is the differentiation induction agent AMP.

1.9.2 Phosphatases

As the enzymatic counterparts to protein kinases, phosphatases represent an equally important contribution to regulation of cellular processes via dephosphorylation. The composition of the *T. brucei* phosphatome is diverged from that of humans, with an expanded complement of serine/threonine phosphatases and reduced tyrosine phosphatases (Brenchley et al., 2007). As described in section 1.8, 2 protein phosphatases have been demonstrated to be key players in a distinct differentiation event, namely the transformation from stumpy to procyclic form. However, a number of phosphatases was also included in the *pos*ST cohort and are described below.

1.9.2.1 PP1/PP2A

The PPP family of serine/threonine phosphatases has been well characterised in eukaryotes and is typically subdivided into types 1, 2A, 4, 6, 2B, 5 and 7 (Cohen, 2002). The *T. brucei* genome encodes 7 PP1 orthologues (Li et al., 2006). Simultaneous knockdown of all 7 results in modest growth inhibition in procyclic forms (Li et al., 2006). PP1-3 has been shown to be essential for correct organelle positioning in procyclics (Gallet et al., 2013) and is also transcribed directly upstream of the largest subunit of RNA pol II, RPB1, leading to speculation that RPB1 could be a substrate of the phosphatase (Evers and Cornelissen, 1990). Members of a PP1 array, PP1-4,5,6 (Tb927.4.3640, Tb927.4.3630, Tb927.4.3620), were identified in the RNAi library screen as *pos*ST components. Simultaneous knockdown of these genes prevents differentiation (Mony et al., 2014) while overexpression of one member enhances stumpy formation (B. Mony and K. R. Matthews, unpublished data). TbPP2A (Tb927.3.1240) is essential for growth and

cell cycle progression in both procyclic and bloodstream forms (Rothberg et al., 2014). Interestingly, the related *Trypanosoma cruzi* PP2A, which shows a high degree of homology to the *T. brucei* protein, has been implicated in the differentiation from trypomastigote to amastigote forms of this parasite (Gonzalez et al., 2003). Although TbPP2A was detected in the RNAi library screen, this may be a consequence of substantial shared homology with the PP1s (Mony et al., 2014).

1.9.2.2 Dual specificity phosphatase

Another identified *pos*ST phosphatase is the dual specificity phosphatase (DSP) with accession no. Tb927.7.7160. It is a kinetoplastid specific DSP with no close homology to DSPs of other species (Brenchley et al., 2007) and was previously identified as being enriched in stumpy forms in a transcriptomic study (Kabani et al., 2009). Knockdown of DSP prevents differentiation to stumpy forms (Mony et al., 2014).

1.9.3 RNA-binding proteins

Further downstream in any signalling cascade operate effectors capable of modulating gene expression. Due to the reliance of *T. brucei* on post-transcriptional mechanisms of regulation (see section 1.3), it stands that RNA-binding proteins are likely candidates for involvement in the stumpy formation pathway. RNA-binding proteins have been implicated in developmental progression of other life cycle stages, including *Tb*ZFP1-3, which are involved in differentiation to procyclic forms (Hendriks et al., 2001; Paterou et al., 2006; Walrad et al., 2012), and RBP6, which plays a central role in the development of various tsetse life stages (Kolev et al., 2012). Potential such effectors among the *pos*ST proteins include HYP2 and RBP7, described below.

1.9.3.1 Hypothetical protein 2

Although the function of the hypothetical protein (HYP2; Tb927.9.4080) is unknown, as eponymously implied, there is evidence to indicate a role in gene regulation. It was shown to upregulate transcripts to which it was artificially tethered in a screen for post-transciptional regulators by Erben *et al.* (2014), although this effect may be indirect, as HYP2 has been shown to interact with DRBD3 (Fernandez-Moya et al., 2012) and MKT1 (Singh et al., 2014), both of which are

known to stabilise mRNAs. HYP2 contains a DskA zinc finger motif and a nucleotide-binding domain (Mony et al., 2014). In *Escherichia coli*, DskA is an RNA polymerase binding protein which regulates rRNA transcription in response to nutritional stress (Paul et al., 2004). Silencing of HYP2 reduces stumpy formation *in vitro* and *in vivo* (Mony et al., 2014).

1.9.3.2 RBP7

RBP7 is encoded by 2 near identical genes, RBP7A and RBP7B (Tb927.10.12090 and Tb927.10.12100), which each contain a single RNA-recognition motif (RRM). RNAi of RBP7 results in reduced responsiveness to the SIF differentiation signal, while overexpression of RBP7B accelerates stumpy formation. Transcriptomic analysis of these 2 perturbations showed upregulation of a number of histone transcripts upon RBP7 depletion, likely reflective of a continued proliferative state, whereas overexpression elevated transcripts associated with the procyclic form, indicative of preparation for the subsequent differentiation event. RBP7 overexpression also increased levels of a number of other RNA-binding protein mRNAs (Mony et al., 2014).

1.9.4 Inhibitors of stumpy formation

Prior to the identification of positive regulators of stumpy formation via the RNAi library screen, a number of inhibitors of this process were already known. A null mutant of a zinc finger kinase (ZFK) in a pleomorphic strain showed increased stumpy formation *in vitro*, though not *in vivo* (Vassella et al., 2001). Similarly, ablation of MAPK5 in pleomorphs resulted in premature differentiation both *in vitro* and *in vivo* (Domenicali Pfister et al., 2006). Crucially, these phenotypes were not observed upon ablation of either gene in a monomorphic strain. However, stumpy formation can be triggered in monomorphs by RNAi of the TOR kinase TOR4 (Barquilla et al., 2012). The action of these negative regulators points to the influence of 2 opposing forces in regulating differentiation: the stumpy inhibitors which act to preserve slender state at low density, and the *pos*ST pathway, which when released from this inhibition by SIF, activates differentiation. This system draws parallels to that of the subsequent development event, in which *Tb*PIP39 triggers differentiation to procyclic forms but is inhibited by the action of *Tb*PTP1

(see section 1.8). It is likely that the components of the conflicting processes operate closely together to enable tight regulation of proliferation versus differentiation and it would therefore be of interest to study where known stumpy inhibitor proteins operate in relation to proteins of the *pos*ST pathway. This is explored in this thesis via TOR4, which is described in detail below.

1.9.4.1 TOR4

The conserved serine/threonine kinases targets of rapamycin (TOR) acts within a complex, TORC, to regulate cell growth in relation to environmental conditions and energy status. They generally operate during favourable conditions and are downregulated upon nutrient depletion (Wullschleger et al., 2006). In *T. brucei*, TOR1 and TOR2 act via TORC1 and TORC2, respectively, to modulate growth in a manner analogous to their mammalian and yeast counterparts (Barquilla et al., 2008). Specifically, TORC1 regulates such aspects as transcription, translation and suppression of autophagy, while TORC2 is implicated in cytoskeletal remodelling, endocytosis and cytokinesis. Kinetoplastids are unusual in that they contain 2 additional TORs which function distinctly from TORC1 and TORC2 signalling (Barquilla et al., 2008). TOR3 is involved in regulation of acidocalcisome and polyphosphate metabolism (de Jesus et al., 2010). TOR4, meanwhile, forms a unique complex, TORC4, which includes proteins not previously associated with TORCs (Barquilla et al., 2012). RNAi of TOR4 triggered differentiation to stumpy forms while membrane-permeable cAMP or AMP treatment downregulated TbTOR4 expression. TOR4-depleted monomorphic cells showed many hallmarks of stumpy development, including growth arrest, PAD upregulation and cis-aconitate hypersensitivity (Barquilla et al., 2012). As these experiments were performed in a monomorphic strain, it is unknown if depletion of TOR4 is able to produce the same effect in pleomorphs.

1.10 Chemical inducers of stumpy formation

The stumpy signalling pathway is of interest not just to our understanding of parasite biology but also due to its potential as a novel therapeutic target. In natural

infections, differentiation to stumpy form occurs at high density, ensuring a sustainable and highly transmissible population (MacGregor et al., 2011; Reuner et al., 1997). Chemical induction of stumpy formation could be used to achieve arrest and clearance of the parasites at sub-transmissible densities. Ablation of negative regulators of stumpy formation (Barquilla et al., 2012; Domenicali Pfister et al., 2006; Vassella et al., 2001) and overexpression of *pos*ST proteins (Mony et al., 2014) have demonstrated the feasibility of targeting the pathway in this manner. In addition, the continued elusiveness of the molecular identity of SIF means that *in vitro* studies of differentiation have long relied on membrane permeable forms of cAMP and AMP (Laxman et al., 2006; Mony et al., 2014; Vassella et al., 1997), highlighting the importance of chemical tools in the investigation of this process.

To identify novel small molecule inducers of differentiation, MacGregor et al. (2014) developed a monomorphic stumpy-specific reporter cell line in which a β-glucuronidase reporter was fused to the 3'UTR of PAD1. A high-throughput screen of 6,764 molecules using this reporter was able to identify DDD00015314 (referred to as E667 in this thesis) as a chemical inducer of differentiation in monomorphs and pleomorphs. This demonstrated the potential of this reporter for use in subsequent high-throughput screens of further compound libraries. In addition, the identification of new differentiation regulators presents the possibility of discovery of new compounds targeted to specific proteins.

1.11 Aims

The aim of this thesis was to study the slender to stumpy signalling pathway in *Trypanosoma brucei* by ordering with respect to one another components known to be involved in this process. This objective takes advantage of the recent identification of many new proteins involved in stumpy formation and was primarily addressed via 3 approaches:

- Relative positioning of *pos*ST proteins via a combinatorial overexpression and knockout strategy as well as phosphoproteomic analysis.

- Ordering of *pos*ST proteins relative to the stumpy inhibitor TOR4 via a similar dual genetic silencing approach.
- Chemical-genetic analysis using small molecules capable of inducing differentiation via unknown mechanisms.

2 Chapter 2: Methods

2.1 Trypanosome strains

The majority of cell lines used in this thesis are based on *T. b. brucei* AnTat 1.1 90:13 (Engstler and Boshart, 2004), a pleomorphic culture-adapted cell line with integrated T7 RNA polymerase and Tet repressor constructs to facilitate conditional genetic manipulations. The monomorphic 2T1 cell line, in which constructs can be specifically targeted to a defined locus containing an incomplete *HYG* ORF to prevent variable position effects (Alsford et al., 2005), was used to generate RNAi lines in monomorphs. The RNAi library line based on this strain (Alsford et al., 2011) was used for the RNAi library screen (section 2.17). Full length and truncated MEKK1 fragments were overexpressed in the 427-derived single marker S16 line, which expresses a tet repressor and T7 RNA polymerase under the control of neomycin (Wirtz et al., 1999). The GUS PAD1 3'UTR reporter line was developed from the Lister 427 strain by MacGregor *et al*. (2014).

2.2 Trypanosome culture

Trypanosomes were maintained in HMI-9 media supplemented with 10% foetal calf serum (Life Technologies) and 100U/ml penicillin and streptomycin (Life Technologies) at 37°C/5% CO_2 (Hirumi and Hirumi, 1989) and grown to densities up to $1x10^6$/ml. Cells were counted using a Beckman Coulter Z2 Particle Count and Size Analyser. For storage, approximately $2x10^6$ cells at a density of $7x10^5$-$1x10^6$/ml were resuspended in 1ml 10% glycerol in HMI-9 and frozen at -80°C in cryovials. Frozen samples were recovered by thawing rapidly at 37°C, centrifuging at 1000g for 5 minutes and transferring to 5ml fresh media.

2.3 Trypanosome infections

All trypanosome infections were performed in MF1 strain mice in the MARCH Building, University of Edinburgh. All animal procedures were carried out either by myself, Julie Young or Keith Matthews according to the terms of the project and personal licenses.

Mice were injected with 200µl 25 mg/ml cyclophosphamide (Sigma) 24 hours before infection to suppress the immune system. This step was omitted for experiments in which only slender parasites were required for harvest. Parasitaemia was monitored at 24 hour intervals from 3 days post infection onwards by making a tail snip and collecting a blood drop on a slide. Parasitaemia was then estimated microscopically according the method described by Herbert and Lumsden (1976). To terminate the infection, whole blood was extracted by cardiac puncture using a 2ml syringe containing 200 µl 2% citrate. Parasites were purified from whole blood by passing through DEAE-cellulose anion exchange resin (Whatman) at pH 7.8.

2.4 Cloning

2.4.1 DNA extraction

Genomic DNA was extracted from *Trypanosoma brucei* using the QIAGEN® DNeasy Blood and Tissue kit according to the manufacturer's instructions.

2.4.2 PCR

PCR was carried out in 0.2ml PCR tubes in a Biometra TProfessional Basic Gradient Thermocycler. Components and conditions of a typical 25 µl reaction are outlined below.

Components:
5 µl 5x buffer
1.5 µl 25 mM $MgCl_2$
2 µl 2.5 mM dNTPs
1.25 µl 10 mM Forward primer
1.25 µl 10 mM Reverse primer
0.5 µl template DNA
0.25 µl Taq polymerase
13.25 µl dH_2O

Reaction conditions:
95°C 5 mins

[95°C 30s
55°C 30s
68°C 1 min/kb amplicon] x30 cycles
68°C 10 mins

All primers used in this thesis were produced by Sigma-Aldrich and are listed in Appendix A.

2.4.3 DNA agarose gel electrophoresis

For the visualisation and separation of DNA fragments, samples were resolved on a 1% agarose gel in 1x TAE buffer containing 0.5 μg/ml ethidium bromide. The gel was cast in a Fisher-brand gel tank and immersed in 1x TAE buffer. DNA samples were loaded into the wells alongside a 1 kb DNA ladder for size estimation and electrophoresed at 130V until the fragments resolved.

2.4.4 Restriction digestion

All restriction enzymes and buffers used were from Promega or NEB. Reactions were carried out in an optimum buffer with 10 units of enzyme and incubated at 37°C (recommended temperature for all enzymes used in this thesis) for a minimum of 1 hour. Double digests were carried out simultaneously where a compatible buffer for both enzymes was available.

2.4.5 DNA purification

DNA was purified from PCR products, restriction digests or agarose gel pieces using the NucleoSpin Extract II kit (Machery-Nagel) following the manufacturer's instructions in order to remove salts, primers and other impurities from previous reactions which may interfere with downstream processing of the sample.

2.4.6 Ligation

PCR products were ligated directly into the pGEM T-Easy vector (Promega) via the A/T overhangs. Restriction digested DNA inserts were ligated into expression vectors digested with the same enzyme(s) to produce complementary sticky ends. Typically ligation reactions were carried out in a 10 μl volume and comprised 1μl

10x T4 DNA ligase buffer (Promega), 0.5 µl T4 DNA ligase, 1 µl DNA vector and 7.5 µl DNA insert. Ligations were incubated at room temperature for 1 hour or 4°C overnight.

2.4.7 Gibson cloning

Some constructs in this thesis – specifically the overexpression of NEK, YAK and MEKK1 with C terminal TY tag in pDEX - were generated by the alternative cloning method of the Gibson cloning system (NEB), which enables the assembly of multiple overlapping DNA fragments. Primers generating overlap sequences were designed using the NEBuilder Assembly tool (http://nebuilder.neb.com) and are listed in Appendix A. These primers were used to amplify insert fragments by PCR (section 2.4.2) while the vector was prepared by restriction digestion (section 2.4.4). The assembly reaction comprised 50-100 ng of vector with 2-3 fold excess of each insert in a 10 µl volume. 10 µl of 2x Gibson Assembly Master Mix was then added and the reaction incubated at 50°C for 15 minutes. 2 µl of the reaction was then transformed in NEB 5-alpha Competent *Escherichia coli* according to the protocol described in section 2.4.9.

2.4.8 Preparation of XL-1 *Escherichia coli* competent cells

XL-1 blue cells were used to inoculate 5 ml LB broth. This was incubated at 37°C overnight with shaking. This starter culture was then used to inoculate 400 ml LB broth, which was divided into 2 x 200 ml cultures in 1L flasks to allow sufficient aeration. These were incubated at 37°C shaking until OD_{600} reached 0.4-0.5, as measured on an Eppendorf Biophotometer. The cells were centrifuged at 2000g for 10 minutes at 15°C in 8 x 50 ml volumes. Each pellet was resuspended in 25 ml sterile ice-cold Buffer RF1 and incubated on ice for 1 hour. The cells were centrifuged at 2000g for 5 minutes at 4°C and resuspended in 8 x 8 ml sterile ice-cold Buffer RF2. The competent cells were then aliquoted into 200 µl volumes, snap frozen in liquid nitrogen and stored at -80°C.

Buffer RF1:	Buffer RF2:
10mM $RbCl_2$	10mM $RbCl_2$

50mM $MnCl_2$
30mM potassium acetate
10mM $CaCl_2$
10% (v/v) glycerol
pH5

10mM MOPS
75mM $CaCl_2$
10% (v/v) glycerol
pH 6.8

2.4.9 Bacterial transformation

For transformation, 5 µl of ligation reactions or plasmids were added to 100 µl of XL-1 blue *E. coli* competent cells (prepared as described in section 2.4.8) and incubated on ice for 20 minutes. The cells were then subjected to heat shock at 42°C for 40s, before addition of 500 µl LB media and incubation at 37°C with shaking for 1 hour. The cells were then pelleted at 2500g for 90s, resuspended in 100 µl of media and spread onto an LB agar plate containing 1 mg/ml ampicillin to enable selection of the plasmid. For ligations into pGEM T-Easy, plates were spread with 100 µl 2% X-gal (5-bromo-4-chloro-3-indolyl-beta-D-galacto-pyranoside) and 20 µl 0.1M IPTG (isopropyl β-D-1-thiogalactopyranoside) prior to addition of cells to screen for successful integration of the insert and consequent disruption of the β-lactamase gene. Plates were then incubated at 37°C overnight.

2.4.10 Small scale plasmid preparation

For preparation of up to 20 µg of plasmid DNA, a bacterial colony was used to inoculate 3 ml LB with 1 mg/ml ampicillin. This was incubated at 37°C with shaking overnight. The cells were then pelleted at 10,000g for 5 minutes and resuspended in 100 µl Mini-prep soln I (50mM glucose, 25mM Tris pH8, 10mM EDTA pH 8). 200µl Soln II (0.2M NaOH, 1% SDS) was added and the sample incubated for 4 mins at room temperature. 150 µl ice cold Soln III (3M potassium acetate, 5M acetic acid) was then added and the sample incubated on ice for 5 mins. It was then spun for 10 mins at 10000g and the supernatant transferred to a fresh tube. 2 volumes of cold 96% ethanol was added and the sample incubated on ice for 15 minutes. It was then spun for 10 mins at 10000g, washed in 70% ethanol and spun again. The pellet was air-dried, resuspended in 40 µl water and treated with 100 µg/ml RNase A (Sigma) for 5 minutes.

2.4.11 Medium scale plasmid preparation

For preparation of larger quantities of plasmid DNA, DNA was purified using the Nucleobond Xtra Midi kit (Macherey-Nagel) according to the manufacturer's instructions.

2.4.12 DNA sequencing

DNA sequencing reactions were carried out at the University of Edinburgh's dedicated sequencing facility Edinburgh Genomics (formerly the GenePool). 6 µl samples were submitted containing 500 ng DNA and 3.2 µM primer in water.

2.5 Trypanosome transfections

Transfection of pleomorphic AnTat 90:13 strains was performed using either cells grown *in vitro* or harvested from mouse blood. In the latter case, whole blood was harvested from a mouse showing slender parasitaemia and added to 25 ml HMI-9 + 10% FCS and allowed to settle for 4-6 hours. 20 ml of this culture was then carefully pipetted from the top and transferred to a new flask containing another 20 ml media. Any remaining blood was allowed to settle overnight. The following day media was then pipetted from the top, transferred to a new flask and used for transfection. Transfection of monomorphic strains exclusively used *in vitro* cultured parasites.

DNA for transfection was prepared by small or medium scale plasmid preparation as described in sections 2.4.10 or 2.4.11 respectively. The plasmid was linearised using the relevant restriction enzyme (see section 2.4.4) and purified as in section 2.4.5. The purified, linearised plamid was then precipitated by addition of 0.1x volume of 3 M sodium acetate and 2.5x volumes of 100% ethanol and incubation at -80°C for minimum 1 hour. The DNA was then pelleted at 18,000g for 10 minutes at 4°C and the supernatant aspirated. The pellet was resuspended in 10 µl water. At least 5 µg DNA was used for each transfection.

2-3x10^7 parasites at a density of 6x10^5-1.2x10^6/ml were centrifuged for 5 mins at 1000g and washed in TDB (Trypanosome Dilution Buffer – see below). They were resuspended in 50-100 µl Amaxa buffer (Lonza) mixed with the DNA. The sample was then transferred to a cuvette and electroporated in an Amaxa Nucleofector II

using program Z-001 – Free Program Choice. The cells were immediately transferred to a flask containing 30ml pre-warmed media and serially diluted 1:10 and 1:100 in 2 additional flasks. After incubation at 37°C for minimum 6 hours, antibiotic was added to each flask for selection of transfectants. Antibiotic concentrations are listed in Appendix C. The cultures were plated in 1ml volumes in 24-well plates. Positive transfectants were identified microscopically and diluted into antibiotic-containing media 4-8 days post transfection.

Trypanosome Dilution Buffer:
5 mM KCl
80 mM NaCl
1 mM $MgSO_4$
20 mM Na_2HPO_4
2 mM NaH_2PO_4
20 mM glucose
pH7.4

2.6 Growth curves

To measure parasite growth, cells were seeded in triplicate in 24-well plates at a concentration of $2x10^5$/ml for pleomorphic cells or $1x10^5$/ml for monomorphic cells. In the case of RNAi and overexpression lines, this was done in the presence and absence of 1 μg/ml tetracycline (Sigma). Cell density was measured at 24-hour intervals using the Beckman Coulter Z2 Particle Count and Size Analyser and diluted to prevent growth above a density of $1x10^6$/ml. Cumulative growth rates were plotted using GraphPad Prism.

To test parasite sensitivity to the compounds pCPTcAMP and E667 (DDD00015314), parasites were treated with or without either 100 μM pCPTcAMP (Sigma) or 50 μM E667 (BioFocus) at the outset, or 24 hours after tetracycline induction in the case of RNAi lines. Growth was monitored as described above.

2.7 Dose response curves

In white-bottomed 96-well plates (Greiner), 150 µl HMI-9 + 10% FCS was added to the outermost wells to prevent evaporation from internal sample wells. 50 µl HMI-9 + 10% FCS was added to wells B2 to G11. 50 µl media + 4x starting concentration of compound was added to wells B2-G2. For E667 and GKI7 (NEU-0001233), a 2-fold serial dilution of the compound was performed by transferring 50 µl from column 2 to column 3, mixing, and repeating along the plate until column 11. In the case of pCPTcAMP, 3-fold serial dilutions were similarly performed by transferring and mixing 25 µl between columns. This resulted in 50 µl media + 2x compound in columns 2 to 10, while 11 was left as an untreated control. 50 µl cells diluted to $1x10^4$/ml, ± 2 µg/ml tetracycline in the case of RNAi lines, were added to wells B2-G11 to give $5x10^4$/ml + 1x compound in each well. All cells were tested in triplicate for each compound and condition. This plate layout and the concentrations of the compounds used are depicted in Figure 2.1.

The plate was incubated at 37°C/5% CO_2 for 72 hours. 10 µl alamarBlue (Bio-Rad) was added to each well and the plate was incubated for 4 hours at the same conditions. Fluorescence was read using a FLUOstar OPTIMA fluorimeter (BMG Labtech) at 544 nM excitation/590 nM emission. Fluorescence values were normalised relative to the untreated control and GraphPad Prism was used to plot sigmoidal dose response curves with variable slopes (4 parameter non linear regression).

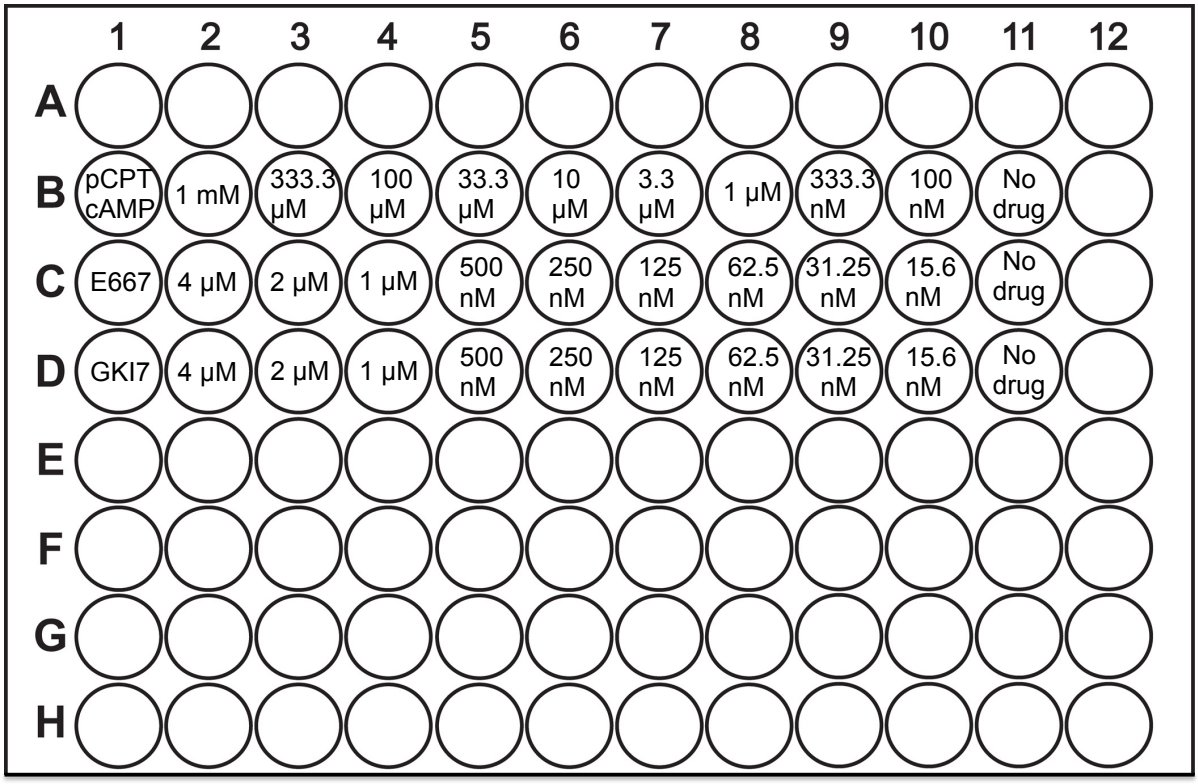

Figure 2.1 Diagram of concentrations of pCPTcAMP, E667 and GKI7 used in dose response assays and column layout in 96 well plate.

GUS assay

GUS enzyme activity was assayed according to MacGregor *et al.* (2014). The β-glucuronidase (GUS) enzyme produces a quantifiable colour change in the fluorescent substrate 4-Methylumbelliferyl-β-D-glucopyranosiduronic acid (MUG). To test BioFocus-synthesised E667, 427 GUS-PAD1 3'UTR cells were incubated with 50 µM of the compound for 48 hours at a starting density of $3x10^5$/ml. Cells were counted and 50% v/v substrate/lysis solution (see below) was added to 100 µl cells in triplicate in 96-well plates and incubated for 2 hours at 37°C. Absorbance was measured with an excitation wavelength of 355 nm and emission wavelength of 460nm on a BioTek Flx800 Fluorescent Microplate Reader with Gen5 data analysis software. For screening of GSK kinase inhibitor (GKI) compounds, 100 µl cells were incubated for 24 hours with EC_{50} concentration of each compound, as determined by Diaz *et al.* (2014). To assay cell density at low volume, 10 µl AlamarBlue was then added and incubated at 37°C for 4 hours and fluorescence read as described in section 2.7. 50% substrate/lysis solution was then added and GUS activity measured

as described above. In all cases, 100 μM pCPTcAMP was used as a positive control and fluorescence was normalised to cell density, as determined by either spectrophotometric count or AlamarBlue assay.

GUS substrate/lysis solution:
1mM MUG (Sigma)
0.82M Tris-HCl pH8
0.6% SDS
0.3mg/ml BSA

2.9 Procyclic differentiation assay

To test the capacity of cells to differentiate to procyclic forms, parasites purified from whole blood were resuspended at $3x10^6$/ml in SDM-79 +10% FCS media supplemented with 6mM *cis*-aconitate (Sigma) to induce procyclic differentiation and incubated at 27°C/5% CO_2. After 0, 4 and 24 hours, 1 ml culture was removed, washed and fixed in 2% formaldehyde/0.05% gluteraldehyde for EP expression analysis by FACS (see section 2.10).

2.10 FACS

Stumpy and procyclic characteristics of trypanosomes were assayed by FACS analysis of PAD1 and EP expression, respectively. Samples were prepared in 5ml FACS tubes (BD Biosciences). Cells were fixed in 2% formaldehyde/0.05% gluteraldehyde at 4°C overnight. Samples were centrifuged at 2000g for 7 minutes, washed in PBS and blocked in 200 μl 2% BSA/PBS for 40 minutes or overnight. They were centrifuged again and resuspended in primary antibody in 2% BSA/PBS for 1 hour or overnight at 4°C. Cells were then washed again and resuspended in fluorescently conjugated secondary antibody for 40 minutes at 4°C. The cells were washed again and finally resuspended in 500 μl 0.2 μg/ml 4',6-diamidino- 2-phenylindole (DAPI)/PBS. Antibody concentrations are listed in Appendix B.

Samples were processed on an LSRII Flow Cytometer (BD Biosciences). A minimum of 10,000 cells were analysed for each sample. Analysis was performed using FlowJo version 9.6.2 (Tree Star).

2.11 Microscopic analysis of cell cycle status

To analyse cell cycle status, trypanosomes were smeared on a glass slide, allowed to dry and then fixed in cold methanol and stored at -20°C. The slides were washed in PBS and stained with 10 μg/ml DAPI/PBS for 2 minutes. They were washed twice with PBS and mounted with 50 μl Mowiol (see below). The slides were dried in the absence of light and stored at 4°C.

Mowiol:
10% (w/v) mowiol 4-88 reagent (Calbiochem catalogue number 475904)
25% (v/v) glycerol
100mM Tris-HCl, pH 8.5
2.5% (v/v) DABCO

Cell cycle was assessed by counting the number of kinetoplasts and nuclei per cell for 250 DAPI stained cells on each slide using a Zeiss Axioskop 2 microscope. Trypanosomes in G_1 and S phase have 1 nucleus (N) and 1 kinetoplast (K) and after S phase division of first the kinetoplast and then the nucleus forms 2K1N and then 2K2N cells, which represent G_2 and post-mitotic phases respectively (Woodward and Gull, 1990).

Morphometric analyses of cell nuclei were performed using ImageJ. The shape descriptor function was used to score nuclei for aspect ratio and solidity. At least 100 nuclei were scored for each condition.
Aspect ratio = maximum diameter/minimum diameter
Solidity = area/convex area

The data was analysed by unpaired t test using GraphPad Prism version 6. P values of less than 0.05 were considered statistically significant.

2.12 Immunofluorescent assay

For immunofluorescent analysis (IFA) of expression, at least $2x10^5$ cells were centrifuged at 1000g for 5 minutes, washed in ice-cold PBS and resuspended in 125 µl ice-cold PBS. 75 µl 8% paraformaldehyde in PBS was added and the tube mixed by inverting. The sample was incubated on ice for 10 minutes. 500 µl PBS was added and the tube centrifuged at 1000g for 5 minutes. The cells were resuspended in 0.1 M glycine/PBS and stored at 4°C.

8 well 6mm slides (Thermo Scientific) were washed sequentially with hot water, ethanol and dH_2O and air-dried. In a humid chamber, 15 µl 0.1 mg/ml poly-L-lysine (Biochrom) was added to each well. After 15 minutes incubation, the slides were rinsed with dH_2O and air-dried.

Samples were resuspended in 15 µl PBS and pipetted onto wells. Slides were incubated in a humid chamber for 1 hour to allow the cells to adhere. Excess solution was then removed using an aspirator. For intracellular proteins, 0.05% Triton X-100 was added for 5 minutes. The wells were washed 3 times in PBS and then blocked in 20% FCS/PBS for 45 minutes. Excess liquid was removed and primary antibody in 20% FCS/PBS was applied for 1 hour. The wells were washed 5 times and then fluorescent dye conjugated secondary antibody in 20% FCS/PBS added for 1 hour. Secondary antibody was aspirated and 10 mg/ml DAPI applied for 1 minute. The wells were washed 5 times in PBS. The slides were removed from the humid chamber and dried for 10 minutes at 37°C, then mounted and dried as described in section 2.11. Antibody concentrations used are listed in Appendix B.

2.13 Western blot

Lysates were prepared by centrifuging cells at 1000g for 5 minutes, washing in PBS and resuspending in Laemmli buffer at $3x10^5$ cells/µl. For PAD1 expression analysis, samples were sonicated using a Bandelin Sonorex Ultrasonic bath to reduce viscosity. All other samples were incubated at 95°C for 5 minutes. Lysates were stored at -20°C until use.

Laemmli buffer:
62.5mM Tris HCl pH 6.8
10% glycerol
2% SDS
0.0025% bromophenol blue
5% 2-mercaptoethanol

Protein samples were resolved by SDS polyacrylamide gel electrophoresis using the Bio-Rad mini Protean II system. An 8-12% resolving gel (depending on expected protein size; see recipe below) was poured between clamped glass plates (1.5 mm spacer plate and short plate) to a height of approximately 2 cm below the top of the short plate, covered with isopropanol and left to set. The isopropanol was washed out and the 5% stacking gel poured to the top of the plate, a comb inserted. Once set, the comb was removed and the gel inserted into the gel running apparatus. The tank was filled with running buffer (25 mM Tris, 200 mM glycine, 0.1% SDS). 10 µl protein (i.e. $3x10^6$ cells) was added to each well alongside Novex sharp prestained Protein Standard (Life Technologies) and the gel run at approx. 120V until the bromophenol blue dye reached the bottom.

Resolving gel:	Stacking gel:
8-12% acrylamide	5% acrylamide
375 mM Tris pH 8.8	125 mM Tris pH 6.8
0.1% SDS	0.1% SDS
0.1% APS	0.1% APS
0.04% TEMED	0.1% TEMED

(APS = ammonium persulphate; TEMED = N,N,N',N'-Tetramethylethylenediamine)

Protein was transferred from the gel to a nitrocellulose membrane (GE Healthcare) using a Bio-Rad Mini Trans-Blot cell according to the manufacturers instructions. The tank was filled with cold transfer buffer (25mM Tris, 200mM glycine, 20% methanol) and run at 200 mA for 90 minutes while stirring.

The membrane was blocked at room temperature with agitation for at least 30 minutes in 5% milk in PBS-0.1% Tween 20 (PBS-T). It was then incubated in

primary antibody in 5% milk in PBS-T for minimum 1 hour with agitation and washed 3 times in PBS-T.

Secondary detection of the antibody used one of two systems. The first used chemiluminescence. The membrane was incubated in secondary antibody conjugated to horseradish peroxidase (HRP) diluted in 5% milk in PBS-T for 1 hour with agitation and washed three times with PBS-T. The membrane was placed between two sheets of polyethylene and Pierce ECL2 Western Blotting substrate applied for 2 minutes. Excess liquid was then removed and the membrane and polyethylene placed inside a film cassette and exposed to X-ray film (Fujifilm). Exposure time varied according to signal strength. The film was developed using a Konica Minolta SRX-101A developer.

Alternatively, the signal was visualised using the LI-COR Odyssey system. In this case, the secondary antibody was conjugated to a fluorescent dye and diluted in 50% Odyssey Blocking Buffer/50% PBS-T. After 1 hour incubation in secondary antibody, the membrane was washed twice in PBS-T and once in PBS, and scanned using a LI-COR Odyssey imager, which uses an infrared laser to detect fluorescence.

2.14 Southern blot

Southern blotting was used to confirm successful gene deletion and correct integration of replacement alleles in null mutants. Probes were prepared using the DIG High Prime DNA labelling Kit (Roche) from 1 μg of a double stranded DNA template produced by either PCR or restriction digestion, according to the manufacturers instructions.

For each sample, 1 μg of gDNA was digested with the appropriate restriction enzyme for minimum 3 hours at 37°C (see section 2.4.4) and run on a 1% agarose gel at 25V overnight. The gel was soaked in Depurination Solution (0.25 M HCl) for 15 minutes with agitation. It was denatured using Denaturation Solution (1.5 M NaCl/0.5 M NaOH) for 2 x 15 minutes with agitation. The gel was rinsed with dH_2O and neutralised with Neutralisation Solution (1 M Tris, 1.5 M NaCl, pH 7.4) for 2 x 15 minutes with agitation.

DNA was then transferred from the gel to a positively charged nylon membrane overnight by capillary transfer. A plastic box was placed upside down in a tray filled to approx. 2 cm depth with 10x SSC (1.5M NaCl, 150mM tri-sodium citrate). The box was covered with filter paper soaked in 10x SSC to form a wick and the gel placed on top. Parafilm was used to seal the edges of the tray to prevent evaporation. The membrane was pre-soaked in 10x SSC and placed on top of the gel, followed by two sheets of filter paper soaked in 2x SSC, a large pile of paper towels and a Perspex sheet to ensure even weight distribution. Finally, a 1 kg weight was placed on top to add weight. The following day, the membrane was allowed to dry. A Stratalinker was used to UV cross-link the membrane at 0.12 joules.

The blot was pre-hybridised in 10 ml hybridisation buffer (see below) at 42°C for 1 hour in a hybridisation oven (Techne Hybridiser HB-1D). This was then replaced with 7 ml hybridization buffer containing 1 µl DIG-labelled DNA probe denatured for 5 mins at 95°C and hybridised overnight.

Hybridisation buffer:
5x SSC
50% formamide
0.02% SDS
2% DIG block

The blot was washed in 2x SSC/0.1% SDS twice for 5 minutes at room temperature with agitation. It was then washed in prewarmed 0.5x SSC/0.1% SDS twice for 15 minutes at 68°C in the hybridisation tube. It was rinsed in maleic acid buffer (100 mM maleic acid, 150 mM NaCl, pH 7.5) with 0.3% Tween 20 for 1 minute at room temperature. The membrane was blocked in 1% DIG block (Roche) in maleic acid buffer for 1 hour at room temperature with agitation and then incubated with Anti-Digoxigenin-AP Fab Fragments (Roche) in 1% DIG block/maleic acid buffer for 30 minutes. Maleic acid buffer with 0.3% Tween 20 was used to wash the membrane 3 times for 10 minutes. The blot was soaked in detection buffer (100 mM Tris pH 9.5, 100 mM NaCl) for 2 minutes and then placed between 2 sheets of polyethylene. 250 µM CDP-Star chemiluminescent substrate (Roche) in detection buffer was applied to the membrane for 2 minutes. Excess substrate was removed and the polythene sealed

using a heat sealer before incubation at 37°C for 15 minutes. The blot was then exposed to X-ray film and developed as for the Western blot (section 2.13).

2.15 Northern blot

For Northern blotting, riborobes were prepared using the DIG RNA labelling Kit (SP6/T7)(Roche). The desired sequence was cloned into the pGEM-T Easy vector, which contains SP6/T7 promoter sites, and amplified using M13 primers. 1 µg purified PCR product was used in the following 20 µl reaction to produce digoxigenin-UTP labelled RNA:

1 µg template DNA
1x NTP Mix
5mM DTT
10U RNase inhibitor
1x transcription buffer
40U SP6 or T7 RNA polymerase (SP6 for forward oriented sequences, T7 for reverse oriented sequences).

The reaction was incubated at 37°C for 2 hours, then 20U RNase-free DNaseI added and a further 15 minutes incubation at 37°C for 15 minutes to remove any remaining DNA. The reaction was stopped by the addition of 20mM EDTA, pH8.0. The sample was then precipitated with 2.5 µl of 4 M LiCl and 75 µl of cold 100% ethanol and incubated at -80°C for 1 hour. The riboprobe was then centrifuged at 16,500 g for 15 minutes and washed in 50µl 70% cold ethanol. The pellet was air dried and resuspended in 50µl dH_2O with 20U RNase inhibitor and stored at -80°C.

RNA was extracted from *Trypanosoma brucei* using the QIAGEN® RNeasy kit according to the manufacturer's instructions. For each RNA sample, 1 µg of RNA was added to 16 µl RNA gel loading buffer (see below) and incubated at 65°C for 5 minutes before immediate loading on an RNA gel (see below). The gel was run for 90 minutes at 150 V.

RNA gel loading buffer:
60 % formamide
20 % formaldehyde
1.5x MOPS
0.01% bromophenol blue
1.25% glycerol

RNA gel:
1.3 % agarose
1x MOPS
1 % formaldehyde

The gel was soaked in 1 µg/ml ethidium bromide in 1x MOPS for 15 minutes with agitation and destained twice with dH_2O for 30-60 minutes. The rRNA bands were visualised and photographed using a Syngene G:box.

RNA was then transferred from the gel to a positively charged nylon membrane and cross-linked exactly as described for Southern blotting (section 2.14).

The blot was pre-hybridised in 10 ml hybridisation buffer (section 2.14) at 68°C for 1 hour in a hybridisation oven (Techne Hybridiser HB-1D). This was then replaced with 7 ml hybridization buffer containing 1 µl riboprobe, which had been denatured for 5 mins at 95°C, and hybridised overnight.

The blot was washed at 68°C in the hybridisation tube, first in 2x SSC/0.1% SDS three times for 30 minutes and then once in 0.5x SSC/0.1% SDS for 30 minutes. It was then removed from the tube and rinsed in maleic acid buffer with 0.3% Tween 20 for 1 minute at room temperature. All subsequent steps were exactly as described for the Southern blot in section 2.14.

2.16 Quantitative RT-PCR

2.16.1 RNA preparation

RNA was extracted from *Trypanosoma brucei* using the QIAGEN® RNeasy kit according to the manufacturer's instructions. Contaminating gDNA was removed using Turbo DNase (Ambion). 5 µg RNA was incubated with 1 U DNase in 1x Turbo DNase reaction buffer for 30 mins at 37°C. A further 0.5µl DNase was then added and the sample again incubated for 30 mins at 37°C. The reaction was then incubated for 2 mins at room temperature with 10µl DNase Inactivation Reagent and centrifuged for 2 mins at 12000g. Supernatant was transferred to a fresh tube and

precipitated with 0.05 volumes of 3M sodium acetate and 3 volumes of 100% ethanol for 1 hour at -80°C. The sample was centrifuged for 10 minutes at 12000g at 4°C, washed in 70% ethanol and the pellet air-dried. Samples were resuspended in 12 µl RNase-free water. 1 µl was run on an RNA gel (see section 2.15) to check the integrity of the RNA.

2.16.2 Generation of cDNA

cDNA was synthesised from the DNased RNA using the ThermoScript RT-PCR system (Invitrogen). For each RNA sample, a parallel reaction was performed without reverse transcriptase (RT-). The following reaction was incubated for 5 mins at 65°C to denature the RNA:

1 µg RNA
2 µl 10 mM dNTPs
1 µl (50 ng) Random Hex primers
Total vol 12 µl

The following components were added and the 20 µl reaction reverse transcribed using the program shown:

4 µl 5x cDNA synthesis buffer	25°C	10 mins
1 µl 0.1 M DTT	50°C	50 mins
1 µl (40 U) RNaseOUT	85°C	5 mins
1 µl (15 U) ThermoScript Reverse Transcriptase		
1 µl RNase free water		

2 U of RNase H was then added to remove any remaining RNA and the reaction incubated at 37°C for 20 mins. 180 µl of nuclease-free water was then added to dilute the cDNA 1:10.

2.16.3 qRT-PCR

Quantitative reverse transcriptase PCR was carried out on a LightCycler 96 machine (Roche) to amplify either TOR4 or ZFP3 mRNA. 25 µl reactions were carried out in triplicate. For each cDNA sample, a fourth reaction was also carried out in which the corresponding RT- product was substituted for cDNA. A melt curve was added to the

end of each qRT-PCR amplification program to ensure amplification of a single product. TOR4 transcript abundance was quantified relative to ZFP3 using the equation $2^{-\Delta\Delta Ct}$, where cycle threshold (Ct) refers to the number of cycles at which fluorescence passes a set threshold, ΔCt = Ct(TOR4) – Ct(ZFP3) and $\Delta\Delta Ct$ = ΔCt(test sample) – ΔCt(reference sample) The data was analysed using the LightCycler 96 software (Roche).

Reaction components:
12.5 µl Power SYBR Green PCR Master Mix (Applied Biosystems)
1.5 µl 10mM FW
1.5 µl 10mM RV
7 µl dH_2O
2.5 µl cDNA

Reaction Conditions:
95°C 10 minutes
[95°C 15 s
60°C 1 minute] x40
Melt curve: 60°C - 95°C 0.03°C/s

2.17 RNAi library screen

2.17.1 Library treatment with GKI7

A vial containing approx. $1x10^7$ RNAi library cells was thawed and inoculated in 50 ml HMI-9/10% FCS supplemented with 2 µg/ml blasticidin and 1 µg/ml phleomycin. After 24 hours incubation at 37°C/5% CO_2, $1x10^7$ cells were frozen in HMI-9 + 25% glycerol to replace the stock and the remaining cells diluted to a density of $2.5x10^5$/ml. 24 hours later, the library was divided into 3 cultures of $2.5x10^7$ cells at $2.5x10^5$/ml. Genomic DNA was extracted from 1 culture according to section 2.4.1 to represent the starting population and 1 µg/ml tetracycline was added to another to induce RNAi. After 24 hours, the 2 cultures were diluted to a concentration of $2.5x10^5$/ml, treated with 1.44 µM GKI7 and each divided into 5 x 50 ml volumes. Cells were counted every 24 hours and diluted back to $2.5x10^5$/ml in 50 ml volumes where required. A minimum of $1.25x10^7$ cells ($2.5x10^5$/ml in 50 ml) was

continuously present in each culture throughout the experiment. After 10 days, when resistant populations had outgrown, genomic DNA was extracted from each replicate (section 2.4.1).

2.17.2 PCR amplification and sequencing

RNAi fragments were amplified from gDNA from each replicate using RNAi insert specific primers Lib3F ATCAAGCTTGGCCTGTGAG and Lib3R CCTCGAGGGCCAGTGAG. These primers represent a more effective version of the Lib2 primers (E. Rico Vidal, personal communication) described in the published protocol by Glover *et al.* (2015). The products were resolved by gel electrophoresis and 6 bands were excised, purified and ligated into pGEM-T Easy. The plasmids were transformed and sequenced using M13 primers.

2.17.3 Ion Torrent sequencing

Ion Torrent sequencing was carried out at the University of Edinburgh Wellcome Trust Clinical Research Facility Genetics Core. PCR products amplified with Lib3F and Lib3R primers from 3 induced replicates (tet+1, tet+2, tet+4) and 1 uninduced replicate (tet-1) were sequenced. For library preparation, the samples were fragmented by Covaris unltrasonication. Each sample was assigned an IonXpress barcode and sequenced using an Ion PGM (Thermo), generating 4,158,002 total reads, with each sample generating 0.9-1.2 million reads. Subsequent data analysis was carried out by Dr. Alasdair Ivens. Quality checking was performed using FASTC software, and the output inspected manually (http://www.bioinformatics.babraham.ac.uk/projects/fastqc/). Cutadapt software was used to identify and remove the Lib3 primer sequences used in amplification (parameters: -O 15 -m 100 -n 5 -q 20). Alignments for all cutadapt-processed sequences were aligned to the *T. b. brucei* 927 genome using bowtie2 (version 2.2.7) software (parameters: --very-sensitive -p 4 --no-unal). Outputs were stored as indexed bam files generated using samtools version 1.3 (http://www.htslib.org/; http://samtools.sourceforge.net/). Read depths at each base were generated from the indexed bam files using samtools and the "depth" parameter. Gene location coordinates, extracted from the genome annotation, were stored in bedtools "bed" format, and bedtools (v2.23.0) used to extract read counts for each gene, using

"multicov -D -bams" parameters (http://bedtools.readthedocs.org/en/latest/); read counts for each gene in each sample were stored as tab-delimited "Excel" files. Plots were generated using R/Bioconductor software (https://cran.r-project.org/; https://www.bioconductor.org/).

2.18 Phosphoproteomic analysis

2.18.1 Cell lysis

For preparation of phosphoproteomic samples, low binding tips and low binding eppendorfs were used. Samples were extracted from 4 replicates each of AnTat 1.1 90:13, MEKK1 KO and YAK KO cell lines. For each, $2.7x10^8$ cells at $9x10^5$/ml were spun at 1000g for 10 mins at 4°C, washed three times in PBS and resuspended in 100 µl lysis buffer. The samples were sonicated using a Bioruptor (Diagenode; 10 cycles of 30s alternating sonication/rest at 18°C).

Lysis buffer:
4% SDS
25 mM Tris(2-carboxyethyl)phosphine (TCEP) (Thermo)
50 mM N-ethylmaleimide (Thermo)
M NaCl
1x PhosSTOP phosphatase inhibitor (Roche)
10 mM Na_2HPO_4 pH6

The samples were then chloroform:methanol precipitated. After 10 minutes incubation at 65°C, 400 µl methanol was added and the samples vortexed. 100 µl of chloroform was added and the samples vortexed again. 300 µl of ddH_2O was added and the samples vortexed for 1 minute. They were then centrifuged for 5 minutes at 9000g and the upper phase aspirated. A further 300 µl of methanol was added and the samples vortexed and centrifuged as before. The supernatants were aspirated and and the pellets air dried.

2.18.2 Tryptic digestion

The pellets were resuspended in 150 µl 8M urea/0.1 M Tris pH8/1 mM $CaCl_2$ and quantified by Bradford assay. The protein concentration was determined by

comparison to a bovine serum albumin (BSA) standard curve (0.1-2.5 mg/ml). 125 µl of Bradford Reagent (Sigma) was added to 2.5 µl protein sample in triplicate in a 96 well plate and absorbance read at 595 nm using a Fluostar Omega plate reader (BMG Labtech). 800 µg of protein for each sample was then diluted with 0.1 M Tris pH8/1 mM $CaCl_2$ to 1 M urea and 8 µl LysC (Wako) added. The samples were digested overnight at 37°C. 8 µg trypsin (Pierce) in 50 mM acetic acid was then added and the samples incubated for 4 hours at 37°C. Finally 1 % v/v trifluoroacetic acid was added.

2.18.3 TMT Labelling

Labelling and mass spectrometry were carried out at the FingerPrints Proteomics Facility at the University of Dundee. The samples were divided into 2 separate runs, each containing 2 replicates of each cell line. They were purified by solid phase extraction and then quantified by bicinchoninic acid assay prior to labeling with isobaric tandem mass tags (TMT). The samples were pooled and fractionated into 13 fractions using hydrophilic interaction liquid chromatography.

2.18.4 Mass spectrometry

5% of each fraction was analysed by nLC-MS/MS (nano liquid chromatography-tandem mass spectrometry) using a Thermo Q-Exactive HF mass spectrometer to generate proteomic quantitation. Phosphopeptides were enriched in the remaining 95% of each fraction and these samples were then also analysed by nLC-MS/MS to generate quantitation of phosphopeptides.

Data analysis was carried out by Dr. Mathieu Cayla. 4,767 and 4,746 proteins were detected in the first and second runs, respectively. This was reduced to 3,237 and 3,128 after exclusion of proteins with a confidence value score less than 20 or TMT reporter intensity less than 10,000. 9,265 phosphopeptides from 2,499 proteins were identified in the first set and 9,473 phosphopeptides from 2,599 proteins in the second set. Phosphopeptides for which protein ratios were not generated were excluded from the analysis. Proteins and phosphopeptides for the knockout samples were normalised to the mean of AnTat 1.1 90:13 control replicates 1 and 2 for the first run and replicates 3 and 4 for the second. Protein ratios were then used to

normalise phosphopeptide ratios. All phosphoproteins for which $\log_2$ of the normalised phosphopeptide ratio was greater than 1 or lower than -1 (i.e. showed greater than 2 fold change) and for which a similar effect was not observed when comparing AnTat replicates was considered to be differentially regulated.

2.19 Statistical analysis

Statistical analysis for all parasitaemia, cell cycle, PAD1 IFA, FACS data collected in triplicate was carried out using either Minitab version 15 or GraphPad Prism version 6. Where only a single timepoint was analysed, the data was analysed by students t test. In the case of multiple timepoints, the data was analysed by general linear model with Tukey's test for multiple comparisons. P values of less than 0.05 were considered statistically significant.

3 Chapter 3: Organising *pos*ST components within the stumpy formation pathway

3.1 Introduction

The recent identification of numerous mediators of stumpy formation via pCPTcAMP/AMP treatment of an RNAi library population (Mony et al., 2014)(see section 1.9) represents a significant step forward in elucidating a pathway which had previously been uncharacterised and opens up countless new avenues for further study. While ongoing validation of the *pos*ST genes continues to confirm their individual roles in differentiation, nothing is known of the contribution of each gene to the pathway. An obvious next step in the investigation of these molecules is to determine their relationship to each other. It has been shown that silencing of *pos*ST genes confers a reduced differentiation phenotype, while overexpression increases stumpy formation. Therefore, overexpression of one *pos*ST gene in a null mutant background of a distinct *pos*ST gene should provide positional information about the relative action of both genes, which will ultimately enable ordering within a signalling pathway. Additionally, the abundance of kinases and phosphatases within this cohort points to the importance of phosphorylation as a means of signalling in stumpy formation. Phosphoproteomic analysis of null mutants of *pos*ST kinases can therefore offer insight into their respective signalling roles and how these fit with the rest of the pathway.

3.2 Validation of *pos*ST genes as mediators of stumpy formation

Mony *et al.* (2014) were able to validate several hits from the pCPTcAMP/AMP RNAi library screen, using individual RNAi lines to demonstrate their involvement in stumpy formation. Here, systematic testing of a number of further hits from this screen are described.

3.2.1 Adenosine Kinase

Adenosine kinase is the enzyme responsible for the cleavage-independent pathway of purine salvage in *T. brucei* (see section 1.9.1.4), in which adenosine is directly phosphorylated to form adenosine monophosphate (Luscher et al., 2007; Vodnala et

al., 2008). AK was idenitified in the *pos*ST cohort along with a number of other purine pathway enzymes. Upon further study, many of these showed no differentiation phenotype but were instead selected due to restoration of purine balance by the cAMP/AMP analogues (Mony et al., 2014). However, AK differs from these enzymes in that RNAi reportedly confers no growth phenotype under normal conditions (Luscher et al., 2007). Hence, it was decided to explore the role of this molecule in stumpy formation.

3.2.1.1 AK RNAi confers reduced responsiveness to pCPTcAMP in monomorphs

To generate an AK RNAi line in a monomorphic strain, an RNAi construct was generated by cloning 2 complementary 363bp fragments corresponding to both AK gene copies, and so capable of forming a stem-loop structure, into a specialised *T. brucei* RNAi vector, pRPa^{iSL} (see map in Appendix D Figure 1). This plasmid was transfected into the monomorphic 2T1 bloodstream form cell line which is capable of tetracycline-regulated gene expression. 2T1s contain an incomplete hygromycin resistance gene within an rRNA spacer locus which is rendered functional by successful integration of the pRPa construct (Alsford and Horn, 2008). Transfectants were selected with 2.5μg/ml hygromycin. One clone was selected and growth was measured for 4 days in cells first either incubated with or without 1μg/ml tetracycline to induce the RNAi. Cells were also treated or not treated with 100μM of the membrane-permeable cAMP analogue 8-(4-chlorophenylthio)-cAMP (pCPTcAMP) after 24 hours to induce differentiation as detailed in section 2.6. Growth was measured in 3 technical replicates for each condition. As seen in Figure 3.1A, tetracycline has little or no effect on growth in the absence of the analogue. This is consistent with the findings of Luscher *et al.* (2007), and indicates that AK did not emerge from the library screen due to rescue of a purine pathway defect. Upon treatment with pCPTcAMP, uninduced cells showed substantial growth inhibition, which was partially rescued in the induced cells. This indicates that knockdown of AK confers resistance to pCPTcAMP-induced differentiation, validating its original selection in the library screen. Figure 3.1B shows confirmation of effective silencing of the AK transcript by Northern blot.

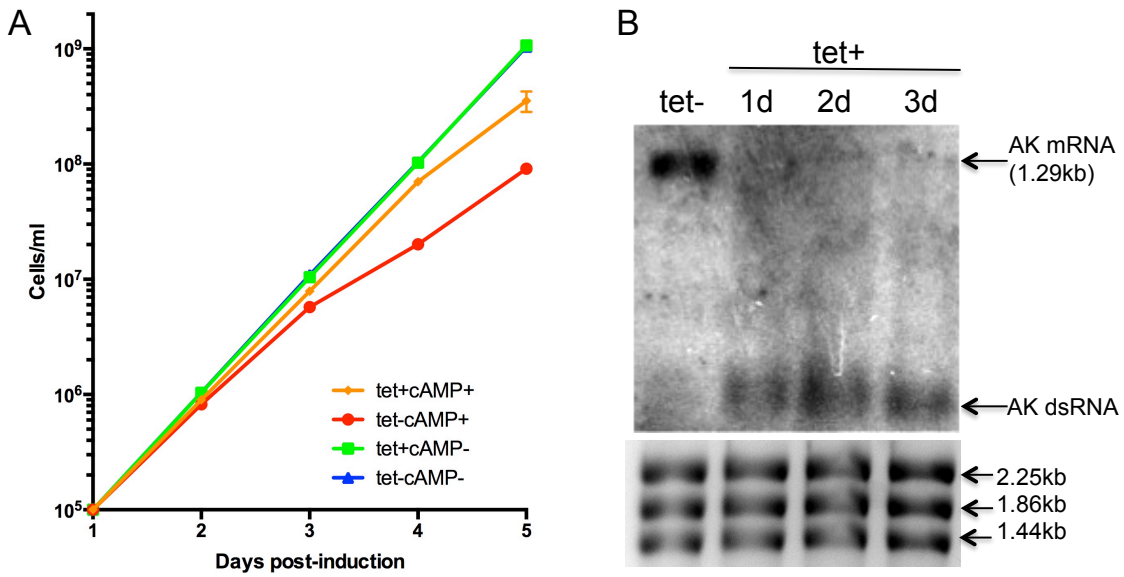

Figure 3.1 A) Growth curve of monomorphic AK RNAi cells incubated with (tet+) or without (tet-) tetracycline and either treated (cAMP+) or untreated (cAMP-) with pCPTcAMP 24 hours post-induction by tetracycline. AK RNAi results in reduced responsiveness to pCPTcAMP. B) Northern blot analysis shows loss of the AK transcript upon RNAi induction. rRNA was used as a loading control.

3.2.1.2 AK RNAi confers reduced responsiveness to pCPTcAMP in pleomorphs

A pleomorphic AK RNAi line was subsequently generated by cloning the same gene fragment as for the pRPa plasmid into the pALC14 vector (plasmid map shown in Appendix D Figure 2). The plasmid is competent for transfection of the *T. brucei* AnTat 1.1 90:13 cell line expressing the Tet repressor and T7 RNA polymerase. Growth in response to pCPTcAMP was measured in puromycin-selected transfectants, as for the monomorphs. Figure 3.2 shows that, as in monomorphs, AK RNAi confers reduced responsiveness to pCPTcAMP.

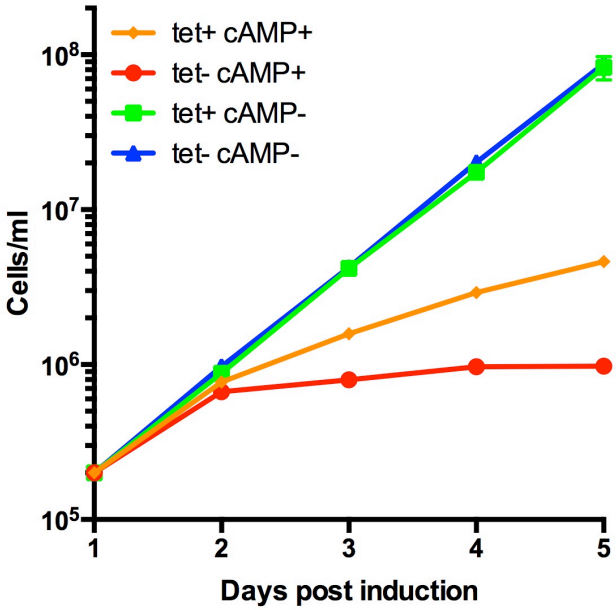

Figure 3.2 Growth curve of pleomorphic AK RNAi cells incubated with (tet+) or without (tet-) tetracycline and either treated (cAMP+) or untreated (cAMP-) with pCPTcAMP 24 hours post-induction by tetracycline. AK RNAi results in reduced responsiveness to pCPTcAMP.

3.2.1.3 AK RNAi has no effect on responsiveness to SIF *in vivo*

To assess responsiveness to SIF in vivo, MF1 mice treated or untreated with doxycycline were infected in triplicate with pleomorphic AK RNAi parasites. From the third day of infection onward, blood samples were taken and the parasitaemia calculated by the rapid matching method (Herbert and Lumsden, 1976). Figure 3.3A shows that doxycycline has no statistically significant effect on parasitaemia ($p = 0.448$). Blood smears taken from the mice from day 3 of infection onwards were stained with DAPI and nuclei and kinetoplast numbers were counted for 250 cells to determine their cell cycle position. Trypanosomes in G1 and S phase have 1 nucleus (N) and 1 kinetoplast (K) and, after S phase division, of first the kinetoplast and then the nucleus forms 2K1N and then 2K2N cells, which represent G2 and post-mitotic phases respectively (Woodward and Gull, 1990). The proportion of 1K1N (G1/S phase) cells increased from day 3 to day 5 and was not significantly different between induced and non-induced samples ($p = 0.376$), indicating that the parasites were arresting at a comparable rate (Figure 3.3B). Loss of the AK transcript was confirmed by Northern blot (Figure 3.3C). Thus it appears that, contrary to its in vitro phenotype, loss of AK does not prevent differentiation in vivo. Possible

explanations for this disparity are explored in Section 3.5.1.

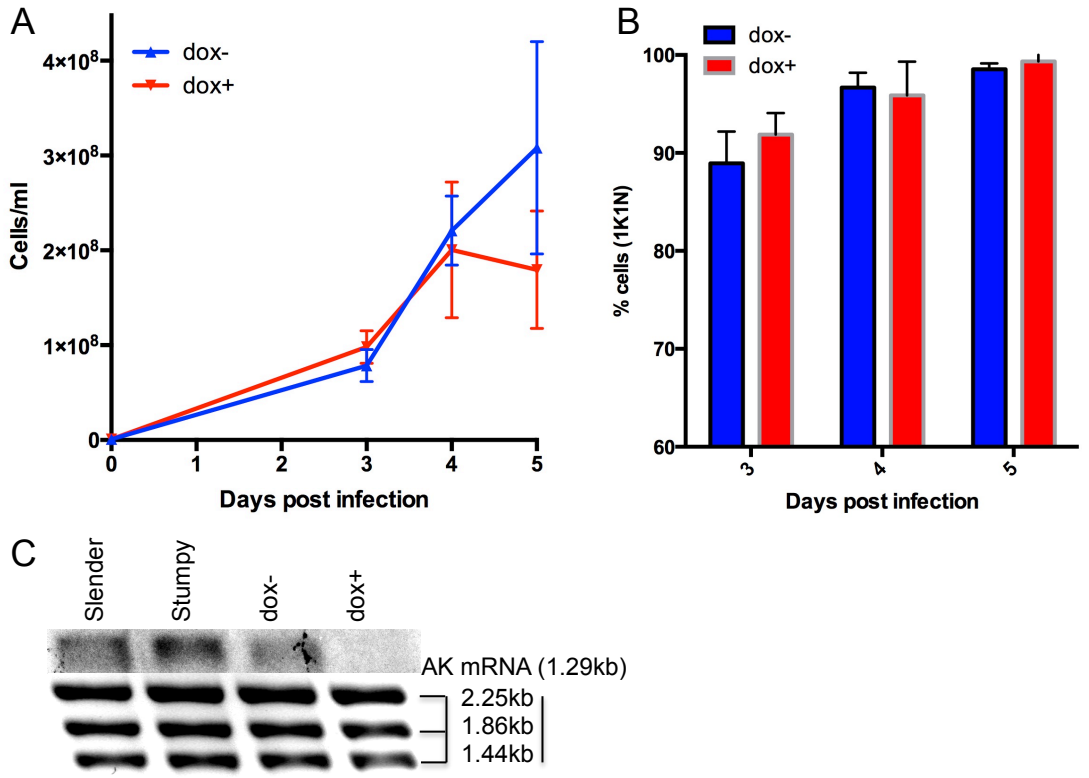

Figure 3.3 AK RNAi has no effect on responsiveness to SIF in vivo A) Parasitaemia of mice infected with AK RNAi cells, estimated by the rapid matching method. Data represents 6 mice, 3 treated with doxycycline (dox+) and 3 non-induced (dox-). No statistical difference was observed upon RNAi induction by general linear model (GLM). B) % 1K1N (representing G_1 and S phase) cells throughout the course of infection. 250 cells were counted for each sample. No statistical difference was observed upon RNAi induction by GLM. C) Northern blot analysis shows upregulation of AK transcript in stumpy forms and loss of the transcript upon RNAi induction. rRNA was used as a loading control.

3.2.2 Protein phosphatase 2A

The serine/threonine phosphatase *Tb*PP2A (Tb927.3.1240) is essential for growth and cell cycle progression in both procyclic and bloodstream forms (see section 1.9.2.1)(Rothberg et al., 2014). It was identified in the RNAi library screen as a *pos*ST component, along with members of a PP1 array, with which it shares substantial homology. The involvement of PP1 in stumpy formation has been experimentally validated (Mony et al., 2014).

3.2.2.1 PP2A is essential in monomorphic bloodstream *T. brucei*

An RNAi line was generated for PP2A in monomorphic *T. brucei* as described for AK and its growth assessed. As seen in Figure 3.4A, RNAi induction by addition of

doxycycline resulted in severe growth inhibition in both the presence and absence of pCPTcAMP. Due to the strong growth defect, this gene was not pursued further in pleomorphic cells.

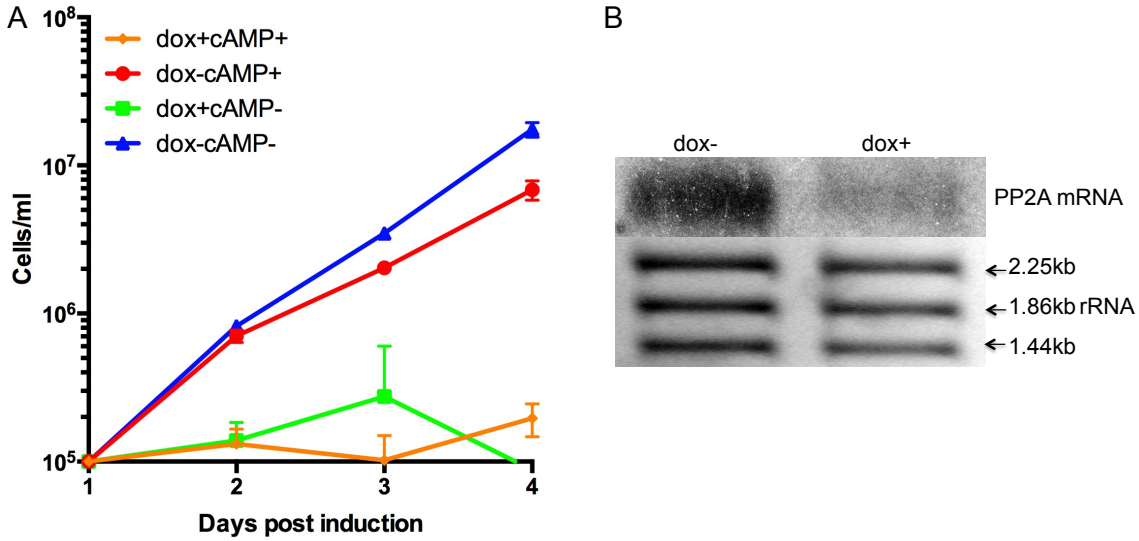

Figure 3.4 A) Growth curve of monomorphic PP2A RNAi cells incubated with (tet+) or without (tet-) tetracycline and either treated (cAMP+) or untreated (cAMP-) with pCPTcAMP 24 hours post-induction by tetracycline. PP2A RNAi is lethal. B) Northern blot analysis shows loss of PP2A transcript upon RNAi induction. rRNA was used as a loading control.

3.2.3 MEKK1

The identification of a putative MEKK, *Tb*MEKK1 (Tb927.2.2720), among the *pos*ST cohort (Mony et al., 2014) was intriguing due to previous implication of various MAPK signalling components in growth and differentiation processes (see section 1.9.1.1). Supporting a potential stage-specific signalling role, MEKK1 was found to be differentially phosphorylated between bloodstream and procyclic forms in a comparative phosphoproteomic study by Urbaniak *et al.* (2013). A monomorphic MEKK1 RNAi line had previously been validated as conferring resistance to pCPTcAMP (Mony et al., 2014).

3.2.3.1 MEKK1 RNAi confers modest loss of responsiveness to pCPTcAMP in pleomorphs.

To determine if responsiveness to pCPTcAMP was still dependent on MEKK1 in pleomorphic trypanosomes, a MEKK1 RNAi line was generated in the AnTat 1.1 90:13 strain as for AK (section 3.2.1.2) and treated with pCPTcAMP. MEKK1 RNAi was found to confer a modest loss of responsiveness to pCPTcAMP (Figure 3.5).

Although this effect was small, it was observed consistently in multiple independent experiments in this cell line, although never confirmed in an independent clone.

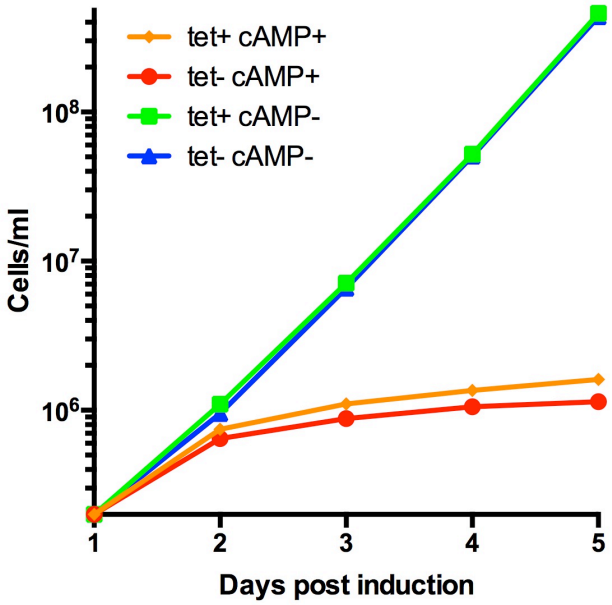

Figure 3.5 Growth curve of pleomorphic MEKK1 RNAi cells incubated with (tet+) or without (tet-) tetracycline and either treated (cAMP+) or untreated (cAMP-) with pCPTcAMP 24 hours post-induction by tetracycline. MEKK1 RNAi results in modestly reduced responsiveness to pCPTcAMP.

3.2.3.2 MEKK1 RNAi confers loss of responsiveness to SIF *in vivo.*

This cell line was subsequently tested *in vivo* to assess its response to SIF. The parasitaemia of uninduced cells ascended for 4 days post infection and then dropped on the fifth day as the population arrested (Figure 3.6A). The parasitaemia was significantly higher on day 5 in the presence of doxycycline, indicating that the population was undergoing a lower rate of arrest. Further, induced cells contained a reduced percentage of 1K1N cells at all timepoints examined (Figure 3.6B), supporting a decrease in G_1 arrest. However, the 1K1N proportion did increase as the infection progressed, indicating that differentiation was not completely eliminated. By day 5, parasites in the uninduced population were visibly stumpy in morphology, while the induced cells remained morphologically slender (Figure 3.6C). In accord, on the same day of infection, PAD1 was low in the induced population relative to uninduced cells (Figure 3.6D). However, a low level of expression was still present, again suggesting that differentiation was occurring but to a lesser extent. Reduction of the MEKK1 transcript in this experiment was confirmed by Northern blot (Figure 3.6E). Thus it appears that MEKK1 RNAi leads to reduced responsiveness to SIF *in*

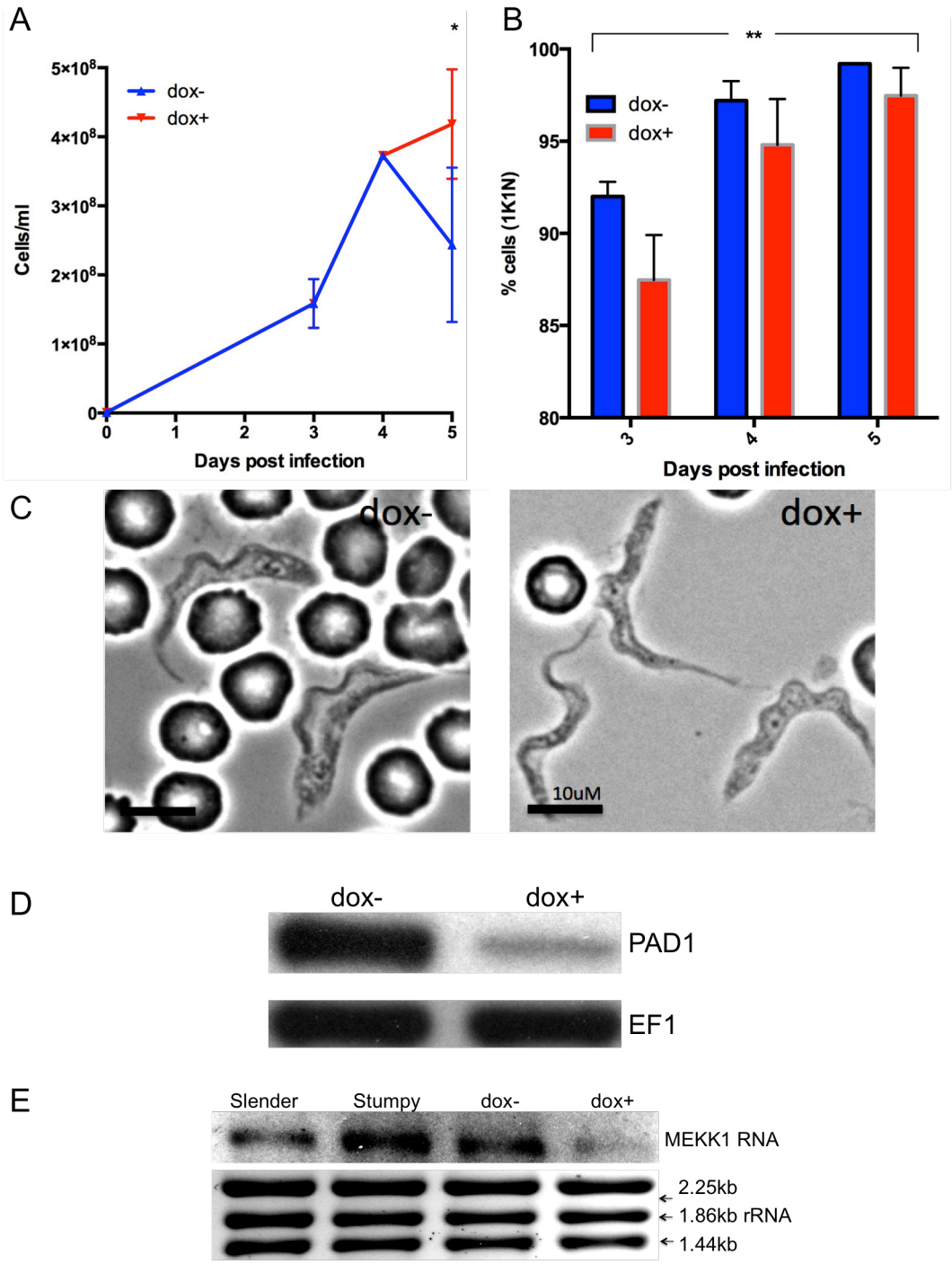

Figure 3.6 MEKK1 RNAi confers loss of responsiveness to SIF *in vivo*. A) Parasitaemia of mice infected with MEKK1 RNAi cells, estimated by the rapid matching method. Data represents 6 mice, 3 treated with doxycycline (dox+) and 3 non-induced (dox-). The parasitaemia was higher for induced cells on day 5 of infection. *P<0.05 GLM and Tukey test for multiple comparisons. B) % 1K1N (representing G_1 and S phase) cells throughout the course of infection. 250 cells were counted for each sample. Induced cells have lower 1K1N **P<0.005 GLM. C) Phase contrast images of parasites on day 5 of infection. Untreated cells appear stumpy in morphology whereas doxycycline-treated cells have remained morphologically slender. D) Western blot analysis of PAD1 expression on day 5 of infection. Expression was lower with dox induction. EF-1 was used as a loading control. E) Northern blot analysis shows upregulation of MEKK1 transcript in stumpy forms and reduction of the transcript upon RNAi induction. rRNA was used as a loading control.

vivo, leading to reduced cell cycle arrest, increased parasitaemia and a reduction in morphological and PAD expression characteristics associated with stumpy forms. However, stumpy formation was still able to proceed at a low level, possibly due to incomplete ablation of the MEKK1 transcript.

3.2.3.3 Generation of a MEKK1 null mutant

As MEKK1 RNAi cells retained some level of differentiation capacity, albeit significantly reduced, a null mutant of this gene was generated to determine the effect on stumpy formation when the kinase is completely absent. This was achieved by replacing the YFP and TY tags of the pEnT6B-Y and pEnT6P-Y vectors with fragments of the 3' and 5'UTRs of MEKK1 (see vector map in Appendix D Figure 4). Restriction digestion of these plasmids between the 3'UTR and 5'UTR sequences produced 2 linear constructs, containing resistance markers to blasticidin and puromycin respectively, which were capable of homologous recombination with, and replacement of, MEKK1 alleles. As shown in Figure 3.7A, the pEnT6B-Y construct contained external UTR fragments located distal to the ORF relative to the internal UTR fragments in the pEnT6P-Y construct. This meant that when the pEnT6B-Y construct was transfected into the AnTat 1.1 90:13 strain in the first of 2 sequential transfections, it would be expected to delete one allele of MEKK1 including the internal UTR fragments. Therefore, when the pEnT6P-Y construct was subsequently transfected, it should be able to recombine only with the remaining MEKK1 allele, producing a double knockout (dKO) line resistant to both antibiotics.

After the second round of transfection, a number of double-resistant clones were selected. To test for gene deletion, genomic DNA was isolated and PCR carried out using primers corresponding to a short fragment of the MEKK1 ORF. As seen in Figure 3.7B, the fragment was amplified from parental AnTat 90:13 gDNA and every drug-resistant clone except for clone E, in which only primer dimers were visible. To confirm that the gene was completely knocked out in this clone, it was further tested by Southern blot. Figure 3.7C schematically depicts the fragments recognised by 2 DNA probes in parental, single knockout (sKO) and dKO genomic DNA digested with PstI. A gene probe was able to detect 2 bands in the parental and sKO but not in the dKO, confirming that the gene has been deleted (Figure 3.7D). A

second probe to determine correct plasmid integration hybridises to bands of 3 different sizes in the WT allele, 1st allelic replacement and 2nd allelic replacement respectively, thereby conferring parental, sKO and dKO cells each with a unique signature and confirming correct integration of the relevant constructs in each case.

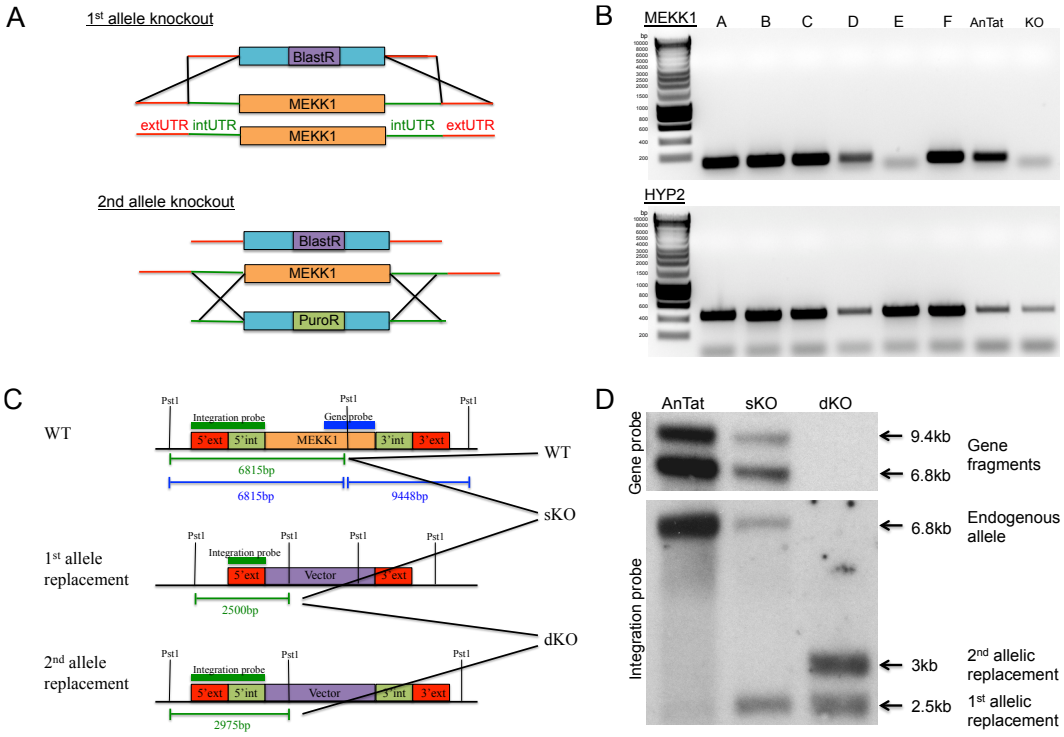

Figure 3.7 Generation of a null mutant of MEKK1. A) Schematic of knockout strategy. In the first step, a plasmid containing the blasticidin resistance gene was targeted to external portions of the 5' and 3' UTRs (extUTR) by homologous recombination, thereby replacing both the ORF and internal UTRs (intUTR) from one allele. Subsequently, a plasmid containing the puromycin resistance gene was targeted to internal portions of the UTRs and could recombine only with the remaining allele so that the second copy of the gene was replaced. B) Blast+Puro resistant clones were tested for MEKK1 deletion by PCR for a 100bp fragment of the ORF, showing successful deletion in clone E (upper panel). PCR with primers specific to a region of the HYP2 ORF confirmed gDNA was present in all samples (lower panel). KO control is previously verified MEKK1 KO + TOR4 KD clone (see section 4.5). C) A diagram shows the fragments recognised by 2 Southern DNA probes in the WT allele and integrated 1st and 2nd replacement constructs following gDNA digestion by Pst1. D) A gene probe complementary to part of the MEKK1 ORF recognises 6815bp and 9448bp fragments in the WT allele only, which were present in parental AnTat 1.1 90:13 cells and single knockout (sKO) cells but absent in the double knockout (dKO) cells, confirming successful gene deletion. A second probe to determine correct integration hybridises to a 6815bp fragment in the WT allele, a 2500bp fragment in the 1st allelic replacement and a 2975bp fragment in the 2nd allelic replacement, thereby conferring parental, sKO and dKO cells each with a unique signature and confirming correct integration of the relevant constructs in each case.

3.2.3.4 MEKK1 knockout confers loss of responsiveness to SIF *in vivo*

The differentiation capacity of the MEKK1 null mutant was tested *in vivo*. It showed uncontrolled proliferation, so that the mice needed to be sacrificed 5 days post

infection due to their very high parasitaemia (Figure 3.8A). A loss of G_1 arrest was supported by a significant reduction in cells with a single nucleus and kinetoplast relative to the parental line, although the 1K1N percentage did increase over the course of infection, indicating that absence of MEKK1 does not prevent differentiation entirely. PAD1 expression was almost completely eliminated in the null mutant, with only 8.6 ± 1.8 % expression on the final day of infection, relative to 60.4 ± 5.2% in the parental line (Figure 3.8C).

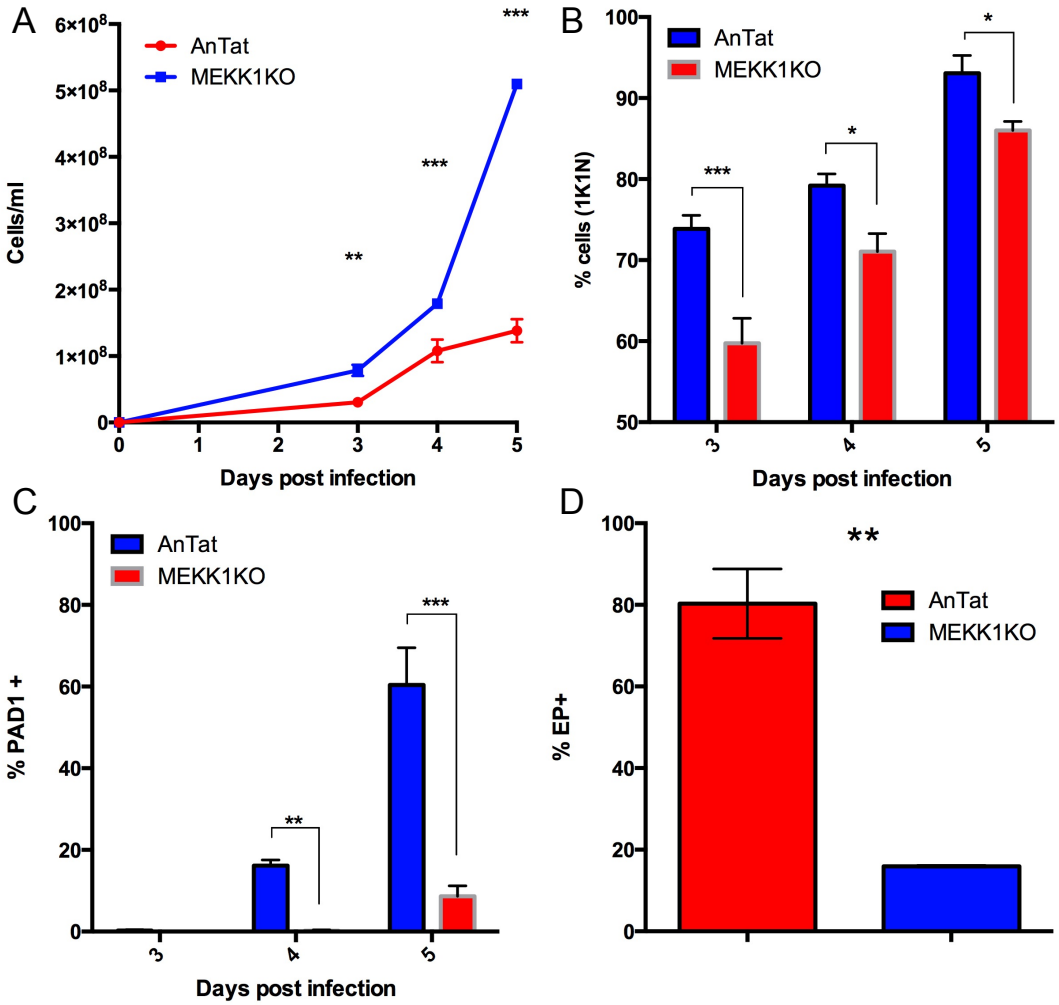

Figure 3.8 MEKK1 KO confers loss of responsiveness to SIF in vivo A) Parasitaemia of 6 mice infected with parental AnTat (n=3) or MEKK1 KO (n=3) cells, estimated by the rapid matching method. The parasitaemia was significantly higher in the KO. B) % 1K1N (representing G_1 and S phase) cells throughout the course of infection. 250 cells were counted for each sample. KO cells have lower % 1K1N. C) % cells expressing PAD1 throughout the course of infection, determined by IFA. 250 cells were counted for each sample. PAD1 expression was almost abolished in the KO cells. D) % EP procyclin expressing cells 4 hours post cis-aconitate treatment. To assess capacity to differentiate to procyclic forms, parasites purified from blood 5 days post infection were incubated in SDM-79 media supplemented with 6mM cis-anonitate at 27°C for 4 hrs and then analysed by FACS. EP expression was significantly reduced in the MEKK1KO line. A)-C) *P<0.05,**P<0.005,***P<0.0005 GLM and Tukey test for multiple comparisons. D) **P<0.005 GLM.

A key distinction between slender and stumpy forms is that only the latter can efficiently differentiate to procyclic forms (Dean et al., 2009; Robertson, 1913). To assess the capacity of the null mutant line to undergo this differentiation, parasites were purified from blood 5 days post infection and incubated at 27°C in the procyclic medium SDM-79 which had been supplemented with 6mM citrate/cis-aconitate (CCA) to stimulate differentiation. After 4 hours incubation, the expression of the procyclic surface marker EP procyclin was analysed by FACS. EP expression was significantly decreased in the null mutant (16 ± 0.1%) relative to the parental line (80.3 ± 4.9%)(Figure 3.8D). In agreement with the concurrent large but not absolute reductions in cell cycle arrest and PAD1 expression, this indicates that ablation of MEKK1 prevents most stumpy formation, but that it is still able to proceed at a low level.

3.2.3.5 Overexpression of full length MEKK1 protein but not the catalytic domain alone inhibits cell growth

In other systems, the N-terminal domain of MEK kinases appears to have a regulatory role and has been shown to interact with and repress the C-terminal catalytic domain so that overexpression of the C-terminal portion alone in yeast and mammalian cells is constitutively active (Mizote et al., 2010; Owen et al., 2013; van Drogen et al., 2000). This phenomenon has also been shown to occur naturally in human MEKK1, where caspase cleavage releases the active catalytic domain to induce apoptosis (Gibson et al., 1999). The possibility that this may also be true for trypanosomes raised the intriguing potential for a cell line with constitutively active differentiation signal transduction. To this end, 2 cell lines were generated in the monomorphic S16 line in which either full length MEKK1 or the catalytic domain alone (CatMEKK1) was overexpressed with an N-terminal TY epitope tag to assist detection (see vector in Appendix D Figure 5). As seen in Figure 3.9, overexpression of full length MEKK1 resulted in growth inhibition. This was as expected as the kinase promotes stumpy formation and therefore cell cycle arrest. However, CatMEKK1 had no effect on cell growth.

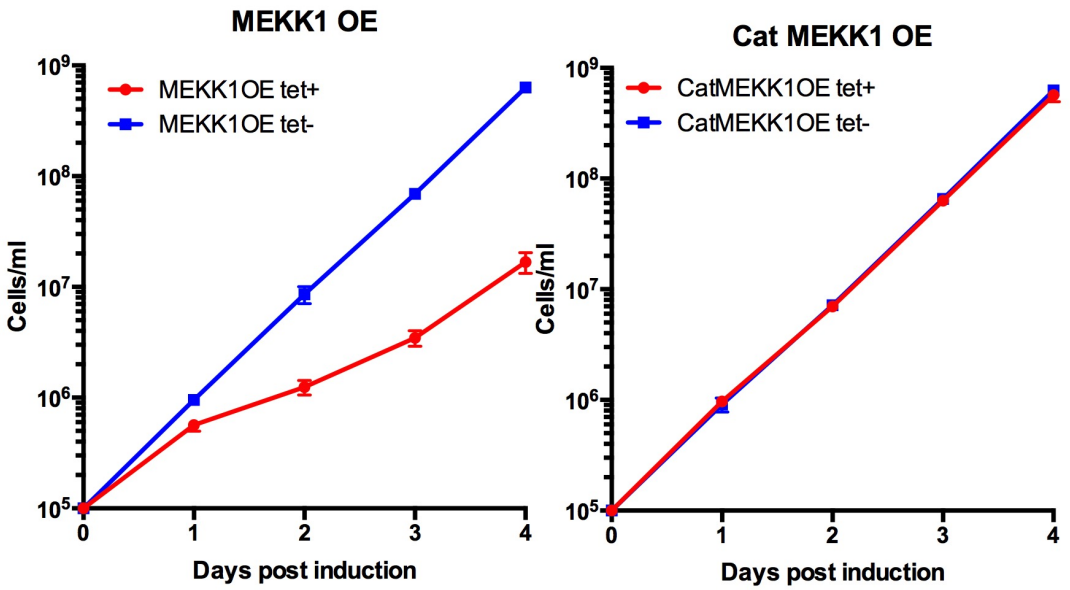

Figure 3.9 *In vitro* growth of monomorphic bloodstream cells was reduced upon overexpression of full length MEKK1 but not by the catalytic domain alone (Cat).

3.2.3.6 Overexpression of full length MEKK1 cannot be detected via the N-terminal TY epitope tag

These cell lines were tested for overexpression using the BB2 antibody which recognises the TY epitope tag. Western analysis revealed no detectable expression of the TY tagged protein upon induction with tetracycline in the full length MEKK1 overexpression line (Figure 3.10A). This was unexpected as these cells exhibited growth inhibition upon tetracycline induction (Figure 3.9), indicating overexpression of a protein which generates a phenotypic response. Equally surprisingly, expression of the catalytic domain was clearly detectable at the expected size of 43kDa in the CatMEKK1 overexpression line (Figure 3.10A), which showed no growth effect. Both of these results were confirmed by immunofluorescence analysis. It appears that overexpression of full length MEKK1 inhibits growth but is not detectable via its N-terminal tag while its catalytic domain detectably overexpresses but has no obvious effect on cell proliferation.

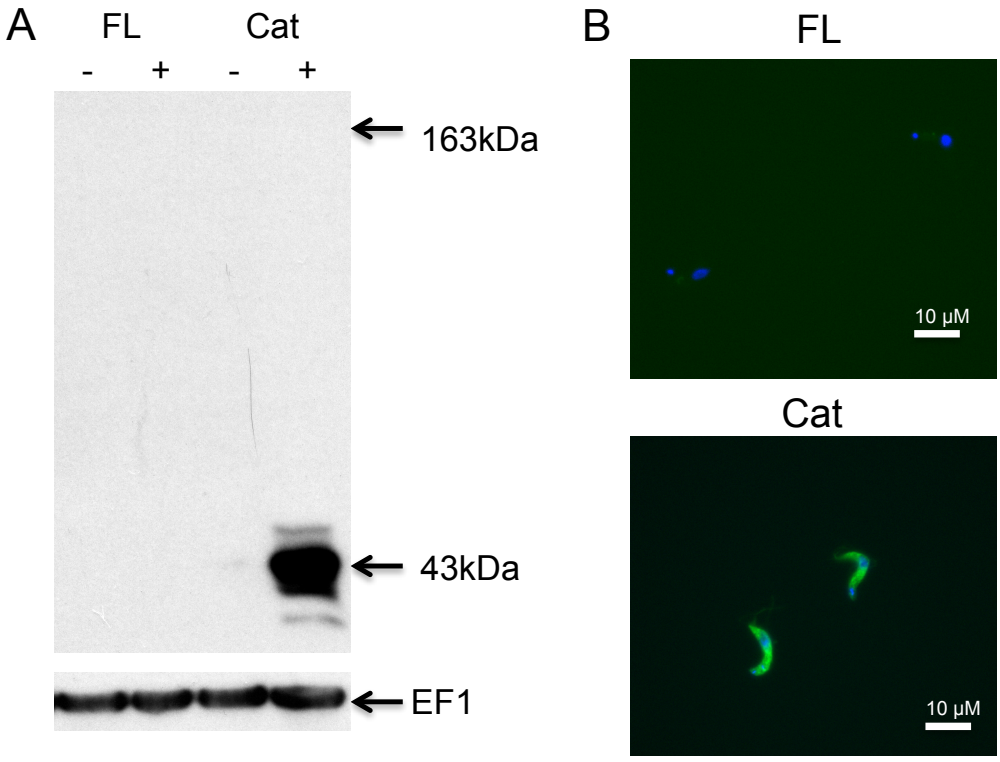

Figure 3.10 Overexpression of full length N-terminally TY tagged MEKK1 (FL) cannot be detected by BB2 antibody but overexpression of the truncated catalytic domain (Cat) was detectable by A) Western blot analysis of FL and Cat – or + tetracycline; EF1 was used as a loading control; or B) immunofluorescence analysis.

3.2.3.7 Overexpression of C-terminally epitope tagged MEKK1 is not detectable.

One possible explanation for the inability to detect TY tagged MEKK1 was that the kinase is targeted to a cellular compartment via an N-terminal targeting signal which is cleaved upon entry, resulting in loss of the epitope tag. To explore this possibility, the overexpression construct was regenerated with a C-terminal TY tag. This plasmid was transfected, along with the CatMEKK1 construct, into the pleomorphic AnTat 1.1 90:13 line. As before, overexpression of the catalytic domain was readily detectable via its TY tag but had no effect on cell growth (Figure 3.11). This would suggest that overexpression of the catalytic domain in this manner does not result in constitutive MEKK1 activity, at least as far as its generation of a detectable phenotype is concerned. Possible explanations for this result are discussed in section 3.5.1. Overexpression of the C-terminally tagged full length protein resulted in growth arrest but, as with the N-terminally tagged version, the protein was not detectable either by Western or IFA (Figure 3.11). Therefore the inability to detect

protein overexpression cannot be simply explained by cleavage of a localisation sequence.

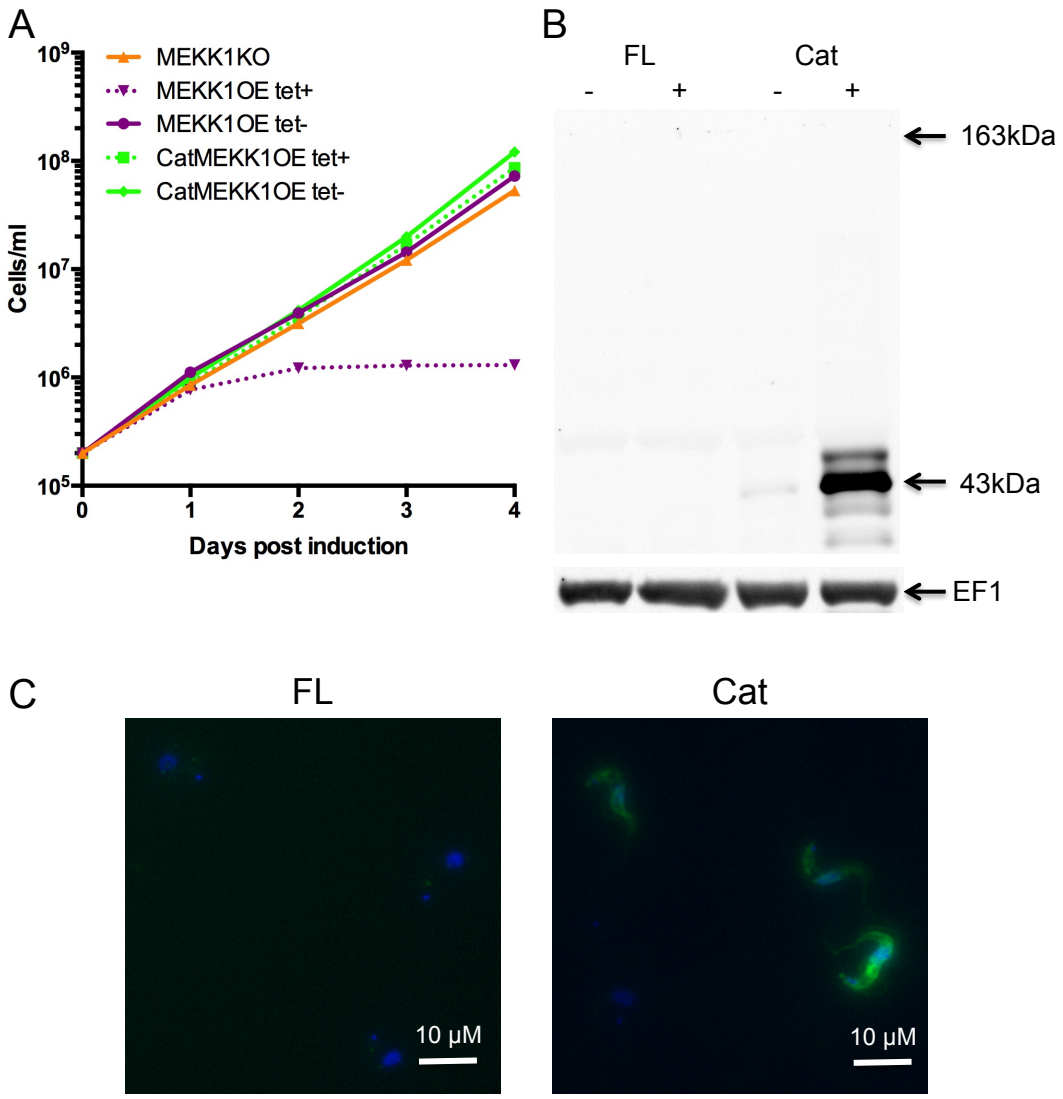

Figure 3.11 A) *In vitro* growth of pleomorphic cells was reduced upon overexpression of C-terminally TY tagged full length MEKK1 (FL) but not by the catalytic domain alone (Cat). Cat but not FL can be detected by the BB2 antibody by B) Western blot analysis of FL and Cat – or + tetracycline; EF1 was used as a loading control; or C) immunofluorescence analysis.

3.2.3.8 Overexpression of MEKK1 does not increase its transcript level but restores it in a null mutant background.

As MEKK1 overexpression could not be detected at the protein level, the abundance of MEKK1 transcript was investigated by Northern blot. As seen in Figure 3.12, doxycycline induction does not affect mRNA level in the C-terminally tagged MEKK1 overexpression line. However, when the same construct was used to

overexpress the protein in the MEKK1 null mutant background, it was able to restore detectable MEKK1 mRNA expression, despite complete absence of the transcript in the absence of doxycycline. This indicates that the plasmid is capable of generating MEKK1 mRNA expression, but is unable either to produce or to sustain a higher than endogenous expression level, possibly due to degradation as a consequence of the toxic effects of high expression or another regulatory mechanism.

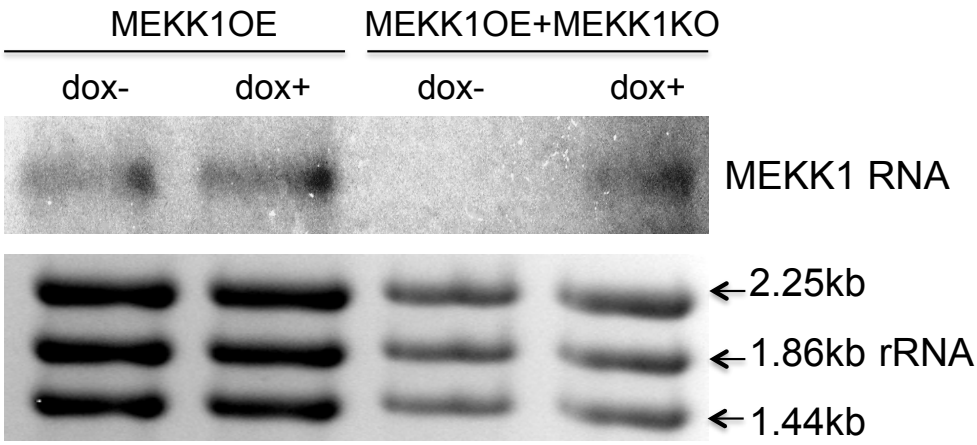

Figure 3.12 Northern analysis showed no increase in MEKK1 transcript level 48 hours after induction of overexpression but was able to restore expression in a MEKK1 null mutant background.

3.2.4 Hypothetical protein 2 (HYP2)

HYP2 is a *pos*ST gene and, although its function is as yet unknown, it is a potential candidate as an effector of gene expression changes acting downstream in the stumpy formation signalling cascade. The presence of a zinc finger motif (Mony et al., 2014), interaction with RNA regulators such as DRBD3 (Fernandez-Moya et al., 2012) and MKT1 (Singh et al., 2014) and its identification in a screen for post-transcriptional regulators (Erben et al., 2014) all point to a role in the regulation of gene expression (see section 1.9.3.1).

3.2.4.1 Generation of a HYP2 null mutant

To analyse the loss of HYP2 in a clean genetic background, as for MEKK1 (see section 3.2.3.3), the same strategy was used to generate a HYP2 null mutant in the AnTat 1.1 90:13 strain. The plasmids were prepared by Eleanor Silvester. After 2 rounds of transfection and selection, a number of clones were isolated with resistance to both blasticidin and puromycin. PCR with internal HYP2 ORF primers

demonstrated that the gene was absent in 3 of these clones. Gene deletion was later confirmed in these clones by Southern blot by Eleanor Silvester, who also demonstrated that HYP2 knockout confers resistance to SIF *in vivo* (E. Silvester, thesis in preparation).

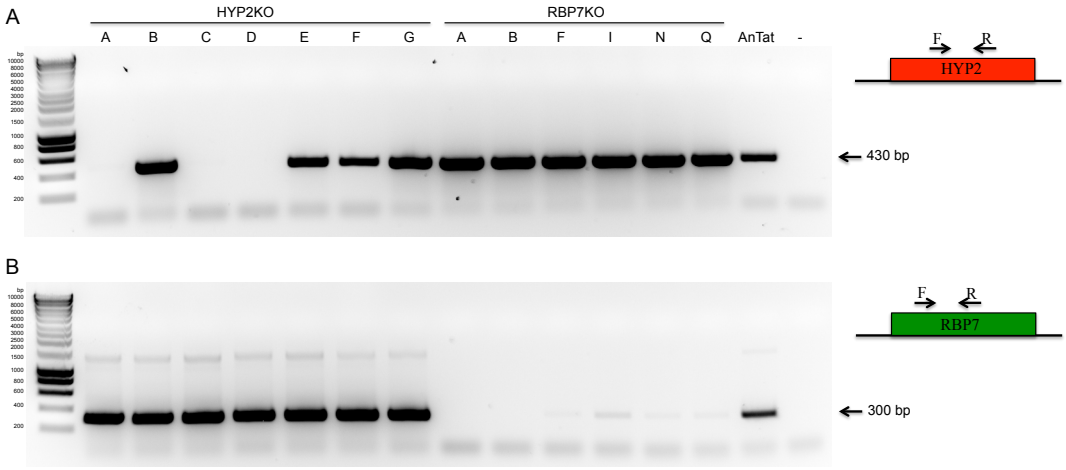

Figure 3.13 PCRs using internal A) HYP2 and B) RBP7 ORF fragments were used to test for successful gene deletion in gDNA from parasites subjected to 2 rounds of allelic replacement. In each case, the respective gene was absent in several clones.

3.2.5 RNA-binding protein 7 (RBP7)

RBP7 comprises two near identical gene copies, RBP7A and RBP7B, arranged in tandem array. It is another potential modulator of gene expression in the differentiation pathway due to the presence of an RNA-recognition motif (RRM) in each copy. RNAi of RBP7 reduces responsiveness to the differentiation signal, while overexpression accelerates stumpy formation. Although transcriptomic analysis of these 2 perturbations showed limited widespread expression changes, RBP7 overexpression increased levels of a number of other RNA-binding protein mRNAs (Mony et al., 2014).

3.2.5.1 Generation of an RBP7 null mutant

A null mutant of RBP7 was generated in the AnTat 1.1 90:13 strain. This was achieved using the same strategy as for MEKK1 and HYP2 (sections 3.2.3.3 and 3.2.4.1), except that the constructs were targeted to the 5'UTR of RBP7A and the 3'UTR of RBP7B, in order to delete the two tandemly arranged gene copies simultaneously. The plasmids were prepared by Eleanor Silvester. After successive transfections with the 2 allelic replacement constructs, a number of clones were

tested for the presence of a fragment of the RBP7 ORF. PCR amplification confirmed this fragment to be absent in all clones tested (Figure 3.13). Gene deletion was later verified by Southern blot (E. Silvester, thesis in preparation).

3.2.5.2 RBP7 KO confers loss of responsiveness to SIF *in vivo*

The SIF response of an RBP7 null mutant cell line was investigated *in vivo*. As seen in Figure 3.14A, the parasitaemia continued to increase throughout the course of the infection, showing no sign of arrest. On the final day of infection, RBP7 KO cells showed a significantly reduced 1K1N population relative to the parental AnTat 1.1 90:13 parasites, indicating a failure to undergo G_1 arrest (Figure 3.14B). PAD1 expression was also significantly lower than in wild type cells (Figure 3.14C) and when induced to differentiate to procyclic forms, EP procyclin expression was almost completely absent in the null mutant, with only 5.9 ± 2.2% expression relative to 70.3 ± 2% parental cells (Figure 3.14D). This all points to reduced differentiation to stumpy forms in response to SIF.

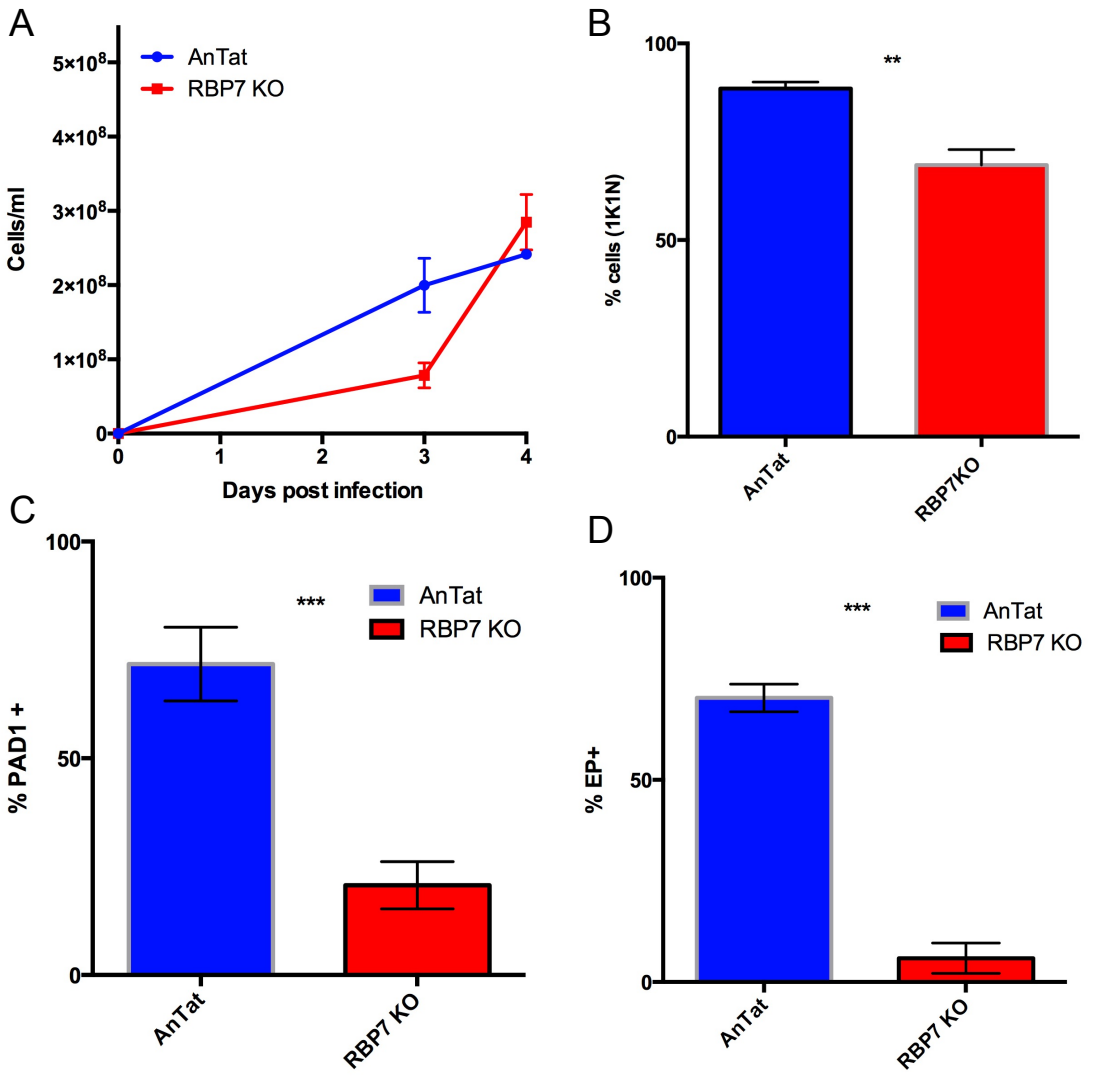

Figure 3.14 RBP7 KO confers loss of responsiveness to SIF in vivo. A) Parasitaemia of 6 mice infected with parental AnTat (n=3) or RBP7 KO (n=3) cells, estimated by the rapid matching method. B) % 1K1N (representing G_1 and S phase) cells 4 days p.i. 250 cells were counted for each sample. KO cells have lower 1K1N. C) % cells expressing PAD1 4 days p.i., determined by FACS. PAD1 expression was significantly reduced in the KO cells. D) Proportions of EP procyclin expressing cells 4 hours post cis-aconitate treatment. To assess capacity to differentiate to procyclic forms, parasites purified from blood 4 days post infection were incubated in SDM-79 media supplemented with 6mM cis-aconitate at 27°C for 4 hrs and then analysed by FACS. EP expression was much lower in RBP7 KO. *P<0.05,**P<0.005,***P<0.0005 GLM.

3.2.5.3 Overexpression of RBP7 restores differentiation in RBP7 KO *in vitro*

RBP7 has previously been overexpressed in the AnTat 1.1 90:13 background and shown to induce differentiation by Mony *et al.* (2014). RBP7 was overexpressed in the RBP7 null mutant background to determine if this could restore its capacity for stumpy formation. As seen in Figure 3.15A, this resulted in growth arrest, suggesting

that exogenously overexpressed RBP7 was able to drive stumpy formation in the absence of endogenous protein. This supports the hypothesis that the block in differentiation which occurs upon knockout of a *pos*ST gene can be overcome by overexpressing it. As this would also be expected to be true for any downstream effector, it adds credence to the approach of ordering the *pos*ST pathway by overexpressing *pos*ST proteins in distinct *pos*ST null mutant backgrounds.

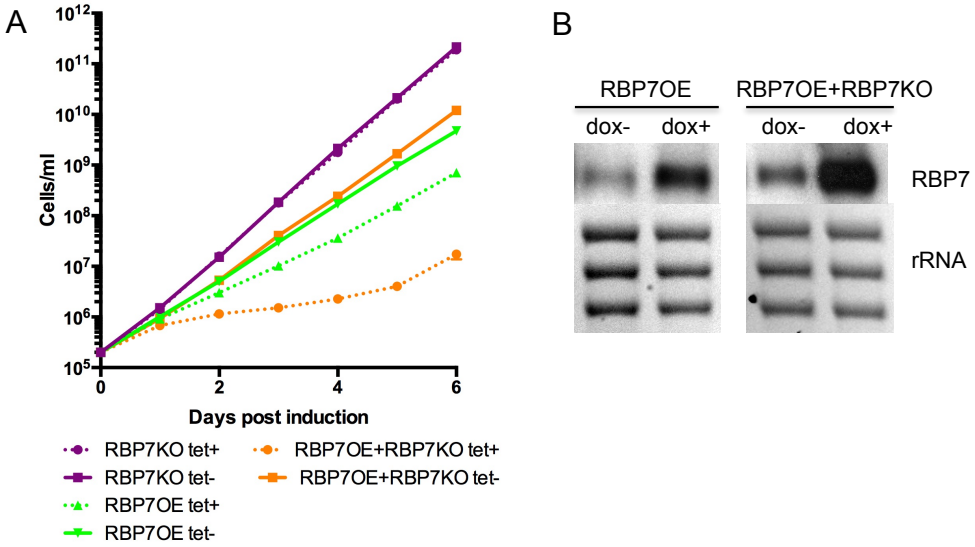

Figure 3.15 A) *In vitro* growth inhibition upon overexpression of RBP7 was still observed in a RBP7 null mutant background. B) Northern blot analysis shows overexpression of RBP7 in an RBP7 null mutant background upon induction with doxycycline.

3.3 Relative positioning of *pos*ST genes via combinatorial knockout and overexpression strategy

It has been demonstrated for various *pos*ST genes that overexpression promotes stumpy formation while gene knockout prevents it (sections 3.2.3.4, 3.2.5.2, 3.2.5.3 and (Mony et al., 2014). It has also been shown in the case of RBP7 that overexpression in a null mutant background can restore differentiation capacity (section 3.2.5.3). Therefore, overexpression of one *pos*ST gene in combination with knockout of a distinct *pos*ST could be used to elucidate the relationship of the 2 genes and facilitate ordering of the pathway. As depicted in Figure 3.16, if overexpressed *pos*ST X is dependent on the deleted *pos*ST Y, the parasites would be unable to differentiate. This would indicate that, for example, Y acts directly

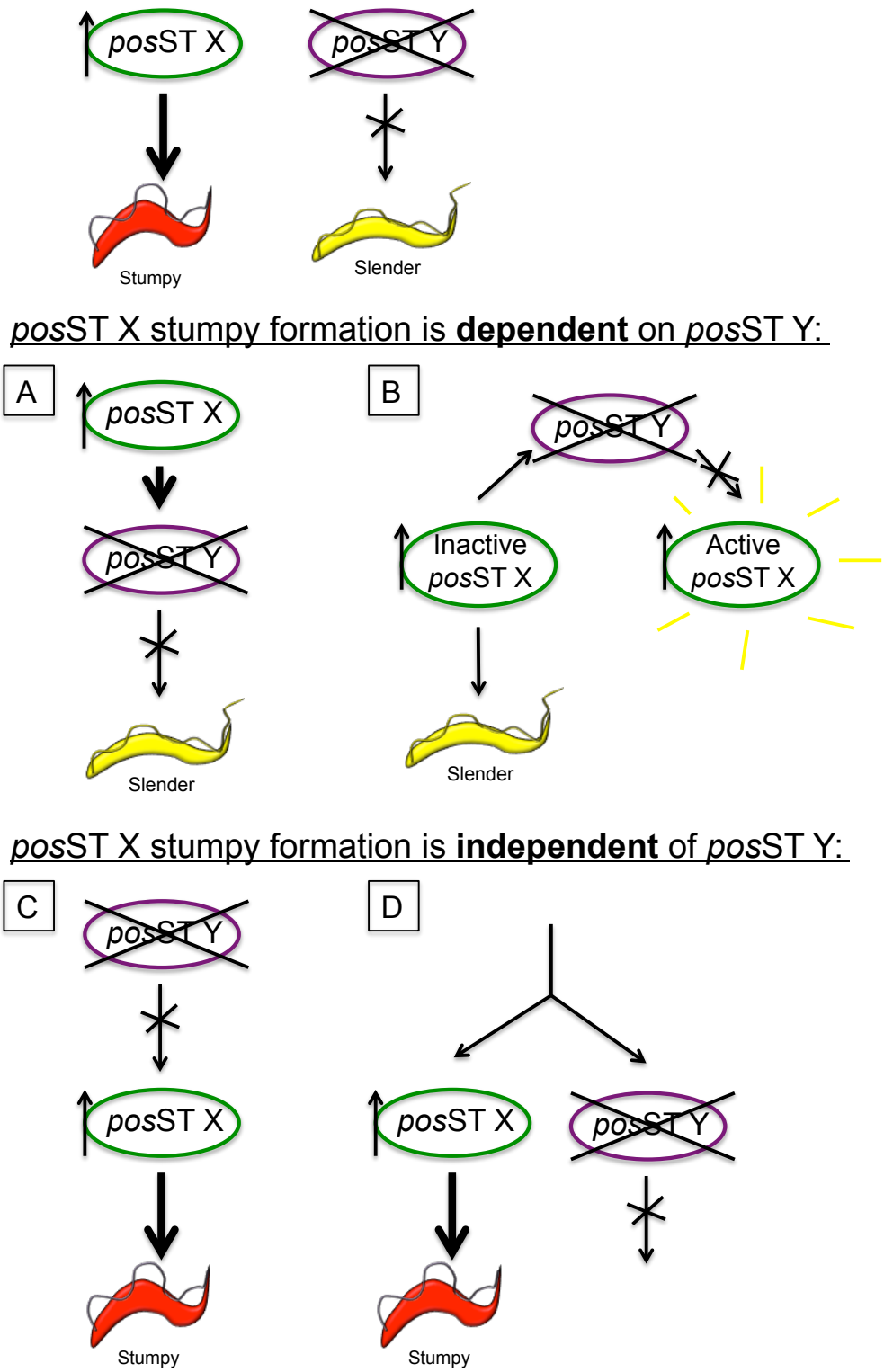

Figure 3.16 Combinatorial knockout and overexpression strategy for ordering *pos*ST genes. Overexpression of *pos*ST X triggers stumpy formation. Knockout of *pos*ST Y results in retention of slender forms. Combined X OE + Y KO gives possible outcomes: *pos*ST X stumpy formation is dependent on *pos*ST Y and cells remain slender if A) X acts upstream of Y or B) Y is required to produce the active form of X. *pos*ST X stumpy formation is dependent on *pos*ST Y and cells differentiate to stumpy forms if C) Y acts upstream of X or D) X and Y act in different branches of the pathway.

downstream of X or alternatively is required to produce the active form of X. If, on the other hand, X is independent of Y, the parasites would differentiate to stumpy forms. This would indicate that Y acts either upstream of X or on a distinct branch of the SIF response pathway.

3.3.1 NEK OE + RBP7 KO: Overexpression of NEK results in RBP7-dependent growth inhibition *in vitro*

A copy of NEK (Tb927.10.5950) with a C-terminal TY tag was overexpressed in AnTat 1.1 90:13 parasites and in the RBP7 KO line using the strategy described for overexpression of MEKK1 (section 3.2.3.7). Figure 3.17A shows that overexpression of NEK alone resulted in growth inhibition but this effect was completely lost in the RBP7 KO background. Interestingly, while both lines showed inducible overexpression using an antibody against the TY epitope tag, the level of overexpression was much higher in the RBP7 null mutant (Figure 3.17B), in which growth was unaffected. Possible explanations for this are discussed in section 3.5.4, but it demonstrated that the absence of arrest was not due to a failure to express the NEK protein. These results demonstrate that NEK-induced stumpy formation is dependent on RBP7 and act as proof of principle that *pos*ST overexpression phenotypes can be rescued by knockout of a distinct gene.

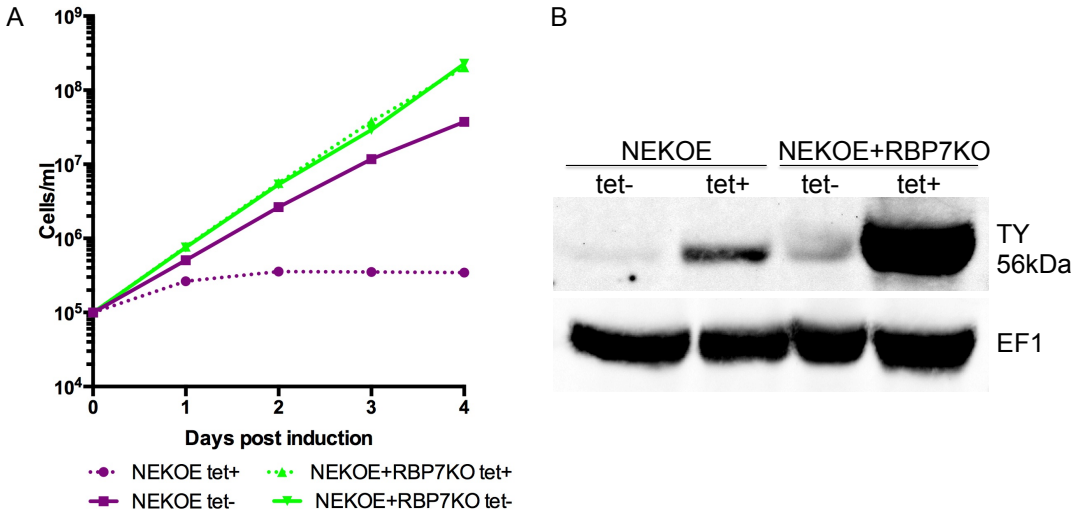

Figure 3.17 A) *In vitro* growth inhibition caused by overexpression of NEK was rescued in an RBP7 null mutant background. B) Western blot analysis using the TY epitope tag specific BB2 antibody 24 hours p.i. shows NEK was ectopically expressed to a higher level in the RBP7 KO. EF1 was used as a loading control.

3.3.2 NEK OE + YAK KO: Overexpression of NEK results in YAK-independent growth inhibition *in vitro*

NEK was also ectopically expressed in a null mutant of YAK generated by Paula MacGregor (unpublished results). Induction of NEK overexpression resulted in growth inhibition in both the wild type and the YAK KO cells (Figure 3.18A), indicating that NEK mediates differentiation independently of YAK. However, western analysis demonstrated that the protein was overexpressed at a much higher level in the null mutant line (Figure 3.18B). It is possible that this reflects a partial rescue by the YAK KO which necessitates a higher level of NEK overexpression in order to produce a similar level of growth inhibition. This possibility is further explored in section 3.5.4. However, the observation of growth arrest in the absence of YAK strongly indicates that stumpy formation by NEK is not dependent on YAK.

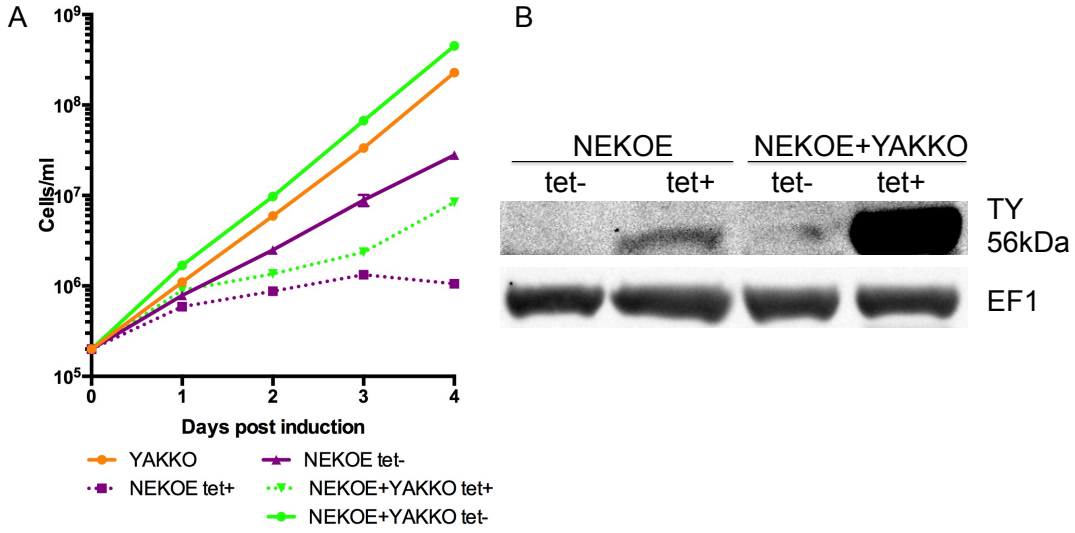

Figure 3.18 *In vitro* growth inhibition caused by overexpression of NEK was still observed in a YAK null mutant background. B) Western blot analysis demonstrated that NEK was overexpressed to a higher level in the YAK KO line. EF1 was used as a loading control.

3.3.3 PP1 OE + RBP7 KO: Overexpression of PP1 results in RBP7-independent growth inhibition in vitro

PP1 has previously been overexpressed in the AnTat 1.1 90:13 background and shown to induce stumpy formation (B. Mony and K. Matthews, unpublished results). To investigate its pathway position, PP1 was overexpressed in the RBP7 null mutant line. Figure 3.19A shows that induction of PP1 overexpression led to immediate arrest lasting 48 hours, after which growth subsequently recovered. A Northern blot was probed for expression of the PP1 transcript, resulting in the detection of 3 bands.

As seen in Figure 3.19B, the lowest of the 3 showed increased intensity 48 hours after induction of PP1 ectopic expression in both the AnTat and RBP7 KO lines. This was no longer apparent 5 days post induction in the PP1 OE + RBP7 KO line, indicating that growth had resumed due to reduced PP1 expression. This suggests that *in vitro*, stumpy formation can be induced by elevated PP1 expression and that this is independent of the presence of RBP7.

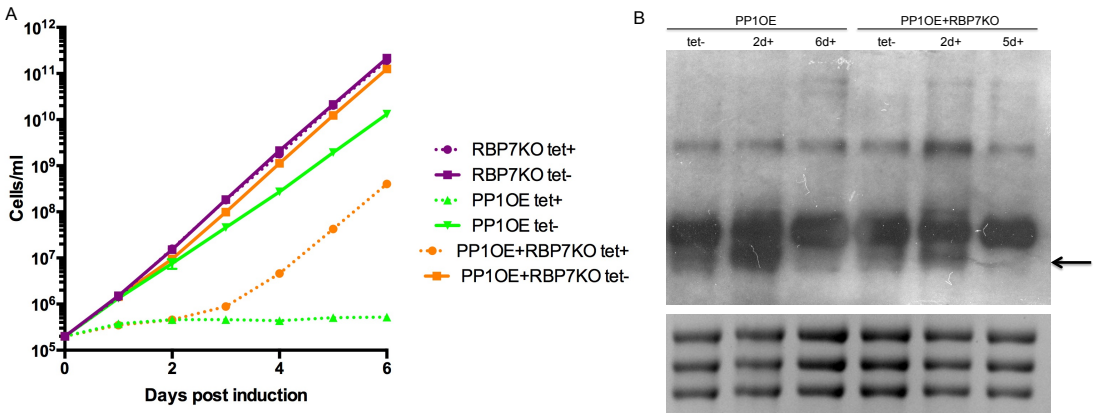

Figure 3.19 A) In vitro growth inhibition caused by overexpression of PP1 was still observed in a RBP7 null mutant background. B) Northern blot analysis of PP1 detects 3 bands, the smallest of which (arrow) was increased 48 hours post induction of overexpression. This increase was abolished at later timepoints when cell growth had recovered.

3.3.4 PP1 OE + RBP7 KO: Overexpression of PP1 results in RBP7-independent stumpy formation *in vivo*

In addition to an *in vitro* growth analysis, the capacity of PP1 overexpression to trigger differentiation in the absence of RBP7 was assessed *in vivo*. As PP1 overexpression results in rapid growth arrest *in vivo* (B. Mony and K. Matthews, unpublished results), doxycycline was not introduced until 3 days post infection. This resulted in the expected growth inhibition in the PP1 OE line (Figure 3.20A). This was also observed in the PP1 OE + RBP7 KO line, showing that PP1 OE induced growth arrest independently of the presence of RBP7. Effective PP1 overexpression in both lines was confirmed by Northern blot (Figure 3.20C). In the absence of doxycycline, the cells appeared slender in morphology on day 4 of infection due to the absence of RBP7. However, addition of doxycycline resulted in the presence of morphologically stumpy forms (Figure 3.20B), showing that PP1 overexpression was able to restore differentiation in this line.

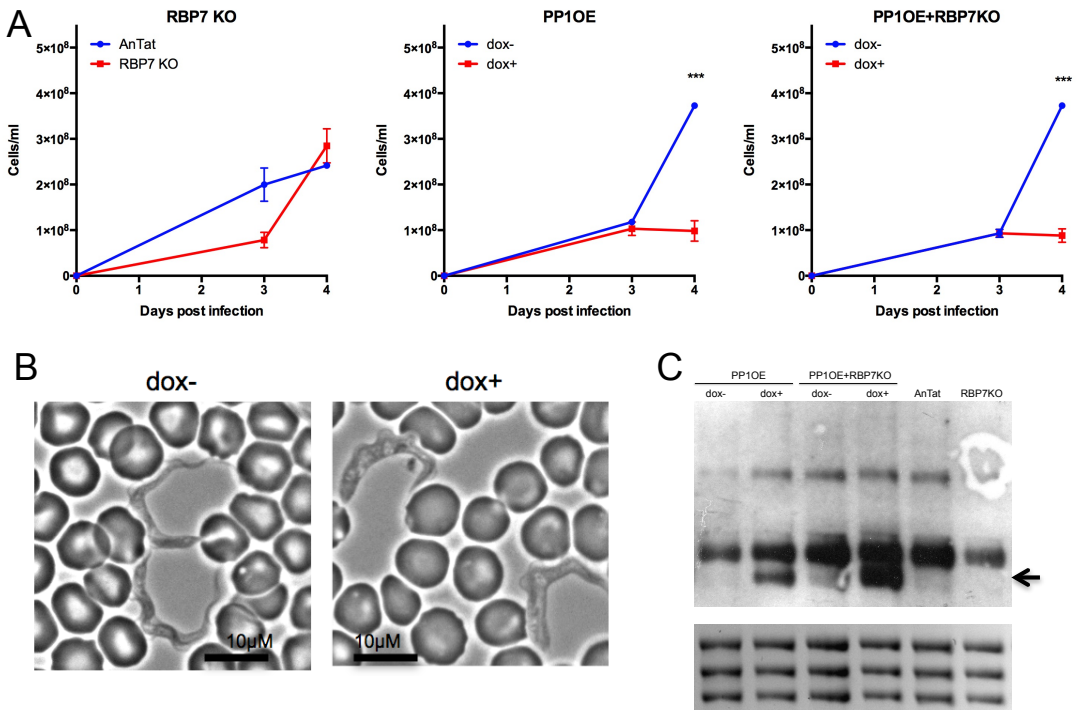

Figure 3.20 PP1 OE restores stumpy formation in RBP7 KO cells *in vivo*. A) Parasitaemia of mice infected with PP1 overexpression and RBP7 knockout cell lines in triplicate, estimated by the rapid matching method. Overexpression was induced with doxycycline at 3 days post infection, resulting in rapid growth inhibition. A strong growth effect upon induction of PP1 overexpression was also observed in the RBP7 null mutant background. ***P<0.0005 t test. B) Phase contrast images of PP1OE+RBP&KO parasites on day 4 of infection. Untreated (dox-) cells appear slender in morphology whereas doxycycline-treated (dox+) cells were morphologically stumpy. C) Northern blot analysis of PP1 detects 3 bands, the smallest of which (arrow) was increased upon overexpression of PP1. rRNA was used as a loading control.

The differentiation status of the parasites 24 hours after induction of PP1 overexpression was further explored by analysing their cell cycle position. PP1 overexpression resulted in increased G_1 arrest in the RBP7 KO, as determined by a 19% increase in 1K1N cells (Figure 3.21A). PAD1 expression was also restored, although a low level of PAD1 expression was also observed in this cell line in the absence of doxycycline. As this was undetectable in the parental RBP7 KO line (Figure 3.21B), this indicated that the overexpression was slightly leaky. The PP1 OE + RBP7 KO population also demonstrated enhanced competence to differentiate to procyclic forms and express EP procyclin upon CCA treatment (Figure 3.21C). A low level of EP expression was also detected in the absence of doxycycline, again likely due to leaky PP1 expression. These results demonstrate that PP1 mediates stumpy formation in an RBP7-independent fashion.

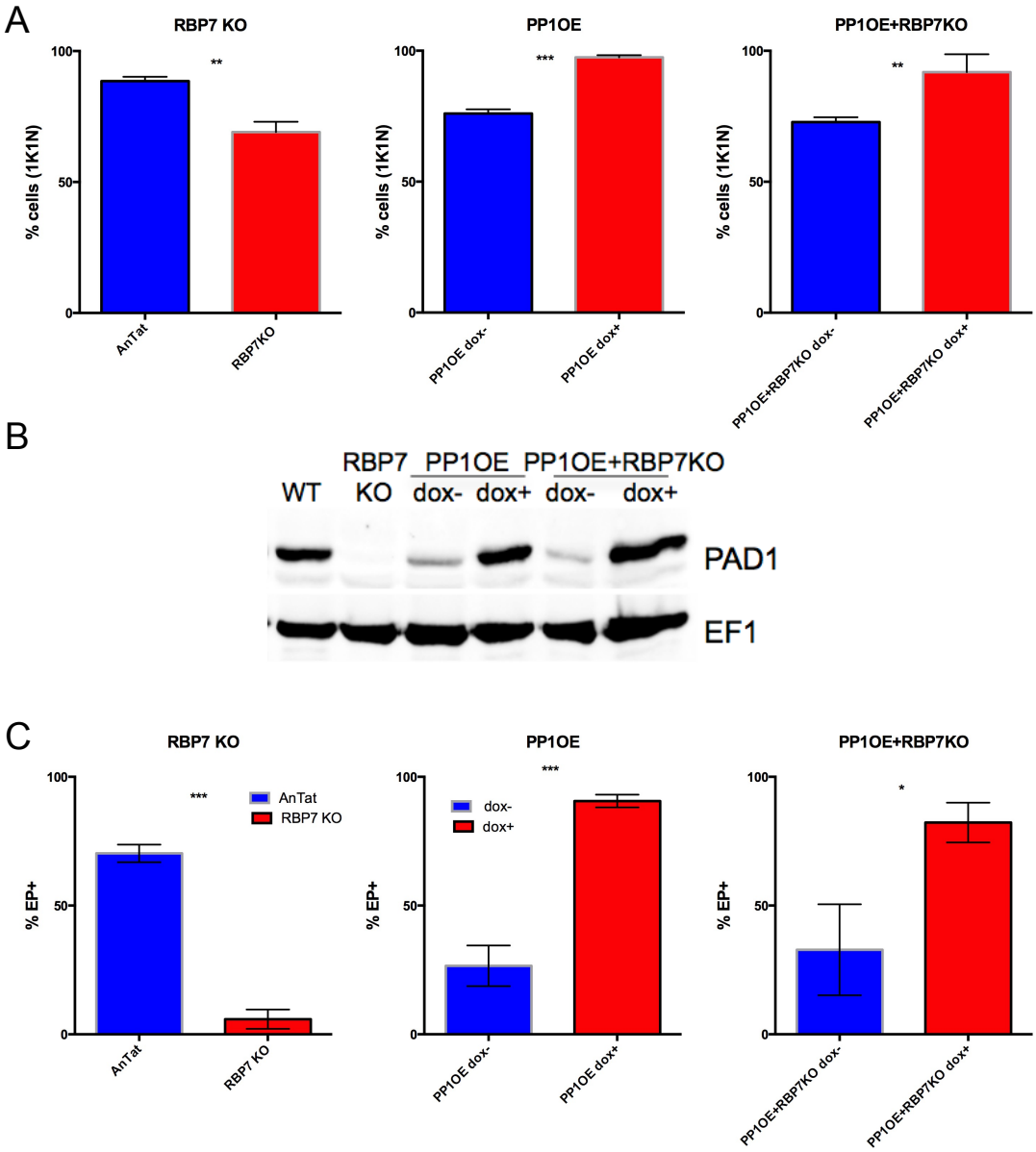

Figure 3.21 Stumpy formation by PP1 was independent of RBP7. A) % 1K1N cells at day 4 p.i. 250 cells were counted for each sample. An increase in G_1 arrest upon PP1 overexpression was still observed in the RBP7 null mutant. **P<0.005,***P<0.0005 t test. B) Western blot analysis on day 4 shows an increase in PAD1 expression upon PP1 overexpression was still observed in the RBP7 null mutant. EF1 was used as a loading control. C) Proportions of EP procyclin expressing cells 4 hours post cis-aconitate treatment. To assess capacity to differentiate to procyclic forms, parasites purified from blood 4 days post infection were incubated in SDM-79 media supplemented with 6mM cis-aconitate at 27°C for 4 hrs and then analysed by FACS. An increase in EP expression upon PP1 overexpression was still observed in the RBP7 null mutant. *P<0.05,**P<0.005,***P<0.0005 t test.

3.3.5 PP1 OE + YAK KO: Overexpression of PP1 results in YAK-independent growth inhibition *in vitro*

To further analyse the role of PP1 in the differentiation pathway, PP1 was overexpressed in the YAK null mutant background. Induction with tetracycline

resulted in growth inhibition (Figure 3.22A), indicating that this phenotype is independent of YAK. Although growth recovered at a later timepoint, this was likely due to loss of PP1 overexpression as this was also observed when PP1 was overexpressed in the RBP7 null mutant background (section 3.3.3). Indeed, PP1 overexpression could no longer be detected by Northern blot 4 days post induction (Figure 3.22B). Surprisingly, the Northern blot also showed enrichment of the lowest band in the uninduced PP1 OE + YAK KO sample. The reason for this is unclear as the cells grew normally.

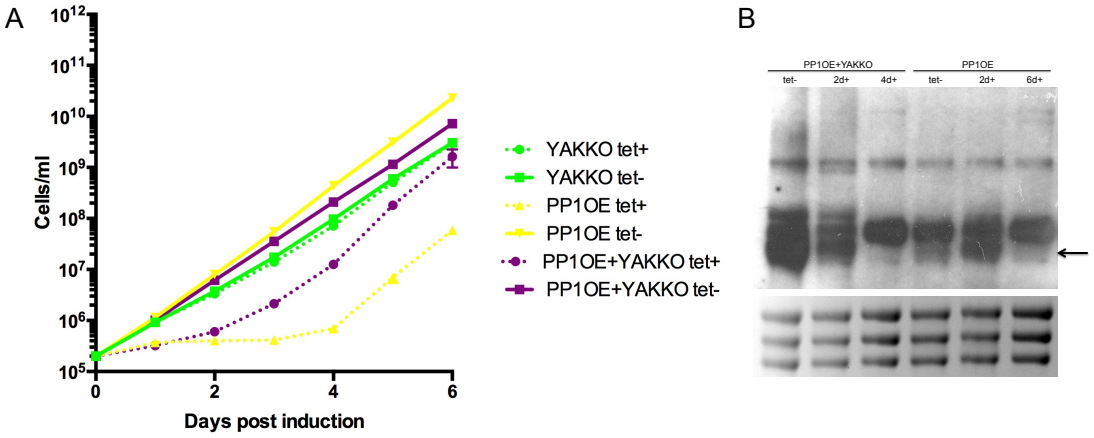

Figure 3.22 A) *In vitro* growth effect upon overexpression of PP1 was still observed in a YAK null mutant background. B) Northern blot analysis of PP1 detects 3 bands, the smallest of which (arrow) was increased 48 hours post induction of overexpression. This increase was abolished at later timepoints when cell growth had recovered.

3.3.6 PP1 OE + YAK KO: Overexpression of PP1 results in YAK-dependent stumpy formation *in vivo*

The capacity of PP1 overexpression to trigger differentiation in the absence of YAK was also assessed *in vivo*. This demonstrated that induction of PP1 overexpression on day 3 of infection resulted in rapid growth inhibition both in the AnTat 1.1 90:13 background and the YAK null mutant (Figure 3.23A). This corresponded to the *in vitro* finding that PP1-induced growth arrest was YAK-independent. However, while PP1 OE + YAK KO cells showed an increase in 1K1N upon doxycycline treatment, this was modest compared to overexpression of PP1 in the wild type background (72.9 ± 1% vs. 97.5 ± 0.5%; Figure 3.23B), indicating that G_1 arrest was tempered by the absence of YAK. When the harvested parasites were induced to differentiate to procyclic forms, PP1 overexpression did not result in an increase in EP expression in

YAK KO cells relative to doxycycline untreated cells (Figure 3.23C), suggesting that the population was mainly slender in characteristic. Consistent with this, PAD1 expression was barely detectable in doxycycline induced PP1 OE + YAK KO parasites (Figure 3.23D). Thus it appears that although growth inhibition by PP1 overexpression is YAK independent, PP1-induced stumpy formation and differentiation competence is YAK dependent. The PP1 overexpression growth phenotype is more severe than that observed for overexpression of other *pos*ST proteins and, unlike most of these, it also exhibited growth inhibition upon RNAi (Mony et al., 2014). This suggests that, in addition to its role in differentiation, PP1 also performs a function essential to proliferative slender cells. Therefore, although its differentiation function is YAK-dependent, YAK has no involvement in its other role in slender forms and as such YAK KO cannot rescue the growth phenotype. Northern analysis showed the previously observed upregulation of the lowest PP1 band in the PP1 OE line (indicated by arrow in Figure 3.23E). However, as observed *in vitro*, this band was upregulated in the PP1 OE + YAK KO line both with and without doxycycline. This was not observed in the parental YAK KO line (Figure 3.23E), which indicates that the PP1 transcript does not accumulate as a consequence of the absence of YAK. As the lack of a growth defect in the absence of doxycycline also rules out leaky overexpression as an explanation for this observation, the reason behind this accumulation is unknown.

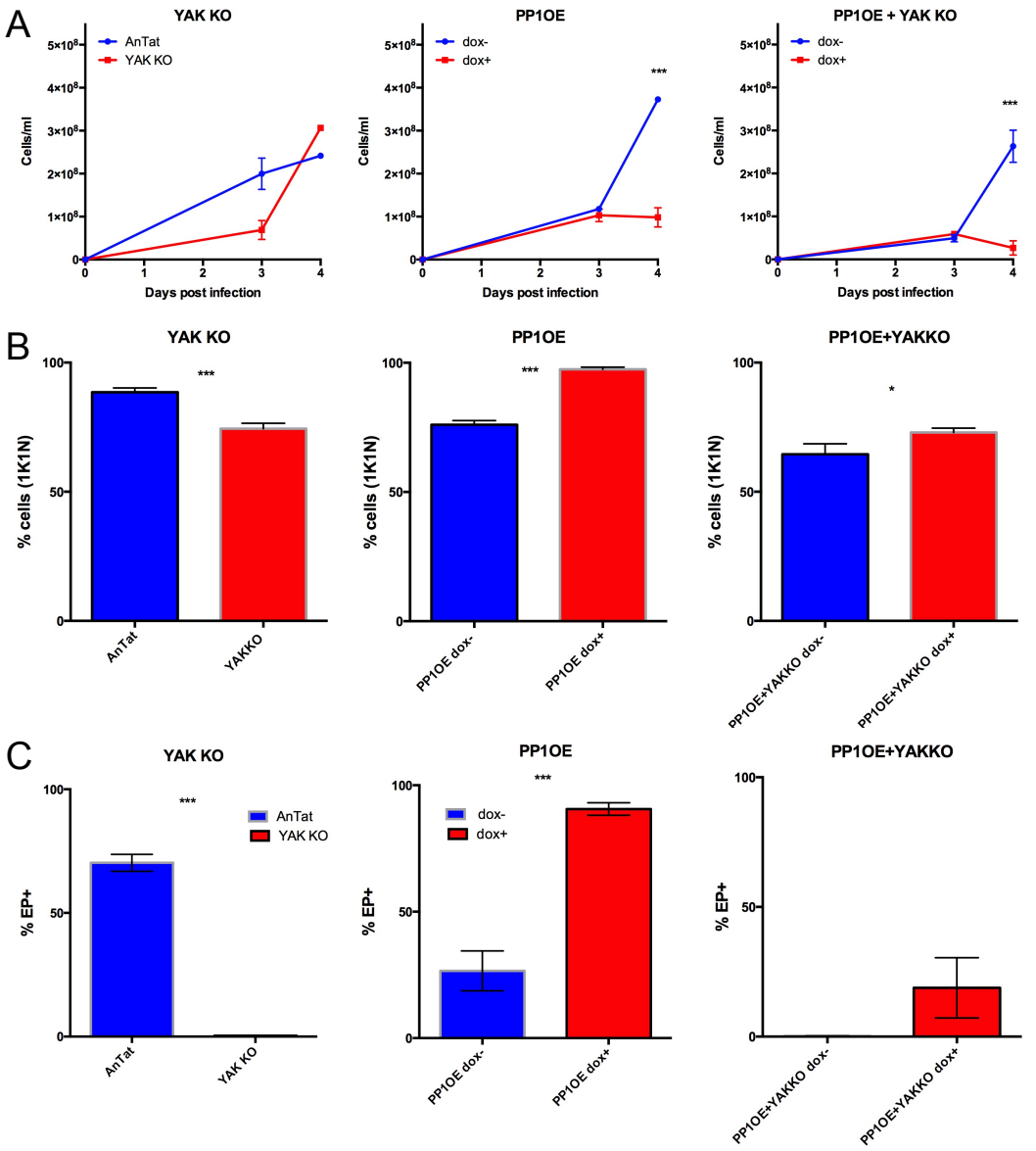
A
YAK KO
AnTat
YAK KO
Cells/ml
Days post infection
PP1OE
dox-
dox+
***
PP1OE + YAK KO
B
% cells (1K1N)
AnTat
YAKKO
PP1OE dox-
PP1OE dox+
PP1OE+YAKKO dox-
PP1OE+YAKKO dox+
*
C
% EP+
D
PP1OE PP1OE+YAKKO YAK
dox- dox+ dox- dox+ KO WT
PAD1
EF1
E
AnTat
YAKKO
PP1OE+YAKKO
PP1OE

Figure 3.23 Stumpy formation by PP1 *in vivo* is dependent on YAK. A) Parasitaemia of mice infected with PP1 overexpression and YAK knockout cell lines in triplicate, estimated by the rapid matching method. Overexpression was induced with doxycycline at 3 days post infection. A strong growth effect upon induction of PP1 overexpression was also observed in an YAK null mutant background. B) % 1K1N cells at day 4 p.i. 250 cells were counted for each sample. An increase in G1 arrest upon PP1 overexpression was diminished in a YAK null mutant. C) % EP procyclin expressing cells 4 hours post cis-aconitate treatment. To assess their capacity to differentiate to procyclic forms, parasites purified from blood 4 days post infection were incubated in SDM-79 media supplemented with 6mM cis-aconitate at 27°C for 4 hrs and then analysed by FACS. An increase in EP expression upon PP1 overexpression was reduced in the YAK null mutant. A)-C) *P<0.05,**P<0.005,***P<0.0005 t test. D) Western blot analysis on day 4 demonstrated that PAD1 expression upon PP1 overexpression was not observed in the YAK null mutant. EF1 was used as a loading control. E) Northern blot analysis of PP1 detects 3 bands, the smallest of which (arrow) was increased upon overexpression of PP1. rRNA was used as a loading control.

Figure 3.24A shows that doxycycline-treated PP1 OE + YAK KO cells appeared morphologically slender, which was in agreement with the findings from Figure 3.23 that PP1-mediated differentiation is YAK-dependent. However, visualisation of these cells using a nuclear stain showed that, in many of these cells, the nucleus had an unusual elongated, curvy shape. An example is shown in Figure 3.24A. This was quantified using 2 shape descriptors: aspect ratio and solidity. Aspect ratio defines the length of the object divided by the width, such that an elongated object such as an oval will have a higher aspect ratio than a compact object such as a circle. Solidity measures the area of an object divided by its convex area and therefore quantifies how concave the shape is. Nuclei of doxycycline-treated cells had a significantly increased aspect ratio and decreased solidity compared to uninduced controls (Figure 3.24B), demonstrating that these nuclei were less circular and more elongated and concave in shape. This phenomenon has not been observed for PP1 OE alone and appears to be specific to the PP1 OE + YAK KO combination, suggesting that these cells have characteristics distinct from wild type slender parasites. Possible explanations for this phenotype are discussed in section 3.5.3.

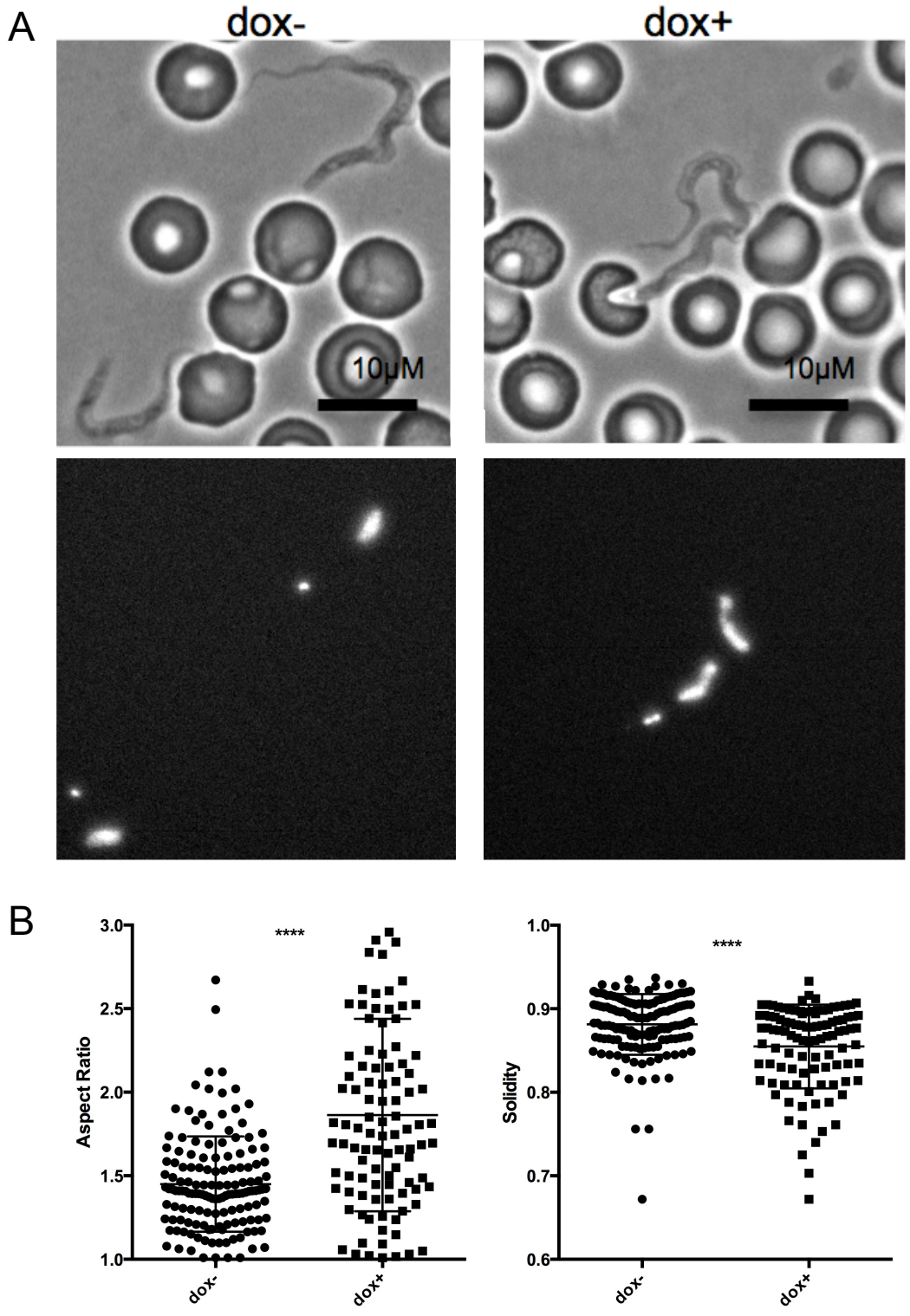

Figure 3.24 PP1 overexpression affects nuclear shape in YAK null mutant cells. A) Phase contrast (upper) and DAPI (lower) images of PP1OE+YAKKO parasites on day 4 of infection. Doxycycline-treated (dox+) cells appear slender in morphology and have elongated nuclei. B) Quantification of nuclear shape changes. Aspect ratio = length/width. Solidity = area/convex area. dox- n=145; dox+ n=102. Doxycycline treated cells show increased aspect ratio and decreased solidity. ****P<0.00005 t test.

3.3.7 RBP7 OE + YAK KO: Overexpression of RBP7 results in YAK-independent growth inhibition *in vitro*

Having investigated the role of PP1 relative to both RBP7 and YAK, RBP7 was overexpressed in the YAK null mutant line to assess the relationship of these 2 proteins. Overexpression of RBP7 led to growth inhibition *in vitro* in the YAK null mutant to an even greater degree than in the wild-type background (Figure 3.25A), possibly due to a higher level of RBP7 overexpression, as demonstrated by Northern blot (Figure 3.25B). This demonstrated that *in vitro* growth inhibition by RBP7 overexpression is YAK-independent.

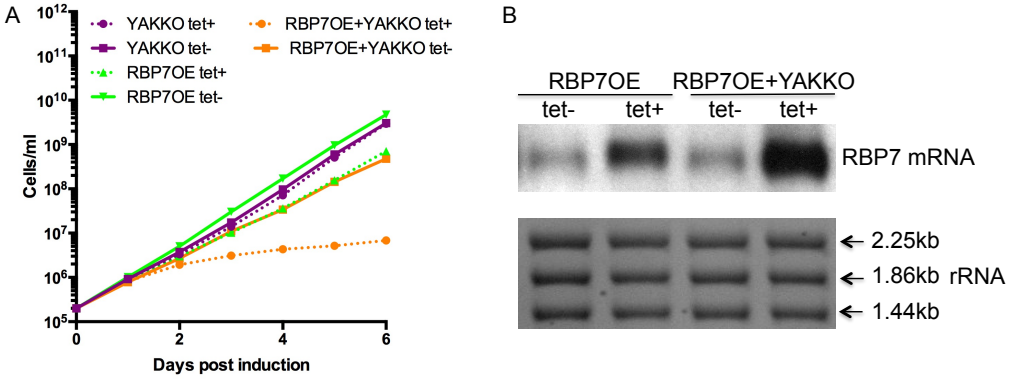

Figure 3.25 A) *In vitro* growth effect upon overexpression of RBP7 was still observed in a YAK null mutant background. B) Northern blot analysis shows upregulation of RBP7 transcript in the presence of tetracycline. rRNA was used as a loading control.

3.3.8 RBP7 OE + YAK KO: Overexpression of RBP7 results in YAK-independent stumpy formation *in vivo*

To explore the genetic interaction between RBP7 and YAK *in vivo*, Mice were infected with RBP7 OE + YAK KO parasites to assess their capacity to differentiate to stumpy forms *in vivo*. Doxycycline was introduced at day 0. In the untreated mice, the parasitaemia ascended rapidly whereas growth was significantly reduced upon the induction of overexpression (Figure 3.26A). Inducible overexpression of RBP7 was confirmed by Northern blot (Figure 3.26E). The induction of RBP7 overexpression also resulted in an increase in G_1 arrest, as determined by a significantly increased proportion of 1K1N cells (Figure 3.26B). The parasite populations in uninduced mice appeared morphologically slender whilst stumpy forms were observed upon the overexpression of RBP7 (Figure 3.26C). RBP7

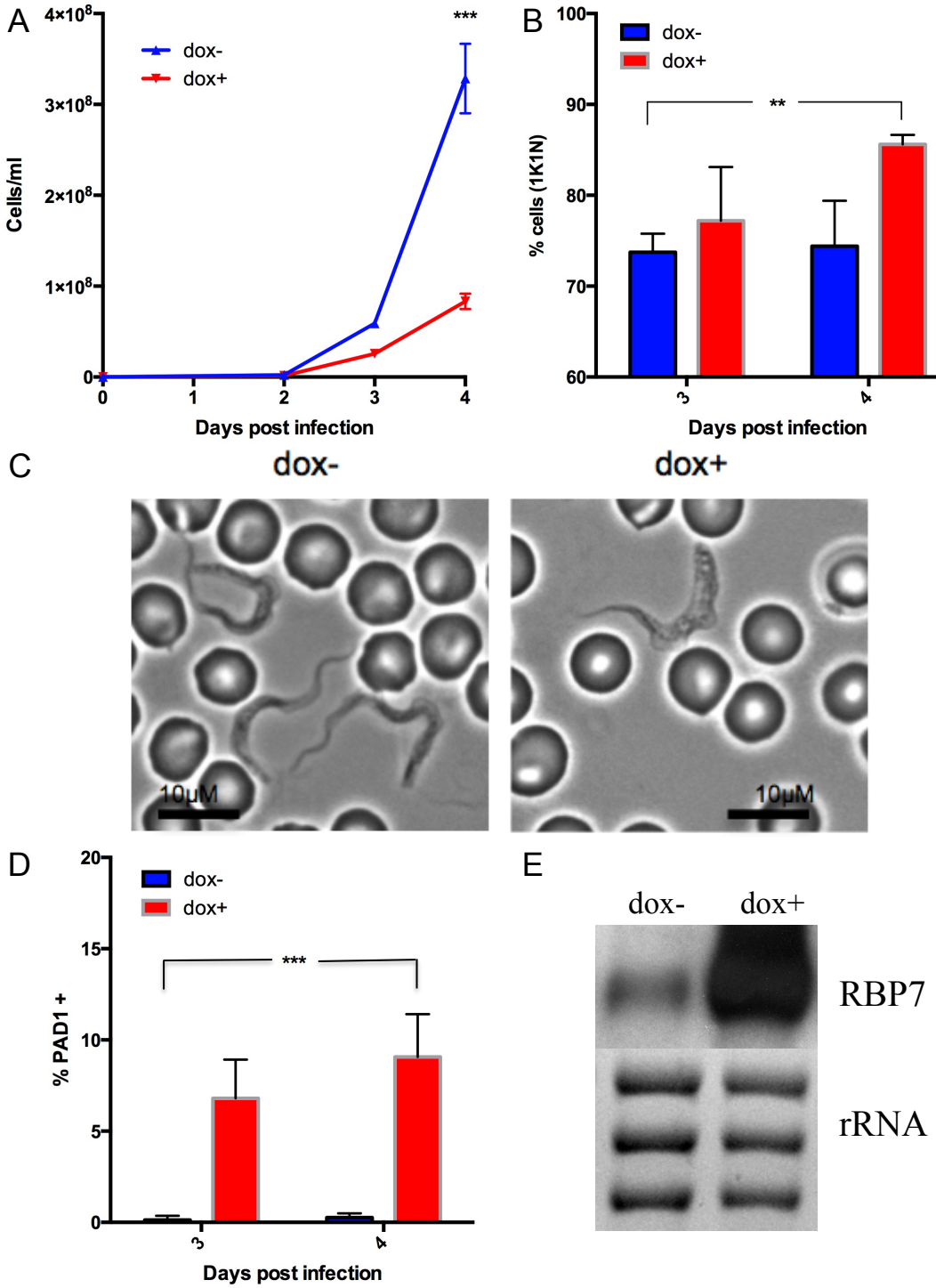

Figure 3.26 Stumpy formation by RBP7 *in vivo* is independent of YAK. A) Parasitaemia of mice infected with RBP7OE+YAKKO cells, estimated by the rapid matching method. Data represents 6 mice, 3 treated with doxycycline (dox+) and 3 non-induced (dox-). Growth was reduced in dox+. ***P<0.0005 GLM and Tukey test for multiplie comparisons. B) % 1K1N (representing G_1 and S phase) cells throughout the course of infection. 250 cells were counted for each sample. Induced cells have a higher proportion of 1K1N cells. **P<0.005 GLM. C) Phase contrast images from day 4 of infection. Untreated cells appear slender in morphology whereas dox+ cells were morphologically stumpy. D) % cells expressing PAD1 throughout the course of infection, determined by IFA. 250 cells were counted for each sample. PAD1 expression increases in dox+. ***P<0.0005 GLM. E) Northern blot analysis shows upregulation of RBP7 transcript in dox+. rRNA was used as a loading control.

overexpression also generated a small but significant upregulation of PAD1 expression from 0% in the untreated population on days 3 and 4 to 6.8 ± 1.2% and 9.1 ± 1.4% respectively in the induced parasites (Figure 3.26D). These results demonstrated that overexpression of RBP7 induces G_1 arrest and differentiation to stumpy forms *in vivo* independently of YAK.

3.3.9 HYP2 OE + RBP7 KO: Overexpression of HYP2 results in RBP7-independent stumpy formation *in vivo*

HYP2 has been overexpressed with an N-terminal TY tag in the AnTat 1.1 90:13 strain and shown to induce stumpy formation by Eleanor Silvester (thesis in preparation). The same construct was used to overexpress HYP2 in the RBP7 null mutant line. Induction of overexpression generated growth inhibition *in vivo* (Figure 3.27A), indicating that this phenotype is RBP7 independent. Although growth recovered later in the timecourse (Figure 3.27A), this was likely due to loss of the overexpression, which could no longer be detected 5 days post-induction (Figure 3.27B). Tagged overexpressed HYP2 has an expected size of 142 kDa. However, the BB2 antibody detected multiple bands of various sizes. With the exception of 1 non-specific band, none of these bands were detectable in the tet- samples, suggesting inducible expression, and the band pattern was consistent between the HYP2 OE and HYP2 OE + RBP7 KO lines (Figure 3.27B). Moreover, the additional bands were lost once growth recovered in the HYP2 OE + RBP7 KO line. This would suggest that these represent HYP2 or HYP2-derived protein products.

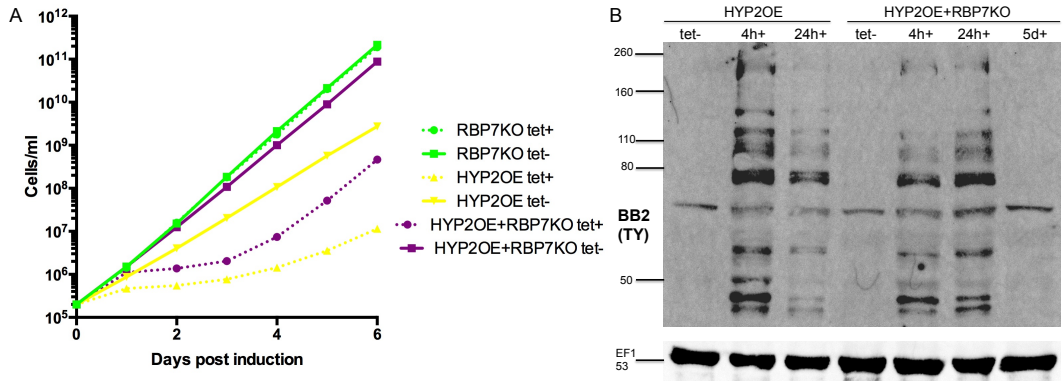

Figure 3.27 A) *In vitro* growth effect upon overexpression of HYP2 is still observed in an RBP7 null mutant background. B) Western blot analysis showed detection of bands of multiple sizes by the BB2 antibody recognizing the TY tag. EF1 was used as a loading control.

3.4 Phosphoproteomic analysis

The generation of null mutant lines of 2 *pos*ST kinases, MEKK1 and YAK, presented the opportunity to investigate changes in the phosphorylation profile on a global scale resulting from the loss of these proteins by phosphoproteomics, and thereby potentially identify downstream substrates. Protein was extracted and trypsinised in the presence of phosphatase inhibitors from quadruplicate *in vitro* cultures of slender MEKK1 KO, YAK KO and parental AnTat 1.1 90:13 parasites. At the FingerPrints Proteomic Facility at the University of Dundee, these samples were labelled with isobaric tandem mass tags (TMTs) and subjected to proteomic and phosphoproteomic quantitation by mass spectrometry. This process was carried out in 2 separate runs each involving 2 replicates of each cell line. Analysis of the data was carried out by Dr. Mathieu Cayla. Ratios were generated for the knockout samples relative to the AnTat 1.1 90:13 control replicates and protein ratios used to normalise phosphopeptide ratios.

The proteomic and phosphoproteomic datasets generated showed unexpected results for the two kinases investigated. In the first of the two runs, MEKK1 protein was unexpectedly detected in the knockout samples. However, it was excluded from the analysis due to detection at a reporter intensity of less than the cutoff value of 10,000 in these samples. In the second run, MEKK1 protein was not detected in any sample, although 7 phosphopeptides were attributed to it. Similarly, YAK protein was not detected in any sample in the first run. Although it was detected in the second run, it did not exceed the cutoff reporter intensity value in any samples. The low level detection of MEKK1 and YAK peptides in their respective null mutant lines may be due to a limitation of the methodology whereby pooling of the samples after TMT labelling and prior to fractionation can lead to co-isolation of peptides of similar sizes during mass spectrometry in fractions of high complexity. This issue can also lead to ratio compression in quantitation.

Overall, 105 proteins in the MEKK1 KO line and 176 proteins in the YAK KO line were found to have greater than 2-fold differential phosphorylation, of which 61 were common to both. In many proteins, multiple peptides were affected. These changes are depicted in Figure 3.29 and Figure 3.30. As shown in Figure 3.28, a

variety of protein classes are represented among the regulated phosphoproteins. As well as affecting a large number of hypothetical proteins, both KO lines resulted in increased and decreased phosphorylation of numerous kinases, phosphatases and RNA-binding proteins, indicating substantial perturbation of signalling pathways. The presence of various differentially regulated motor proteins, including many dyneins and kinesins, and flagellar proteins suggested effects on transport and motility.

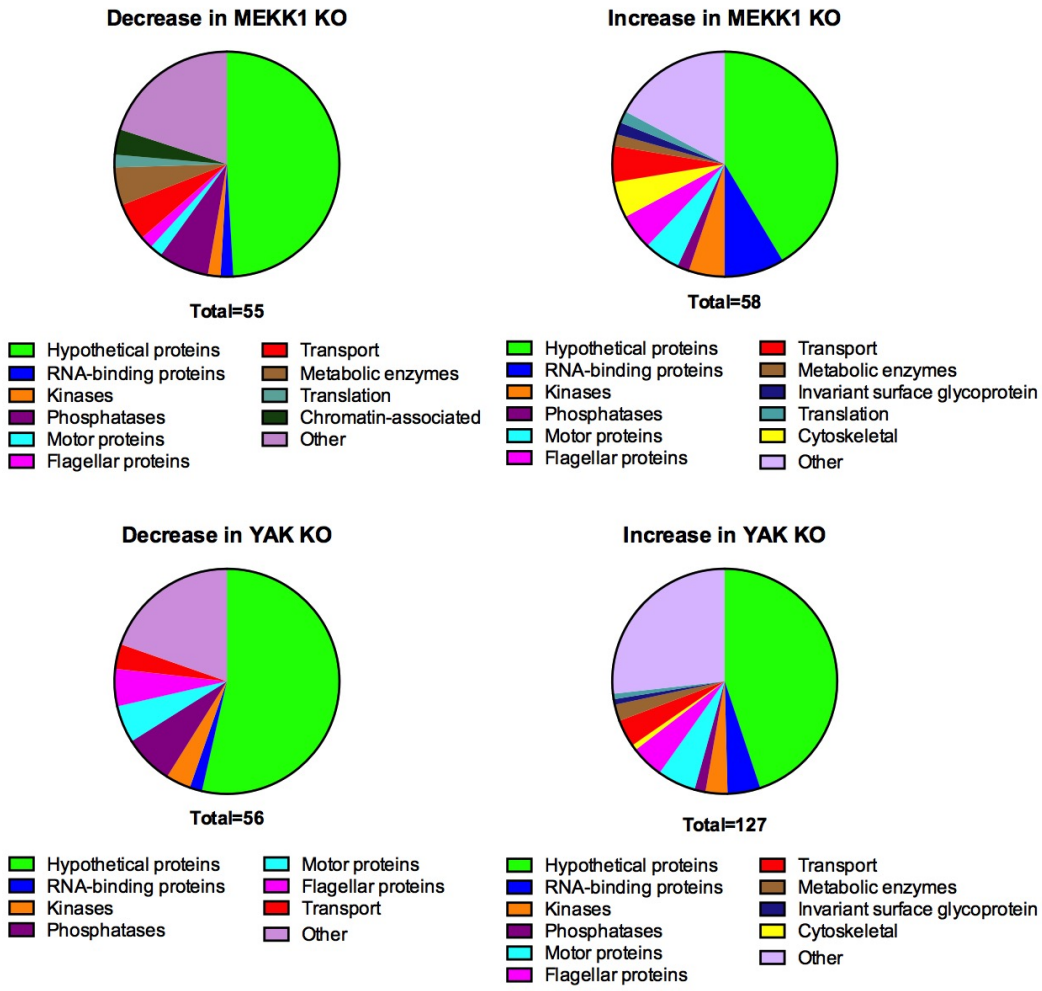

Figure 3.28 Differentially phosphorylated proteins grouped according to protein class.

Loss of MEKK1 affected the phosphorylation status of numerous cellular proteins. A number of examples of affected proteins are listed in Table 3.1. 55 proteins showed reduced phosphorylation, potentially including direct targets of the kinase, as well as proteins in which phosphorylation status is changed due to secondary or indirect effects. Notable among these was the *pos*ST component NEK, which indicates that

NEK likely operates downstream of MEKK1 in the *pos*ST pathway. A number of other proteins which showed reduced phosphorylation also had predicted roles in signal transduction, including 2 putative phosphatase 2C proteins (Tb927.4.4510 and Tb927.7.4020) and a predicted TFIIF-stimulated CTD phosphatase (Tb927.10.4180), while ZC3H34 (Tb927.10.12330) is a CCCH-type zinc finger RNA-binding protein (Kramer et al., 2010) shown to act as a post-transcriptional activator (Erben et al., 2014), making it a good candidate for a role as a downstream effector in a signalling cascade perturbed by loss of MEKK1. A predicted subunit of eukaryotic translation initiation factor 3 (eIF-3 beta) also showed reduced phosphorylation. Interestingly, according to RNAseq data (E. Silvester, thesis in preparation), eIF-3 beta mRNA is enriched 1.8 fold in the stumpy form, a stage associated with widespread repression of translation (Kabani et al., 2009).

Distinct signalling molecules were among the 58 proteins which showed increased phosphorylation upon MEKK1 KO (Figure 3.28 and Figure 3.29). One of these was the AMPK β subunit Tb927.8.2450, which is particularly intriguing as an α subunit of AMPK is a known *pos*ST component (Mony et al., 2014). 4 potential regulators showed increased phosphorylation. Of these, RBP42 (Tb927.6.4440), which acts on transcripts involved in energy metabolism (Das et al., 2012) and DRBD4 (Tb927.11.14100), were shown to result in post-transcriptional activation of an artificially tethered mRNA (Erben et al., 2014). In contrast, RBP12 (Tb927.10.13540) acted to repress mRNAs (Erben et al., 2014). Silencing of RBP35 (Tb927.9.12360) resulted in increased fitness during differentiation (Alsford et al., 2011). A putative C3HC4 zinc finger RING-type protein (Tb927.8.4570) contained the most highly upregulated phosphopeptides in both the MEKK1 and YAK KO lines. RING finger domain containing proteins are often involved in ubiquitination (Lorick et al., 1999).

Figure 3.29 Distribution of phosphopeptides showing greater than 2 fold differential phosphorylation in MEKK1 KO cells relative to parental AnTat 1.1 90:13 cells. Log_2 of the phosphopeptide:protein ratio normalised to AnTat controls is shown for each replicate of each phosphopeptide in which the value is greater than 1 or less than -1. Dot size is proportional to TMT reporter intensity.

56 proteins showed reduced phosphorylation in the YAK KO line (Figure 3.28 and Figure 3.30), and were therefore potential YAK targets. These included two predicted PPP phosphatases, one of which (Tb927.4.4510) was also dephosphorylated in the MEKK1 KO line. Two paraflagellar rod components (Tb927.8.1550 And Tb927.8.6660) also showed reduced phosphorylation. KKT4 (Tb927.8.3680), a member of the unusual kinetoplastid specific kinetochore proteins (Akiyoshi and Gull, 2014), showed both increased and decreased phosphorylation on different residues, and was also dephosphorylated in the MEKK1 KO line. Interestingly, a NEK kinase, NRKC (Tb927.10.460), was dephosphorylated in the absence of YAK. Unlike NEK and NRKA/B (Domingo-Sananes et al., 2015), NRKC has not been previously implicated in differentiation, but has been shown to have a role in basal body separation (Pradel et al., 2006).

A much larger cohort of proteins showed enriched phosphorylation in the YAK KO line. This included a large complement of motor proteins (6). Phosphopeptides were also enriched for six flagellar proteins, including four of the eight FLAM (FLAgellar Member) proteins recently identified by proteomic analysis and experimentally validated by Subota *et al.* (2014), which showed distinct suborganellar localisations and dynamics. All 4 RNA-binding proteins with increased phosphorylation in the MEKK1 KO line showed the same effect in the YAK KO. In addition, the RNA-binding protein ZC3H34, which was dephosphorylated in the absence of MEKK1, showed increased phosphorylation at a different residue in the YAK KO line. The mRNA-stabilising factor MKT1 also showed increased phosphorylation. This is intriguing as MKT1 has been shown to interact with HYP2 (Singh et al., 2014) and also ZC3H20, a zinc finger protein identified in an RNAi library screen for resistance to the stumpy inducing compound GKI7 (see section 5.6). A selection of proteins of interest showing differential phosphorylation in one or both null mutant lines are listed in Table 3.1.

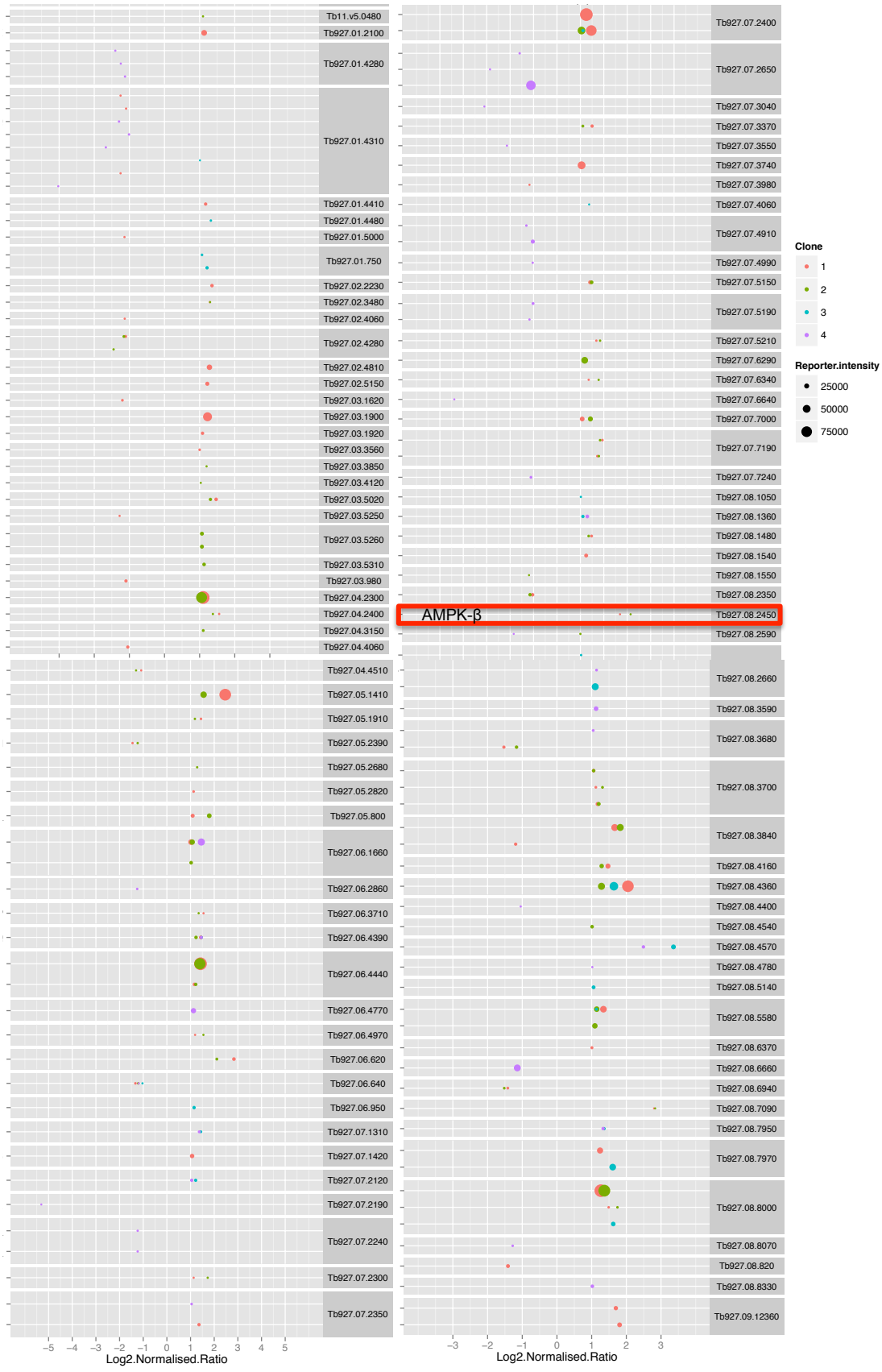
Tb11.v5.0480
Tb927.01.2100
Tb927.01.4280
Tb927.01.4310
Tb927.01.4410
Tb927.01.4480
Tb927.01.5000
Tb927.01.750
Tb927.02.2230
Tb927.02.3480
Tb927.02.4060
Tb927.02.4280
Tb927.02.4810
Tb927.02.5150
Tb927.03.1620
Tb927.03.1900
Tb927.03.1920
Tb927.03.3560
Tb927.03.3850
Tb927.03.4120
Tb927.03.5020
Tb927.03.5250
Tb927.03.5260
Tb927.03.5310
Tb927.03.980
Tb927.04.2300
Tb927.04.2400
Tb927.04.3150
Tb927.04.4060
Tb927.04.4510
Tb927.05.1410
Tb927.05.1910
Tb927.05.2390
Tb927.05.2680
Tb927.05.2820
Tb927.05.800
Tb927.06.1660
Tb927.06.2860
Tb927.06.3710
Tb927.06.4390
Tb927.06.4440
Tb927.06.4770
Tb927.06.4970
Tb927.06.620
Tb927.06.640
Tb927.06.950
Tb927.07.1310
Tb927.07.1420
Tb927.07.2120
Tb927.07.2190
Tb927.07.2240
Tb927.07.2300
Tb927.07.2350
−5 −4 −3 −2 −1 0 1 2 3 4 5
Log2.Normalised.Ratio
Tb927.07.2400
Tb927.07.2650
Tb927.07.3040
Tb927.07.3370
Tb927.07.3550
Tb927.07.3740
Tb927.07.3980
Tb927.07.4060
Tb927.07.4910
Tb927.07.4990
Tb927.07.5150
Tb927.07.5190
Tb927.07.5210
Tb927.07.6290
Tb927.07.6340
Tb927.07.6640
Tb927.07.7000
Tb927.07.7190
Tb927.07.7240
Tb927.08.1050
Tb927.08.1360
Tb927.08.1480
Tb927.08.1540
Tb927.08.1550
Tb927.08.2350
AMPK-β
Tb927.08.2450
Tb927.08.2590
Tb927.08.2660
Tb927.08.3590
Tb927.08.3680
Tb927.08.3700
Tb927.08.3840
Tb927.08.4160
Tb927.08.4360
Tb927.08.4400
Tb927.08.4540
Tb927.08.4570
Tb927.08.4780
Tb927.08.5140
Tb927.08.5580
Tb927.08.6370
Tb927.08.6660
Tb927.08.6940
Tb927.08.7090
Tb927.08.7950
Tb927.08.7970
Tb927.08.8000
Tb927.08.8070
Tb927.08.820
Tb927.08.8330
Tb927.09.12360
−3 −2 −1 0 1 2 3
Log2.Normalised.Ratio
Clone
1
2
3
4
Reporter.intensity
25000
50000
75000

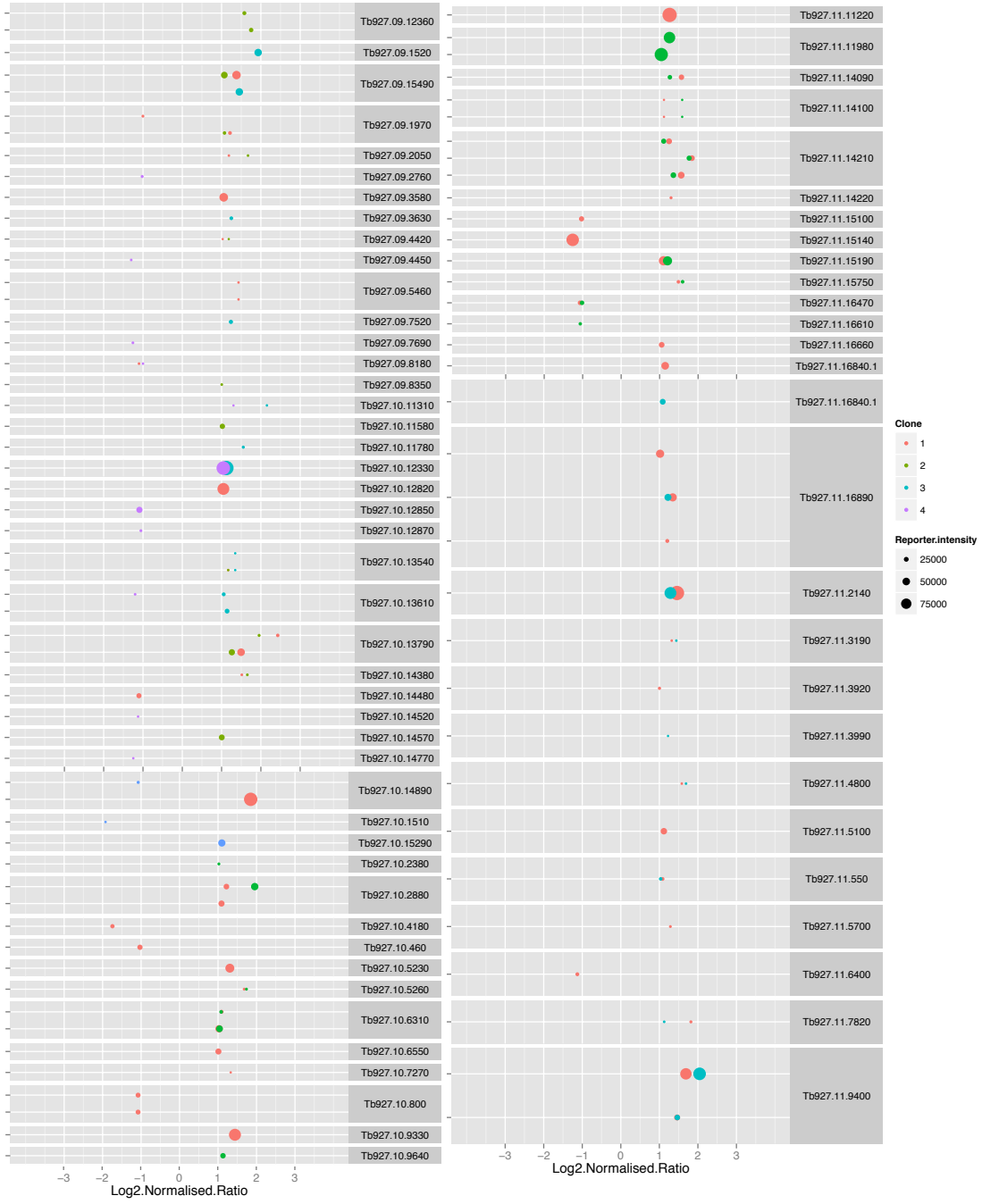

Figure 3.30 Distribution of phosphopeptides showing greater than 2 fold differential phosphorylation in YAK KO cells relative to parental AnTat 1.1 90:13 cells. Log_2 of the phosphopeptide:protein ratio normalised to AnTat controls is shown for each replicate of each phosphopeptide in which the value is greater than 1 or less than -1. Dot size is proportional to TMT reporter intensity.

Accession no.	Description	MEKK1KO	YAKKO	Diff
Tb927.3.5020	Flagellar Member 6 (FLAM6)		+	No
Tb927.4.4510	protein phosphatase 2C, putative	-	-	No
Tb927.6.640	kinetoplastid-specific phospho-protein phosphatase, putative		-	No
Tb927.6.4770	protein mkt1, putative (MKT1)		+	Yes
Tb927.6.4440	RNA-binding protein 42 (RNA-binding motif protein 42) (RBP42)	+	+	Yes
Tb927.7.4020	protein phosphatase 2C, putative	-		No
Tb927.8.1550	paraflagellar rod component, putative (PFC3)		-	Yes
Tb927.8.2450	5'-AMP-activated protein kinase subunit beta (AMPKB)	+	+	No
Tb927.8.3680	kinetoplastid kinetochore protein 4 (kkt4)	-	-/+	Yes
Tb927.8.4570	Zinc finger, C3HC4 type (RING finger), putative	+	+	No
Tb927.8.4780	Flagellar Member 3 (FLAM3)	+	+	Yes
Tb927.8.6660	paraflagellar rod component, putative (PFC1)		-	Yes
Tb927.8.7950	Flagellar Member 4 (FLAM4)		+	No
Tb927.9.12360	RNA-binding protein, putative (RBP35)	+	+	No
Tb927.9.5460	Eukaryotic translation initiation factor 4 gamma type 2 (eif4g2)		+	No
Tb927.10.460	NIMA-related protein kinase (NRKC)		-	No
Tb927.10.4180	TFIIF-stimulated CTD phosphatase, putative	-		Yes
Tb927.10.5950	NEK kinase	-		No
Tb927.10.11310	intraflagellar transport protein 57/55 (IFT57/55)		+	Yes
Tb927.10.12330	zinc finger protein family member, putative (ZC3H34)	-	+	Yes
Tb927.10.13540	RNA-binding protein, putative (RBP12)	+	+	No
Tb927.11.9610	eukaryotic translation initiation factor 3 subunit 2, putative (eIF-3 beta)	-		No
Tb927.11.14100	DRBD4 (DRBD4)	+	+	No
Tb927.11.16890	Tetratricopeptide-like helical domain containing protein (FLAM7)		+	Yes
Tb927.3.5310	paraflagellar rod protein		+	Yes

Table 3.1 Selection of proteins showing greater than 2 fold differential phosphorylation in the MEKK1 or YAK null mutant lines. Phosphopeptides were either increased (+) or decreased (-).The final column refers to whether a reduced fitness phenotype was observed upon differentiation in a RIT-seq screen (Alsford et al., 2011).

3.5 Discussion

3.5.1 Involvement of a number of *pos*ST screen hits in stumpy formation has been clarified.

To determine the full complement of stumpy signalling molecules which can be extracted from the *pos*ST RNAi library screen, independent validation of each hit is necessary. This had already been carried out for many candidate genes by the generation of individual RNAi lines, and in the majority of cases this confirmed that silencing of these genes conferred loss of responsiveness to the SIF differentiation signal (Mony et al., 2014). In several cases where this phenotype was not observed, the hits in question were enzymes involved in purine metabolism and homeostasis. Hence, analysis of RNAi lines of adenylosuccinate synthetase (ADSS) and adenylosuccinate lyase (ADSL), which are involved in conversion of inosine monophosphate (IMP) to AMP, showed growth inhibition which could be alleviated by pCPTcAMP treatment. This suggests that these enzymes were selected in the screen due to a restoration of purine balance in the parasites by the analogues, alleviating growth inhibition. Adenosine kinase is another purine pathway enzyme identified in the screen, but unlike ADSS and ADSL, it showed no growth inhibition upon RNAi. This is in agreement with observations by Luscher *et al.* (2007). However, AK RNAi did confer loss of responsiveness to pCPTcAMP in both monomorphs (section 3.2.1.1) and pleomorphs (section 3.2.1.2). While this initially indicated a role in differentiation, no corresponding resistance to SIF could be observed when the cell line was analysed *in vivo* (section 3.2.1.3). This disparity may be due to the distinct properties of the pCPTcAMP analogue used in the *in vitro* experiment when compared to the biological activity of SIF. This analogue is hydrolysed and dephosphorylated to a corresponding adenosine analogue in culture, and therefore rephosphorylation would be required after cell entry (Laxman et al., 2006). It is possible that this dephosphorylated analogue is recognised by AK, but not the enzymes of the alternative cleavage-dependent pathway, such that its action is dependent on AK. Hence, while the analogue is prevented at this stage from inducing differentiation in AK RNAi induced cells, *in vivo*, endogenous adenosine could circumvent this loss by phosphorylation via the alternative pathway such that differentiation remains unaffected. An alternative explanation for these findings is

that AK acts in a stage of the cAMP-induced differentiation pathway upstream of its intersection with the SIF signaling pathway.

Another enzyme identified in the screen, PP2A, was independently analysed by RNAi in a monomorphic strain (section 3.2.2.1). In accordance with a previous study by Rothberg *et al.* (2014), this resulted in severe growth inhibition which precluded further analysis. It is likely that the identification of PP2A resulted from its substantial shared homology with validated *pos*ST, PP1.

Mony *et al*. (2014) determined that MEKK1 RNAi conferred loss of responsiveness to pCPTcAMP in a monomorphic strain. Generation of an RNAi line in a pleomorphic strain was used to demonstrate a role for the kinase in differentiation *in vitro* (section 3.2.3.2) and *in vivo* (section 3.2.3.1). This is intriguing as it suggests involvement of the MAPK pathway in SIF signal transduction.

To further investigate the role of MEKK1 in stumpy formation, 2 forms of the kinase were overexpressed in pleomorphic trypanosomes: the full length protein and the truncated C-terminal catalytic domain. In a number of other systems, expression of the latter is constitutively active due to loss of repression by the regulatory N-terminal domain (Gibson et al., 1999; Mizote et al., 2010; Owen et al., 2013; van Drogen et al., 2000). Overexpression of the full length MEKK1 inhibited growth *in vitro* (section 3.2.3.5 and 3.2.3.7), similar to the differentiation-associated growth arrest which has been observed upon overexpression of other *pos*ST proteins. Interestingly, this was observed even in a monomorphic strain, suggesting that MEKK1 is able to drive stumpy formation in parasites unresponsive to the SIF signal. Surprisingly, despite the growth phenotype, the overexpressed protein could not be detected by an antibody to its TY epitope tag (section 3.2.3.6). The result was the same when the epitope tag was switched from the N terminal to the C terminal of the protein, excluding the possibility that the tag was lost upon cleavage of an N-terminal targeting signal (section 3.2.3.7). When analysed at the transcript level, there was no apparent increase in MEKK1 mRNA upon induction of overexpression. However, when the same construct was used to overexpress MEKK1 in a MEKK1 null mutant background, MEKK1 transcript abundance was restored, though not

enriched (section 3.2.3.8). This suggests that MEKK1 can be exogenously expressed by the construct, but is unable to increase transcript abundance above endogenous levels. This may be an indication of an unknown regulatory mechanism, which is discussed further in section 3.5.4. Overexpression of the catalytic domain, in contrast, had no effect on growth, but was clearly detectable via its epitope tag (section 3.2.3.5). In the absence of kinase assays to determine the activity of the truncated protein, it can only be speculated as to whether it is indeed constitutively active. However, as constitutive transduction of the differentiation signal would be predicted to be antiproliferative, the absence of any growth phenotype indicates that this is not the case. This may reflect differences between the trypanosome kinase and those of other systems. Another possibility is that the truncated protein is active but mislocalised. There are 2 predicted transmembrane domains in the excised N-terminal portion which may confer targeting essential for protein function. CatMEKK1 expression can be detected by immunofluorescence (sections 3.2.3.6 and 3.2.3.7) but in the absence of detectable full length MEKK1, it is impossible to determine whether the staining pattern reflects typical MEKK1 localisation.

3.5.2 Null mutants of *pos*ST genes reduce differentiation in vivo and represent a clean genetic background in which to carry out further manipulations.

RNAi has been used to effectively demonstrate involvement of numerous *pos*ST components in stumpy signalling (section 3.2.3.2)(Mony et al., 2014). However, in most cases, some degree of differentiation is still observed. Using RNAi, it is not possible to determine whether residual stumpy formation represents a non-absolute requirement for the *pos*ST component in question for differentiation to proceed or is a consequence of incomplete transcript knockdown. It is also problematic to use in combination with overexpression to analyse the relative positioning of distinct *pos*ST proteins. This is because RNAi and overexpression systems may proceed with different kinetics but cannot be separately controlled, since both are subject to tetracycline induction. The generation of null mutants represents an alternative option with the capacity to clarify the absolute requirement of different *pos*ST components for differentiation and to provide a “clean” background in which to execute further genetic manipulations. Fortunately, existing RNAi data indicated that

most *pos*ST components studied were non-essential, with the notable exception of PP1 (section 3.2.3.2)(Mony et al., 2014), making null mutant production feasible. An established transfection protocol in the pleomorphic strain AnTat 1.1 90:13 has been extensively used in our laboratory for generation of RNAi and overexpression lines (MacGregor et al., 2013). However, YAK was the first gene to be successfully knocked out in these parasites (P. MacGregor and K Matthews, unpublished), demonstrating the feasibility of generating null mutants in this strain using the system of sequential allelic replacement outlined in section 3.2.3.3. In this chapter, the generation of null mutants of 3 more *pos*ST components – MEKK1, HYP2 and RBP7 – is described (sections 3.2.3.3, 3.2.4.1 and 3.2.5.1). *In vivo*, these lines proliferate rapidly to high parasitaemia and show dramatically compromised stumpy formation. However, the continued increase in the proportion of 1K1N cells throughout the course of infection and the appearance of some PAD1 expression at later timepoints indicate that a limited level of stumpy formation remains possible in the total absence of each of these 3 components (sections 3.2.3.4 and 3.2.5.2; E. Silvester, thesis in preparation). The YAK and RBP7 null mutant lines have successfully been further modified to overexpress distinct *pos*ST components, revealing information about the dependency relationships of the signalling pathway components, discussed in the following section, while phosphoproteomic analysis of MEKK1 and YAK null mutants has provided insight into the downstream effects of these signalling molecules, discussed in section 3.5.5.

3.5.3 Combined overexpression and knockout of *pos*ST proteins can be used to reveal the organisation of the differentiation signalling pathway.

To explore the dependency relationships between *pos*ST components with respect to each other, a combinatorial overexpression and knockout approach was used in which one *pos*ST gene was overexpressed in the a null mutant background of a distinct *pos*ST gene and the differentiation phenotype analysed, as depicted in Figure 3.16. First, to demonstrate proof of principle, RBP7 was overexpressed in an RBP7 null mutant background (section 3.2.5.3). This resulted in growth inhibition *in vitro* similar to the effect observed when RBP7 is overexpressed in a wild type

background, demonstrating that stumpy formation could be restored by exogenous introduction of RBP7.

Overexpression of NEK in a wild type background resulted in growth inhibition *in vitro*. This growth defect was completely rescued when NEK was overexpressed in the RBP7 null mutant line (section 3.3.1), indicating that stumpy formation by NEK is RBP7 dependent. It is likely that RBP7 operates downstream of NEK and that NEK is part of a signalling relay which triggers RBP7 to induce expression changes related to differentiation. In contrast, the growth defect was retained when NEK was overexpressed in the YAK null mutant (section 3.3.2), indicating that stumpy formation by NEK is independent of YAK.

Overexpression of PP1 in the RBP7 null mutant line resulted in growth inhibition *in vitro* as in the wild type background (section 3.3.3). When overexpression was induced *in vivo*, it resulted in a rapid inhibition of the ascending parasitaemia accompanied by appearance of morphologically stumpy forms, increased G_1 arrest, PAD1 expression and capacity to differentiate to procyclic forms (section 3.3.4). Stumpy formation by PP1 therefore appears to be independent of RBP7. While it is possible that PP1 operates directly downstream of RBP7, this seems unlikely given their putative roles in signalling and modulation of expression respectively. An alternative hypothesis is that PP1 and RBP7 act on separate branches of the differentiation pathway and their actions are therefore independent. A cell line with opposing gene modifications – ie. RBP7 overexpression and PP1 knockout – would be useful in exploring this hypothesis but unfortunately the apparent essentiality of PP1 (Mony et al., 2014) likely precludes successful generation of a knockout using this strategy.

As in the wild type and RBP7 knockout backgrounds, overexpression of PP1 in the YAK null mutant background resulted in severe growth inhibition *in vitro* and *in vivo* (sections 3.3.5 and 3.3.6). In contrast, PAD1 expression in this cell line was negligible, and when induced to differentiate to procyclic forms, EP procyclin expression was not significantly elevated relative to uninduced parasites. This would suggest that PP1-induced stumpy formation is in fact YAK-dependent and that the 2 proteins act on the same branch of the stumpy signalling pathway. One possibility is

that PP1 operates directly upstream of YAK and its action is therefore blocked downstream when YAK is absent. An alternative explanation is that PP1 is activated by YAK phosphorylation and loss of the latter blocks its action by locking PP1 in an inactive form. However, phosphoproteomic analysis of the YAK null mutant showed no evidence of changes in the phosphorylation status of PP1 (section 3.4). Another question posed by this result is why deletion of YAK blocked differentiation by PP1, but not growth inhibition. The growth phenotype observed upon PP1 overexpression is more severe than for other *pos*ST components, with proliferation completely arrested within 24 hours of induction *in vivo*. In addition, PP1 RNAi results in growth inhibition in culture, suggesting it is essential for normal growth of slender forms as well as differentiation. One possibility is that PP1 has one function unrelated to differentiation which is independent of YAK and a separate YAK-dependent function in stumpy formation. The discrepancy between the YAK-dependent differentiation and YAK-independent growth inhibition also highlights the importance of *in vivo* analysis in ordering *pos*ST components using this strategy, as *in vitro* evidence alone indicated an entirely different relationship between these 2 proteins.

Microscopic examination of DAPI-stained cells revealed that PP1 overexpression in the YAK null mutant background also affected nuclear shape. Nuclei in these cells were unusually elongated and curved in morphology (Figure 3.24). The reason for this phenotype, which is not observed with either PP1 overexpression or YAK knockout alone, is unknown. Although the cells have a KN profile similar to that of slender cells, this measure of cell cycle only accounts for kinetoplast segregation and nuclear division and does not take account of DNA replication. It is unknown if the misshapen nuclei contain an atypical quantity of DNA. One possibility is that the combined excess of PP1 and absence of YAK locks the cells in a stasis in which DNA proliferation proceeds but nuclear division is prevented, resulting in amorphous nuclei with multiple genomic copies, although it is worth noting that this morphology is also observed in dividing 2K1N and 2K2N cells. This could be explored in future by using flow cytometry to quantify DNA content. Another possibility is that the morphological rearrangements associated with differentiation to stumpy forms are

disturbed by the opposing developmental influences of PP1 overexpression and YAK knockout.

From the above results, it is hypothesised that PP1 acts on the same branch of the pathway as YAK, but on a distinct branch to RBP7. Therefore, it would be expected that YAK and RBP7 would be positioned on different branches to each other. This was explored by overexpression of RBP7 in the YAK null mutant line. Growth inhibition *in vitro* and *in vivo* and restoration of stumpy formation demonstrated that differentiation by RBP7 is YAK independent (sections 3.3.7 and 3.3.8). This is consistent with the hypothesis that PP1 and YAK act on a branch of the pathway distinct to that of RBP7.

Overexpression of HYP2 in the RBP7 null mutant line resulted in RBP7-independent growth inhibition *in vitro*. While it could be speculated that HYP2 might therefore be found on the pathway branch separate from that of RBP7, the example of the PP1 overexpression plus YAK knockout line demonstrates that an independent growth phenotype does not necessarily equate to an independent differentiation phenotype. Hence, this position remains highly tentative until this cell line is tested *in vivo*.

A further piece of information regarding ordering of the *pos*ST components is provided by the phosphoproteomic analysis of the MEKK1 null mutant, which shows a significant reduction in phosphorylation of NEK (section 3.4), suggesting that NEK is a direct or indirect substrate of MEKK1. This would place MEKK1 upstream of NEK and consequently RBP7.

OE	**KO**	Stumpy formation
PP1	RBP7	PP1 is independent of RBP7
PP1	YAK	PP1 is dependent on YAK
RBP7	YAK	RBP7 is independent of YAK
NEK	RBP7	NEK is dependent on RBP7
NEK	YAK	NEK is independent of YAK
HYP2	RBP7	HYP2 is independent of RBP7 (in vitro)

Table 3.2 Summary of overexpression (OE) and knockout (KO) combinations of *pos*ST components. OE promotes differentiation determined to be either dependent or independent of KO gene.

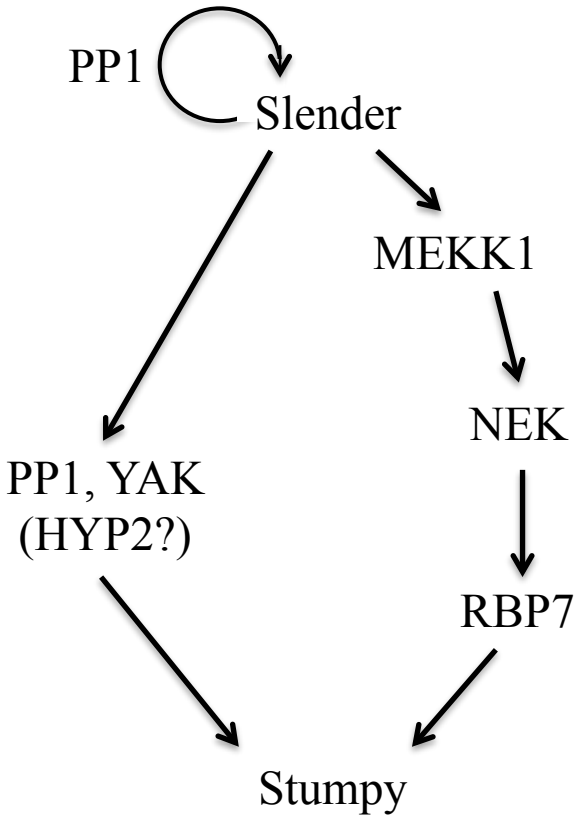

Figure 3.31 Model of *pos*ST stumpy signalling pathway according to results listed in Table 3.2.

The results from the numerous overexpression and knockout combinations tested are collated in Table 3.2 and enable construction of a model of the *pos*ST signalling pathway. According to the model depicted in Figure 3.31, the pathway can be divided into 2 branches. One branch includes PP1 and YAK in an as yet unknown order. It also tentatively includes HYP2 pending *in vivo* analysis of HYP2 OE + RBP7 KO and generation of further combinations including HYP2. PP1 likely also performs a separate role in slender forms. On the other branch of the pathway, MEKK1 acts upstream of NEK according to phosphoproteomic data, which in turn acts upstream of RBP7.

The pathway described here bears analogy to the signalling networks associated with glucose depletion in yeast. Similar to stumpy formation in trypanosomes, this response triggers metabolic adaptation to oxidative phosphorylation, G_1 arrest and widespread transcriptional changes (Brauer et al., 2008; DeRisi et al., 1997). Homologues of PP1 and YAK are implicated in this process (Garrett and Broach, 1989; Tu and Carlson, 1995), while homologues of an AMP-activated kinase

(AMPK) and a regulatory subunit of protein kinase A (PKA-R), both identified in the *pos*ST cohort (Mony et al., 2014) but not investigated in this thesis, act as central regulators (Toda et al., 1987; Woods et al., 1994). Yeast Yak1 performs an analogous quiescence-promoting role which is at least partially dependent on PKA (Garrett et al., 1991; Lee et al., 2011). In contrast to the trypansosome pathway, the yeast PP1 Glc7, in conjunction with its regulatory subunit Reg1, inactivates the yeast AMPK homologue Snf1 in the presence of glucose, inhibiting energy production by alternative carbon sources (Tu and Carlson, 1995). This indicates differences between the two systems, as PP1 and AMPK are both positive regulators of differentiation in *T. brucei* (B. Mony and K. Matthews, unpublished results). However, given that both systems involve an external signal (glucose depletion/SIF) triggering parallel, interconnected signalling pathways which include multiple common components and induce multiple common cellular processes, the established relationships of the yeast pathway may serve as a useful guide in further ordering of the trypanosome pathway.

Overall, these results validate overexpression and null mutant combinations as an effective strategy to identify dependency relationships in the *pos*ST signalling pathway. The model here can be built on, strengthened and expanded as further combinations are tested. Null mutants exist for both HYP2 and MEKK1, relatively unexplored via combinations at this point, which should facilitate further incorporation of these components into the model. In addition, there exist numerous other validated *pos*ST components which were not studied in this chapter and are excellent candidates for future inclusion.

3.5.4 A regulatory mechanism controls expression of differentiation signalling components?

A number of *pos*ST overexpression lines studied here showed evidence of potential limitation of expression levels. Firstly, overexpression of NEK in the RBP7 null mutant line showed a far greater level of protein expression than when overexpressed in the wild type background (section 3.3.1). As RBP7 knockout completely rescues the growth phenotype associated with NEK overexpression and is consequently hypothesised to act directly downstream of NEK, it is possible that the enhanced

expression level reflects accumulation of upstream pathway components in the absence of RBP7. The antibody used to measure expression levels of NEK recognises the epitope tag rather than the protein. As such, it can only identify the exogenous copy which does not include the endogenous NEK UTRs and it is therefore likely that any such accumulation would be mediated via the coding region or at a post-translational level. Enhanced NEK expression levels were also apparent when NEK is overexpressed in the YAK null mutant background, although growth inhibition is still observed in this line (section 3.3.2). Although other lines would need to be tested, if repeated it might indicate a general regulatory mechanism which limits overexpression in stumpy forms. In this case, NEK overexpression is restricted in the AnTat 1.1 90:13 background as a relatively low amount of protein induces differentiation. As knockout of RBP7 completely rescues this arrest, the cells remain slender and NEK overexpression is consequently unrestricted and is therefore expressed to a much higher level. Similarly, overexpression of MEKK1 cannot be detected at mRNA or protein level despite its ability to inhibit growth and restore transcript detection in a MEKK1 null mutant line (section 3.2.3.8).

It is possible that *T. brucei* harbours an intrinsic regulatory mechanism which limits *pos*ST-mediated stumpy formation to a maximum tolerated level of arrest at low density. However, another explanation is that overexpression is downregulated in stumpy forms due to the properties of the pDex577-Y plasmid. Sequences transcribed from this plasmid are conjugated to the aldolase 3'UTR (see map in Appendix D Figure 5). According to RNAseq data, aldolase is downregulated 3.5-fold in stumpy forms relative to slender forms (E. Silvester, thesis in preparation). Work is currently underway to modify the plasmid, replacing the aldolase 3'UTR with an actin 3'UTR which remains unchanged during differentiation (E. Vidal, unpublished). The new vector should be capable of robust overexpression in stumpy forms, a key resource for future *pos*ST analyses.

3.5.5 Phosphoproteomic analysis of null mutants reveals downstream effects of MEKK1 and YAK.

To further investigate the *pos*ST signalling pathway, changes in the phosphoproteome were examined in null mutant lines of two *pos*ST kinases,

MEKK1 and YAK. Four replicates of each cell line were subjected to proteomic and phosphoproteomic analysis, although the samples were split into two distinct sets of two replicates each at the labelling stage. The final dataset showed inconsistencies between the two sets, with MEKK1 protein being detected only in the first set of replicates and YAK protein detected only in the second, although due to the low level of detection, this was later excluded from the analysis. MEKK1 protein was detected in the MEKK1 KO samples in the first replicate set, but did not exceed the cutoff reporter intensity value and was therefore removed in these samples. YAK was not detected above the cutoff value in any samples, indicating low expression in slender bloodstream cells. The low level detection of MEKK1 and YAK in their respective null mutant lines may be a consequence of the TMT labelling procedure, in which the samples are pooled prior to fractionation. If high complexity is retained after fractionation, this can lead to co-isolation of peptides of similar sizes during mass spectrometry. This issue can also lead to ratio compression in quantitation. As a result, it is likely that some proteins with altered phosphorylation status were not detected in this analysis and that the effect on others was reduced.

220 proteins showed a greater than 2-fold change in phosphorylation in one or both KO lines, many of which had not previously been implicated in differentiation. 105 proteins in the MEKK1 KO line and 176 proteins in the YAK KO line were differentially regulated, of which 61 proteins were common to both. This indicated that both kinases elicit common downstream responses as well as additional effects specific to each. One explanation for this is that MEKK1 and YAK act through distinct branches of the stumpy signalling pathway which converge later in the process. However, it is entirely possible that these kinases have additional roles unrelated to differentiation which result in distinct effects.

The set of differentially phosphorylated proteins included many hypothetical proteins, as well as a large number of signalling molecules (Figure 3.28). Numerous kinases and phosphatases indicated that signalling cascades were affected in the KO lines, while a large representation of RNA-binding proteins and other post-transcriptional regulators presented potential downstream effectors of these pathways. Interestingly, differential phosphorylation was also observed in a large

number of motor proteins, including various kinesins and dynein components. While kinesins and dyneins are involved in a wide range of cellular processes, the concomitant changes in phosphorylation of a substantial set of flagellar proteins, and the predicted flagellum localisation of various identified motor proteins, indicated that this may be due to effects of MEKK1 and YAK on flagellar processes. Flagellar motility is powered by axonemal dynein motors (Langousis and Hill, 2014) while kinesins have been implicated in PFR assembly (Demonchy et al., 2009) and intraflagellar transport (Kozminski et al., 1995). Flagellum transcripts have previously been shown to be enriched in slender forms relative to stumpy forms (Jensen et al., 2009). It is possible that the action of MEKK1 and YAK mediates deactivation of flagellum formation in arrested stumpy forms.

The 55 proteins in which phosphorylation decreased in the MEKK1 KO line represent a set of potential kinase substrates (Figure 3.29). The most notable of these, in terms of *pos*ST pathway organisation, was the *pos*ST component NEK. The relationship between MEKK1 and NEK has not been investigated by combinatorial overexpression and knockout. However, this result indicates that NEK acts downstream of MEKK1 and may even be directly phosphorylated by MEKK1. Collated with the results from the overexpression and knockout combinations, this would place MEKK1 upstream of both NEK and RBP7 in the signalling pathway (Figure 3.31).

Other potential effectors of signal transduction which showed reduced phosphorylation in the MEKK1 KO line and would therefore be predicted to operate downstream of MEKK1 included two predicted phosphatase 2C proteins, a putative TFIIF-stimulated CTD phosphatase and the CCCH-type zinc finger RNA-binding protein ZC3H34, which was shown to act as a post-transcriptional activator in an mRNA tethering screen (Erben et al., 2014). This suggests that loss of MEKK1 has substantial effects on downstream signalling pathways, including kinases and phosphatases as well as regulators of gene expression.

Phosphorylation was also depleted in the predicted translation initiation factor subunit eIF-3 beta. Translation undergoes global repression during the transition to the stumpy form (Brecht and Parsons, 1998). However, comparison of the slender

and stumpy transcriptomes by RNAseq (E. Silvester, thesis in preparation) showed that eIF-3 beta mRNA was upregulated in the stumpy form. This raises the intriguing possibility that this subunit may be involved in activating translation of a subset of stumpy-specific transcripts in this life stage.

Potential substrates of YAK kinase among the 56 proteins which showed reduced phosphorylation in the YAK KO line (Figure 3.30) included another NIMA-related kinase, NRKC. While NEK has a role in stumpy formation (Mony et al., 2014) and NRKA/B is involved in the stumpy to procyclic transition (Domingo-Sananes et al., 2015), the identification of NRKC as a downstream target of YAK suggests extensive involvement of this kinase family in parasite differentiation. The YAK-dependent role of NRKC may or may not be related to its known function in basal body separation in procyclic forms (Pradel et al., 2006).

The large number of proteins in which phosphorylation increased in one or both null mutant lines testified to wide-ranging secondary effects to loss of these kinases. These likely include effects of reduced differentiation processes, including increased activation of slender-specific proteins, but may also reflect compensatory mechanisms whereby cells upregulate alternative pathways to overcome the block. Thus the signalling molecules which showed increased phosphorylation have the potential to include both positive and negative regulators of stumpy formation.

This is particularly important to bear in mind in the case of AMPK, which showed highly enriched phosphorylation in both KO lines. An α subunit of AMPK, AMPK α2, was previously identified as a *pos*ST component (Mony et al., 2014). Its position in the pathway relative to other *pos*ST components has not yet been investigated. In mammalian and yeast cells, the β subunit of AMPK acts as a scaffold, binding the catalytic α and AMP-binding γ subunits (Woods et al., 1996) The β subunit is required for AMPK activation and substrate definition in yeast (Schmidt and McCartney, 2000), where as discussed in section 3.5.3, the *Saccharomyces* AMPK α homologue Snf1 plays a central role in the glucose depletion response networks in which various other *pos*ST homologues are also implicated. In *T. brucei*, AMPK β RNAi has been shown to affect surface glycoprotein expression in response to glucose availability in procyclics (Clemmens et al., 2009). The nature of the

interaction between the α and β subunits of AMPK in *T. brucei* is unknown. AMPK β may regulate AMPK α2 activity in response to MEKK1 KO and YAK KO. This could suggest that AMPK acts downstream of both MEKK1 and YAK in the signalling pathway. Alternatively, it may act via a distinct arm which is upregulated to compensate for the blocked MEKK1 and YAK pathways.

A putative C3HC4 zinc finger RING-type protein showed the greatest degree of increased phosphorylation, with greater than 8-fold phosphopeptide upregulation in both the MEKK1 and YAK KO lines. The function of this protein in *T. brucei* is unknown, but RING finger domain containing proteins are often involved in ubiquitination (Lorick et al., 1999), which suggests that absence of MEKK1 and YAK may affect this process.

Phosphorylation was increased in numerous RNA-binding proteins. Four of these – RBP12, RBP35, RBP42 and DRBD4 – were increased in both the MEKK1 and YAK KO lines, and distinct residues of ZC3H34 showed decreased phosphorylation in the MEKK1 KO and increased phosphorylation in the YAK KO. This suggests that loss of these kinases elicit common gene expression responses. According to a genome-wide mRNA tethering screen, RBP42 and DRBD4 are post-transcriptional activators, while RBP12 represses mRNAs (Erben et al., 2014). RNAi of RBP35 has been shown to increase fitness during differentiation while RBP42 regulates transcripts associated with energy metabolism, which could suggest that MEKK1 and YAK are involved in the metabolic adaptations associated with stumpy formation. One regulatory factor which showed increased phosphorylation in the YAK KO line is intriguing as it potentially links a number of components potentially implicated in stumpy formation via independent approaches. MKT1 stabilises mRNAs through interactions with a variety of gene regulators. These include HYP2 (Singh et al., 2014), ZC3H20, a zinc finger protein identified in an RNAi library screen for resistance to the stumpy inducing compound GKI7 (section 5.6), and PAB1-binding protein PBP1 (Singh et al., 2014), in which increased phosphorylation was also observed in the YAK KO.

Overall, this analysis has identified many potentially interesting proteins which showed differential phosphorylation in the absence of MEKK1, YAK or both,

although none have yet been experimentally validated. Hopefully, future analysis of these proteins will enable separation of direct substrates from secondary effects, validation of proteins involved in stumpy formation and ultimately the identification of which differentiation processes are activated by different branches of the signalling pathway.

4 Chapter 4: Positioning of TOR4 within the stumpy formation pathway

4.1 Introduction

In contrast to the *pos*ST genes, which positively regulate stumpy formation, a number of inhibitors of differentiation are known. Ablation of either ZFK or MAPK5 has been shown to increase stumpy formation in pleomorphs (Domenicali Pfister et al., 2006; Vassella et al., 2001). More recently, an unusual kinetoplastid-specific TOR kinase, TOR4, was shown to negatively regulate stumpy formation in a monomorphic strain. RNAi of TOR4 *in vitro* triggered differentiation, as characterised by stumpy morphology, G_1 cell cycle arrest, upregulation of PAD transcripts and an enhanced capacity to differentiate to procyclic forms. In addition, membrane permeable cAMP/AMP analogues were found to downregulate TOR4 expression (Barquilla et al., 2012). Clearly this kinase plays an important role in preventing differentiation but it is unknown if it acts via the same pathway as the *pos*ST genes, and if so, at what point. The differentiation-enhancing phenotype of TOR4 RNAi is in effect antagonistic to the reduced differentiation observed upon loss of posST proteins. Therefore, dual ablation of TOR4 and a *pos*ST protein should facilitate ordering of these proteins relative to each other, akin to the combinatorial knockout and overexpression approach detailed in the previous chapter, and provide insight into how differentiation preventing and promoting mechanisms link.

4.2 TOR4 silencing triggers stumpy formation *in vitro* in pleomorphs, as in monomorphs.

As TOR4 had previously been studied only in a monomorphic strain (Barquilla et al., 2012), RNAi lines of TOR4 were produced in monomorphic and pleomorphic *T. brucei* to enable comparison of the phenotypes of these strains. To produce the monomorphic line, opposing fragments of TOR4 were cloned into the pRPa vector and transfected into 2T1s as in section 3.2.1.1 (vector map in Appendix D Figure 1). For the pleomorphic line, a single fragment of the gene was cloned between 2 opposing T7 promoters of the p2T7-177 vector and transfected into the AnTat 1.1 90:13 line (vector map in Appendix D Figure 3). In both cases, induction of RNAi resulted in growth inhibition in culture (Figure 4.1A). Pleomorphic parasites analysed 72 hours post induction appeared stumpy in morphology (Figure 4.1B) and

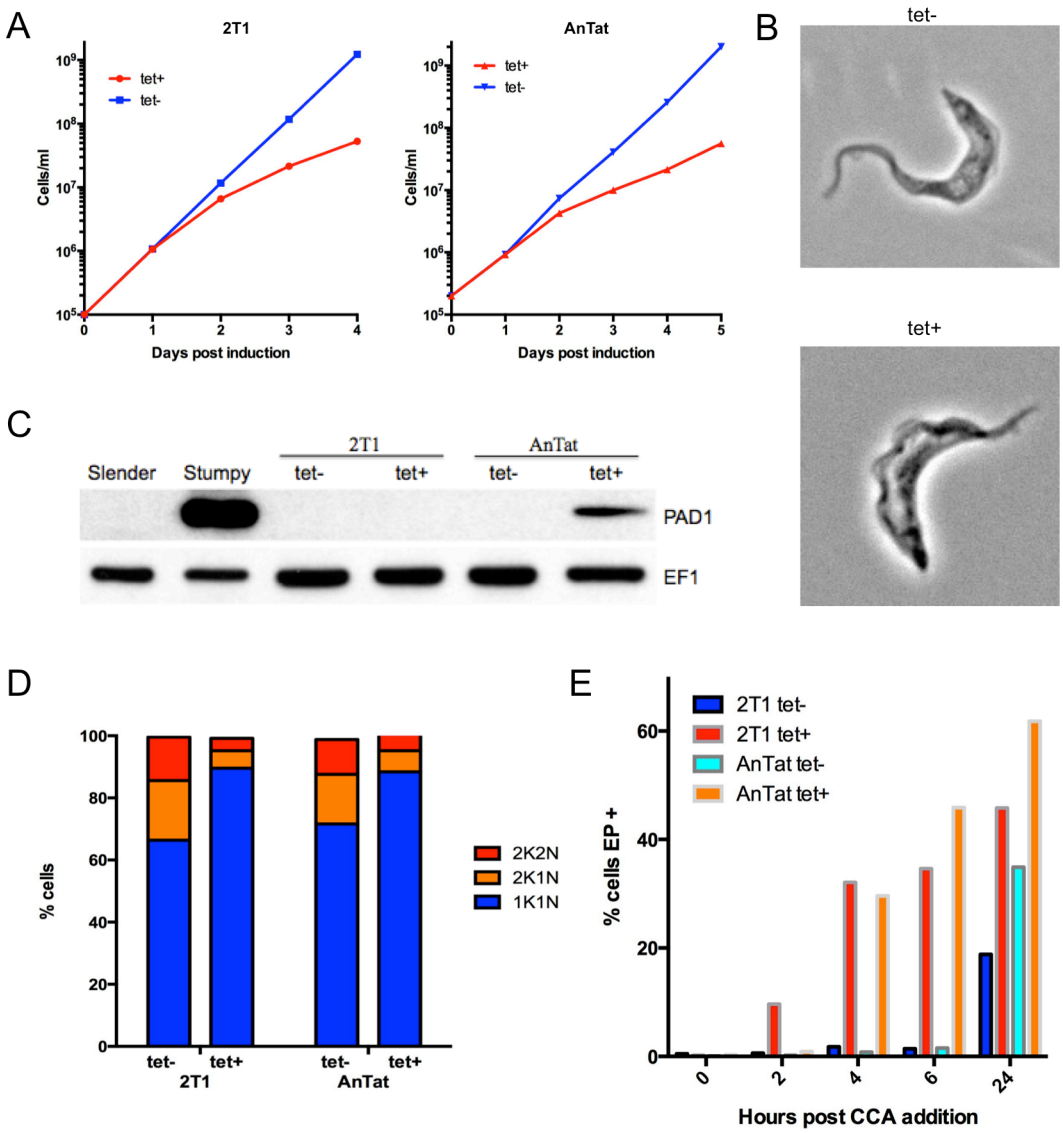

Figure 4.1 Effect of TOR4 RNAi on monomorphic 2T1s and pleomorphic AnTat 1.1 90:13s *in vitro*. A) Cells grown in the presence of tetracycline (tet+) show reduced growth. B) 72-hour induced pleomorphic cells show stumpy morphology. C) Western blot analysis shows expression of PAD1 in pleomorphic cells 72 hours after induction. D) DAPI-stained slides scored for kinetoplast (K) and nucleus (N) configuration 72 hours post induction show G_1 arrest. E) Timecourse of EP procyclin protein expression. Parasites cultured in presence or absence of tetracycline for 72 hours were incubated at 27°C in procyclic SDM-79 medium with 6mM citrate/cis-aconitate (CCA), which induces differentiation to procyclic forms, and analysed by FACS. TOR4 RNAi leads to increased EP procyclin expression upon CCA treatment.

expressed the stumpy marker PAD1 (Figure 4.1C). Cell cycle status was analysed by scoring kinetoplast (K) and nucleus (N) configuration on DAPI-stained slides (see section 3.2.1.3). In both parasite strains, an increase in the proportion of 1K1N cells was observed, indicating arrest in G_1 (Figure 4.1D). To test the capacity of TOR4 RNAi cells to differentiate to procyclic forms, cells were transferred to SDM-79 at

27°C and triggered to differentiate with cis-aconitate. Expression of EP procyclin was then measured by FACS. At all timepoints analysed, EP expression was increased when TOR4 RNAi was induced, both in monomorphs and pleomorphs, indicating greater differentiation capacity (Figure 4.1E). It appears that TOR4's role in differentiation is shared between monomorphs and pleomorphs, as its silencing in a pleomorphic strain results in the appearance of the various hallmark characteristics of stumpy forms.

4.3 TOR4 silencing results in premature differentiation to stumpy forms in vivo.

To explore the *in vivo* role of TOR4, the pleomorphic RNAi line was used to infect mice. As seen in Figure 4.2A, mice which were treated with doxycycline show reduced parasitaemia. Despite this, the degree of cell cycle arrest in these cells, as indicated by the proportion of parasites with a single nucleus and kinetoplast, did not significantly differ from the non-induced cells, with the exception of day 5, at which point it was lower (Figure 4.2C). This indicates that the cells were arresting at a lower parasite density. Likewise, when cells were scored for staining with the stumpy-specific marker PAD1, there was no significant difference in expression at any timepoint except for day 5 (Figure 4.2D). This suggests that RNAi induced cells show characteristics of stumpy forms at low parasitaemia. It would therefore appear that loss of TOR4 results in differentiation at low density *in vivo*.

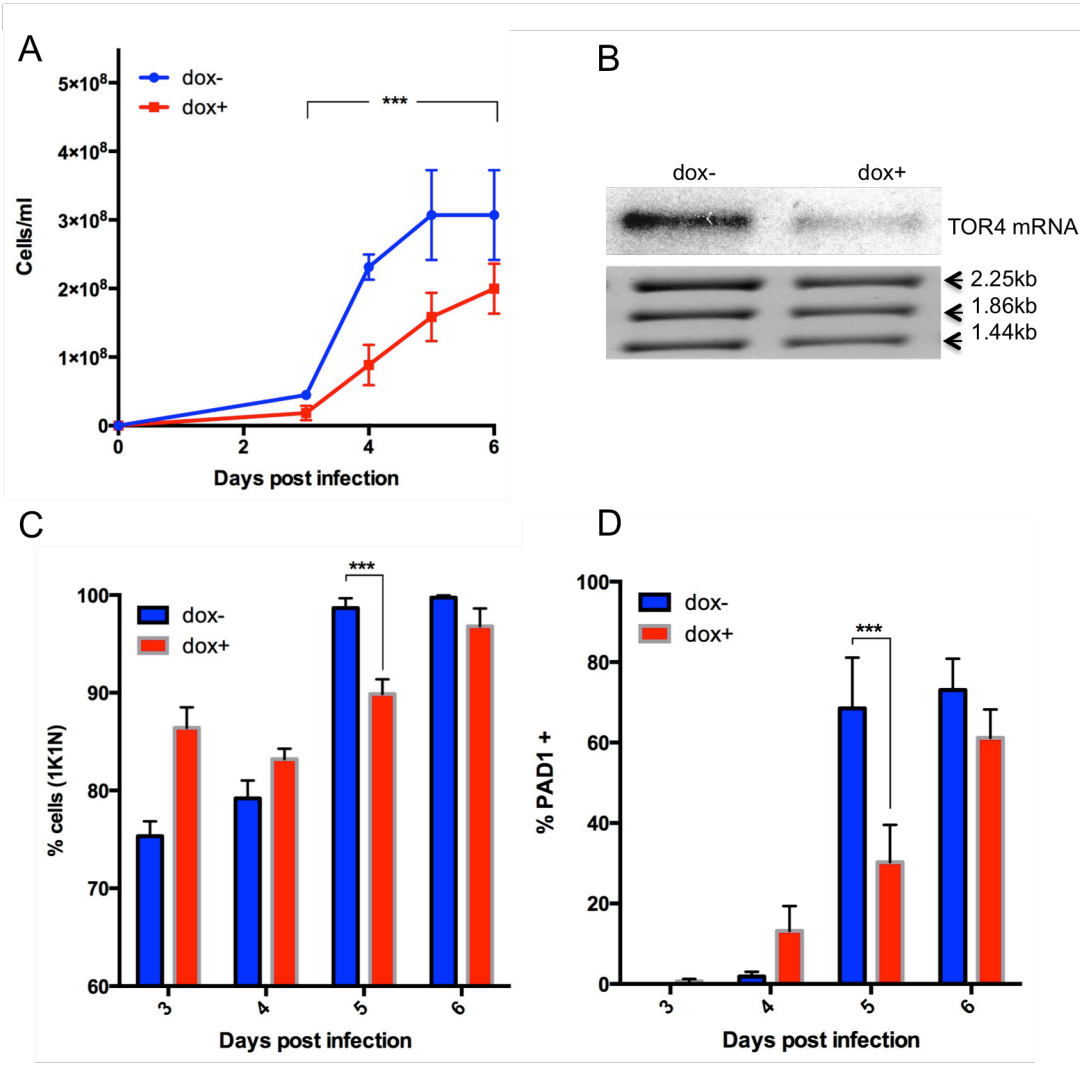

Figure 4.2 TOR4 RNAi triggers premature stumpy formation in vivo. A) Parasitaemia of mice infected with TOR4 RNAi cells, estimated by the rapid matching method. Data represents 6 mice, 3 treated with doxycycline (dox+) and 3 non-induced (dox-). TOR4 RNAi induced mice have reduced parasitaemia. B) Northern analysis shows decreased TOR4 transcript level 6 days post induction. C) % 1K1N (representing G_1 and S phase) cells throughout the course of infection. 250 cells were counted for each sample. D) % cells expressing PAD1 throughout the course of infection, determined by IFA. 250 cells were counted for each sample. ***P<0.0005 GLM and Tukey test for multiple comparisons.

4.4 Simultaneous RNAi of NEK and TOR4 has complex effects on differentiation.

To investigate the role of TOR4 in relation to the *pos*ST kinase NEK, a double RNAi line was generated in which both genes were silenced by RNAi. The AnTat 1.1 90:13 TOR4 RNAi line contains an integrated p2T7-177 construct under the control of phleomycin. A corresponding NEK RNAi line was previously produced using the pALC14 vector to validate this kinase as a positive regulator of differentiation (Mony et al., 2014). As this construct contains a puromycin resistance gene, it could be compatibly transfected into the phleomycin-resistant TOR4 RNAi line to generate a combined NEK and TOR4 RNAi line. The capacity of this cell line to differentiate *in vitro* was assessed using pCPTcAMP. As shown in Figure 4.3, induction of NEK RNAi results in reduced responsiveness to pCPTcAMP, as expected. In contrast, TOR4 RNAi results in growth inhibition both in the presence and absence of pCPTcAMP, again as expected. NEK+TOR4 RNAi showed a similar growth inhibition in response to tetracycline, indicating that it is the loss of TOR4 which has the dominant phenotype *in vitro*.

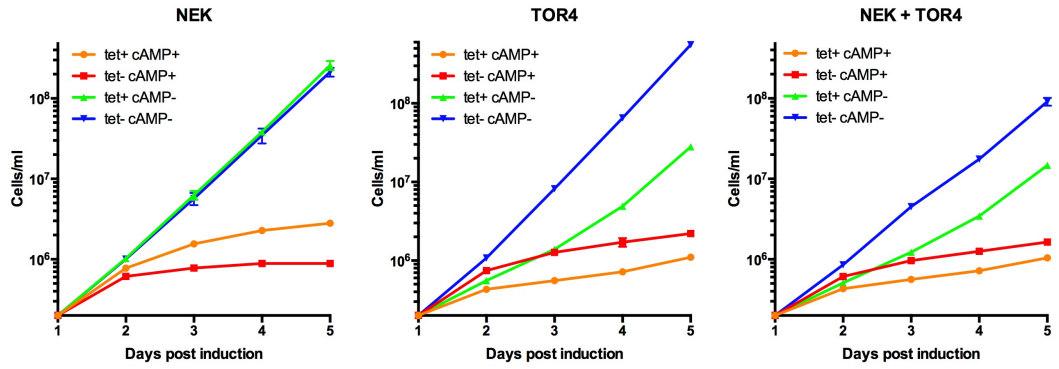

Figure 4.3 Growth curve of NEK/TOR4 RNAi cell lines incubated with (tet+) or without (tet-) tetracycline and either treated (cAMP+) or untreated (cAMP-) with pCPTcAMP 24 hours post-induction by tetracycline. NEK RNAi cells show resistance to pCPTcAMP. NEK+TOR4 RNAi cells show reduced growth upon RNAi induction similar to TOR4 RNAi alone.

These lines were subsequently analysed *in vivo*. Consistent with data from Mony *et al.* (2014), the parasitaemia of induced NEK RNAi cells continued to increase throughout the infection, showing no signs of arrest while TOR4 RNAi cells were unable to reach a high parasitaemia (Figure 4.46A). Each of these lines was compared to that of the double NEK+TOR4 RNAi line, in the left

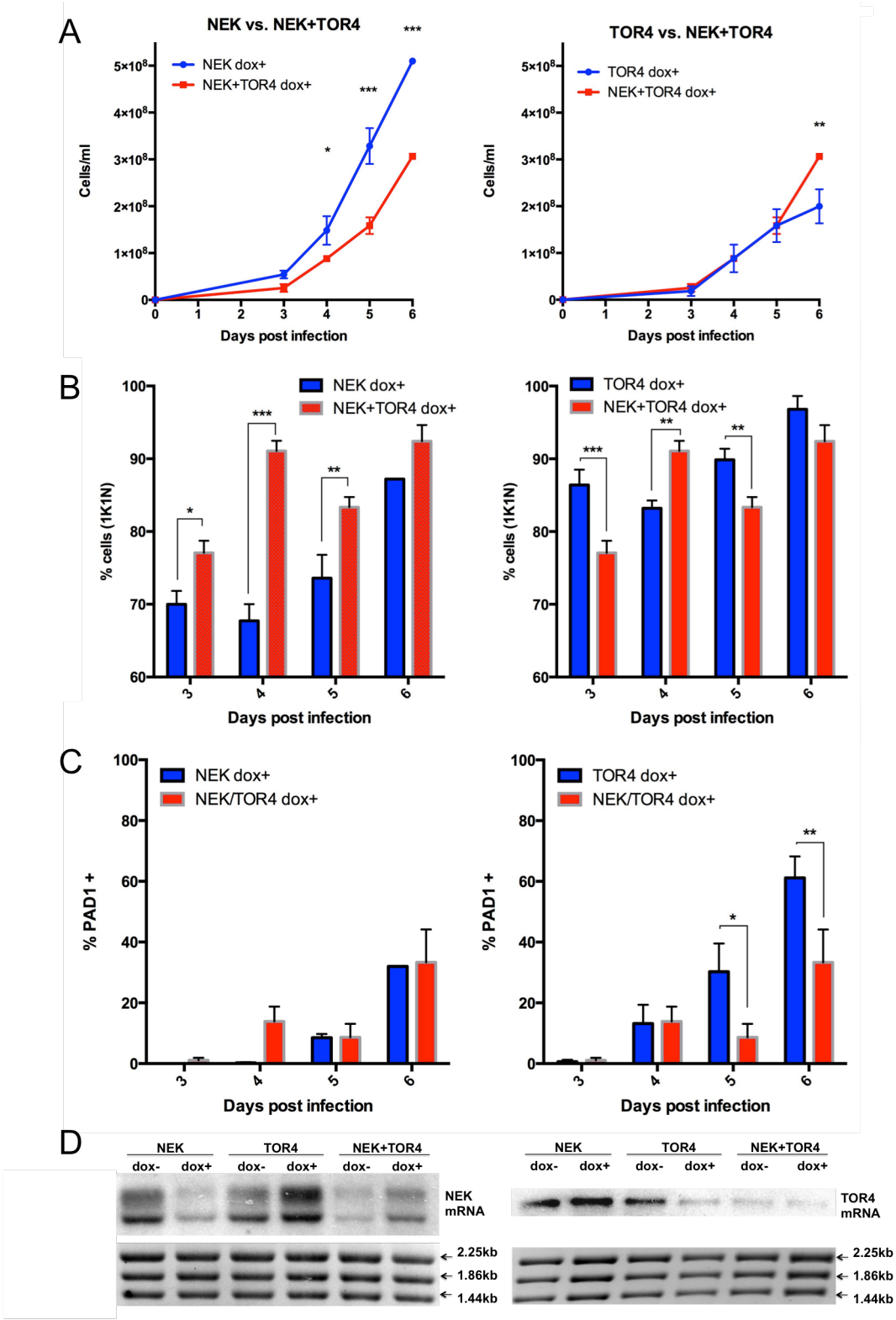

Figure 4.46 Effects of combined NEK+TOR4 RNAi on stumpy formation in vivo. A)-C) Data from infections with NEK+TOR4 RNAi in the presence of doxycycline is shown relative to NEK RNAi (left) and TOR4 RNAi (right) alone. *P<0.05,**P<0.005,***P<0.0005 GLM and Tukey test for multiple comparisons. A) Parasitaemia was estimated by the rapid matching method B) % 1K1N (G1/S phase) cells throughout the course of infection. 250 cells were counted for each sample. C) % cells expressing PAD1 throughout the course of infection, determined by IFA. 250 cells were counted for each sample. D) Northern analysis of RNA 6 days p.i. shows effect of doxycycline treatment on NEK/TOR4 transcript level in the respective RNAi cell lines. rRNA was used as a loading control.

and right panels respectively. The NEK+TOR4 RNAi parasitaemia was significantly lower than NEK RNAi, indicating that loss of TOR4 remains capable of driving arrest, even in the absence of NEK. Indeed, the profile of the parasitaemia closely matched that of TOR4 RNAi until the fifth day of infection. On day 6, however, there was an increase in parasitaemia, indicating that the silencing of NEK reduces arrest late in infection (Figure 4.46A). NEK+TOR4 RNAi cells also showed a higher proportion of 1K1N cells relative to NEK RNAi from days 3 to 5 of infection, indicating that the loss of TOR4 was still able to promote G_1 arrest in this cell line. However, atypically, the percentage of 1K1N cells actually dropped between days 4 and 5 from 91.1 ± 0.8% to 83.3 ± 0.8%. Again this suggests that the effect of NEK RNAi is able to overcome the TOR4 RNAi induced arrest at a later stage of infection (Figure 4.46B). The level of PAD1 expression remained low throughout infection in NEK+TOR4 RNAi cells, reaching a maximum of 33.3 ± 6.3% on day 6 similar to that of NEK RNAi and significantly lower than with TOR4 RNAi at later timepoints (Figure 4.46C). It would therefore appear that although loss of TOR4 is able to drive cell cycle arrest in the absence of NEK, it is not able to upregulate PAD1. Northern analysis confirmed depletion of NEK and TOR4 in their respective single RNAi lines. Both transcripts were also present at low abundance in the double RNAi line (Figure 4.46D). However, as this was true even in the absence of doxycycline, it appears that dsRNA expression may be leaky in these cells.

4.5 Combined knockout of MEKK1 and knockdown of TOR4 has complex effects on differentiation.

The complex effects on differentiation observed upon simultaneous RNAi of NEK and TOR4 may have been influenced by the respective levels of depletion of each transcript, as neither was completely silenced (Figure 4.4D). This possibility could be overcome by the use of null mutants to eradicate expression completely. As TOR4 appears to be essential, it is a poor candidate for gene deletion. However, the *pos*ST kinase MEKK1 is non-essential and was successfully knocked out in the parental AnTat 1.1 90:13 strain, as described in section 3.2.3.3. The same vectors were used to sequentially delete both alleles of MEKK1 in the TOR4 RNAi line. Successful

deletion of the MEKK1 gene and correct integration of both replacement alleles was confirmed by Southern blot (Figure 4.5C).

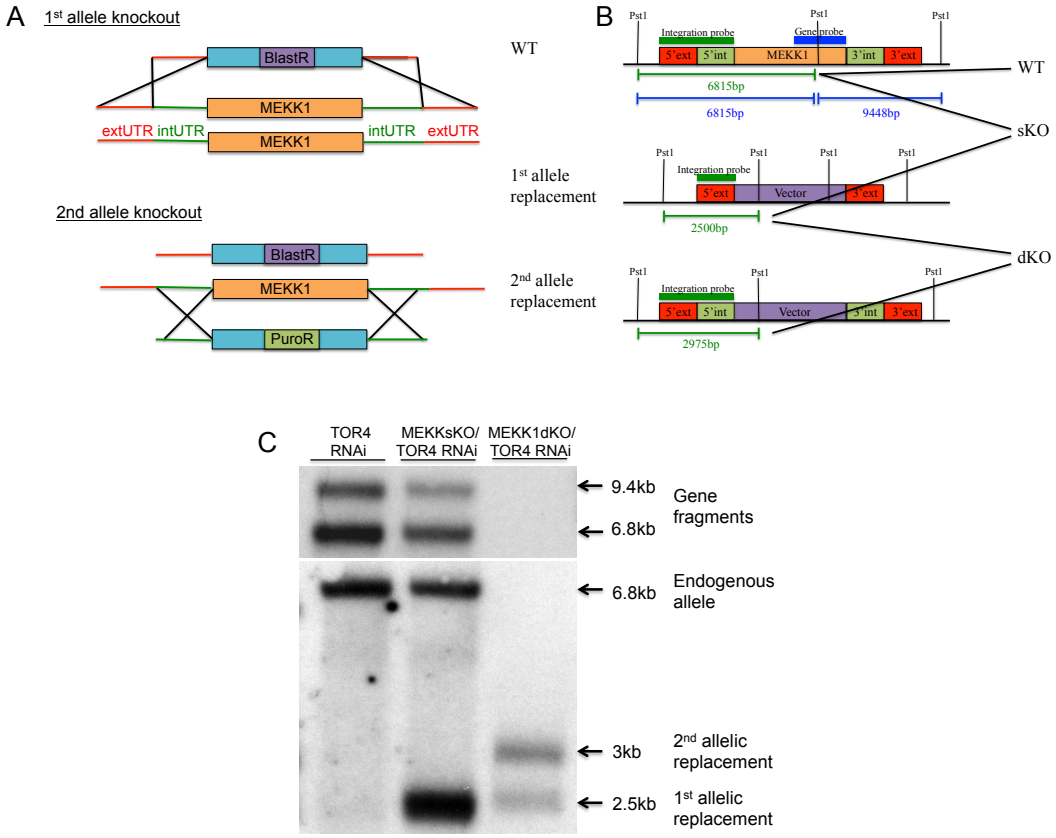

Figure 4.5 Generation of a null mutant of MEKK1 in the TOR4 RNAi line. A) Schematic representation of the knockout strategy. In the first step, a plasmid containing the blasticidin resistance gene was targeted to external portions of the 5' and 3' UTRs (extUTR) by homologous recombination, thereby replacing both the ORF and internal UTRs (intUTR) from one allele. Subsequently, a plasmid containing the puromycin resistance gene was targeted to internal portions of the UTRs and could recombine only with the remaining allele so that the second copy of the gene was replaced. B) A diagram shows the fragments recognised by 2 DNA probes in the WT allele and integrated 1st and 2nd replacement constructs following gDNA digestion by Pst1. C) A gene probe complementary to part of the MEKK1 ORF recognised 6815bp and 9448bp fragments in the WT allele only, which were present in the parental TOR4 RNAi cells and the single knockout (sKO) cells but absent in double knockout (dKO) cells, confirming successful gene deletion. A second probe to determine correct integration hybridised to a 6815bp fragment in the WT allele, a 2500bp fragment in the 1st allelic replacement and a 2975bp fragment in the 2nd allelic replacement, thereby conferring parental, sKO and dKO cells each with a unique signature and confirming correct integration of the relevant constructs in each case.

The single and double knockouts were analysed *in vitro* for their capacity to differentiate. As shown in Figure 4.6, deletion of either one or both alleles of MEKK1 results in decreased responsiveness to the pCPTcAMP signal. However, concomitant silencing of TOR4 by tetracycline induction arrests growth in these

cells. This indicates that the *in vitro* growth effect observed upon TOR4 RNAi is independent of MEKK1.

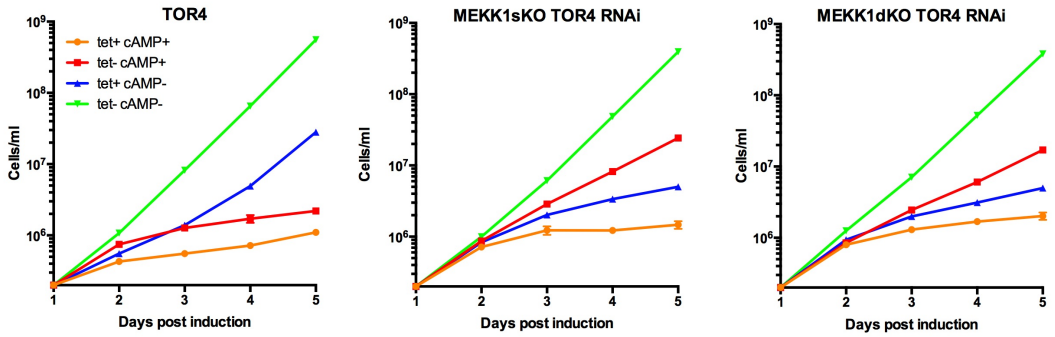

Figure 4.6 Growth curve of MEKK1KO TOR4 RNAi cell lines incubated with (tet+) or without (tet-) tetracycline and either treated (cAMP+) or untreated (cAMP-) with pCPTcAMP 24 hours post-induction by tetracycline. MEKK1sKO TOR4 RNAi and MEKK1dKO TOR4 RNAi cells show resistance to pCPTcAMP in the absence of tetracycline and reduced growth upon induction.

The differentiation capacity of the MEKK1 KO + TOR4 RNAi line was subsequently investigated *in vivo*. In Figure 4.7A, data from infections with induced MEKK1KO + TOR4 RNAi parasites were compared to their non-induced counterparts in the left panel and to the induced parental TOR4 RNAi line on the right. In the presence of doxycycline, MEKK1 KO + TOR4 RNAi parasitaemia remains low, showing a similar profile to the induced parental TOR4 RNAi line. In the absence of doxycycline, the parasitaemia in the null mutant line increased so dramatically that all 3 mice had died by day 5 of infection (Figure 4.7A). This suggests that the growth effect observed upon TOR4 RNAi is not dependent on MEKK1. MEKK1 KO parasites in which TOR4 RNAi has not been induced showed a low proportion of 1K1N cells indicative of a non-arrested population. In the presence of doxycycline, this percentage was significantly higher (Figure 4.7B), suggesting that TOR4 RNAi leads to G1 arrest even in the absence of MEKK1. Uninduced MEKK1 KO + TOR4 RNAi parasites express no detectable PAD1 on the days of infection for which data is available. Where the RNAi was induced, 11.2 ± 2.2% and 19.7 ± 1.6% PAD1 expression was detectable on days 4 and 5 respectively but this was significantly lower than in the parental TOR4 RNAi line, which expresses 38.4 ± 7.6 % and 57.4 ± 10.2% on the same days (Figure 4.7C). This data indicated that, similar to the results seen for the NEK+TOR4 RNAi line, silencing of

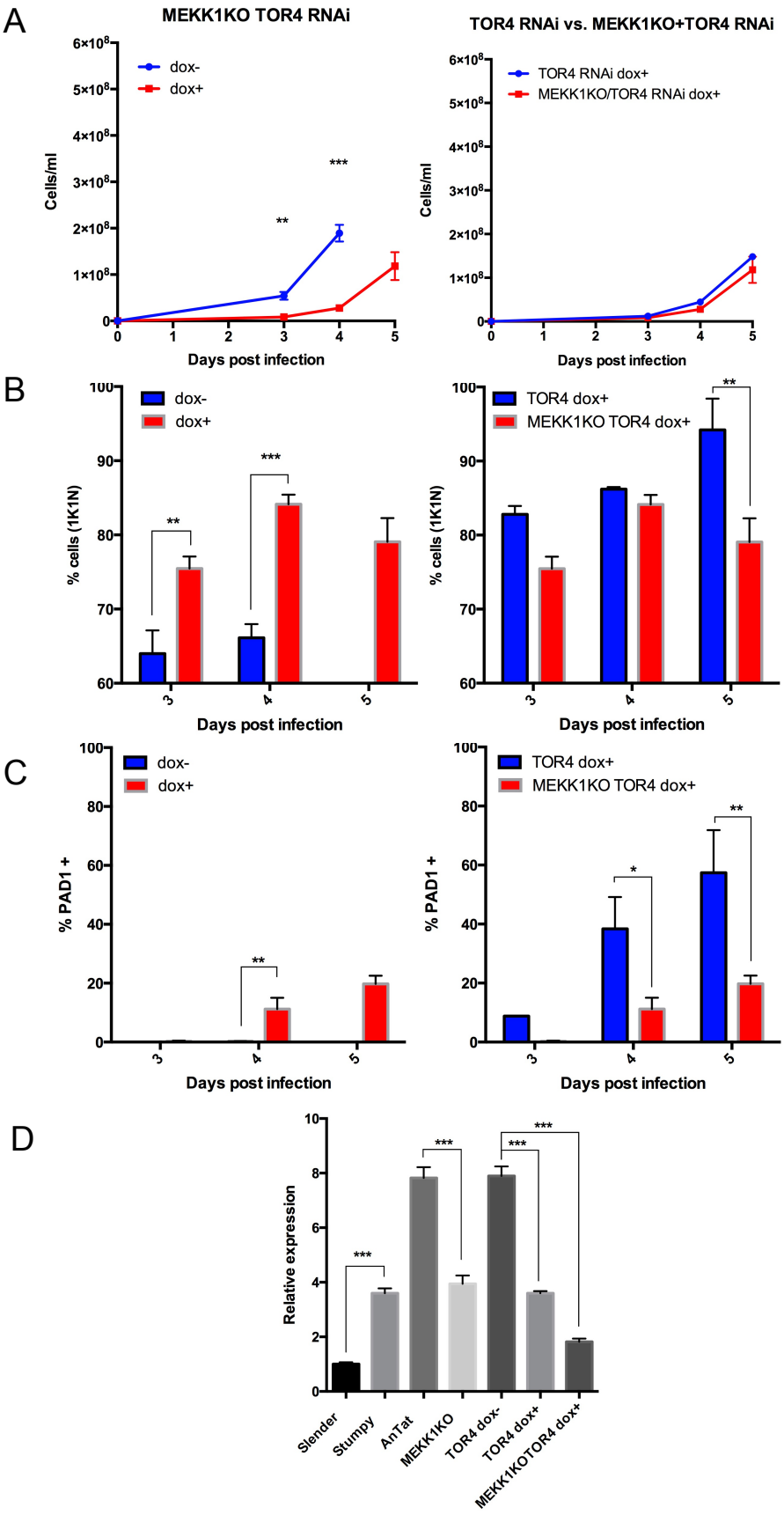
A
MEKK1KO TOR4 RNAi
dox-
dox+
Cells/ml
Days post infection
TOR4 RNAi vs. MEKK1KO+TOR4 RNAi
TOR4 RNAi dox+
MEKK1KO/TOR4 RNAi dox+
B
% cells (1K1N)
TOR4 dox+
MEKK1KO TOR4 dox+
C
% PAD1 +
D
Relative expression
Slender
Stumpy
AnTat
MEKK1KO
TOR4 dox-
TOR4 dox+
MEKK1KOTOR4 dox+

Figure 4.7 Effects of combined MEKK1 KO + TOR4 RNAi on stumpy formation in vivo. A)-C) Data from infections with MEKK1 KO + TOR4 RNAi in the presence of doxycycline is shown relative to uninduced (left) and TOR4 RNAi (right) alone. *P<0.05,**P<0.005,***P<0.0005 GLM and Tukey test for multiple comparisons. A) Parasitaemia as estimated by the rapid matching method. B) Proportions of 1K1N (G1/S phase) cells throughout the course of infection. 250 cells were counted for each sample. C) Proportions of cells expressing PAD1 throughout the course of infection, determined by IFA. 250 cells were counted for each sample. D) qRT-PCR analysis of TOR4 mRNA 6 days p.i. normalised to ZFP3.

TOR4 is sufficient to promote cell cycle arrest *in vivo* independent of MEKK1 but PAD1 upregulation is MEKK1 dependent. qRT-PCR analysis was used to confirm that TOR4 was depleted upon RNAi induction in both parental and MEKK1 KO cell lines. In the latter case, this was compared to the uninduced parental TOR4 RNAi line, as corresponding data for the null mutant line was unavailable due to death of the mice. This analysis also revealed upregulation of TOR4 in stumpy forms relative to slender forms (Figure 4.7D). As loss of TOR4 promotes stumpy formation, this may affect the degree of transcript depletion observed.

4.6 Discussion

4.6.1 TOR4 is an inhibitor of stumpy formation in pleomorphs

Barquilla *et al.* (2012) have shown previously that TOR4 negatively regulates stumpy formation in monomorphic trypanosomes. Here RNAi is used to demonstrate that silencing of TOR4 also induces differentiation in a pleomorphic strain. A comparison of monomorphic and pleomorphic RNAi lines highlights that loss of TOR4 results in a more pronounced stumpy formation phenotype in pleomorphs, which show PAD1 upregulation *in vitro* not observed in the monomorphic line (Figure 4.1C) and enhanced CCA-induced differentiation to procyclic forms (Figure 4.1E). *In vivo*, TOR4 RNAi results in reduced parasitaemia (section 4.3). Despite this, cells show similar levels of G_1 arrest and PAD1 expression to uninduced parasites, indicating that loss of TOR4 drives stumpy formation at low cell density. The exception to this was on day 5, in which both the proportion of 1K1N and PAD1 expression levels were significantly lower than in uninduced cells (Figure 4.2). This likely represents the point at which the uninduced population reached threshold density and the majority of differentiation occurred, leading to a sudden surge in arrested, PAD1 expressing cells whereas TOR4 RNAi-induced stumpy formation occurs as a more continuous process at sub-threshold parasitaemia. In addition, it is

possible that some selection of RNAi resistant parasites occurs in the induced population, leading to outgrowth of slender cells, although the observed increase in arrested, PAD1-expressing cells from day 5 to day 6 (Figure 4.2) points to continued differentiation later in the infection.

4.6.2 Complex interactions between TOR4 and *pos*ST kinases NEK and MEKK1

The relationship of the differentiation inhibitor TOR4 to the components of the stumpy promoting *pos*ST pathway was investigated using the kinases NEK and MEKK1. This was explored first using a double RNAi line in which NEK and TOR4 were simultaneously silenced. This cell line was used to demonstrate that TOR4 RNAi induces *in vitro* growth inhibition independently of NEK (section 4.4). Likewise *in vivo*, the NEK + TOR4 RNAi cells showed reduced growth, although the parasitaemia significantly increased on the final day of infection relative to TOR4 RNAi cells, indicating that NEK RNAi is able to exert a contrary effect on arrest only at a late stage of infection. NEK + TOR4 RNAi cells showed increased G_1 arrest relative to NEK RNAi alone. However, these two lines showed similarly low levels of PAD1 expression throughout the infection. This indicates that TOR4 RNAi induces cell cycle arrest independently of NEK but its upregulation of PAD1 is NEK-dependent. As G_1 arrest precedes PAD1 expression in the differentiation program (MacGregor et al., 2011), this suggests a role for TOR4 in the early stages of differentiation, while NEK appears to be implicated in both arrest and later PAD1 expression components of the process. However, the increase in the NEK + TOR4 RNAi parasitaemia on the final day of infection suggests that NEK-independent growth arrest is lost at this stage. While this may reflect a physiologically dominant role for NEK in relation to TOR4 in predominantly stumpy populations, it may alternatively be a side effect of the kinetics of RNAi. NEK and TOR4 RNAi may proceed with different kinetics due to factors such as the efficiency of their respective dsRNA expression systems and differential protein turnover. As with TOR4 RNAi alone, it is possible that the growth effect of TOR4 RNAi exerts a selective pressure for RNAi escapees, which emerge later in infection as single NEK RNAi cells. To complicate matters, TOR4 mRNA shows several-fold upregulation in stumpy forms according to qRT-PCR analysis (Figure 4.7D), so the phenotype it

induces may in fact counteract its own silencing by upregulating TOR4 transcription as the population differentiates. However, this depends on whether cells have been driven to irreversible arrest, as TOR4 upregulation would have to occur before the point of commitment to be effective in reversing the effect of the RNAi. In a comparison of KN counts between TOR4 RNAi and NEK + TOR4 RNAi populations, the latter showed a significant decrease in 1K1N cells on day 3, a significant increase on day 4, a significant decrease again on day 5 and no change on day 6. With unknown variation in levels of each knockdown at these timepoints of infection, it can be difficult to interpret which of these differences reflect physiological effects and which reflect uneven mRNA silencing, or a combination of the two.

In an alternative approach which attempted to remove some of this variability, both alleles of MEKK1 were deleted in the TOR4 RNAi line, providing a constitutively MEKK1-negative background in which only TOR4 was under inducible control. As with NEK, TOR4 RNAi induced MEKK1-independent growth inhibition *in vitro* and cell cycle arrest *in vivo*. However, PAD1 expression in the MEKK1 KO + TOR4 RNAi line was significantly reduced relative to TOR4 RNAi alone. This supports the hypothesis suggested by the NEK + TOR4 RNAi phenotype that TOR4 acts early in differentiation at the stage of cell cycle arrest, while like NEK, MEKK1 is involved in both arrest and later in the process at the stage of PAD1 expression. This is summarised in Figure 4.4.8.

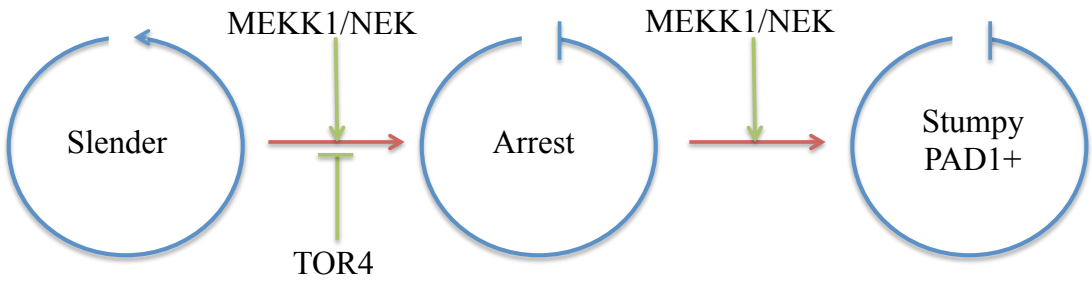

Figure 4.4.8 Model of action of stumpy inhibitor TOR4 and *pos*ST components MEKK1 and NEK at different stages of differentiation.

This model of TOR4 and *pos*ST action makes sense if it is supposed that differentiation is controlled by two opposing mechanisms: one responsible for

retaining the slender state and the other for inducing stumpy formation. As an inhibitor of stumpy formation, TOR4 is likely active in proliferating slender forms at low density to prevent initiation of the differentiation process. As such, it is logical that it should function in the primary steps, specifically in cell cycle arrest. When TOR4 RNAi removes this inhibition, the *pos*ST pathway activates the entire differentiation program, resulting in the production of PAD1-positive cells. However, when MEKK1 or NEK is also removed, G_1 arrest proceeds but subsequent steps in stumpy formation which require activation by the compromised *pos*ST pathway do not occur.

One of many aspects of the intersection of the opposing mechanisms of differentiation control which remains to be determined is the role of MAPK5 and ZFK, two other kinases which have been implicated in negative regulation of stumpy formation. In contrast to TOR4, loss of neither MAPK5 or ZFK has any effect in a monomorphic strain (Domenicali Pfister et al., 2006; Vassella et al., 2001). This positions them upstream of both TOR4 and the *pos*ST components, which were identified using a monomorphic RNAi library (Mony et al., 2014). It is unknown if ZFK and/or MAPK5 act directly upstream of TOR4 and therefore intersect with the *pos*ST pathway at the same stage or if they act independently to ensure redundant layers of protection against premature differentiation.

As is the case for numerous *pos*ST components, as discussed in section 3.5.3, a TOR kinase acts as a central regulator in nutrient signalling in yeast. TORC1 and *pos*ST component homologues are integrated into a complex signalling network of antagonistic interactions. TORC1 has been shown to negatively regulate Yak1 via control of subcellular localisation (Martin et al., 2004; Schmelzle et al., 2004; Zhang et al., 2013). Conversely, the yeast AMPK Snf1 represses signalling through the TOR pathway (Hallett et al., 2014), a finding also observed in mammalian cells (Gwinn et al., 2008; Inoki et al., 2003). The interactions described between TORC1 and *pos*ST component homologues in these signalling networks may offer clues as to how slender retention and stumpy induction pathways intersect in *T. brucei*.

5 Chapter 5: Ordering components of the stumpy signalling pathway via chemical-genetic analysis

5.1 Introduction

With the continued elusiveness of the molecular identity of SIF, small molecule inducers of differentiation to stumpy forms have long been invaluable as chemical tools for *in vitro* studies of this process. Specifically, membrane permeable forms of cAMP and AMP have been used to this end and were integral to the discovery of the *pos*ST genes. Subsequent validation has shown that individual *pos*ST RNAi lines show a reduced response to the pCPTcAMP signal. Identification of further differentiation inducing compounds with different points of action to cAMP/AMP could provide additional information about the organisation of the stumpy formation pathway and could even be useful as therapeutic agents, as differentiation at low, sub-transmission, parasite densities should lead to population arrest and clearance. For example, a small molecule which acts downstream of AMP would be expected to select only a subset of *pos*ST genes if applied to an RNAi library screen, whereas RNAi lines of any *pos*ST proteins which act upstream would be fully sensitive to the compound. This is represented in Figure 5.1.

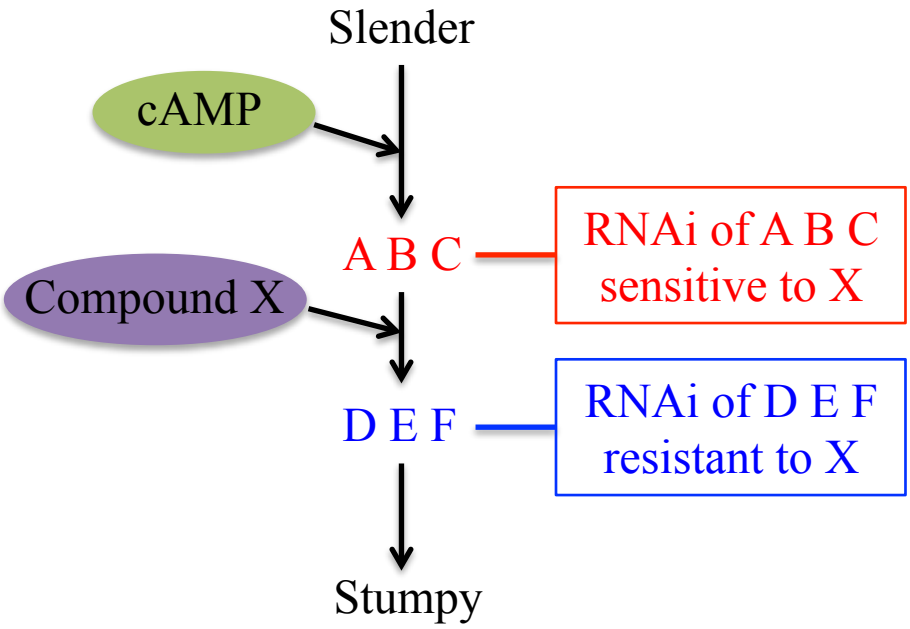

Figure 5.1 Organisation of the *pos*ST pathway via positioning of stumpy inducing compounds. If compound X activates stumpy formation via the *pos*ST pathway but downstream of cAMP, RNAi cells of all *pos*ST components upstream of its action (A, B, C) will retain sensitivity to X and RNAi cells of all *pos*ST components downstream (D, E, F) will be resistant, revealing A, B and C to act upstream of D, E and F in the stumpy signalling pathway.

Using a fluorescent reporter assay for stumpy formation, MacGregor *et al.* (2014) conducted a high-throughput screen for such compounds and were able to identify E667 as a small molecule capable of inducing differentiation in monomorphs and pleomorphs. Its target within the differentiation signalling pathway remains unknown and is explored here via its relation to the *pos*ST genes as described above. Given the involvement of various kinases in differentiation, kinase inhibitors represent an intriguing potential source of downstream stumpy inducers. A recent compound screen of a kinase inhibitor library identified a set of small molecules capable of inhibiting trypanosome growth (Diaz et al., 2014). Here, this compound set is screened for stumpy induction phenotypes.

5.2 Validation of E667 as an inducer of stumpy formation

The compound DDD00015314 (here referred to as E667) was identified from a high throughput screen for developmental phenotypes and shown to induce stumpy formation (MacGregor et al., 2014). Due to the inability to commercially source E667 which previously hindered further investigation, new chemically identical compound was synthesised by BioFocus and tested for differentiation activity using the monomorphic GUS-PAD1 3'UTR reporter line. This cell line, in which the fluorescent reporter β-glucuronidase (GUS) is conjugated to the stumpy-specific PAD1 3'UTR, was used in the original identification of E667 (MacGregor et al., 2014). Consistent with previous observations, treatment of these cells with newly synthesised E667 upregulated reporter activity several fold (Figure 5.2).

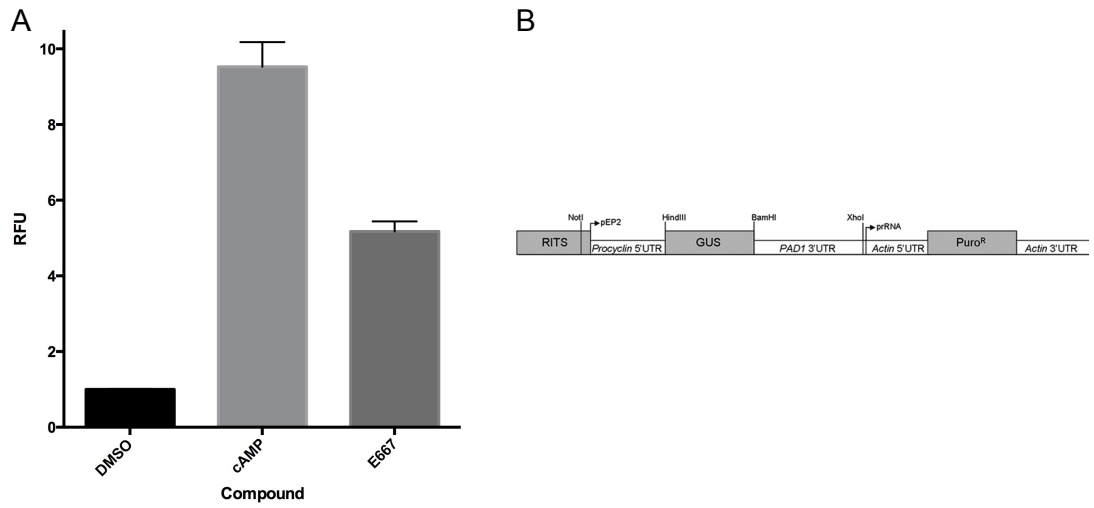

Figure 5.2 E667 upregulates a PAD1 reporter. A) The monomorphic GUS-PAD1 3'UTR line showed an increase in reporter activity after 48 hours treatment with 100 μM pCPTcAMP or 50 μM E667. RFU = relative fluorescence units. B) Schematic diagram of the reporter construct from MacGregor *et al.* (2014).

5.3 Kinase inhibitor library screen for stumpy induction phenotypes

Diaz *et al.* (2014) recently identified hundreds of compounds from a GlaxoSmithKline kinase inhibitor (GKI) set which effected inhibition of trypanosome growth, including 52 for which the chemical structure was disclosed. To identify additional compounds capable of inducing stumpy formation, these 52 compounds were tested for differentiation phenotypes using the GUS-PAD1 3'UTR reporter line previously employed.

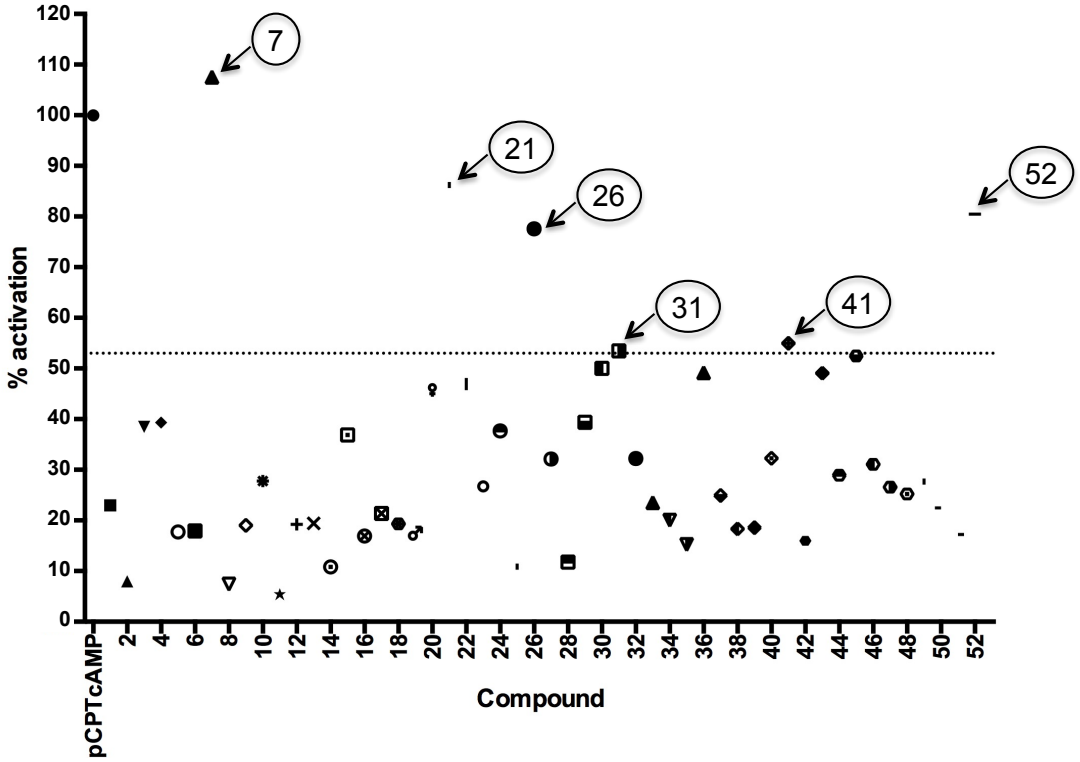

Figure 5.3 Primary screen for differentiation effects of GKI compound set. GUS-PAD1 3'UTR reporter line cells were incubated with EC_{50} conc. of each compound for 24 hours and % activation calculated relative to pCPTcAMP upregulation (set at 100% activation). Threshold for selection (dotted line) was set at 53%.

The level of upregulation of the fluorescent reporter caused by incubation with pCPTcAMP was set at 100% activation and any compounds which resulted in >53% activation were selected for further analysis, according to the selection parameters used in MacGregor *et al.* (2013). Six compounds met this criterion (Figure 5.3).

RBP7 is predicted to act relatively far down in the *pos*ST pathway (section 1.9.3.2) and is therefore likely to be necessary for the action of any drug which drives differentiation via this pathway. In consequence, the six GKI compounds selected from the primary screen were subsequently screened for reduced activity in the RBP7 null mutant line.

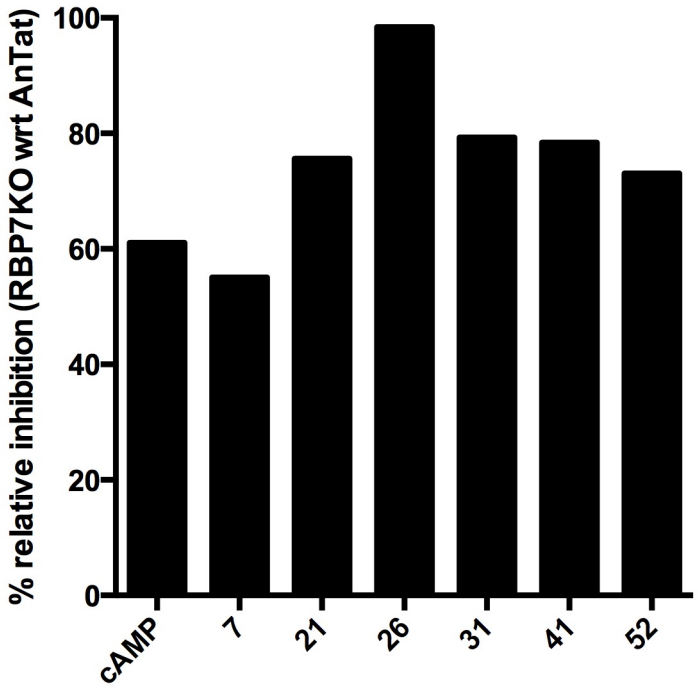

Figure 5.4 Inhibition of RBP7 KO by GKI compounds relative to parental AnTat 1.1 90:13. Cells were treated with EC_{50} compound conc. for 24 hours and growth inhibition determined by Alamar blue assay.

As expected, the RBP7 null mutant cells showed reduced sensitivity to pCPTcAMP, with only 60% inhibition relative to the parental line. Reduced sensitivity was also observed for five of the six GKI compounds tested (7, 21, 31, 41, 52; Figure 5.4), supporting roles for them as activators of stumpy formation.

Of the GKI compounds tested, NEU-0001233, referred to here as GKI7, showed both the highest degree of activation of the PAD1-specific reporter, at 108% (Figure 5.3), as well as the lowest relative inhibition of RBP7 null mutant parasites (Figure 5.4). It was therefore selected for further analysis. Further supporting its differentiation promoting activity, treatment of pleomorphic AnTat 90:13 parasites with GKI7 resulted in G_1 arrest, as denoted by a significant increase in 1K1N cells (Figure 5.5A), and upregulation of PAD1 protein (Figure 5.5B).

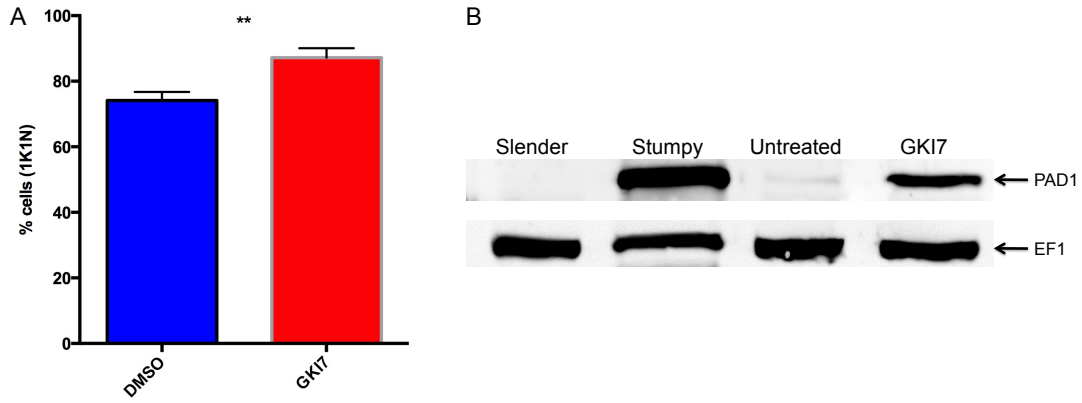

Figure 5.5 GKI7 induces stumpy formation in the pleomorphic AnTat 1.1 90:13 strain. Cells were treated with 1.44 μM GKI7 for 24 hours. A) % 1K1N (representing G_1 and S phase) cells throughout the course of infection. 250 cells were counted for each sample. **P<0.005 t test. B) Western blot analysis of PAD1 expression. EF-1 was used as a loading control.

5.4 Sensitivity of *pos*ST RNAi lines to E667 and GKI7

To examine if E667 and GKI7 act via the *pos*ST pathway to activate stumpy formation, and to determine the point of their respective actions within this pathway, several *pos*ST RNAi lines were tested for sensitivity to these compounds.

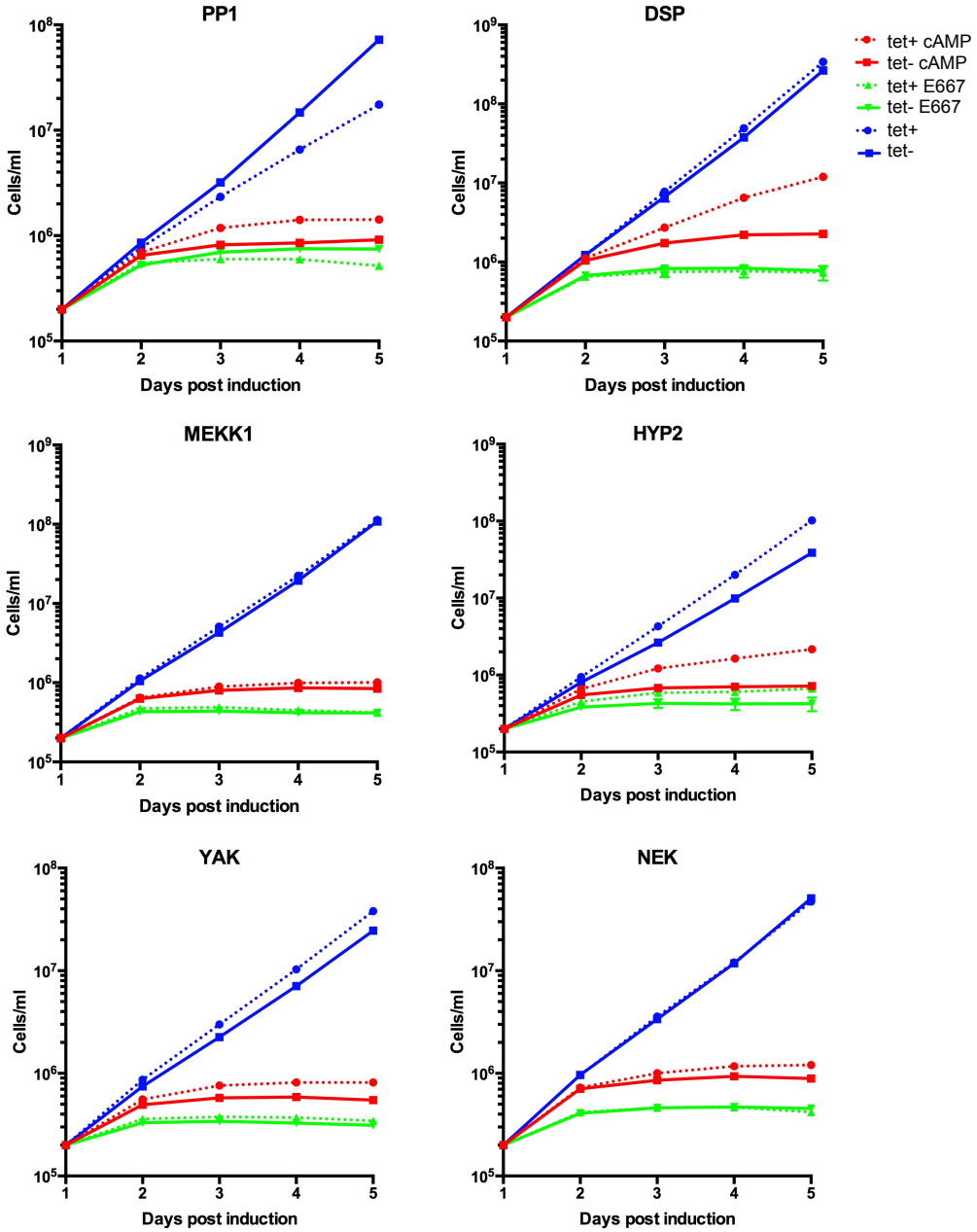

Figure 5.6 Growth curve of *pos*ST RNAi cells treated with pCPTcAMP or E667 24 hours post-induction by tetracycline.

Six *pos*ST RNAi lines were tested for sensitivity to E667. Induction of RNAi had no effect on the sensitivity to E667 in any of these lines (Figure 5.6). However, several lines also showed very limited resistance to pCPTcAMP, suggesting that the level of *in vitro* differentiation resistance previously observed in Mony *et al.* (2014) may be diminished. As this could potentially mask subtle phenotypes at a single compound concentration, their sensitivity to each compound was instead analysed using a range of concentrations to plot dose response curves.

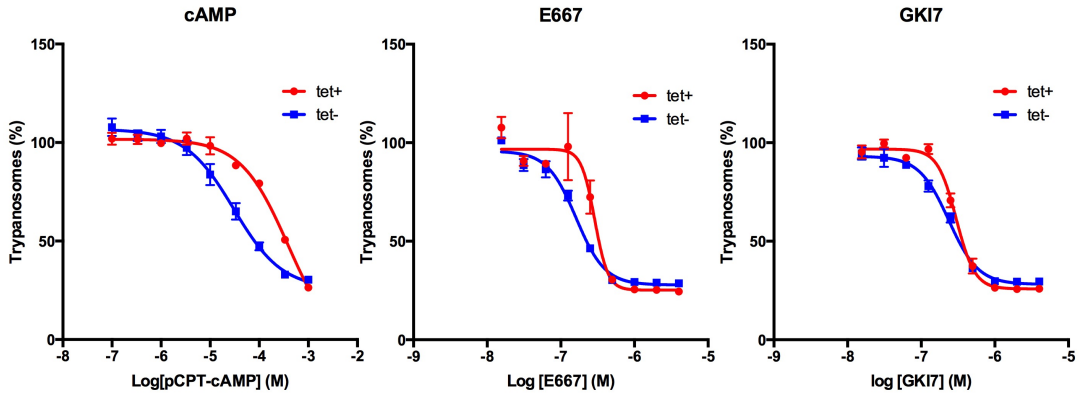

Figure 5.7 Growth of PP1 RNAi cells 72 hours post treatment with stumpy-inducing compounds, determined by alamarBlue assay. 100% indicates density of untreated cells.

As seen in Figure 5.7, induction of PP1 (Tb927.4.3640, Tb927.4.3630, Tb927.4.3620) RNAi resulted in an increase in the concentration of pCPTcAMP required to elicit a response. This was in accordance with previous observations that PP1 RNAi confers loss of responsiveness to pCPTcAMP (Mony et al., 2014). Modest dose-dependent shifts were also observed for both E667 and GKI7 (Figure 5.7), indicating that growth inhibition by both compounds is moderated by PP1.

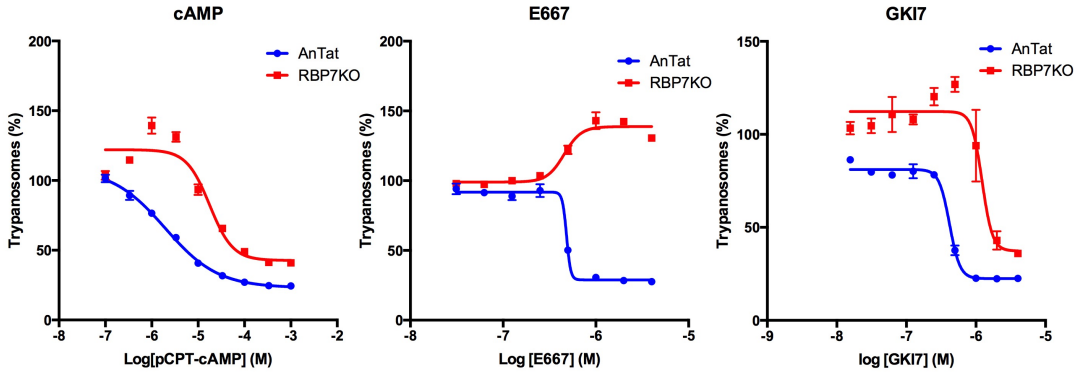

Figure 5.8 Growth of RBP7 KO cells relative to parental AnTat 1.1 90:13 cells 72 hours post treatment with stumpy-inducing compounds, determined by alamarBlue assay. 100% indicates density of untreated cells.

Due to poor regulation of dsRNA expression in the RBP7 (Tb927.10.12090 and Tb927.10.12100) RNAi line (Mony et al., 2014), the RBP7 null mutant line was tested instead and compared to the parental line. In this case, clear resistance to all 3 compounds was observed (Figure 5.8). Intriguingly, the cells were completely resistant to E667, and cell density actually increased at high concentrations of the compound. This demonstrated that both E667 and GKI7 act in an RBP7-dependent manner.

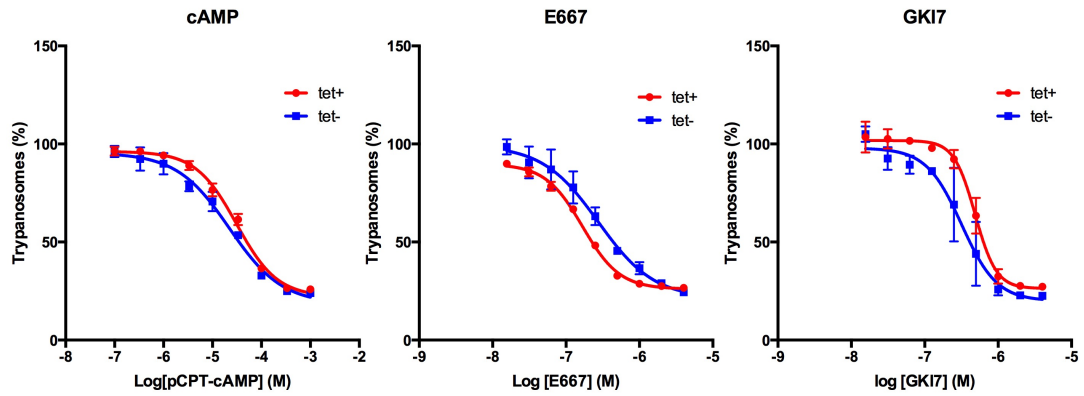

Figure 5.9 Growth of DSP RNAi cells 72 hours post treatment with stumpy-inducing compounds, determined by alamarBlue assay. 100% indicates density of untreated cells.

The dual specificity phosphatase (DSP) Tb927.7.7160 was another *pos*ST component identified in the screen by Mony *et al.* (2014) and a role in stumpy formation has been subsequently validated (B. Mony and K. Matthews, unpublished). DSP RNAi showed no effect on the cells response to E667 or GKI7, suggesting that the compounds act independently of the phosphatase. However, this interpretation was complicated by the absence of any effect of pCPTcAMP in this experiment, contrary to previous observations by Mony *et al.* (2014).

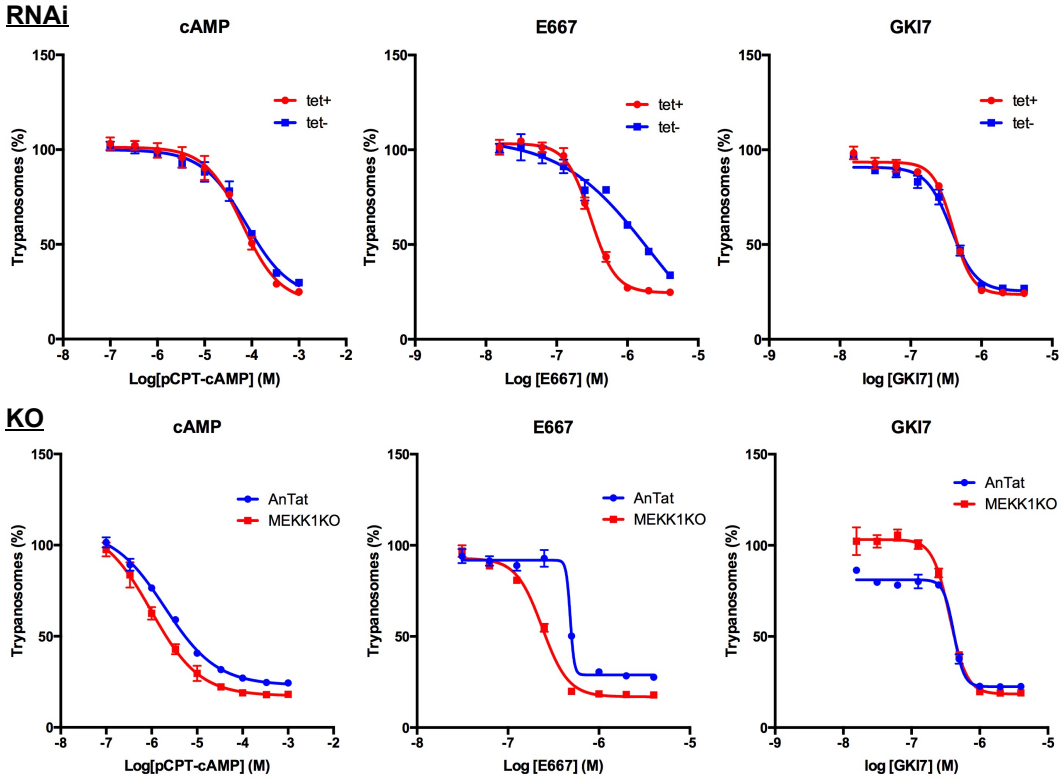

Figure 5.10 Growth of MEKK1 RNAi/KO cells 72 hours post treatment with stumpy-inducing compounds, determined by alamarBlue assay. 100% indicates density of untreated cells.

The involvement of MEKK1 in drug action was tested using both RNAi and null mutant lines. While loss of MEKK1 had no effect on GKI7 sensitivity, it actually increased sensitivity to E667 (Figure 5.10).

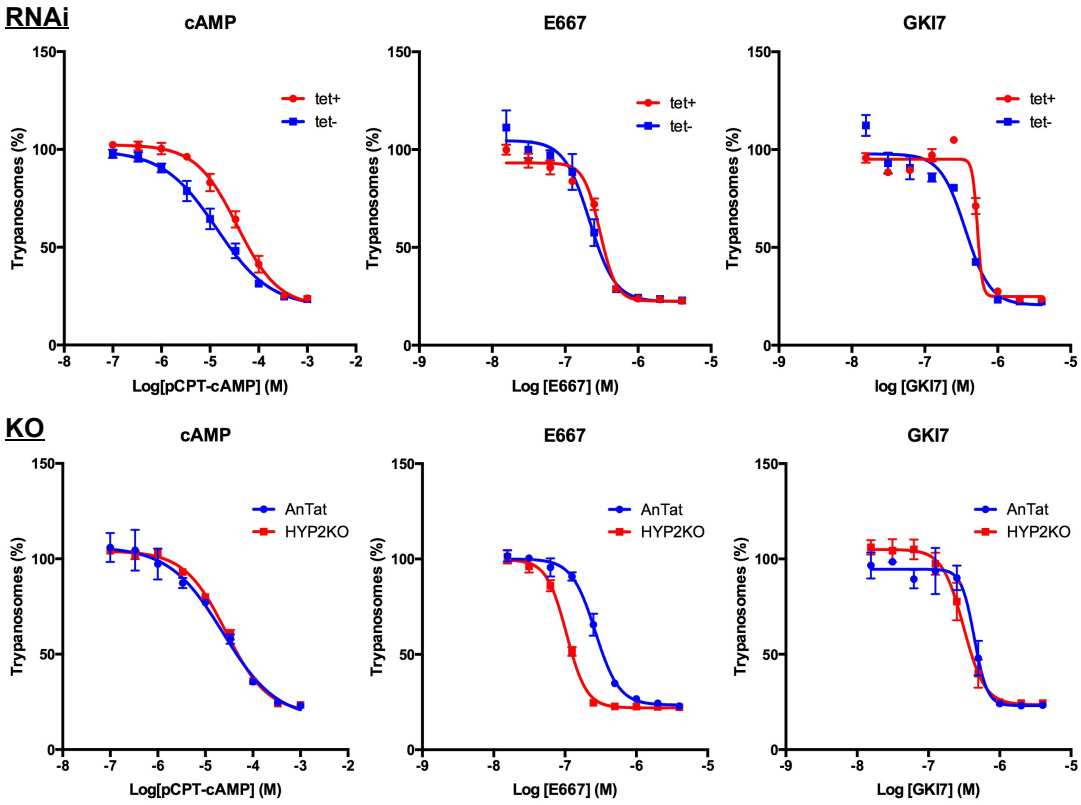

Figure 5.11 Growth of HYP2 RNAi/KO cells 72 hours post treatment with stumpy-inducing compounds, determined by alamarBlue assay. 100% indicates density of untreated cells.

HYP2 RNAi led to the expected decreased sensitivity to pCPTcAMP. It also showed decreased sensitivity to GKI7, while sensitivity to E667 was unaffected (Figure 5.11). While this would suggest that stumpy induction by GKI7, but not E667, is HYP2-dependent, this was not supported when the experiment was conducted on the HYP2 null mutant line, which showed no difference in sensitivity to GKI7 (Figure 5.11; lower panel).

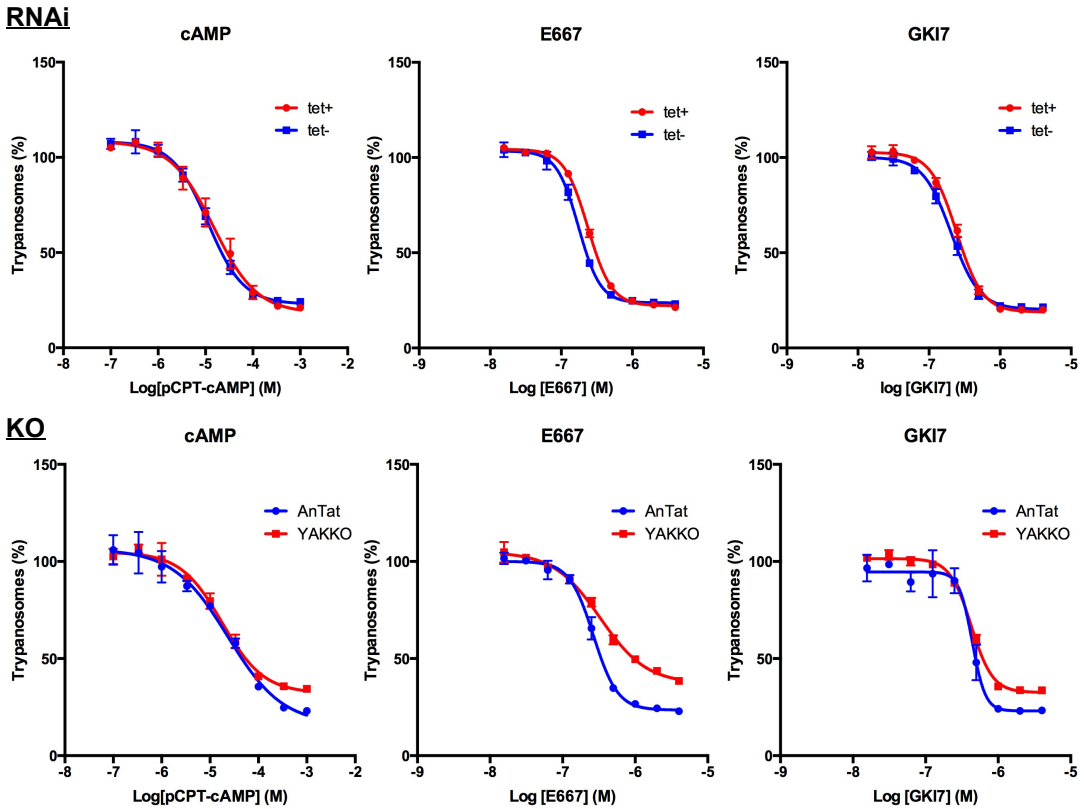

Figure 5.12 Growth of YAK RNAi/KO cells 72 hours post treatment with stumpy-inducing compounds, determined by alamarBlue assay. 100% indicates density of untreated cells.

Loss of YAK had no effect on sensitivity to any of the 3 compounds tested (Figure 5.12). This was unexpected as YAK RNAi had previously shown a pCPTcAMP resistance phenotype (P. MacGregor and K. Matthews, unpublished), but as observed for several other *pos*ST RNAi lines, this appears to have been lost in this assay.

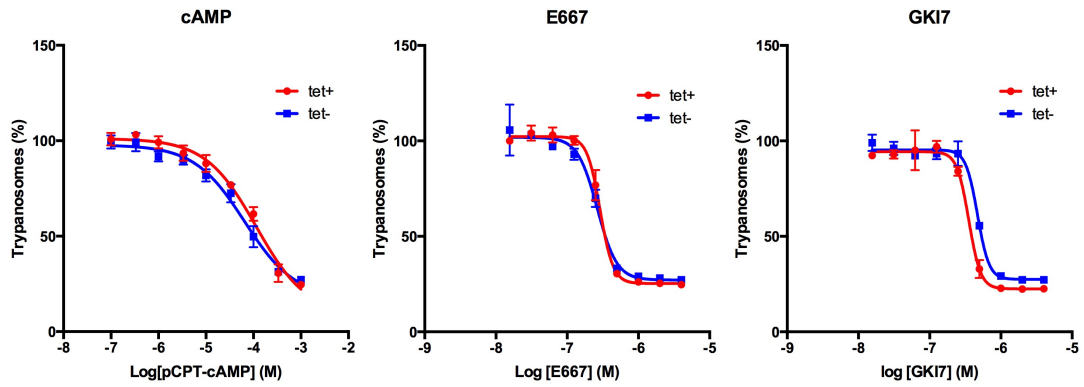

Figure 5.13 Growth of NEK RNAi cells 72 hours post treatment with stumpy-inducing compounds, determined by alamarBlue assay. 100% indicates density of untreated cells.

NEK RNAi had no effect on sensitivity to any of the compounds (Figure 5.13). As for many other *pos*ST RNAi lines discussed above, it is difficult to interpret the relevance of NEK to the actions of E667 and GKI7 as no phenotype was observed for pCPTcAMP, which is known to induce stumpy formation via NEK (Mony et al., 2014).

Overall therefore, only PP1 and RBP7 showed resistance to E667 and GKI7. For the other *pos*ST genes an absence of resistance was complicated by a concomitant lack of resistance to pCPTcAMP.

5.5 Rapid generation of resistance to E667

Treating an RNAi library population with E667 would allow a more comprehensive identification of the downstream effectors of the compound. Previous experiments with E667, carried out on the monomorphic GUS-PAD1 3'UTR reporter line and the pleomorphic AnTat 1.1 90:13 line, used a concentration of 50 µM as standard (MacGregor et al., 2014). Therefore, E667 was tested at this concentration on an RNAi library population (Lib2) to determine its effect on growth.

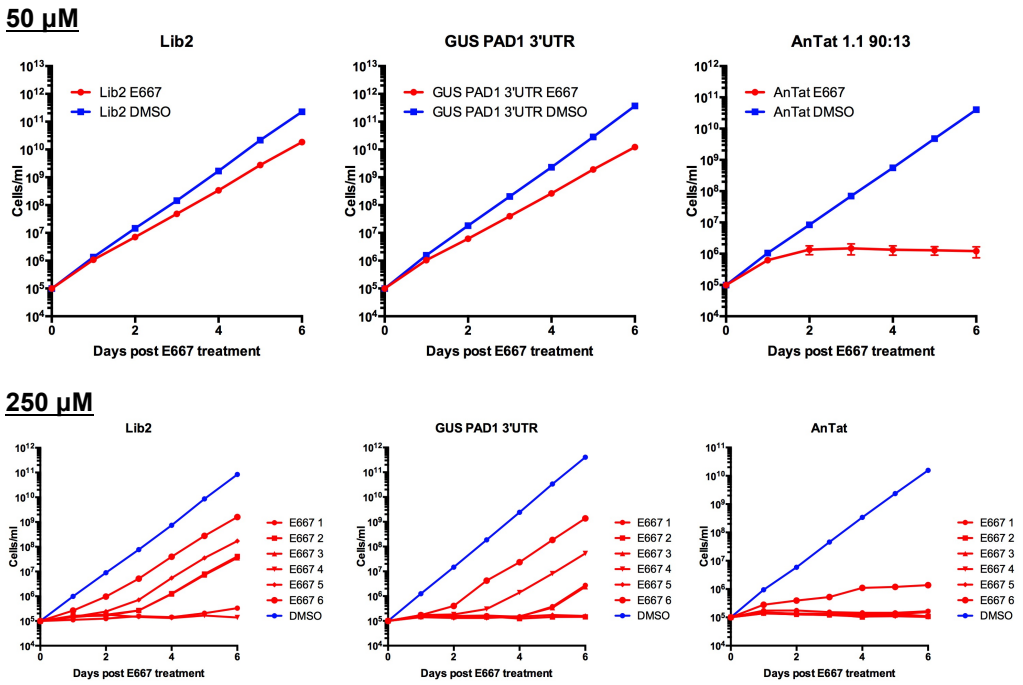

Figure 5.14 Growth effect of E667 on RNAi library (Lib2), GUS-PAD1 3'UTR and AnTat 1.1 90:13 cell lines at 50 µM (upper panel, 3 replicates) and 250 µM (lower panel, 6 replicates). Growth inhibition of monomorphic strains was modest at 50 µM but resistance was rapidly generated at 250 µM.

At 50 μM, E667 had only a modest effect on the uninduced RNAi library population relative to the AnTat 1.1 90:13 strain (Figure 5.14), consistent with previous findings that its effect is less pronounced in monomorphic than pleomorphic trypanosomes (MacGregor et al., 2014). As this level of inhibition would be insufficient for effective selection of resistant RNAi cells, the concentration was increased to 250 μM. This concentration resulted in immediate growth arrest in both monomorphic strains. However, several replicates rapidly recovered and resumed normal growth within 2-6 days of drug addition. It therefore appears that E667 is not suitable for analysis by RNAi library screening as the cells were able to rapidly develop resistance to the compound in the absence of RNAi induction. When 250 μM E667 was tested on pleomorphic trypanosomes, the cells exhibited an immediate and sustained growth arrest. However, 1 replicate recovered growth 12 days after induction and was able to grow continuously at a normal rate in 250 μM E667. This resistance required continuous drug selection to be maintained as when E667 was removed for 12 days and then reintroduced, the cells died (data not shown). Hence, the resistance to the drug selection was not stable over time.

5.6 An RNAi library screen identifies putative GKI7 effectors

Unlike E667, GKI7 was found to effectively inhibit the library population at the concentration used in previous experiments i.e. 1.44 μM, the EC_{50} defined by Diaz *et al.* (2014). To identify downstream effectors of the compound, the RNAi library was induced and subsequently treated with GKI7, resulting in growth arrest. Growth gradually resumed in RNAi induced replicate populations from 5-6 days after treatment. Unexpectedly, this also occurred in non-induced replicates, albeit the effect was delayed by approximately 48 hours (Figure 5.15). This could represent outgrowth of resistant cells, or outgrowth of leaky RNAi lines silencing genes required for GKI7 action.

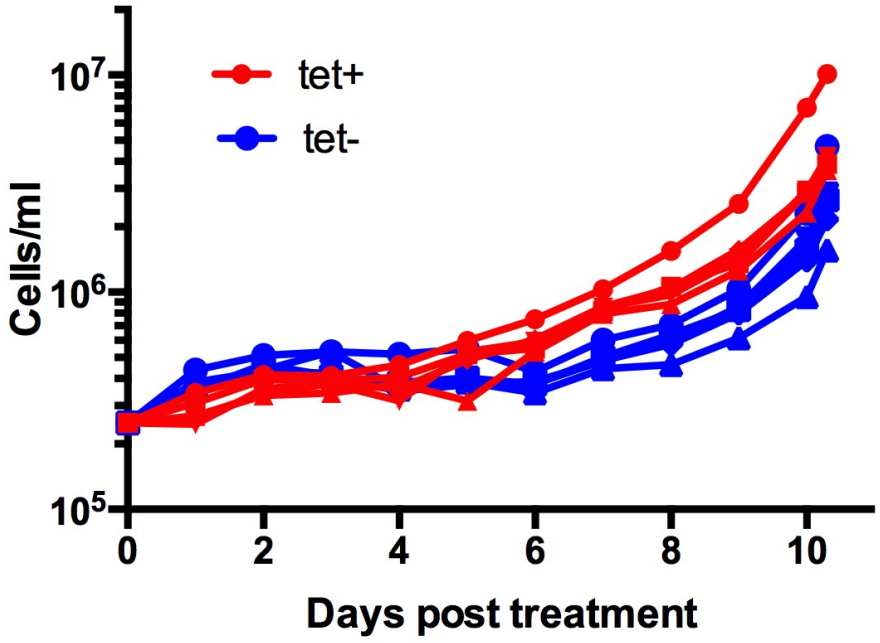

Figure 5.15 Growth of RNAi library cells treated with 1.44 μM E667 24 hours post induction with tetracycline (tet). 5 replicate flasks were analysed in independent assays to provide sufficient library coverage.

After 10 days drug treatment, gDNA was isolated from all treated replicates of the RNAi library, both induced and uninduced, and RNAi inserts amplified by PCR. As seen in Figure 5.16, a continuous smear was observed in a sample isolated at the outset of the experiment due to the presence of a genome-wide representation of RNAi inserts. However, a more specific banding pattern was observed for the GKI7-treated samples, indicating selection of a narrower range of RNAi cells. While this was partially true for uninduced replicate samples, in which distinct bands were visible, a greater degree of selection was evident in the RNAi induced replicates which showed a still more specific profile with far fewer bands. In addition, the banding pattern was similar between replicates, indicating that GKI7 treatment had selected for RNAi of many of the same gene fragments independently.

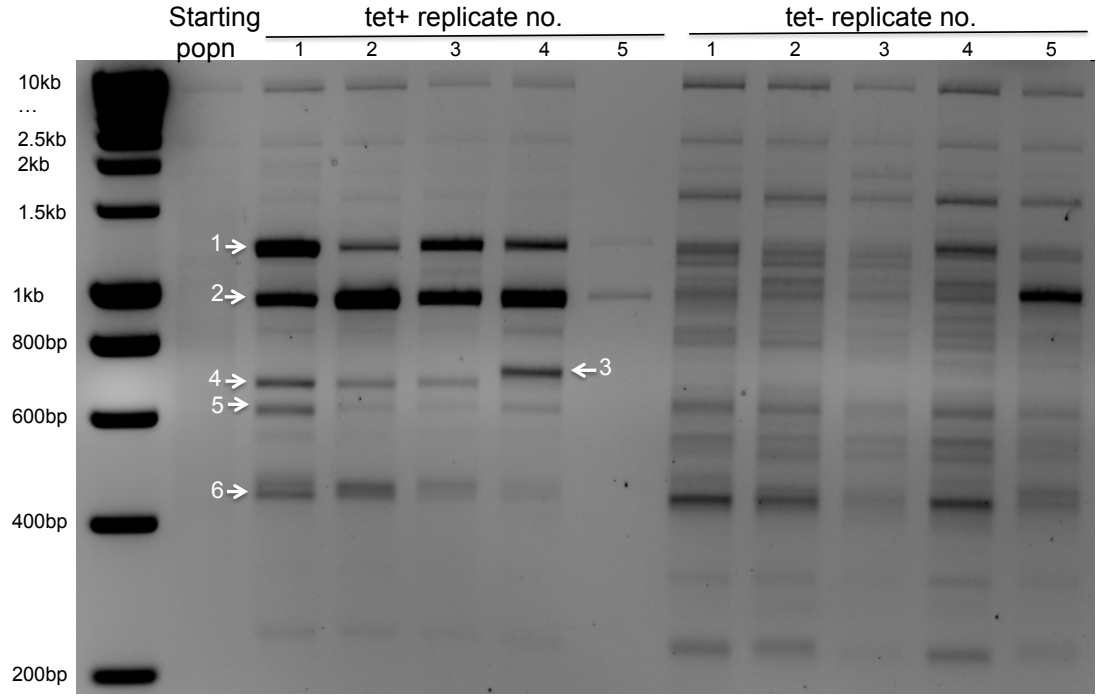

Figure 5.16 RNAi insert amplicon profiles from gDNA of RNAi library cells 10 days post GKI7 treatment. Induced (tet+) replicates show a greater degree of selection. Bands indicated by white arrows were excised and identified by sequencing.

Six amplified RNAi inserts, indicated by white arrows in Figure 5.16, were purified from the gel, cloned into the pGEM T Easy vector (Promega) and sequenced. They were found to correspond to five *T. brucei* genes, listed in Table 5.1. In agreement with hypothetical roles in GKI7-induced stumpy formation, two of these, an N-terminal synaptojanin orthologue and zinc finger protein ZC3H20, showed reduced fitness upon differentiation in a RIT-seq screen by Alsford *et al.* (2011). Synaptojanin is an inositol phosphatase implicated in endocytic recycling (Guo et al., 1999) while ZC3H20 is a zinc finger protein which has been shown to act as a post-transcriptional activator (Erben et al., 2014), and interacts with MKT1, a factor associated with numerous components involved in post-transcriptional regulation (Singh et al., 2014). MKT1 has also been shown to interact with HYP2 (Singh et al., 2014) and showed enriched phosphorylation in the YAK KO line (section 3.5.3). Also included were the methyltransferase MTQ1, which corresponded to two distinct amplified RNAi fragments, as well as two hypothetical proteins.

No.	Accession no.	Function	Additional information	Diff?
1	Tb927.6.2520	Hyp		No
2	Tb927.10.14400	Hyp	Identified in kinome (Urbaniak et al., 2012).	No
3	Tb927.7.3490	synaptojanin (N-term)	Inositol phosphatase domain involved in endocytic recycling.	Yes
4 and 6	Tb927.10.9860	MTQ1	S-adenosylmethionine-dependent methyltransferase. Yeast MTQ1 methylates translational release factor Mrf1p. Non-essential.	No
5	Tb927.7.2660	ZC3H2O	Identified in an silico screen for CCCH-type zinc finger proteins (Kramer et al., 2010). Post-transcriptional activator (Erben et al., 2014). Interacts with MKT1 (Singh et al., 2014).	Yes

Table 5.1 List of genes from the GKI7 RNAi library screen identified by purification and sequencing of RNAi insert specific PCR products. Numbers correspond to the band labels in Figure 5.16. The final column refers to whether a reduced fitness phenotype was observed upon differentiation in a RIT-seq screen (Alsford et al., 2011).

To allow comprehensive identification of selected RNAi fragments, PCR products for 3 induced replicates and 1 uninduced replicate were subject to Ion Torrent sequencing. RNAi insert amplification primers were identified and trimmed and reads aligned to the *T. brucei* TREU 927 genome. A map of read density is shown for all chromosomes in Figure 5.17A. Consistent with the band pattern observed in Figure 5.16, the uninduced replicate showed a greater degree of random widespread mapping at low read density across the genome, indicating reduced specificity relative to the induced samples, although a number of peaks of high read density in the induced samples were also present in the uninduced. Possible explanations for this pattern are discussed in section 5.7.4. Some peaks, such as that at Tb927.10.14400, appeared to be common between induced replicates, while others, such as at RBP7A, were specific to a single replicate, suggesting that parasites silencing these genes were not selected in the other replicates sequenced. This indicated incomplete genomic coverage of the RNAi library population within single replicates, although the use of multiple replicates should provide maximum coverage overall. As each replicate was therefore liable to contain unique hits, the top 20 hits for each RNAi-induced replicate were selected, giving a collated total set of 31 genes. As 4 of these corresponded to only 2 unique sequence targets, this gave a final list of 29 hits, which are listed in Table 5.2. The alignment of reads to each of these genes is depicted in Appendix F Figure 1. The overlap between the 3 sets is depicted in Figure 5.17B. 13 hits are common to all replicates.

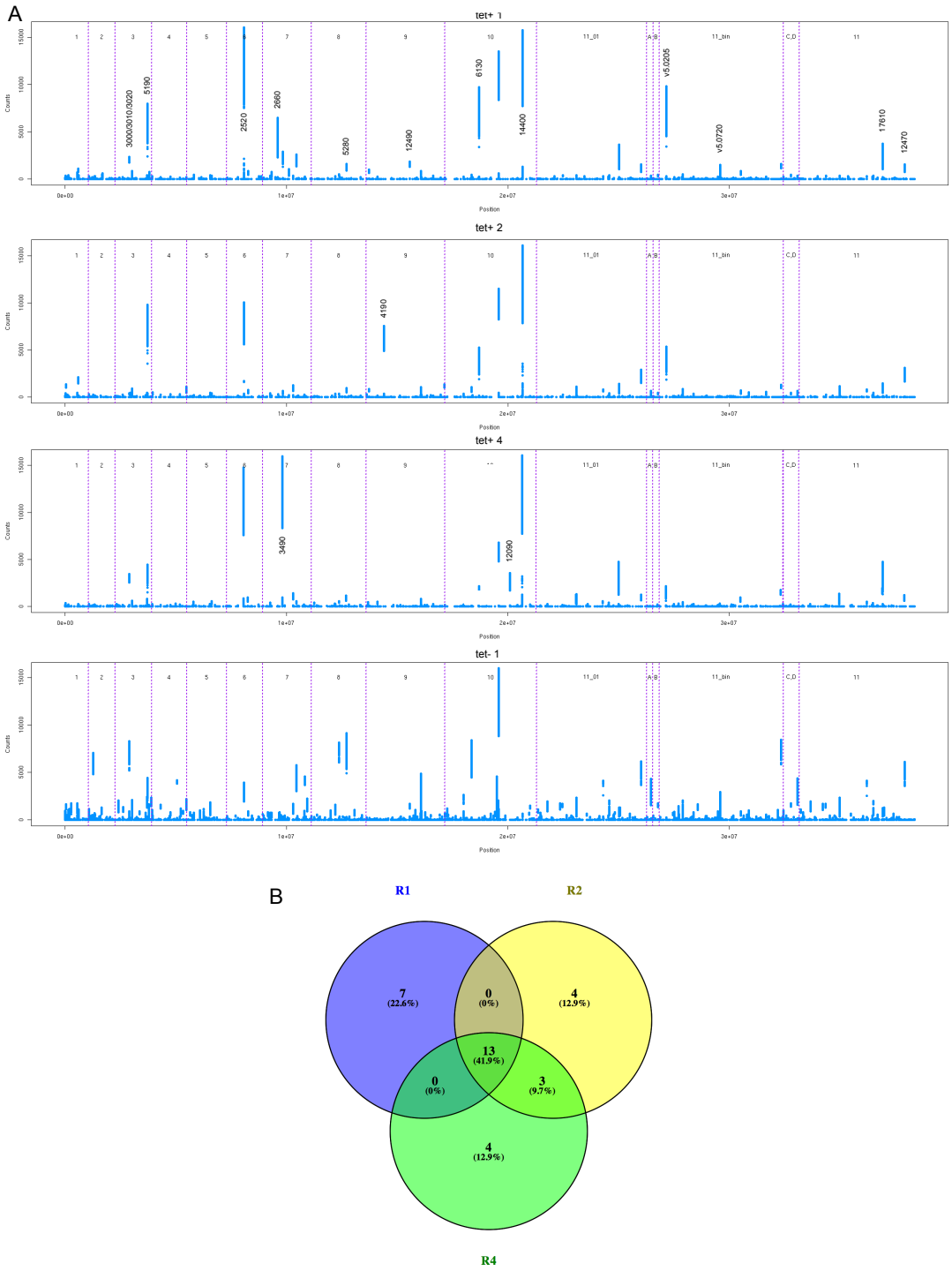

Figure 5.17 Ion Torrent sequencing of RNAi insert specific PCR products from GKI7 RNAi library screen. A) Read density of sequenced replicates aligned to the TREU 927 genome. Pink dotted lines denote divisions between chromosomes. Chromosome numbers are indicated at the top of each graph. A=11_02; B=11_03; C=11_LHfork; D=11_RHfork. Accession numbers of the highest peaks are marked. B) Venn diagram showing overlap of top 20 genes for each induced replicate.

Accession no.	Description	R1	R2	R4	All	Diff
Tb927.10.14400	hypothetical protein, conserved	2	1	1	Yes	No
Tb927.6.2520	hypothetical protein, conserved	1	2	3	Yes	No
Tb927.7.3490	synaptojanin (N-terminal domain), putative	-	-	2	No	Yes
Tb11.v5.0205/ Tb927.10.6130	hypothetical protein, conserved (gene copies)	3	5	9	Yes	Yes
Tb927.9.4190	fatty acyl CoA syntetase 1	-	3	-	No	Yes
Tb927.3.5190	hypothetical protein, conserved	5	4	6	Yes	Yes
Tb927.10.12090	RBP7A	-	-	4	No	Yes
Tb927.3.3000	PIFTC3	6	7	5	Yes	Yes
Tb927.7.2660	ZC3H2O	7	-	-	No	Yes
Tb927.3.5530	Tb-292 membrane associated protein	8	-	-	No	No
Tb927.7.5620	SET domain containing protein, putative	9	-	-	No	No
Tb927.9.12490	hypothetical protein, conserved	10	-	-	No	No
Tb927.7.5210	Putative phosphatase/protein of unknown function DUF89	-	8	7	No	No
Tb927.6.3220/ Tb11.v5.0720	hypothetical protein, conserved, post transcriptional activation (gene copies)	11	12	8	Yes	No
Tb927.11.17610	variant surface glycoprotein (VSG), frameshifted and point mutation	-	9	19	No	No
Tb927.8.5280	TbMRPS34	13	17	13	Yes	No
Tb927.5.3160	protein kinase, putative	16	10	16	Yes	No
Tb927.11.12470	hypothetical protein, conserved	15	11	14	Yes	Yes
Tb927.7.1640	Mitochondrial LSU ribosomal protein, putative	14	-	-	No	No
Tb927.7.4440	NAD dependent epimerase/dehydratase family, putative	16	-	-	No	No
Tb927.5.3330	hypothetical protein, conserved	-	18	12	No	No
Tb927.2.3320	65 kDa invariant surface glycoprotein	18	-	-	No	Yes
Tb927.3.3010	hypothetical protein, conserved	20	14	18	Yes	No
Tb927.3.3020	actin-like protein, putative	19	15	17	Yes	No
Tb09.v4.0072	variant surface glycoprotein (VSG, pseudogene), putative	-	16	-	No	Yes
Tb927.9.2220	SUMO1/Ulp2, putative	-	-	15	No	No
Tb927.4.240	retrotransposon hot spot protein (RHS, pseudogene), putative	-	19	-	No	No
Tb927.11.1680	vesicular-fusion protein SEC18, putative	-	-	20	No	No
Tb927.10.4790	hypothetical protein, conserved	-	20	-	No	Yes

Table 5.2 List of genes from the GKI7 RNAi library screen identified by Ion Torrent sequencing of RNAi insert specific PCR products including the top 20 hits for each induced replicate. Ranking of each gene is shown for each induced replicate in columns 3 to 5. The final column refers to whether a reduced fitness phenotype was observed upon differentiation in a RIT-seq screen (Alsford et al., 2011). Highlighted rows: previously identified by cloning; known *pos*ST component; yellow and green pair gene copies; pseudogenes.

Of the genes previously identified by sequencing in the pGEM-T Easy vector, reads aligning to hypothetical proteins Tb927.6.2520 and Tb927.10.14400 were highly abundant in all 3 induced replicates sequenced while reads from synaptojanin and ZC3H20 were abundant only in replicates 4 and 1 respectively. This matched the PCR product profile shown in Figure 5.16. Surprisingly, MTQ1 was not detected by Ion Torrent sequencing, despite being independently identified from cloning of two distinct PCR fragments.

Of the known *pos*ST components, RBP7A was the fourth highest hit in replicate 4. This is in agreement with the dose response analysis shown in Figure 5.8, in which of all the *pos*ST RNAi and KO lines tested, the RBP7 null mutant most convincingly showed decreased sensitivity to GKI7. None of the other *pos*ST components studied were identified, suggesting that stumpy formation by GKI7 follows a pathway largely distinct to that induced by cAMP, but that both involve the action of RBP7.

Also identified were numerous genes of wide-ranging predicted functions not previously implicated in stumpy formation. The inclusion of metabolic enzymes fatty acyl-coA synthetase 1 (Tb927.9.4190) and a putative member of the NAD dependent epimerase/dehydratase family (Tb927.7.4440) likely relates to the metabolic changes which occur during differentiation in preparation for survival in a new host. Tb927.7.4440 is predicted to be upregulated in stumpy forms according to a recent proteomic study (Dejung et al., 2016). The presence of two components of mitochondrial ribosomes (Tb927.8.5280 and Tb927.7.1640) may also reflect the upregulation of mitochondrial activity in stumpy formation prior to uptake by the tsetse. Tb927.8.5280 is also predicted to be upregulated in stumpy forms (Dejung et al., 2016). Similar to the cAMP-responsive *pos*ST pathway, the cohort includes signalling components including a putative kinase (Tb927.5.3160) and putative phosphatase (Tb927.7.5210). The kinase is upregulated both in stumpy forms and during subsequent differentiation to procyclic forms, while the phosphatase is upregulated during procyclic differentiation (Dejung et al., 2016). There are also a number of candidates which could potentially be involved in regulation of expression. This includes epigenetic regulation, in the case of Tb927.7.5620, which contains a SET domain associated with lysine methyltransferases (Dillon et al.,

2005), and the predicted SUMO protease SUMO1/Ulp2 (Tb927.9.2220). In addition, the hypothetical protein Tb927.6.3220 was implicated in post-transcriptional activation when artificially tethered to a reporter mRNA (Erben et al., 2014). Curiously, three pseudogenes were also selected. It is possible that these transcribe non-protein coding RNAs with regulatory roles. RNAi of one of these, the VSG pseudogene Tb09.v4.0072, was previously found to reduce fitness upon differentiation in a RIT-seq screen (Alsford et al., 2011). Additional hits included an actin-like protein (Tb927.3.3020), an intraflagellar transport protein (Tb927.3.3000) and various hypothetical proteins.

As independent validation of individual RNAi lines has yet to be completed for any of the above hits, their involvement in stumpy formation remains hypothetical. RNAi of some transcripts may select for resistance to GKI7 by mechanisms distinct from differentiation. As such, the selection of the putative vesicular fusion protein SEC18 (Tb927.11.1680) may reflect reduced uptake or increased export of the compound via vesicular transport. A 65 kDa invariant surface glycoprotein (Tb927.2.3320) was also selected. RNAi of another ISG, ISG75, was selected for resistance to suramin and resulted in reduced binding of the drug (Alsford et al., 2012). Interestingly, ISG65 was downregulated upon RNAi of RDK1, which promotes bloodstream to procyclic differentiation (Jones et al., 2014).

5.7 Discussion

5.7.1 Identification of a GKI7, a compound capable of inducing stumpy formation.

MacGregor *et al.* (2014) previously developed a monomorphic reporter line in which the PAD1 3'UTR was conjugated to the β-glucuronidase reporter to use in high-throughput screening assays for stumpy-inducing compounds. This reporter line was used to identify E667, a small molecule capable of inducing differentiation in monomorphic and pleomorphic trypansosomes, demonstrating its efficacy as a phenotypic screening tool and the value of its use in the screening of further compound libraries. The subsequent identification of potent inhibitors of trypanosome growth from a kinase-targeted library by Diaz *et al.* (2014) provided an excellent compound set for such analysis. 52 small molecules were tested for

upregulation of the PAD1 reporter, of which 6 resulted in greater than 53% reporter activation relative to pCPTcAMP (Figure 5.3). GKI7 resulted in the greatest level of activation and was selected for further analysis. Subsequent validation in a pleomorphic line demonstrated that this molecule caused G_1 arrest and upregulation of the PAD1 protein (Figure 5.5). Again, this validated the effectiveness of the reporter assay in the identification of stumpy-inducing small molecules which can be used both as research tools and potentially as novel therapeutics. Although only GKI7 was analysed further in this thesis, the other five compounds also merit subsequent validation. As the tested compound set was previously selected for potency of growth inhibition, GKI7 was capable of triggering differentiation at a substantially lower concentration (1.44 μM) than E667 (50 μM) and thus represents a useful tool for future analysis.

5.7.2 Sensitivity to E667 and GKI7 of *pos*ST RNAi and KO lines.

E667 and GKI7 have been shown to induce stumpy formation but it is unknown if they act via the same pathway as cAMP and, if so, at what point on this pathway. If either compound acts on a *pos*ST component downstream of cAMP, RNAi silencing of those components downstream of this action would confer resistance to the compound while any which acts upstream would remain sensitive (Figure 5.1). RNAi lines for 6 *pos*ST components (PP1, DSP, MEKK1, HYP2, YAK and NEK) were tested for sensitivity to E667 at 50 μM (Figure 5.6). RNAi did not appear to confer resistance in any case. However, contrary to previous observations by Mony *et al.* (2014), many of these lines concurrently showed little or no resistance to pCPTcAMP. To negate the possibility that subtle resistance phenotypes were being masked at a single drug concentration, the sensitivity of *pos*ST RNAi and null mutant lines to pCPTcAMP, E667 and GKI7 were instead analysed using a range of concentrations and dose response curves generated. For many cell lines tested, resistance to pCPTcAMP still was not observed. This was unexpected as the *pos*ST components were originally selected for resistance to pCPTcAMP upon RNAi silencing and this was validated in each independent RNAi line (Mony et al., 2014). In addition, all cell lines recently tested *in vivo* still effectively reduce stumpy formation in response to SIF (K. McWilliam and K. Matthews, unpublished). It is

possible that the loss of the cAMP resistance phenotype was due to adaptation of the cells in culture over time. As any such adaptation may also affect the response to other stumpy-inducing compounds, it complicated interpretation of E667 and GKI7 sensitivity analyses. RNAi of DSP, MEKK1, YAK and NEK all had no apparent effect on sensitivity to either compound, indicating that they operate independently of these proteins. HYP2 RNAi resulted in a modest decrease in sensitivity to GKI7 but this was not replicated in the HYP2 null mutant line. PP1 RNAi also showed a modest decrease in sensitivity to pCPTcAMP, E667 and GKI7. The most obvious effect, however, was observed in the RBP7 null mutant line, which showed a substantial reduction in sensitivity to pCPTcAMP and GKI7 and was completely resistant to E667. This indicated that stumpy formation by both E667 and GKI7 is dependent on RBP7, which is consistent with the prediction that this protein acts relatively low down in the pathway. This could indicate that these compounds activate the *pos*ST pathway at a position low down in the signalling cascade or alternatively that they activate an alternative stumpy formation pathway which converges with the cAMP-responsive *pos*ST pathway at or above RBP7. However, the muted response to pCPTcAMP of various *pos*ST RNAi and KO lines means that the possibility cannot be excluded that E667 and/or GKI7 act higher up in the *pos*ST signalling pathway but that the effects of these manipulations were masked by adaptation of the parasites.

5.7.3 Cells rapidly generate resistance to E667

An RNAi library screen offers a more global approach to identifying downstream effectors of stumpy-inducing compounds, as was used for pCPTcAMP/AMP (Mony et al., 2014). However, in the case of E667, a high concentration of drug (250 μM) was required to sufficiently inhibit the uninduced monomorphic RNAi library cells and, in most replicates, growth resumed within 2-6 days of drug treatment (Figure 5.14). This rapid development of resistance in the absence of RNAi induction precluded the use of an RNAi library screen to identify components responsive to this compound.

Treatment of pleomorphic AnTat 1.1 90:13 cells with an equivalent concentration of E667 resulted in a higher degree of growth inhibition relative to monomorphic cells

(Figure 5.14). However, after 12 days of treatment with 250 μM E667, one of six replicates tested in this cell line developed resistance to the compound and growth was restored to wild type levels. Although this cell line was able to grow continuously in the presence of the compound, the resistance phenotype was lost when drug pressure was removed for 12 days. This indicated that the cells developed resistance via an adaptation which arises in independent replicates, is not cell line specific and can be both acquired and lost rapidly. It is currently unknown if resistant cells display cross-resistance to other differentiation signals. The E667 resistant AnTat 1.1 90:13 cell line may prove a useful tool in future studies of this kind.

5.7.4 RNAi library screen with GKI7 reveals putative novel differentiation factors.

GKI7 was found to effectively inhibit the RNAi library population at the concentration used for all previous experiments (1.44 μM). So in order to comprehensively identify downstream effectors of this compound, the RNAi library was induced and treated with GKI7. A resistant population gradually outgrew in all 5 replicates and amplification of RNAi inserts showed selection of specific RNAi fragments, with the majority of replicates showing a similar profile (Figure 5.16). Unexpectedly, a resistant population also outgrew in the uninduced replicates, although this effect was delayed by approximately 48 hours relative to the replicates in which RNAi had been induced (Figure 5.15). The amplified RNAi insert profile of these cells showed a less specific profile than in the induced replicates with a far greater number of bands present (Figure 5.16) and a greater degree of widespread random mapping to the genome at low read density by Ion Torrent sequencing (Figure 5.17). However, the visibility of distinct bands indicated that some degree of selection had occurred for specific RNAi inserts in the absence of tetracycline, possibly due to leaky dsRNA expression. Indeed, a number of hits identified in the induced replicates by Ion Torrent sequencing were also highly abundant in the uninduced replicate sequenced. An alternative explanation for the emergence of a resistant population in the absence of induction is that either GKI7 or by-products of GKI7 are mutagenic, leading to background genomic mutations unrelated to RNAi.

RNAi inserts of the selected parasites were identified, first by sequencing of distinct amplified bands cloned into the pGEM-T Easy vector, and then more comprehensively by Ion Torrent sequencing. PCR products for 3 induced replicates and 1 uninduced replicate were subject to the latter method. The hits identified by each method were in good agreement, with four out of five cloned genes appearing as top hits in the Ion Torrent dataset and variation between replicates consistently reflected.

A number of hits showed very high read density in one of the replicates sequenced but were low or absent in others, indicating that parasites silencing certain genes were selected in some replicates and not others. For example, Tb927.7.3490 was cloned from a PCR band only visible in induced replicate 4. When sequenced by Ion Torrent, read density for this gene was the second highest for that replicate but this was more than 300 fold lower in the other replicates sequenced. For this reason, the top 20 hits were calculated for each replicate sequenced as many genuine hits may be unrepresented in some replicates due to incomplete genomic coverage within a single replicate. Alsford *et al.* (2011) reported that the library included 5 RNAi targets per gene in an uninduced population. While maintenance of the library at $>5x10^6$ cells and use of $>1x10^7$ cells for each replicate should be sufficient to sustain this level of complexity, it is likely that complexity has been lost over time due to growth and passage of the cells in our lab. This may have been exacerbated by the progressive dilutions entailed in the 48 hour period between thawing of the cells and induction of the library (see section 2.17). Overall, this should be resolved by the use of multiple replicates to increase genomic coverage.

Collation of these hits gave a total of 29 candidate genes. It is possible that some of these genes may be false positives due to sequence homology with the RNAi insert primers. Glover *et al.* (2015) recommended filtering reads using construct-specific tags internal to the sequences used in amplification to confirm construct as opposed to genomic origin. This step was not included in the analysis presented in this thesis. However, a preliminary analysis which did detect and remove construct tags produced an identical list of candidate genes with only very minor variations in the

ranking positions of a few genes, which would indicate that all 29 candidates were identified from genuine RNAi fragments.

The 29 candidates include many novel genes not previously implicated in stumpy formation with a wide range of predicted functions. 11 of these showed reduced fitness upon differentiation in a RIT-seq screen (Alsford et al., 2011). Included were the metabolic enzymes fatty acyl coA synthetase 1 and a putative NAD dependent epimerase/dehydratase, as well as two mitochondrial ribsome components, which may reflect the altered energy metabolism and upregulated mitochondrial activity in the stumpy form in preparation for transmission to the tsetse vector. Also present were a number of potential gene regulators, including a hypothetical protein and a zinc finger protein (ZC3H20) both shown to result in post-transcriptional activation when tethered to a reporter transcript (Erben et al., 2014). Interestingly, a number of hits had putative roles in chromatin remodelling. These include a predicted SUMO protease and a protein containing a SET domain, associated with lysine methyltransferases (Dillon et al., 2005). These could be involved in the loss of mono-allelic control of VSG expression associated with stumpy forms (Amiguet-Vercher et al., 2004; Navarro and Gull, 2001), which involves delocalisation of polymerase I from the expression site body (ESB) containing the active VSG expression site (Barquilla et al., 2012), as SUMOylation has been shown to positively regulate VSG expression at the ESB in slender forms (Lopez-Farfan et al., 2014). Another hit identified by PCR product cloning was the predicted S-adenosylmethionine-dependent methyltransferase MTQ1, although this was not found by Ion Torrent sequencing. 2 predicted kinases and a predicted phosphatase also indicated the involvement of signal transduction in relaying the GKI7 response.

A number of hits had putative functions in endocytic and vesicular transport processes. These include an N-terminal synaptojanin orthologue and putative vesicular fusion protein SEC18. It is possible that RNAi of these genes confers resistance to GKI7 independently of stumpy formation pathways, for example via decreased uptake or increased export of the compound. However, RNAi of the synaptojanin orthologue results in reduced fitness upon differentiation (Alsford et al., 2011), supporting a role in stumpy formation. ISG65 was also identified in the

screen. It is possible that this could be involved in binding and uptake of the compound as RNAi of another ISG, ISG75, was selected for resistance to suramin due to reduced binding of the drug (Alsford et al., 2012). However, a role specific to the differentiation process is supported by the fact that ISG65 was downregulated upon RNAi of RDK1, which promotes bloodstream to procyclic differentiation (Jones et al., 2014).

The inclusion of 3 pseudogenes among the screen hits indicated the involvement of non-protein factors in the response to GKI7. One of these, the VSG pseudogene Tb09.v4.0072, has previously been implicated in differentiation due to reduced fitness in the RIT-seq screen (Alsford et al., 2011). It is possible that these pseudogenes transcribe ncRNAs with regulatory functions.

RBP7A was also identified in the screen. This was in agreement with previous results which showed that the RBP7 null mutant line was less sensitive to GKI7 (Figure 5.4 and Figure 5.8), supporting the hypothesis that stumpy formation by GKI7 is dependent on RBP7. In contrast, none of the other posST components were detected, indicating that GKI7 acts independently or downstream of these proteins, as depicted in Figure 5.18. The number of novel hits identified would favour the option that GKI7 induces differentiation via a pathway distinct to pCPTcAMP and that the two pathways converge upstream of RBP7.

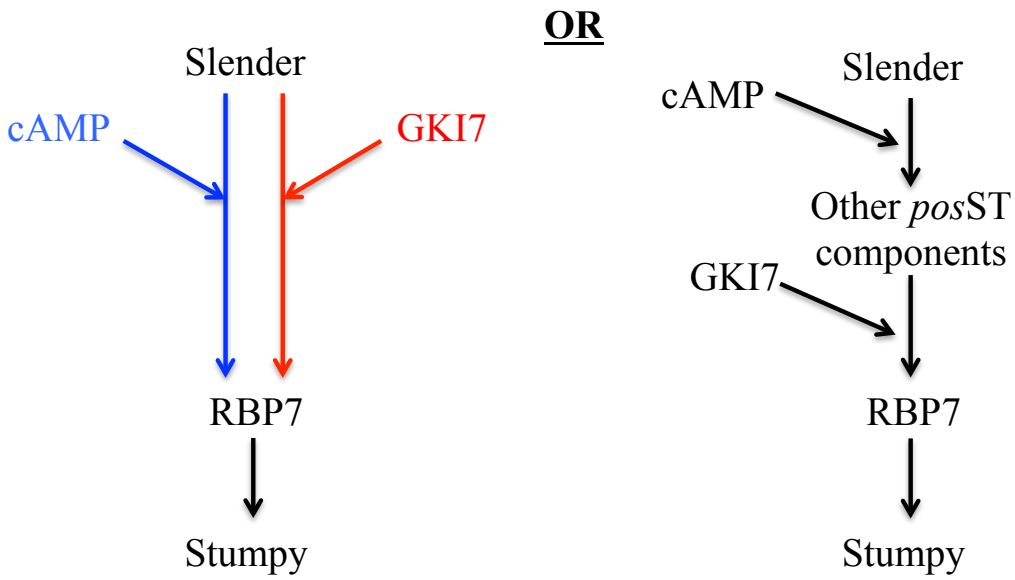

Figure 5.18 Alternative models of stumpy formation induced by cAMP or GKI7. Left: cAMP and GKI7 induce distinct stumpy signalling pathways involving different effectors. The pathways converge upstream of RBP7. Right: Alternatively, GKI7 induces the same stumpy signalling pathway as cAMP, but acts upstream of RBP7 and downstream of other *pos*ST components.

The identification of so many genes that had not previously been implicated in stumpy formation, and which may operate in a distinct arm of the pathway to those previously studied, represents an intriguing prospect for future analysis. All of these hits remain to be independently validated. Stumpy signalling can then be further explored by examining the interactions between these novel components and also their relationship to the actions of the cAMP-responsive *pos*ST components, revealing further organisation of the pathways involved.

6 Chapter 6: Summary and future directions

The differentiation of *Trypanosoma brucei*, from proliferative slender forms to arrested, transmissible, stumpy forms in the mammalian bloodstream involves extensive morphological and metabolic adaptations in preparation for uptake by the tsetse fly vector. The signalling pathway which transduces the unindentified parasite-derived stumpy induction factor signal to produce these adaptations remained uncharacterised until Mony *et al.* (2014) carried out an RNAi library screen for resistance to the stumpy inducing molecules pCPTcAMP and pCPTAMP. This identified a cohort of positive mediators of stumpy formation (*pos*ST), many of which were individually demonstrated to be involved in differentiation *in vitro* and *in vivo*. How these proteins function together to drive stumpy formation remains unknown and this thesis aimed to order known components of the process within the signalling pathway.

Firstly, the organisation of the pathway was explored using knockout and overexpression combinations of distinct *pos*ST components in pleomorphic trypanosomes to determine the dependency relationships between these proteins. The effect on differentiation of these manipulations was analysed for numerous combinations, in particular those involving the *pos*ST components PP1, RBP7, YAK and NEK, revealing a pathway structure predicted to divide into two separate branches with PP1 and YAK acting via one arm and NEK and RBP7 through the other (Figure 3.31). This demonstrated simultaneous knockout and overexpression to be an effective method of elucidating the organisation of the stumpy signalling pathway. Future use in further combinations will not only allow the incorporation of additional components into the model, but will enable corroboration of the predicted positions of those components already investigated in multiple combinations and clarification for components such as HYP2 and MEKK1, which have been tested in fewer combinations to date and for which positioning remains tentative.

Further contributions to the proposed pathway organisation came from the phosphoproteomic analysis of two *pos*ST kinases, MEKK1 and YAK (section 3.4). The first was that NEK is dephosphorylated in the MEKK1 null mutant line, which indicated that MEKK1 acts upstream of NEK. This placed MEKK1 on the branch of the signalling pathway containing NEK and RBP7 (Figure 3.31). It would be

interesting to explore by enzymatic assay whether MEKK1 directly phosphorylates NEK and how this affects its activity. However, recombinant expression of MEKK1 could prove complicated, based on the difficulties experienced in its overexpression (sections 3.2.3.6 and 3.2.3.7). The second contribution is that phosphorylation of AMPK β is increased, indicating that activity of the known *pos*ST component AMPK α2 may either be regulated downstream of MEKK1 and YAK or alternatively can be independently upregulated to compensate for the loss of these kinases. While these changes remain to be independently validated, and involvement of many of the proteins affected in differentiation remains hypothetical, the differences observed between MEKK1 KO and YAK KO raises the interesting possibility that global analysis of the downstream effects of these signalling components could be used to identify which differentiation processes are activated by different branches of the pathway, as both kinases affected phosphorylation of proteins involved in a wide range of cellular processes.

A number of inhibitors of stumpy formation have also been identified previously (Barquilla et al., 2012; Domenicali Pfister et al., 2006; Vassella et al., 2001). The relationship between differentiation promoting and differentiation inhibiting mechanisms was explored using a pleomorphic TOR4 RNAi line. TOR4 RNAi had previously been shown to trigger stumpy formation *in vitro* in a monomorphic line (Barquilla et al., 2012) and this phenotype was also observed in a pleomorphic line (Figure 4.1). RNAi induction also resulted in stumpy formation at low parasite density *in vivo* (Figure 4.2). Ablation of *pos*ST components in combination with TOR4 RNAi was used to explore the dependency relationships between positive and negative regulators of stumpy formation. TOR4 RNAi in conjunction with either NEK RNAi or MEKK1 KO resulted in growth inhibition *in vitro* and *in vivo* (Figure 4.3 and Figure 4.6). TOR4 RNAi still caused cell cycle arrest independently of either *pos*ST component but was unable to upregulate PAD1 expression (Figure 4.4 and Figure 4.7), indicating that this process is dependent on MEKK1 and NEK. This indicated that TOR4 acts at an early stage of differentiation to inhibit cell cycle arrest, while MEKK1 and NEK are implicated in both arrest and later stages of the process including PAD1 expression (Figure 4.4.8). These results support the model proposed by Mony *et al.* (2015) in which stumpy formation is regulated by two

opposing mechanisms, in which TOR4 and other inhibitors of differentiation act to retain the slender state, while the *pos*ST components activate stumpy formation. The slender retention mechanism, including TOR4, would be predicted to be active in slender forms at low density in blocking the initial stages of differentiation, including cell cycle arrest. This inhibition is removed upon TOR4 RNAi, and the *pos*ST pathway activates the entire differentiation program.

It would be interesting to further explore the intersection of these two opposing mechanisms in differentiation. However, this would likely require a change in strategy from the TOR4 RNAi + *pos*ST RNAi/KO combinations used here. TOR4 RNAi does not offer the "clean" genetic background provided by *pos*ST null mutant lines in which to perform further genetic manipulations. TOR4 RNAi line infections proceeded with complex kinetics, possibly in part due to temporal variablility in the level of silencing, and this complicated analysis when used in combination with RNAi/KO of other genes. Although the growth phenotype observed upon TOR4 RNAi suggests that it is essential and therefore not amenable to knockout, Vassella *et al.* (2001) were able to successfully delete both alleles of another stumpy inhibitor, ZFK, in a pleomorphic strain, despite this resulting in a similar slow growth phenotype to TOR4 RNAi.

The organisation of the stumpy signalling pathway was further interrogated using chemical-genetic analysis. The identification of small molecules capable of inducing stumpy formation at low density has potential both in the discovery of novel therapeutics and for use as chemical tools in the investigation of the process. MacGregor *et al*. (2014) identified one such compound, E667, using a stumpy-specific reporter line to screen a compound library. This reporter line was used here to screen 52 compounds selected for trypanosome growth inhibition (Diaz et al., 2014), identifying a further six compounds capable of inducing stumpy formation (Figure 5.3), one of which, GKI7, was selected for further analysis (Figure 5.5). Nothing is known about the mechanism by which either E667 or GKI7 induce stumpy formation: whether they act at the same point of the stumpy signalling pathway to cAMP, or indeed whether they act via the same pathway at all. A compound which acts via the *pos*ST pathway, but at a point downstream of cAMP,

would offer an invaluable tool to investigate ordering of the pathway, as known components could essentially be phenotypically separated into two subsets using RNAi/KO lines: downstream components which confer resistance to the compound, and those upstream or on separate branches, for which sensitivity would be retained (Figure 5.1).

Genes involved in resistance to E667 and GKI7 were therefore investigated using a combination of individual *pos*ST RNAi and KO lines and RNAi library screens. The first approach was hindered by the fact that many of these lines appeared to have lost resistance to pCPTcAMP, possibly due to adaptation through culture, which complicated interpretation for many cell lines. However, the PP1 RNAi line showed a modest reduction in sensitivity to both E667 and GKI7 (Figure 5.7), and the RBP7 KO line showed clear resistance to both compounds (Figure 5.8), indicating that E667 and GKI7 action is dependent on RBP7 and possibly PP1. Resistance to GKI7 was more comprehensively explored using an RNAi library screen, which identified mainly genes not previously implicated in differentiation (Table 5.1 and Table 5.2). The exception was RBP7, consistent with the result observed using the RBP7 KO line. As no other *pos*ST components were identified, this would suggest that GKI7 induces stumpy formation via a largely separate pathway to cAMP involving distinct components, but that the two pathways converge upstream of RBP7. This supports the hypothesis that RBP7 is a central regulator of differentiation which acts far down in the signalling pathway. In addition, this screen has identified many potential novel mediators of stumpy formation which remain to be validated using individual RNAi lines.

It was not possible to carry out an RNAi library screen to identify genes involved in resistance to E667 as the parasites rapidly and consistently developed resistance to the compound in the absence of tetracycline and were again able to proliferate normally (Figure 5.14). A pleomorphic line similarly developed resistance to the compound. Although these cells grew at a rate comparable to untreated parasites, continuous drug pressure was required to maintain resistance. This indicated that *T. brucei* are easily able to generate resistance to E667 via a mechanism which can be both acquired and lost rapidly. The E667 resistant pleomorphic line may serve as a

useful tool in future studies of stumpy formation pathways. It would be interesting to explore its competence to differentiate in response to other signals such as pCPTcAMP and SIF.

While mapping the signalling pathway mediating differentiation to stumpy forms is still in its very preliminary stages, the work described here provides a valuable framework upon which subsequent analyses can be built and existing predictions corroborated, as well as validating strategies which will facilitate this work. It has also identified many potential novel mediators of stumpy formation to be individually analysed and ultimately incorporated into an increasingly characterised pathway.

Bibliography

Akiyoshi, B., and K. Gull, 2013, Evolutionary cell biology of chromosome segregation: insights from trypanosomes: Open Biology, v. 3, p. 13.

Akiyoshi, B., and K. Gull, 2014, Discovery of Unconventional Kinetochores in Kinetoplastids: Cell, v. 156, p. 1247-1258.

Alsford, S., S. Eckert, N. Baker, L. Glover, A. Sanchez-Flores, K. F. Leung, D. J. Turner, M. C. Field, M. Berriman, and D. Horn, 2012, High-throughput decoding of antitrypanosomal drug efficacy and resistance: Nature, v. 482, p. 232-6.

Alsford, S., and D. Horn, 2008, Single-locus targeting constructs for reliable regulated RNAi and transgene expression in Trypanosoma brucei: Mol Biochem Parasitol, v. 161, p. 76-9.

Alsford, S., T. Kawahara, L. Glover, and D. Horn, 2005, Tagging a T. brucei RRNA locus improves stable transfection efficiency and circumvents inducible expression position effects: Mol Biochem Parasitol, v. 144, p. 142-8.

Alsford, S., D. J. Turner, S. O. Obado, A. Sanchez-Flores, L. Glover, M. Berriman, C. Hertz-Fowler, and D. Horn, 2011, High-throughput phenotyping using parallel sequencing of RNA interference targets in the African trypanosome: Genome Research, v. 21, p. 915-924.

Amiguet-Vercher, A., D. Perez-Morga, A. Pays, P. Poelvoorde, H. Van Xong, P. Tebabi, L. Vanhamme, and E. Pays, 2004, Loss of the mono-allelic control of the VSG expression sites during the development of Trypanosoma brucei in the bloodstream: Molecular Microbiology, v. 51, p. 1577-1588.

Barquilla, A., J. L. Crespo, and M. Navarro, 2008, Rapamycin inhibits trypanosome cell growth by preventing TOR complex 2 formation: Proc Natl Acad Sci U S A, v. 105, p. 14579-84.

Barquilla, A., M. Saldivia, R. Diaz, J. M. Bart, I. Vidal, E. Calvo, M. N. Hall, and M. Navarro, 2012, Third target of rapamycin complex negatively regulates development of quiescence in Trypanosoma brucei: Proc Natl Acad Sci U S A, v. 109, p. 14399-404.

Berriman, M., E. Ghedin, C. Hertz-Fowler, G. Blandin, H. Renauld, D. C. Bartholomeu, N. J. Lennard, E. Caler, N. E. Hamlin, B. Haas, W. Bohme, L. Hannick, M. A. Aslett, J. Shallom, L. Marcello, L. H. Hou, B. Wickstead, U. C. M. Alsmark, C. Arrowsmith, R. J. Atkin, A. J. Barron, F. Bringaud, K. Brooks, M. Carrington, I. Cherevach, T. J. Chillingworth, C. Churcher, L. N. Clark, C. H. Corton, A. Cronin, R. M. Davies, J. Doggett, A. Djikeng, T. Feldblyum, M. C. Field, A. Fraser, I. Goodhead, Z. Hance, D. Harper, B. R. Harris, H. Hauser, J. Hostetter, A. Ivens, K. Jagels, D. Johnson, J. Johnson, K. Jones, A. X. Kerhornou, H. Koo, N. Larke, S. Landfear, C. Larkin, V. Leech, A. Line, A. Lord, A. MacLeod, P. J. Mooney, S. Moule, D. M. A. Martin, G. W. Morgan, K. Mungall, H. Norbertczak, D. Ormond, G. Pai, C. S. Peacock, J. Peterson, M. A. Quail, E. Rabbinowitsch, M. A. Rajandream, C. Reitter, S. L. Salzberg, M. Sanders, S. Schobel, S. Sharp, M. Simmonds, A. J. Simpson, L. Talton, C. M. R. Turner, A. Tait, A. R. Tivey, S. Van Aken, D. Walker, D. Wanless, S. L. Wang, B. White, O. White, S. Whitehead, J. Woodward, J. Wortman, M. D. Adams, T. M. Embley, K. Gull, E. Ullu, J. D. Barry, A. H. Fairlamb, F. Opperdoes, B. G. Barret, J. E. Donelson, N. Hall, C. M. Fraser, et al., 2005, The genome of the African trypanosome Trypanosoma brucei: Science, v. 309, p. 416-422.

Besteiro, S., M. P. Barrett, L. Riviere, and F. Bringaud, 2005, Energy generation in insect stages of Trypanosoma brucei: metabolism in flux: Trends in Parasitology, v. 21, p. 185-191.
Brauer, M. J., C. Huttenhower, E. M. Airoldi, R. Rosenstein, J. C. Matese, D. Gresham, V. M. Boer, O. G. Troyanskaya, and D. Botstein, 2008, Coordination of growth rate, cell cycle, stress response, and metabolic activity in yeast: Molecular Biology of the Cell, v. 19, p. 352-367.
Brecht, M., and M. Parsons, 1998, Changes in polysome profiles accompany trypanosome development: Molecular and Biochemical Parasitology, v. 97, p. 189-198.
Breidbach, T., E. Ngazoa, and D. Steverding, 2002, Trypanosoma brucei: in vitro slender-to-stumpy differentiation of culture-adapted, monomorphic bloodstream forms: Exp Parasitol, v. 101, p. 223-30.
Brenchley, R., H. Tariq, H. McElhinney, B. Szoor, J. Huxley-Jones, R. Stevens, K. Matthews, and L. Tabernero, 2007, The TriTryp Phosphatome: analysis of the protein phosphatase catalytic domains: Bmc Genomics, v. 8, p. 22.
Brickman, M. J., and A. E. Balber, 1994, TRYPANASOMA BRUCEI BRUCEI AND T-B-GAMBIENSE - STUMPY BLOOD-STREAM FORMS EXPRESS MORE CB1 EPITOPE IN ENDOSOMES AND LYSOSOMES THAN SLENDER FORMS: Journal of Eukaryotic Microbiology, v. 41, p. 533-536.
Capewell, P., S. Monk, A. Ivens, P. MacGregor, K. Fenn, P. Walrad, F. Bringaud, T. K. Smith, and K. R. Matthews, 2013, Regulation of Trypanosoma brucei Total and Polysomal mRNA during Development within Its Mammalian Host: Plos One, v. 8, p. 14.
Chang, L., and M. Karin, 2001, Mammalian MAP kinase signalling cascades: Nature, v. 410, p. 37-40.
Clemmens, C. S., M. T. Morris, T. A. Lyda, A. Acosta-Serrano, and J. C. Morris, 2009, Trypanosoma brucei AMP-activated kinase subunit homologs influence surface molecule expression: Experimental Parasitology, v. 123, p. 250-257.
Cohen, P. T. W., 2002, Protein phosphatase 1 - targeted in many directions: Journal of Cell Science, v. 115, p. 241-256.
Cross, G. A. M., H. S. Kim, and B. Wickstead, 2014, Capturing the variant surface glycoprotein repertoire (the VSGnome) of Trypanosoma brucei Lister 427: Molecular and Biochemical Parasitology, v. 195, p. 59-73.
Das, A., R. Morales, M. Banday, S. Garcia, L. Hao, G. A. M. Cross, A. M. Estevez, and V. Bellofatto, 2012, The essential polysome-associated RNA-binding protein RBP42 targets mRNAs involved in Trypanosoma brucei energy metabolism: Rna-a Publication of the Rna Society, v. 18, p. 1968-1983.
Das, A., Q. Zhang, J. B. Palenchar, B. Chatterjee, G. A. M. Cross, and V. Bellofatto, 2005, Trypanosomal TBP functions with the multisubunit transcription factor tSNAP to direct spliced-leader RNA gene expression: Molecular and Cellular Biology, v. 25, p. 7314-7322.
de Jesus, T. C., R. R. Tonelli, S. C. Nardelli, L. da Silva Augusto, M. C. Motta, W. Girard-Dias, K. Miranda, P. Ulrich, V. Jimenez, A. Barquilla, M. Navarro, R. Docampo, and S. Schenkman, 2010, Target of rapamycin (TOR)-like 1 kinase is involved in the control of polyphosphate levels and acidocalcisome maintenance in Trypanosoma brucei: J Biol Chem, v. 285, p. 24131-40.

De Virgilio, C., 2012, The essence of yeast quiescence: Fems Microbiology Reviews, v. 36, p. 306-339.
Dean, S., R. Marchetti, K. Kirk, and K. R. Matthews, 2009, A surface transporter family conveys the trypanosome differentiation signal: Nature, v. 459, p. 213-7.
DeJesus, E., R. Kieft, B. Albright, N. A. Stephens, and S. L. Hajduk, 2013, A Single Amino Acid Substitution in the Group 1 Trypanosoma brucei gambiense Haptoglobin-Hemoglobin Receptor Abolishes TLF-1 Binding: Plos Pathogens, v. 9, p. 10.
Dejung, M., I. Subota, F. Bucerius, G. Dindar, A. Freiwald, M. Engstler, M. Boshart, F. Butter, and C. J. Janzen, 2016, Quantitative Proteomics Uncovers Novel Factors Involved in Developmental Differentiation of Trypanosoma brucei: PLoS Pathog, v. 12, p. e1005439.
Demonchy, R., T. Blisnick, C. Deprez, G. Toutirais, C. Loussert, W. Marande, P. Grellier, P. Bastin, and L. Kohl, 2009, Kinesin 9 family members perform separate functions in the trypanosome flagellum: Journal of Cell Biology, v. 187, p. 615-622.
DeRisi, J. L., V. R. Iyer, and P. O. Brown, 1997, Exploring the metabolic and genetic control of gene expression on a genomic scale: Science, v. 278, p. 680-686.
Diaz, R., S. A. Luengo-Arratta, J. O. D. Seixas, E. Amata, W. Devine, C. Cordon-Obras, D. I. Rojas-Barros, E. Jimenez, F. Ortega, S. Crouch, G. Colmenarejo, J. M. Fiandor, J. J. Martin, M. Berlanga, S. Gonzalez, P. Manzano, M. Navarro, and M. P. Pollastri, 2014, Identification and Characterization of Hundreds of Potent and Selective Inhibitors of Trypanosoma brucei Growth from a Kinase-Targeted Library Screening Campaign: Plos Neglected Tropical Diseases, v. 8, p. 14.
Dillon, S. C., X. Zhang, R. C. Trievel, and X. D. Cheng, 2005, The SET-domain protein superfamily: protein lysine methyltransferases: Genome Biology, v. 6, p. 10.
Docampo, R., W. de Souza, K. Miranda, P. Rohloff, and S. N. J. Moreno, 2005, Acidocalcisomes - Conserved from bacteria to man: Nature Reviews Microbiology, v. 3, p. 251-261.
Domenicali Pfister, D., G. Burkard, S. Morand, C. K. Renggli, I. Roditi, and E. Vassella, 2006, A Mitogen-activated protein kinase controls differentiation of bloodstream forms of Trypanosoma brucei: Eukaryot Cell, v. 5, p. 1126-35.
Domingo-Sananes, M. R., B. Szoor, M. A. J. Ferguson, M. D. Urbaniak, and K. R. Matthews, 2015, Molecular control of irreversible bistability during trypanosome developmental commitment: Journal of Cell Biology, v. 211, p. 455-468.
Engstler, M., and M. Boshart, 2004, Cold shock and regulation of surface protein trafficking convey sensitization to inducers of stage differentiation in Trypanosoma brucei: Genes Dev, v. 18, p. 2798-811.
Engstler, M., T. Pfohl, S. Herminghaus, M. Boshart, G. Wiegertjes, N. Heddergott, and P. Overath, 2007, Hydrodynamic flow-mediated protein sorting on the cell surface of trypanosomes: Cell, v. 131, p. 505-515.
Engstler, M., L. Thilo, F. Weise, C. G. Grunfelder, H. Schwarz, M. Boshart, and P. Overath, 2004, Kinetics of endocytosis and recycling of the GPI-anchored variant surface glycoprotein in Trypanosoma brucei: Journal of Cell Science, v. 117, p. 1105-1115.
Erben, E. D., A. Fadda, S. Lueong, J. D. Hoheisel, and C. Clayton, 2014, A Genome-Wide Tethering Screen Reveals Novel Potential Post-Transcriptional Regulators in Trypanosoma brucei: Plos Pathogens, v. 10, p. 15.

Evans, D. A., and R. C. Brown, 1972, UTILIZATION OF GLUCOSE AND PROLINE BY CULTURE FORMS OF TRYPANOSOMA-BRUCEI: Journal of Protozoology, v. 19, p. 686-690.
Evers, R., and A. Cornelissen, 1990, THE TRYPANOSOMA-BRUCEI PROTEIN PHOSPHATASE GENE - POLYCISTRONIC TRANSCRIPTION WITH THE RNA POLYMERASE-II LARGEST SUBUNIT GENE: Nucleic Acids Research, v. 18, p. 5089-5095.
Fernandez-Moya, S. M., A. Garcia-Perez, S. Kramer, M. Carrington, and A. M. Estevez, 2012, Alterations in DRBD3 Ribonucleoprotein Complexes in Response to Stress in Trypanosoma brucei: Plos One, v. 7, p. 10.
Field, M. C., and M. Carrington, 2009, The trypanosome flagellar pocket: Nature Reviews Microbiology, v. 7, p. 775-786.
Fry, A. M., L. O'Regan, S. R. Sabir, and R. Bayliss, 2012, Cell cycle regulation by the NEK family of protein kinases: J Cell Sci, v. 125, p. 4423-33.
Furger, A., N. Schurch, U. Kurath, and I. Roditi, 1997, Elements in the 3' untranslated region of procyclin mRNA regulate expression in insect forms of Trypanosoma brucei by modulating RNA stability and translation: Molecular and Cellular Biology, v. 17, p. 4372-4380.
Gale, M., Jr., V. Carter, and M. Parsons, 1994, Translational control mediates the developmental regulation of the Trypanosoma brucei Nrk protein kinase: J Biol Chem, v. 269, p. 31659-65.
Gallet, C., R. Demonchy, C. Koppel, P. Grellier, and L. Kohl, 2013, A Protein Phosphatase 1 involved in correct nucleus positioning in trypanosomes: Molecular and Biochemical Parasitology, v. 192, p. 49-54.
Garrett, S., and J. Broach, 1989, LOSS OF RAS ACTIVITY IN SACCHAROMYCES-CEREVISIAE IS SUPPRESSED BY DISRUPTIONS OF A NEW KINASE GENE, YAKI, WHOSE PRODUCT MAY ACT DOWNSTREAM OF THE CAMP-DEPENDENT PROTEIN-KINASE: Genes & Development, v. 3, p. 1336-1348.
Garrett, S., M. M. Menold, and J. R. Broach, 1991, THE SACCHAROMYCES-CEREVISIAE YAK1-GENE ENCODES A PROTEIN-KINASE THAT IS INDUCED BY ARREST EARLY IN THE CELL-CYCLE: Molecular and Cellular Biology, v. 11, p. 4045-4052.
Gibson, S., C. Widmann, and G. L. Johnson, 1999, Differential involvement of MEK kinase 1 (MEKK1) in the induction of apoptosis in response to microtubule-targeted drugs versus DNA damaging agents: Journal of Biological Chemistry, v. 274, p. 10916-10922.
Gjini, E., D. T. Haydon, J. D. Barry, and C. A. Cobbold, 2010, Critical Interplay between Parasite Differentiation, Host Immunity, and Antigenic Variation in Trypanosome Infections: American Naturalist, v. 176, p. 424-439.
Glover, L., S. Alsford, N. Baker, D. J. Turner, A. Sanchez-Flores, S. Hutchinson, C. Hertz-Fowler, M. Berriman, and D. Horn, 2015, Genome-scale RNAi screens for high-throughput phenotyping in bloodstream-form African trypanosomes: Nature Protocols, v. 10, p. 106-133.
Gonzalez, J., A. Cornejo, M. R. Santos, E. M. Cordero, B. Gutierrez, P. Porcile, R. A. Mortara, H. Sagua, J. F. Da Silveira, and J. E. Araya, 2003, A novel protein phosphatase 2A (PP2A) is involved in the transformation of human protozoan parasite Trypanosoma cruzi: Biochem J, v. 374, p. 647-56.

Gould, M. K., and H. P. de Koning, 2011, Cyclic-nucleotide signalling in protozoa: FEMS Microbiol Rev, v. 35, p. 515-41.
Gunasekera, K., D. Wuethrich, S. Braga-Lagache, M. Heller, and T. Ochsenreiter, 2012, Proteome remodelling during development from blood to insect-form Trypanosoma brucei quantified by SILAC and mass spectrometry: BMC Genomics, v. 13, p. 1-14.
Gunzl, A., T. Bruderer, G. Laufer, B. Schimanski, L. C. Tu, H. M. Chung, P. T. Lee, and M. G. S. Lee, 2003, RNA polymerase I transcribes procyclin genes and variant surface glycoprotein gene expression sites in Trypanosoma brucei: Eukaryotic Cell, v. 2, p. 542-551.
Gunzl, A., J. K. Kirkham, T. N. Nguyen, N. Badjatia, and S. H. Park, 2015, Mono-allelic VSG expression by RNA polymerase I in Trypanosoma brucei: Expression site control from both ends?: Gene, v. 556, p. 68-73.
Guo, S. L., L. E. Stolz, S. M. Lemrow, and J. D. York, 1999, SAC1-like domains of yeast SAC1, INP52, and INP53 and of human synaptojanin encode polyphosphoinositide phosphatases: Journal of Biological Chemistry, v. 274, p. 12990-12995.
Gwinn, D. M., D. B. Shackelford, D. F. Egan, M. M. Mihaylova, A. Mery, D. S. Vasquez, B. E. Turk, and R. J. Shaw, 2008, AMPK phosphorylation of raptor mediates a metabolic checkpoint: Molecular Cell, v. 30, p. 214-226.
Haanstra, J. R., M. Stewart, V. D. Luu, A. van Tuijl, H. V. Westerhoff, C. Clayton, and B. M. Bakker, 2008a, Control and regulation of gene expression - Quantitative analysis of the expression of phosphoglycerate kinase in bloodstream form Trypanosoma brucei: Journal of Biological Chemistry, v. 283, p. 2495-2507.
Haanstra, J. R., A. van Tuijl, P. Kessler, W. Reijnders, P. A. M. Michels, H. V. Westerhoff, M. Parsons, and B. M. Bakker, 2008b, Compartmentation prevents a lethal turbo-explosion of glycolysis in trypanosomes: Proceedings of the National Academy of Sciences of the United States of America, v. 105, p. 17718-17723.
Hallett, J. E. H., X. X. Luo, and A. P. Capaldi, 2014, State Transitions in the TORC1 Signaling Pathway and Information Processing in Saccharomyces cerevisiae: Genetics, v. 198, p. 773-U452.
Hammarton, T. C., S. Kramer, L. Tetley, M. Boshart, and J. C. Mottram, 2007, Trypanosoma brucei Polo-like kinase is essential for basal body duplication, kDNA segregation and cytokinesis: Molecular Microbiology, v. 65, p. 1229-1248.
Hendriks, E. F., D. R. Robinson, M. Hinkins, and K. R. Matthews, 2001, A novel CCCH protein which modulates differentiation of Trypanosoma brucei to its procyclic form: EMBO J, v. 20, p. 6700-11.
Herbert, W. J., and W. H. Lumsden, 1976, Trypanosoma brucei: a rapid "matching" method for estimating the host's parasitemia: Exp Parasitol, v. 40, p. 427-31.
Hirumi, H., and K. Hirumi, 1989, CONTINUOUS CULTIVATION OF TRYPANOSOMA-BRUCEI BLOOD STREAM FORMS IN A MEDIUM CONTAINING A LOW CONCENTRATION OF SERUM-PROTEIN WITHOUT FEEDER CELL-LAYERS: Journal of Parasitology, v. 75, p. 985-989.
Horn, D., 2014, Antigenic variation in African trypanosomes: Molecular and Biochemical Parasitology, v. 195, p. 123-129.
Imboden, M. A., P. W. Laird, M. Affolter, and T. Seebeck, 1987, TRANSCRIPTION OF THE INTERGENIC REGIONS OF THE TUBULIN GENE-CLUSTER OF TRYPANOSOMA-BRUCEI - EVIDENCE FOR A POLYCISTRONIC

TRANSCRIPTION UNIT IN A EUKARYOTE: Nucleic Acids Research, v. 15, p. 7357-7368.
Inoki, K., T. Q. Zhu, and K. L. Guan, 2003, TSC2 mediates cellular energy response to control cell growth and survival: Cell, v. 115, p. 577-590.
Inoue, M., K. Okamoto, H. Uemura, K. Yasuda, Y. Motohara, K. Morita, M. Hiromura, E. P. Reddy, T. Fukuma, and N. Horikoshi, 2015, Identification and characterization of a cell division-regulating kinase AKB1 (associated kinase of Trypanosoma brucei 14-3-3) through proteomics study of the Tb14-3-3 binding proteins: Journal of Biochemistry, v. 158, p. 49-60.
James, D. M., and G. V. Born, 1980, Uptake of purine bases and nucleosides in African trypanosomes: Parasitology, v. 81, p. 383-93.
Jensen, B. C., D. Sivam, C. T. Kifer, P. J. Myler, and M. Parsons, 2009, Widespread variation in transcript abundance within and across developmental stages of Trypanosoma brucei: Bmc Genomics, v. 10, p. 24.
Jones, N. G., E. B. Thomas, E. Brown, N. J. Dickens, T. C. Hammarton, and J. C. Mottram, 2014, Regulators of Trypanosoma brucei Cell Cycle Progression and Differentiation Identified Using a Kinome-Wide RNAi Screen: Plos Pathogens, v. 10, p. 16.
Kabani, S., K. Fenn, A. Ross, A. Ivens, T. K. Smith, P. Ghazal, and K. Matthews, 2009, Genome-wide expression profiling of in vivo-derived bloodstream parasite stages and dynamic analysis of mRNA alterations during synchronous differentiation in Trypanosoma brucei: BMC Genomics, v. 10, p. 427.
Kelly, S., J. Reed, S. Kramer, L. Ellis, H. Webb, J. Sunter, J. Salje, N. Marinsek, K. Gull, B. Wickstead, and M. Carrington, 2007, Functional genomics in Trypanosoma brucei: A collection of vectors for the expression of tagged proteins from endogenous and ectopic gene loci: Molecular and Biochemical Parasitology, v. 154, p. 103-109.
Kessler, P. S., and M. Parsons, 2005, Probing the role of compartmentation of glycolysis in procyclic form Trypanosoma brucei RNA interference studies of PEX14, hexokinase, and phosphofructokinase: Journal of Biological Chemistry, v. 280, p. 9030-9036.
Kieft, R., P. Capewell, C. M. R. Turner, N. J. Veitch, A. MacLeod, and S. Hajduk, 2010, Mechanism of Trypanosoma brucei gambiense (group 1) resistance to human trypanosome lytic factor: Proceedings of the National Academy of Sciences of the United States of America, v. 107, p. 16137-16141.
Kolev, N. G., K. Ramey-Butler, G. A. M. Cross, E. Ullu, and C. Tschudi, 2012, Developmental Progression to Infectivity in Trypanosoma brucei Triggered by an RNA-Binding Protein: Science, v. 338, p. 1352-1353.
Kozminski, K. G., P. L. Beech, and J. L. Rosenbaum, 1995, THE CHLAMYDOMONAS KINESIN-LIKE PROTEIN FLA10 IS INVOLVED IN MOTILITY ASSOCIATED WITH THE FLAGELLAR MEMBRANE: Journal of Cell Biology, v. 131, p. 1517-1527.
Kramer, S., N. C. Kimblin, and M. Carrington, 2010, Genome-wide in silico screen for CCCH-type zinc finger proteins of Trypanosoma brucei, Trypanosoma cruzi and Leishmania major: Bmc Genomics, v. 11, p. 13.
Kristjanson, P. M., B. M. Swallow, G. J. Rowlands, R. L. Kruska, and P. N. de Leeuw, 1999, Measuring the costs of African animal trypanosomosis, the potential benefits of control and returns to research: Agricultural Systems, v. 59, p. 79-98.

Langousis, G., and K. L. Hill, 2014, Motility and more: the flagellum of Trypanosoma brucei: Nature Reviews Microbiology, v. 12, p. 505-518.
Laxman, S., A. Riechers, M. Sadilek, F. Schwede, and J. A. Beavo, 2006, Hydrolysis products of cAMP analogs cause transformation of Trypanosoma brucei from slender to stumpy-like forms: Proc Natl Acad Sci U S A, v. 103, p. 19194-9.
Lebowitz, J. H., H. Q. Smith, L. Rusche, and S. M. Beverley, 1993, COUPLING OF POLY(A) SITE SELECTION AND TRANSSPLICING IN LEISHMANIA: Genes & Development, v. 7, p. 996-1007.
Lecordier, L., P. Uzureau, P. Tebabi, D. Perez-Morga, D. Nolan, G. S. Burkard, I. Roditi, and E. Pays, 2014, Identification of Trypanosoma brucei components involved in trypanolysis by normal human serum: Molecular Microbiology, v. 94, p. 625-636.
Lee, P., B. R. Cho, H. S. Joo, and J. S. Hahn, 2008, Yeast Yak1 kinase, a bridge between PKA and stress-responsive transcription factors, Hsf1 and Msn2/Msn4: Molecular Microbiology, v. 70, p. 882-895.
Lee, P., S. M. Paik, C. S. Shin, W. K. Huh, and J. S. Hahn, 2011, Regulation of yeast Yak1 kinase by PKA and autophosphorylation-dependent 14-3-3 binding: Molecular Microbiology, v. 79, p. 633-646.
Lemercier, G., S. Dutoya, S. H. Luo, F. A. Ruiz, C. O. Rodrigues, T. Baltz, R. Docampo, and N. Bakalara, 2002, A vacuolar-type H+-pyrophosphatase governs maintenance of functional acidocalcisomes and growth of the insect and mammalian forms of Trypanosoma brucei: Journal of Biological Chemistry, v. 277, p. 37369-37376.
Lemercier, G., B. Espiau, F. A. Ruiz, M. Vieira, S. H. Luo, T. Baltz, R. Docampo, and N. Bakalara, 2004, A pyrophosphatase regulating polyphosphate metabolism in acidocalcisomes is essential for Trypanosoma brucei virulence in mice: Journal of Biological Chemistry, v. 279, p. 3420-3425.
Li, Z., X. Tu, and C. C. Wang, 2006, Okadaic acid overcomes the blocked cell cycle caused by depleting Cdc2-related kinases in Trypanosoma brucei: Exp Cell Res, v. 312, p. 3504-16.
Lopez-Farfan, D., J. M. Bart, D. I. Rojas-Barros, and M. Navarro, 2014, SUMOylation by the E3 Ligase TbSIZ1/PIAS1 Positively Regulates VSG Expression in Trypanosoma brucei: Plos Pathogens, v. 10, p. 18.
Lorick, K. L., J. P. Jensen, S. Y. Fang, A. M. Ong, S. Hatakeyama, and A. M. Weissman, 1999, RING fingers mediate ubiquitin-conjugating enzyme (E2)-dependent ubiquitination: Proceedings of the National Academy of Sciences of the United States of America, v. 96, p. 11364-11369.
Luscher, A., P. Onal, A. M. Schweingruber, and P. Maser, 2007, Adenosine kinase of Trypanosoma brucei and its role in susceptibility to adenosine antimetabolites: Antimicrob Agents Chemother, v. 51, p. 3895-901.
MacGregor, P., A. Ivens, S. Shave, I. Collie, D. Gray, M. Auer, and K. R. Matthews, 2014, High-Throughput Chemical Screening for Antivirulence Developmental Phenotypes in Trypanosoma brucei: Eukaryotic Cell, v. 13, p. 412-426.
MacGregor, P., F. Rojas, S. Dean, and K. R. Matthews, 2013, Stable transformation of pleomorphic bloodstream form Trypanosoma brucei: Molecular and Biochemical Parasitology, v. 190, p. 60-62.

MacGregor, P., N. J. Savill, D. Hall, and K. R. Matthews, 2011, Transmission stages dominate trypanosome within-host dynamics during chronic infections: Cell Host Microbe, v. 9, p. 310-8.
Martin, D. E., A. Soulard, and M. N. Hall, 2004, TOR regulates ribosomal protein gene expression via PKA and the forkhead transcription factor FHL1: Cell, v. 119, p. 969-979.
Matthews, K. R., 2005, The developmental cell biology of Trypanosoma brucei: J Cell Sci, v. 118, p. 283-90.
Matthews, K. R., C. Tschudi, and E. Ullu, 1994, A Common Pyrimidine-Rich Motif Governs Transsplicing and Polyadenylation of Tubulin Polycistronic Pre-Messenger-Rna in Trypanosomes: Genes Dev, v. 8, p. 491-501.
McLintock, L. M. L., C. M. R. Turner, and K. Vickerman, 1993, COMPARISON OF THE EFFECTS OF IMMUNE KILLING MECHANISMS ON TRYPANOSOMA-BRUCEI PARASITES OF SLENDER AND STUMPY MORPHOLOGY: Parasite Immunology, v. 15, p. 475-480.
Melville, S. E., V. Leech, C. S. Gerrard, A. Tait, and J. M. Blackwell, 1998, The molecular karyotype of the megabase chromosomes of Trypanosoma brucei and the assignment of chromosome markers: Molecular and Biochemical Parasitology, v. 94, p. 155-173.
Mizote, I., O. Yamaguchi, S. Hikoso, T. Takeda, M. Taneike, T. Oka, T. Tamai, J. Oyabu, Y. Matsumura, K. Nishida, I. Komuro, M. Hori, and K. Otsu, 2010, Activation of MTK1/MEKK4 induces cardiomyocyte death and heart failure: Journal of Molecular and Cellular Cardiology, v. 48, p. 302-309.
Mony, B. M., P. MacGregor, A. Ivens, F. Rojas, A. Cowton, J. Young, D. Horn, and K. Matthews, 2014, Genome-wide dissection of the quorum sensing signalling pathway in Trypanosoma brucei: Nature, v. 505, p. 681-+.
Mony, B. M., and K. R. Matthews, 2015, Assembling the components of the quorum sensing pathway in African trypanosomes: Molecular Microbiology, v. 96, p. 220-232.
Morand, S., C. K. Renggli, I. Roditi, and E. Vassella, 2012, MAP kinase kinase 1 (MKK1) is essential for transmission of Trypanosoma brucei by Glossina morsitans: Mol Biochem Parasitol, v. 186, p. 73-6.
Moriya, H., Y. Shimizu-Yoshida, A. Omori, S. Iwashita, M. Katoh, and A. Sakai, 2001, Yak1p, a DYRK family kinase, translocates to the nucleus and phosphorylates yeast Pop2p in response to a glucose signal: Genes & Development, v. 15, p. 1217-1228.
Morris, J. C., Z. Wang, M. E. Drew, and P. T. Englund, 2002, Glycolysis modulates trypanosome glycoprotein expression as revealed by an RNAi library: EMBO J, v. 21, p. 4429-38.
Muller, I. B., D. Domenicali-Pfister, I. Roditi, and E. Vassella, 2002, Stage-specific requirement of a mitogen-activated protein kinase by Trypanosoma brucei: Mol Biol Cell, v. 13, p. 3787-99.
Navarro, M., and K. Gull, 2001, A pol I transcriptional body associated with VSG mono-allelic expression in Trypanosoma brucei: Nature, v. 414, p. 759-763.
Ngo, H., C. Tschudi, K. Gull, and E. Ullu, 1998, Double-stranded RNA induces mRNA degradation in Trypanosoma brucei: Proceedings of the National Academy of Sciences of the United States of America, v. 95, p. 14687-14692.

Nilsson, D., K. Gunasekera, J. Mani, M. Osteras, L. Farinelli, L. Baerlocher, I. Roditi, and T. Ochsenreiter, 2010, Spliced Leader Trapping Reveals Widespread Alternative Splicing Patterns in the Highly Dynamic Transcriptome of Trypanosoma brucei: Plos Pathogens, v. 6, p. 13.
Nolan, D. P., S. Rolin, J. R. Rodriguez, J. Van Den Abbeele, and E. Pays, 2000, Slender and stumpy bloodstream forms of Trypanosoma brucei display a differential response to extracellular acidic and proteolytic stress: Eur J Biochem, v. 267, p. 18-27.
Odiit, M., P. G. Coleman, W. C. Liu, J. J. McDermott, E. M. Fevre, S. C. Welburn, and M. E. J. Woolhouse, 2005, Quantifying the level of under-detection of Trypanosoma brucei rhodesiense sleeping sickness cases: Tropical Medicine & International Health, v. 10, p. 840-849.
Ogbadoyi, E. O., D. R. Robinson, and K. Gull, 2003, A high-order trans-membrane structural linkage is responsible for mitochondrial genome positioning and segregation by flagellar basal bodies in trypanosomes: Molecular Biology of the Cell, v. 14, p. 1769-1779.
Ouellette, M., and B. Papadopoulou, 2009, Coordinated gene expression by post-transcriptional regulons in African trypanosomes: Journal of Biology (London), v. 8, p. 8.
Owen, G. R., I. Achilonu, and H. W. Dirr, 2013, High yield purification of JNK1 beta 1 and activation by in vitro reconstitution of the MEKK1 -> MKK4 -> JNK MAPK phosphorylation cascade: Protein Expression and Purification, v. 87, p. 87-99.
Parsons, M., E. A. Worthey, P. N. Ward, and J. C. Mottram, 2005, Comparative analysis of the kinomes of three pathogenic trypanosomatids: Leishmania major, Trypanosoma brucei and Trypanosoma cruzi: BMC Genomics, v. 6, p. 127.
Paterou, A., P. Walrad, P. Craddy, K. Fenn, and K. Matthews, 2006, Identification and stage-specific association with the translational apparatus of TbZFP3, a CCCH protein that promotes trypanosome life-cycle development: Journal of Biological Chemistry, v. 281, p. 39002-39013.
Paul, B. J., M. M. Barker, W. Ross, D. A. Schneider, C. Webb, J. W. Foster, and R. L. Gourse, 2004, DksA: A critical component of the transcription initiation machinery that potentiates the regulation of rRNA promoters by ppGpp and the initiating NTP: Cell, v. 118, p. 311-322.
Peacock, L., V. Ferris, R. Sharma, J. Sunter, M. Bailey, M. Carrington, and W. Gibson, 2011, Identification of the meiotic life cycle stage of Trypanosoma brucei in the tsetse fly: Proceedings of the National Academy of Sciences of the United States of America, v. 108, p. 3671-3676.
Perez-Morga, D., B. Vanhollebeke, F. Paturiaux-Hanocq, D. P. Nolan, L. Lins, F. Homble, L. Vanhamme, P. Tebabi, A. Pays, P. Poelvoorde, A. Jacquet, R. Brasseur, and E. Pays, 2005, Apolipoprotein L-1 promotes trypanosome lysis by forming pores in lysosomal membranes: Science, v. 309, p. 469-472.
Pradel, L. C., M. Bonhivers, N. Landrein, and D. R. Robinson, 2006, NIMA-related kinase TbNRKC is involved in basal body separation in Trypanosoma brucei: J Cell Sci, v. 119, p. 1852-63.
Priotto, G., S. Kasparion, W. Mutombo, D. Ngouama, S. Ghorashian, U. Arnold, S. Ghabri, E. Baudin, V. Buard, S. Kazadi-Kyanza, M. Ilunga, W. Mutangala, G. Pohlig, C. Schmid, U. Karunakara, E. Torreele, and V. Kande, 2009, Nifurtimox-

eflornithine combination therapy for second-stage African Trypanosoma brucei gambiense trypanosomiasis: a multicentre, randomised, phase III, non-inferiority trial: Lancet, v. 374, p. 56-64.
Reuner, B., E. Vassella, B. Yutzy, and M. Boshart, 1997, Cell density triggers slender to stumpy differentiation of Trypanosoma brucei bloodstream forms in culture: Mol Biochem Parasitol, v. 90, p. 269-80.
Robertson, M., 1913, Notes on the life-history of Trypanosoma gambiense, with a brief reference to the cycles of Trypanosoma nanum and Trypanosoma pecoum in Glossina palpalis: Philosophical Transactions of the Royal Society of London Series B-Containing Papers of a Biological Character, v. 203, p. 161-U46.
Rohloff, P., A. Montalvetti, and R. Docampo, 2004, Acidocalcisomes and the contractile vacuole complex are involved in osmoregulation in Trypanosoma cruzi: Journal of Biological Chemistry, v. 279, p. 52270-52281.
Rolin, S., J. Hanocq-Quertier, F. Paturiaux-Hanocq, D. P. Nolan, and E. Pays, 1998, Mild acid stress as a differentiation trigger in Trypanosoma brucei: Molecular and Biochemical Parasitology, v. 93, p. 251-262.
Rothberg, K. G., N. Jetton, J. G. Hubbard, D. A. Powell, V. Pandarinath, and L. Ruben, 2014, Identification of a protein phosphatase 2A family member that regulates cell cycle progression in Trypanosoma brucei: Molecular and Biochemical Parasitology, v. 194, p. 48-52.
Schmelzle, T., T. Beck, D. E. Martin, and M. N. Hall, 2004, Activation of the RAS/cyclic AMP pathway suppresses a TOR deficiency in yeast: Molecular and Cellular Biology, v. 24, p. 338-351.
Schmidt, M. C., and R. R. McCartney, 2000, beta-subunits of Snf1 kinase are required for kinase function and substrate definition: Embo Journal, v. 19, p. 4936-4943.
Schumann Burkard, G., S. Kaser, P. R. de Araujo, B. Schimanski, A. Naguleswaran, S. Knusel, M. Heller, and I. Roditi, 2013, Nucleolar proteins regulate stage-specific gene expression and ribosomal RNA maturation in Trypanosoma brucei: Molecular microbiology, v. 88, p. 827-40.
Schwede, A., N. Jones, M. Engstler, and M. Carrington, 2011, The VSG C-terminal domain is inaccessible to antibodies on live trypanosomes: Molecular and Biochemical Parasitology, v. 175, p. 201-204.
Shalaby, T., M. Liniger, and T. Seebeck, 2001, The regulatory subunit of a cGMP-regulated protein kinase A of Trypanosoma brucei: Eur J Biochem, v. 268, p. 6197-206.
Shapiro, S. Z., J. Naessens, B. Liesegang, S. K. Moloo, and J. Magondu, 1984, Analysis by flow cytometry of DNA synthesis during the life cycle of African trypanosomes: Acta Trop, v. 41, p. 313-23.
Sharma, R., L. Peacock, E. Gluenz, K. Gull, W. Gibson, and M. Carrington, 2008, Asymmetric cell division as a route to reduction in cell length and change in cell morphology in trypanosomes: Protist, v. 159, p. 137-151.
Shlomai, J., 2004, The structure and replication of kinetoplast DNA: Current Molecular Medicine, v. 4, p. 623-647.
Siegel, T. N., D. R. Hekstra, L. E. Kemp, L. M. Figueiredo, J. E. Lowell, D. Fenyo, X. N. Wang, S. Dewell, and G. A. M. Cross, 2009, Four histone variants mark the boundaries of polycistronic transcription units in Trypanosoma brucei: Genes & Development, v. 23, p. 1063-1076.

Siegel, T. N., D. R. Hekstra, X. N. Wang, S. Dewell, and G. A. M. Cross, 2010, Genome-wide analysis of mRNA abundance in two life-cycle stages of Trypanosoma brucei and identification of splicing and polyadenylation sites: Nucleic Acids Research, v. 38, p. 4946-4957.
Simarro, P. P., G. Cecchi, M. Paone, J. R. Franco, A. Diarra, J. A. Ruiz, E. M. Fevre, F. Courtin, R. C. Mattioli, and J. G. Jannin, 2010, The Atlas of human African trypanosomiasis: a contribution to global mapping of neglected tropical diseases: International Journal of Health Geographics, v. 9, p. 18.
Singh, A., I. Minia, D. Droll, A. Fadda, C. Clayton, and E. Erben, 2014, Trypanosome MKT1 and the RNA-binding protein ZC3H11: interactions and potential roles in post-transcriptional regulatory networks: Nucleic Acids Research, v. 42, p. 4652-4668.
Souza, G. M., S. J. Lu, and A. Kuspa, 1998, YakA, a protein kinase required for the transition from growth to development in Dictyostelium: Development, v. 125, p. 2291-2302.
Sturm, N. R., and L. Simpson, 1990, KINETOPLAST DNA MINICIRCLES ENCODE GUIDE RNAS FOR EDITING OF CYTOCHROME-OXIDASE SUBUNIT-III MESSENGER-RNA: Cell, v. 61, p. 879-884.
Subota, I., D. Julkowska, L. Vincensini, N. Reeg, J. Buisson, T. Blisnick, D. Huet, S. Perrot, J. Santi-Rocca, M. Duchateau, V. Hourdel, J. C. Rousselle, N. Cayet, A. Namane, J. Chamot-Rooke, and P. Bastin, 2014, Proteomic Analysis of Intact Flagella of Procyclic Trypanosoma brucei Cells Identifies Novel Flagellar Proteins with Unique Sub-localization and Dynamics: Molecular & Cellular Proteomics, v. 13, p. 1769-1786.
Szoor, B., N. A. Dyer, I. Ruberto, A. Acosta-Serrano, and K. R. Matthews, 2013, Independent Pathways Can Transduce the Life-Cycle Differentiation Signal in Trypanosoma brucei: Plos Pathogens, v. 9, p. 14.
Szoor, B., J. R. Haanstra, M. Gualdron-Lopez, and P. A. M. Michels, 2014, Evolution, dynamics and specialized functions of glycosomes in metabolism and development of trypanosomatids: Current Opinion in Microbiology, v. 22, p. 79-87.
Szoor, B., I. Ruberto, R. Burchmore, and K. R. Matthews, 2010, A novel phosphatase cascade regulates differentiation in Trypanosoma brucei via a glycosomal signaling pathway: Genes Dev, v. 24, p. 1306-16.
Szoor, B., J. Wilson, H. McElhinney, L. Tabernero, and K. R. Matthews, 2006, Protein tyrosine phosphatase TbPTP1: A molecular switch controlling life cycle differentiation in trypanosomes: J Cell Biol, v. 175, p. 293-303.
Toda, T., S. Cameron, P. Sass, M. Zoller, J. D. Scott, B. McMullen, M. Hurwitz, E. G. Krebs, and M. Wigler, 1987, CLONING AND CHARACTERIZATION OF BCY1, A LOCUS ENCODING A REGULATORY SUBUNIT OF THE CYCLIC AMP-DEPENDENT PROTEIN-KINASE IN SACCHAROMYCES-CEREVISIAE: Molecular and Cellular Biology, v. 7, p. 1371-1377.
Tu, J. L., and M. Carlson, 1995, REG1 BINDS TO PROTEIN PHOSPHATASE TYPE-1 AND REGULATES GLUCOSE REPRESSION IN SACCHAROMYCES-CEREVISIAE: Embo Journal, v. 14, p. 5939-5946.
Tu, X. M., and C. C. Wang, 2004, The involvement of two cdc2-related kinases (CRKs) in Trypanosoma brucei cell cycle regulation and the distinctive stage-specific phenotypes caused by CRK3 depletion: Journal of Biological Chemistry, v. 279, p. 20519-20528.

Turner, C. M. R., J. D. Barry, I. Maudlin, and K. Vickerman, 1988a, AN ESTIMATE OF THE SIZE OF THE METACYCLIC VARIABLE ANTIGEN REPERTOIRE OF TRYPANOSOMA-BRUCEI-RHODESIENSE: Parasitology, v. 97, p. 269-276.
Turner, C. M. R., J. D. Barry, and K. Vickerman, 1988b, LOSS OF VARIABLE ANTIGEN DURING TRANSFORMATION OF TRYPANOSOMA-BRUCEI-RHODESIENSE FROM BLOOD-STREAM TO PROCYCLIC FORMS IN THE TSETSE-FLY: Parasitology Research, v. 74, p. 507-511.
Urbaniak, M. D., D. M. A. Martin, and M. A. J. Ferguson, 2013, Global Quantitative SILAC Phosphoproteomics Reveals Differential Phosphorylation Is Widespread between the Procyclic and Bloodstream Form Lifecycle Stages of Trypanosoma brucei: Journal of Proteome Research, v. 12, p. 2233-2244.
Urbaniak, M. D., T. Mathieson, M. Bantscheff, D. Eberhard, R. Grimaldi, D. Miranda-Saavedra, P. Wyatt, M. A. J. Ferguson, J. Frearson, and G. Drewes, 2012, Chemical Proteomic Analysis Reveals the Drugability of the Kinome of Trypanosoma brucei: Acs Chemical Biology, v. 7, p. 1858-1865.
Uzureau, P., S. Uzureau, L. Lecordier, F. Fontaine, P. Tebabi, F. Homble, A. Grelard, V. Zhendre, D. P. Nolan, L. Lins, J. M. Crowet, A. Pays, C. Felu, P. Poelvoorde, B. Vanhollebeke, S. K. Moestrup, J. Lyngso, J. S. Pedersen, J. C. Mottram, E. J. Dufourc, D. Perez-Morga, and E. Pays, 2013, Mechanism of Trypanosoma brucei gambiense resistance to human serum: Nature, v. 501, p. 430-+.
van Drogen, F., S. M. O'Rourke, V. M. Stucke, M. Jaquenoud, A. M. Neiman, and M. Peter, 2000, Phosphorylation of the MEKK Ste11p by the PAK-like kinase Ste20p is required for MAP kinase signaling in vivo: Current Biology, v. 10, p. 630-639.
Vanhamme, L., F. Paturiaux-Hanocq, P. Poelvoorde, D. P. Nolan, L. Lins, J. Van den Abbeele, A. Pays, P. Tebabi, H. Van Xong, A. Jacquet, N. Moguilevsky, M. Dieu, J. P. Kane, P. De Baetselier, R. Brasseur, and E. Pays, 2003, Apolipoprotein L-I is the trypanosome lytic factor of human serum: Nature, v. 422, p. 83-87.
Vanhollebeke, B., P. Uzureau, D. Monteyne, D. Perez-Morga, and E. Pays, 2010, Cellular and Molecular Remodeling of the Endocytic Pathway during Differentiation of Trypanosoma brucei Bloodstream Forms: Eukaryotic Cell, v. 9, p. 1272-1282.
Vassella, E., and M. Boshart, 1996, High molecular mass agarose matrix supports growth of bloodstream forms of pleomorphic Trypanosoma brucei strains in axenic culture: Molecular and Biochemical Parasitology, v. 82, p. 91-105.
Vassella, E., R. Kramer, C. M. R. Turner, M. Wankell, C. Modes, M. van den Bogaard, and M. Boshart, 2001, Deletion of a novel protein kinase with PX and FYVE-related domains increases the rate of differentiation of Trypanosoma brucei: Mol Microbiol, v. 41, p. 33-46.
Vassella, E., B. Reuner, B. Yutzy, and M. Boshart, 1997, Differentiation of African trypanosomes is controlled by a density sensing mechanism which signals cell cycle arrest via the cAMP pathway: J Cell Sci, v. 110 (Pt 21), p. 2661-71.
Vassella, E., J. Van den Abbeele, P. Butikofer, C. K. Renggli, A. Furger, R. Brun, and I. Roditi, 2000, A major surface glycoprotein of Trypanosoma brucei is expressed transiently during development and can be regulated post-transcriptionally by glycerol or hypoxia: Genes & Development, v. 14, p. 615-626.
Vercesi, A. E., S. N. J. Moreno, and R. Docampo, 1994, CA2+/H+ EXCHANGE IN ACIDIC VACUOLES OF TRYPANOSOMA-BRUCEI: Biochemical Journal, v. 304, p. 227-233.

Vickerman, K., 1965, Polymorphism and mitochondrial activity in sleeping sickness trypanosomes: Nature, v. 208, p. 762-6.
Vickerman, K., 1985, Developmental cycles and biology of pathogenic trypanosomes: Br Med Bull, v. 41, p. 105-14.
Vodnala, M., A. Fijolek, R. Rofougaran, M. Mosimann, P. Maser, and A. Hofer, 2008, Adenosine kinase mediates high affinity adenosine salvage in Trypanosoma brucei: J Biol Chem, v. 283, p. 5380-8.
Walrad, P. B., P. Capewell, K. Fenn, and K. R. Matthews, 2012, The post-transcriptional trans-acting regulator, TbZFP3, co-ordinates transmission-stage enriched mRNAs in Trypanosoma brucei: Nucleic Acids Research, v. 40, p. 2869-2883.
Wei, Y., and Z. Y. Li, 2014, Distinct Roles of a Mitogen-Activated Protein Kinase in Cytokinesis between Different Life Cycle Forms of Trypanosoma brucei: Eukaryotic Cell, v. 13, p. 110-118.
Welburn, S. C., I. Beange, M. J. Ducrotoy, and A. L. Okello, 2015, The neglected zoonoses-the case for integrated control and advocacy: Clinical Microbiology and Infection, v. 21, p. 433-443.
Welburn, S. C., K. Picozzi, E. M. Fevre, P. G. Coleman, M. Odiit, M. Carrington, and I. Maudlin, 2001, Identification of human-infective trypanosomes in animal reservoir of sleeping sickness in Uganda by means of serum-resistance-associated (SRA) gene: Lancet, v. 358, p. 2017-2019.
WHO, 2015, WHO | Trypanosomiasis, human African (sleeping sickness): WHO.
Wickstead, B., K. Ersfeld, and K. Gull, 2002, Targeting of a tetracycline-inducible expression system to the transcriptionally silent minichromosomes of Trypanosoma brucei: Molecular and Biochemical Parasitology, v. 125, p. 211-216.
Wickstead, B., K. Ersfeld, and K. Gull, 2004, The small chromosomes of Trypanosoma brucei involved in antigenic variation are constructed around repetitive palindromes: Genome Research, v. 14, p. 1014-1024.
Wirtz, E., S. Leal, C. Ochatt, and G. A. M. Cross, 1999, A tightly regulated inducible expression system for conditional gene knock-outs and dominant-negative genetics in Trypanosoma brucei: Molecular and Biochemical Parasitology, v. 99, p. 89-101.
Woods, A., P. C. F. Cheung, F. C. Smith, M. D. Davison, J. Scott, R. K. Beri, and D. Carling, 1996, Characterization of AMP-activated protein kinase beta and gamma subunits - Assembly of the heterotrimeric complex in vitro: Journal of Biological Chemistry, v. 271, p. 10282-10290.
Woods, A., M. R. Munday, J. Scott, X. L. Yang, M. Carlson, and D. Carling, 1994, YEAST SNF1 IS FUNCTIONALLY RELATED TO MAMMALIAN AMP-ACTIVATED PROTEIN-KINASE AND REGULATES ACETYL-COA CARBOXYLASE IN-VIVO: Journal of Biological Chemistry, v. 269, p. 19509-19515.
Woodward, R., and K. Gull, 1990, Timing of nuclear and kinetoplast DNA replication and early morphological events in the cell cycle of Trypanosoma brucei: J Cell Sci, v. 95 (Pt 1), p. 49-57.
Wullschleger, S., R. Loewith, and M. N. Hall, 2006, TOR signaling in growth and metabolism: Cell, v. 127, p. 5-19.
Yabu, Y., and T. Takayanagi, 1988, TRYPSIN-STIMULATED TRANSFORMATION OF TRYPANOSOMA-BRUCEI-GAMBIENSE BLOOD-

STREAM FORMS TO PROCYCLIC FORMS INVITRO: Parasitology Research, v. 74, p. 501-506.
Zhang, N. S., Z. Z. Quan, B. Rash, and S. G. Oliver, 2013, Synergistic effects of TOR and proteasome pathways on the yeast transcriptome and cell growth: Open Biology, v. 3, p. 14.
Ziegelbauer, K., M. Quinten, H. Schwarz, T. W. Pearson, and P. Overath, 1990, Synchronous differentiation of Trypanosoma brucei from bloodstream to procyclic forms in vitro: Eur J Biochem, v. 192, p. 373-8.

Appendix A: Primers

Nomenclature guide:

F/FW – forward; R/RV – reverse

MKD – monomorph knockdown; PKD – pleomorph knockdown

OE – overexpression

KO – knockout

5/3 ext/int – external/internal 5'/3'UTR;

2300 – AK; 1240 – PP2A; 2720 – MEKK1; 1930 – TOR4

GC – Gibson cloning (see section 2.4.7)

RNAi primers for pRPa constructs:

MKD2300F	(XbaI/BamHI)	TCTAGAGGATCCAGTTTGTATCACCGGCAAGG
MKD2300R	(XhoI/SmaI)	CTCGAGCCCGGGCTTGCAATCTCCTCGACACA
MKD1240F	(XbaI/BamHI)	TCTAGAGGATCCCGAAAGTATGGCAGTGCAAA
MKD1240R	(XhoI/SmaI)	CTCGAGCCCGGGGCACGAGCAATTGTTTTCAA
MKD1930F	(XbaI/BamHI)	TCTAGAGGATCCCTGCAGACGTATCTCGACCA
MKD1930R	(XhoI/SmaI)	CTCGAGCCCGGGCTTTGAAAAGACCTCCAGCG

RNAi primers for p2T7-177 constructs:

PKD1930F	(BamHI/HindIII)	GGATCCAAGCTTCTGCAGACGTATCTCGACCA
PKD1930R	(XhoI/XbaI)	CTCGAGTCTAGACTTTGAAAAGACCTCCAGCG

RNAi primers for pALC14 constructs:

PKD2300F	(BamHI/HindIII)	GGATCCAAGCTTAGTTTGTATCACCGGCAAGG
PKD2300R	(XhoI/XbaI)	CTCGAGTCTAGACTTGCAATCTCCTCGACACA
PKD2720F	(BamHI/HindIII)	GGATCCAAGCTTTTATGTAATGCAGCGAAGCG
PKD2720R	(XhoI/XbaI)	CTCGAGTCTAGAACCGTTGTCACGCTTATTCC

Overexpression primers for pDEX 577-Y constructs:

MEKK1OE FW (for N-terminal TY tagged copy)	(SpeI)	ACTAGTCCCTTCGCGGCAAAT
CatMEKK1OE FW	(SpeI)	ACTAGTTCTTACACGTTGGGGCG
MEKK1OE RV	(BamHI)	GGATCCCTAAACAACTCCCTGATCACCA
MEKK1OECtTY GC Pt1FW		GTATGGACCTCTCTAGAAACAACTCCCTGATCACC
MEKK1OECtTY GC Pt1RV		GTGCAAGTAATGGTGCTATTAGCAGTG

MEKK1OECtTY GC Pt2FW		AGCACCATTACTTGCACCCGAAGAGC
MEKK1OECtTY GC Pt2RV		AGTAAAATTCACAAGCTTATGATGCCCTTCGCGGCAAAT
NEKOE FW GC	(XbaI)	GTATGGACCTCTCTAGACAATCCAAGAACCTCCTGTATTTTC
NEKOE RV GC	(HindIII)	AGTAAAATTCACAAGCTTATGATGTCGTCAACGGATGCAATG
182 (YAK GC Pt1 FW)	(SpeI)	TCACACTAGTACGTTGTGAGTATACCTG
179 (YAK GC Pt1RV)		TCGGTGATCCCTCAATGGTACCAACCCATAC
178 (YAK GC Pt2 FW)		TACCATTGAGGGATCACCGAATGGTATATACGTGTG
175 (YAK GC Pt2 RV)	(SpeI)	ACCAAAAAGTAAAATTCACAAGCTTATGGACGCTGACGAG GGC

Knockout primers for pEnT6B-Y/pEnT6P-Y constructs:

MEKK1 KO internal UTR primers:

2720KO 5U F	(SpeI)	ACTAGTTTATCAGGGGGTTCGAG
2720KO 5U R	(BamHI)	GGATCCGGGTGGTCACCTGCTC
2720KO 3U F	(HindIII)	AAGCTTGAATATATGTAAAAGGGAAGAAGG
2720KO 3U R	(SpeI)	ACTAGTCGATTACCCTCTTCCCC

MEKK1 KO external UTR primers:

MEKK1 5extF	(SpeI)	ACTAGTGTACGTCATTTGCTCCATT
MEKK1 5extR	(BamHI)	GGATCCGGGTGGTCACCTGCTC
MEKK1 3extF	(HindIII)	AAGCTTGAATATATGTAAAAGGGAAGAAGG
MEKK1 3extF	(SpeI)	ACTAGTCGATTACCCTCTTCCCC

RNAi library primers:

Lib3F	ATCAAGCTTGGCCTGTGAG
Lib3R	CCTCGAGGGCCAGTGAG

qRT-PCR primers:

TOR4qF	ACTGCATGGACAAGCAAGTG
TOR4qR	TCAGCAATAACAGGCACGAG
17 (ZFP3qF)	CAGGGGAAACGCAAAACTAA
19 (ZFP3qR)	TGTCACCCCAACTGCATTCT

Appendix B: Antibody concentrations

rabbit α-PAD1 (Eurogentec)	Western	1:1000
	IFA	1:1000
	FACS	1:200
mouse α-EF1 (Millipore)	Western	1:7000
mouse α-EP procyclin (VH Bio)	FACS	1:500
mouse α-BB2 (in house)	Western	1:20
	IFA	1:2
α-rabbit-HRP (Sigma)	Western	1:1000
α-mouse-HRP (Sigma)	Western	1:7000
α-rabbit IRDye 800CW (LiCor)	Western	1:7500
α-mouse IRDye 800CW (LiCor)	Western	1:7500
α-rabbit IRDye 680 (LiCor)	Western	1:7500
α-mouse IRDye 680 (LiCor)	Western	1:7500
α-rabbit Alexa fluor 488 (Life Technologies)	IFA	1:1000
α-mouse Alexa fluor 488 (Life Technologies)	IFA	1:1000
α-rabbit Cy5 (Jackson ImmunoResearch)	FACS	1:1000
α-mouse FITC (Sigma)	FACS	1:1000

Appendix C: Drug concentrations

Drug	2T1	427/S16	AnTat 1.1 90:13
Hygromycin	2.5	2	0.5
G418	-	2.5	2.5
Phleomycin	0.5	2.5	1.5
Puromycin	0.2	0.5	0.5
Blasticidin	2	-	10
Tetracycline	1	1	1

Table 1 Table of drug concentrations used for selection and maintenance of *T. brucei* in culture. Concentrations are in μg/ml.

Appendix D: Plasmid maps

pRPa

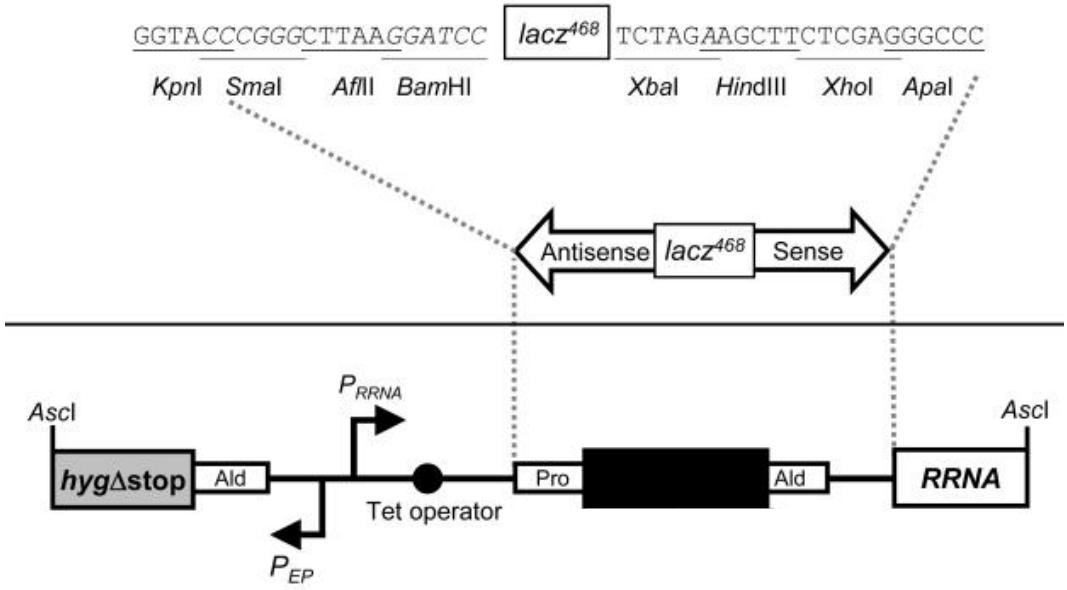

Figure 1 pRPa vector map. RNAi construct for *T. brucei* 2T1 cell line containing the terminal component of a hygromycin resistance gene (HYG) and RRNA spacer sequences for targeting to RRNA locus containing the remaining portion of HYG and the complete puromycin resistance gene (PAC) on chromosome 2a in 2T1 cells. Correct integration generates an intact HYG ORF under the control of the EP procyclin promoter and deletes the PAC ORF. Within, a stem-loop component, in which the 'loop' is a 468-bp lacz fragment, contains unique cloning sites, shown in the upper panel, to facilitate insertion of sense and antisense gene fragments for RNAi targeting. This component is under the control of an RRNA promoter and a tet operator which represses expression of the stem-loop RNA in the absence of tetracycline and allows expression on its presence. From Alsford and Horn (2008).

pALC14

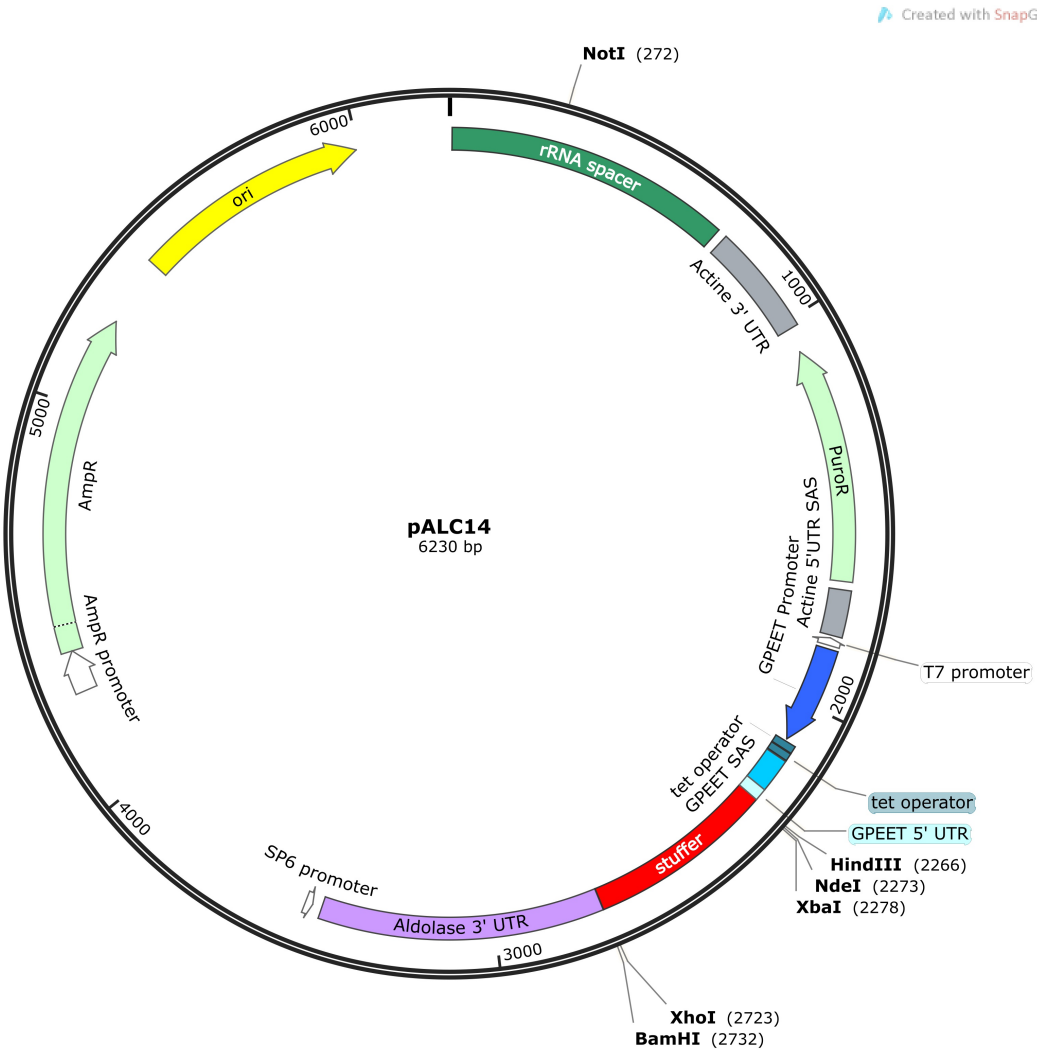

Figure 2 pALC14 vector map. RNAi construct suitable for *T. brucei* lines with integrated expression cassettes for T7 polymerase and a tet repressor (Bochud-Allemann and Schneider, 2002). The plasmid contains a puromycin resistance gene (PuroR) under the control of a T7 promoter and rRNA spacer sequence to enable targeting to RDNA locus. To enable RNAi, a stem-loop component contains unique cloning sites to facilitate insertion of sense and antisense gene fragments either side of the stuffer region for RNAi targeting. This component is under the control of a procyclin promoter and a tet operator which represses expression of the stem-loop RNA in the absence of tetracycline and allows expression on its presence.

p2T7-177

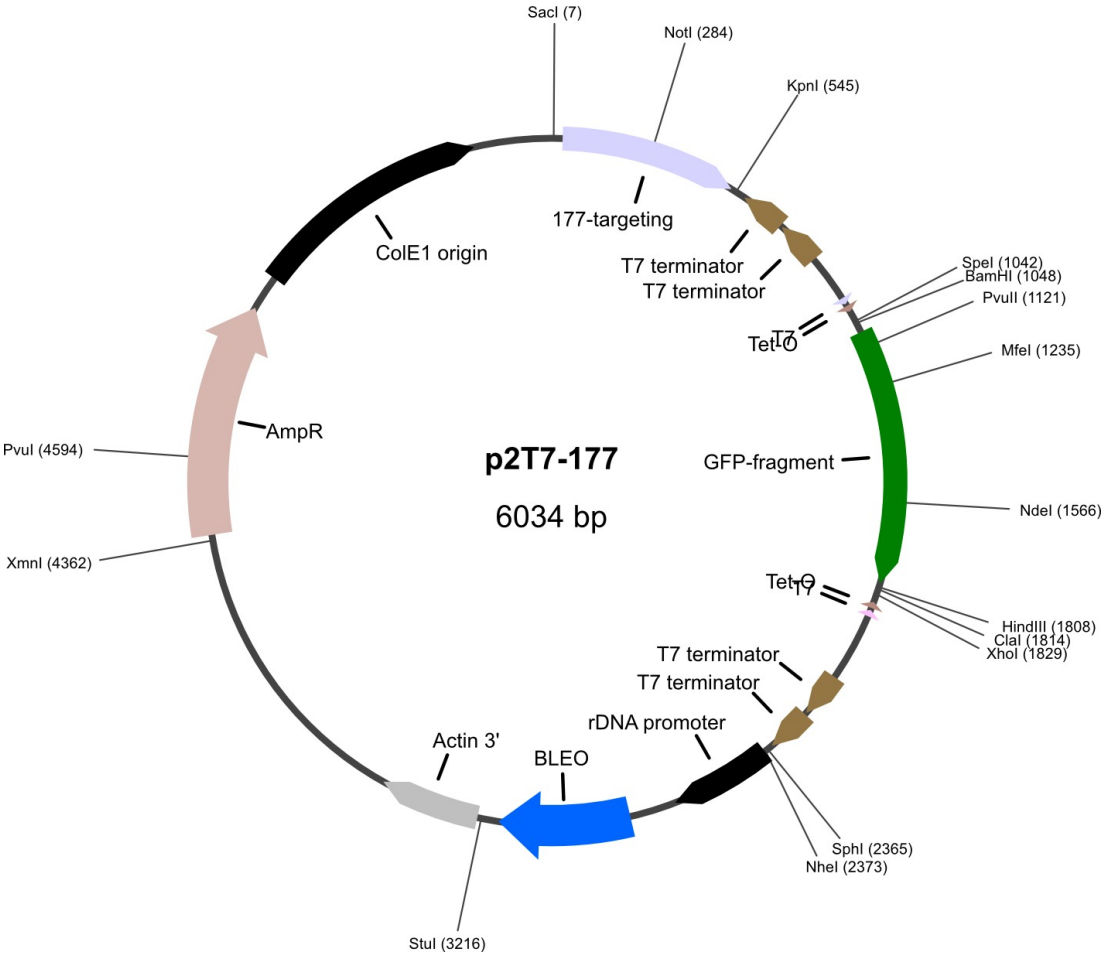

Figure 3 p2T7-177 Wickstead map. RNAi construct suitable for *T. brucei* 427 and AnTat 1.1 90:13 lines with integrated expression cassettes for T7 polymerase and a tet repressor (Wickstead et al., 2002). The plasmid contains a phleomycin resistance gene under the control of an rDNA promoter and 177bp repeat sequences to enable targeting to the transcriptionally silent mini-chromosomes. The RNAi component is flanked by opposing T7 promoters to enable double-stranded RNA synthesis and tet operators to repress its expression in the absence of tetracycline.

MEKK1 KO pEnT6B-Y

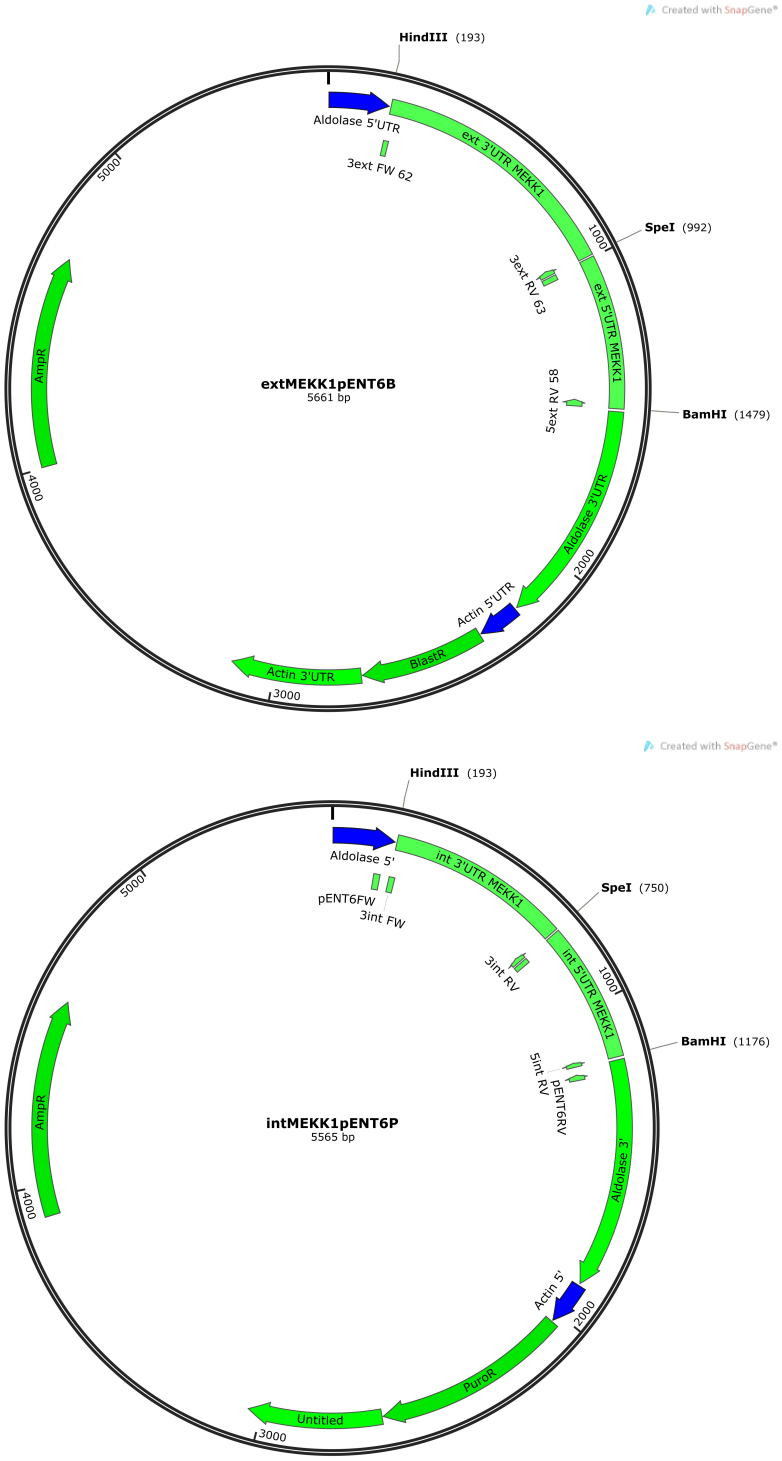

Figure 4 Constructs for generation of MEKK1 null mutant line. External fragments of the 3'UTR and 5'UTR of MEKK1 were cloned into the pEnT6B-Y plasmid (Kelly et al., 2007) replacing the YFP and TY tags (extMEKK1pEnt6B-Y). Internal fragments of the 3'UTR and 5'UTR of MEKK1 were cloned into the pEnT6P-Y plasmid (intMEKK1pEnT6P-Y). Linearisation of the first plasmid using SpeI between the 3'UTR and 5'UTR fragments and transfection into AnTat 1.1 90:13 cells enabled recombination of the entire construct, including the BlastR gene, into the MEKK1 locus. SpeI linearisation of the intMEKK1 pEnT6P-Y plasmid then produced a PuroR containing construct capable of recombination only with the remaining MEKK1 allele.

(Cat)MEKK1 pDEX577-Y

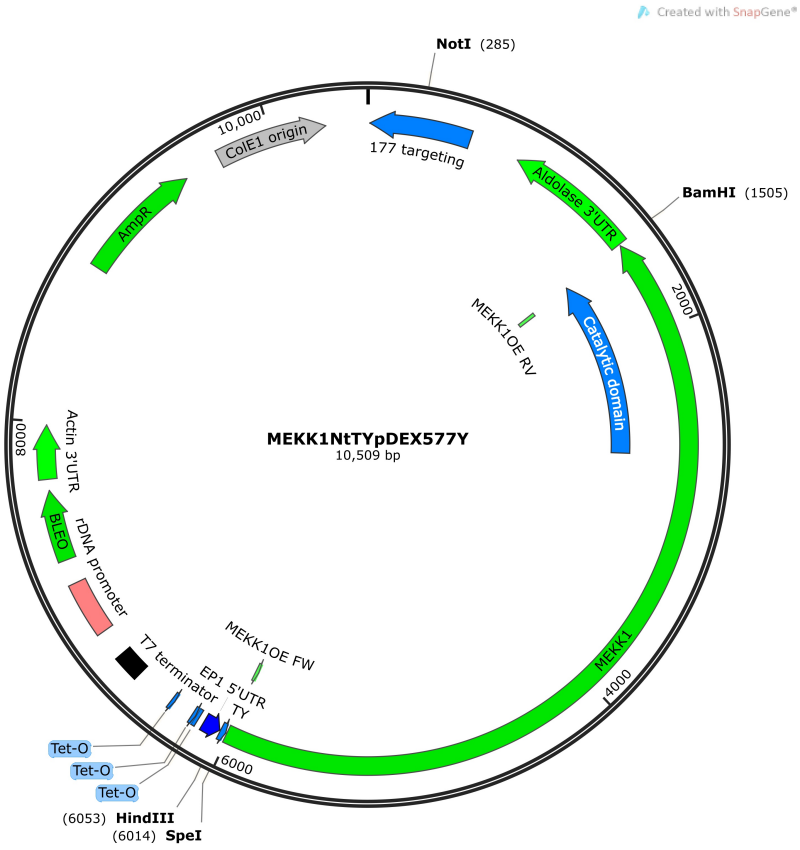

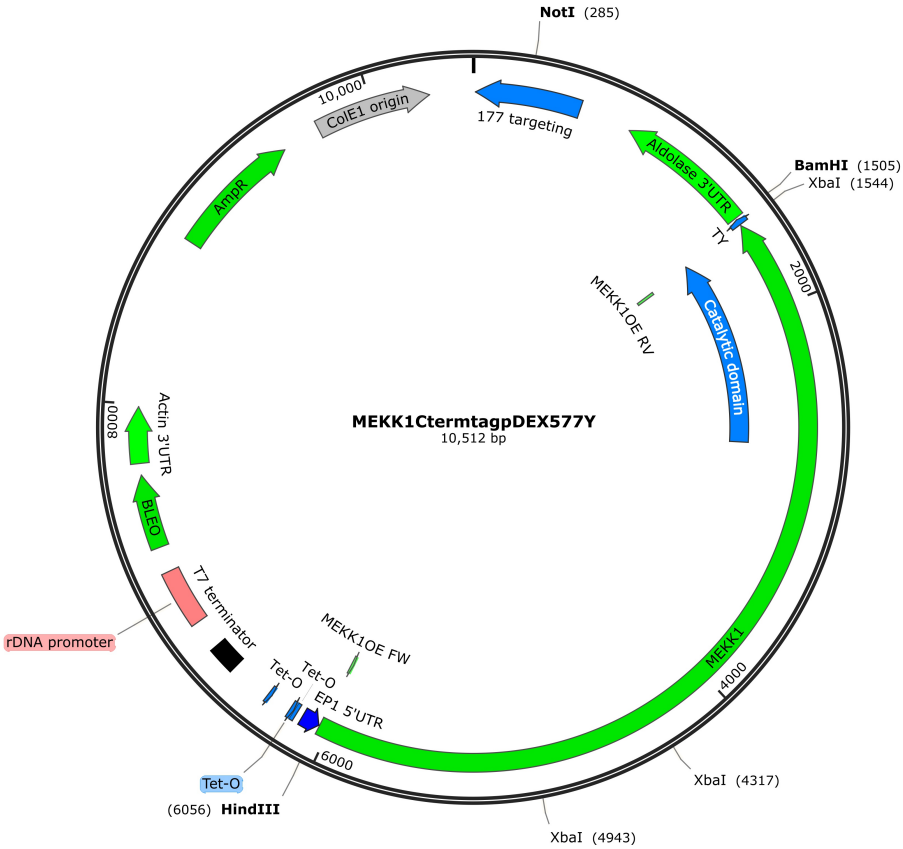

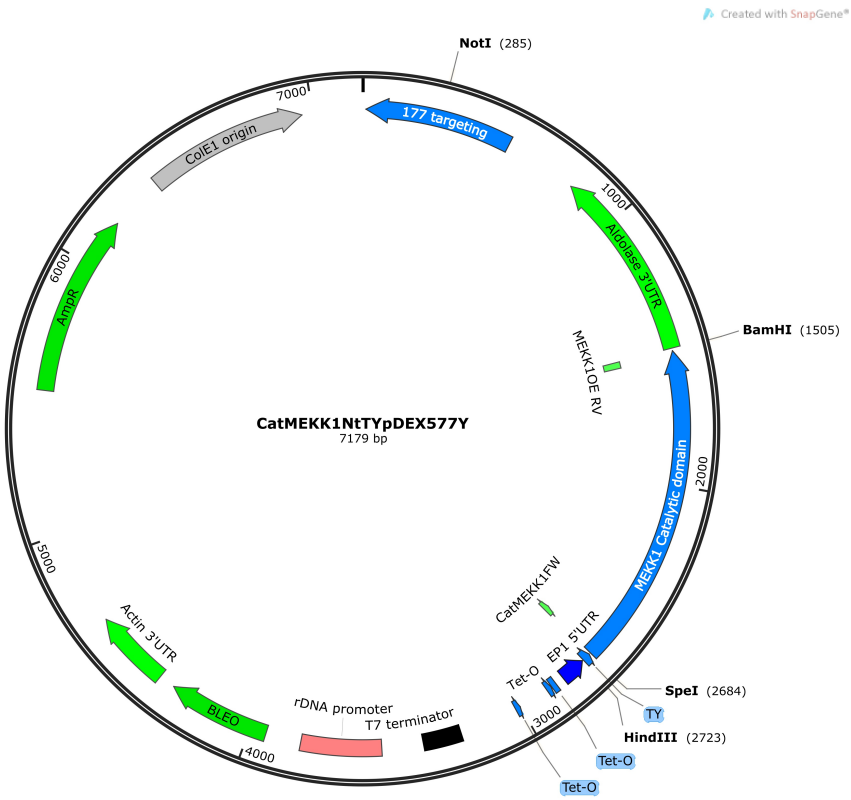

Figure 5 pDex577-Y constructs used for overexpression of MEKK1. The MEKK1 ORF was cloned into the pDex577-Y plasmid, which facilitates tetracycline-inducible expression from an EP promoter (Kelly et al., 2007), using either BamHI and SpeI restriction sites to produce an N-terminal TY epitope tag or HindIII and XbaI to produce a C-terminal TY tag, replacing the vector's YFP tag in both cases. In the final construct, the catalytic domain (Cat) of MEKK1 was cloned into pDex577-Y using BamHI and SpeI restriction sites to produce an N-terminal TY tag. NotI was used to linearise all 3 constructs.

Appendix E: Ion Torrent Read Alignments

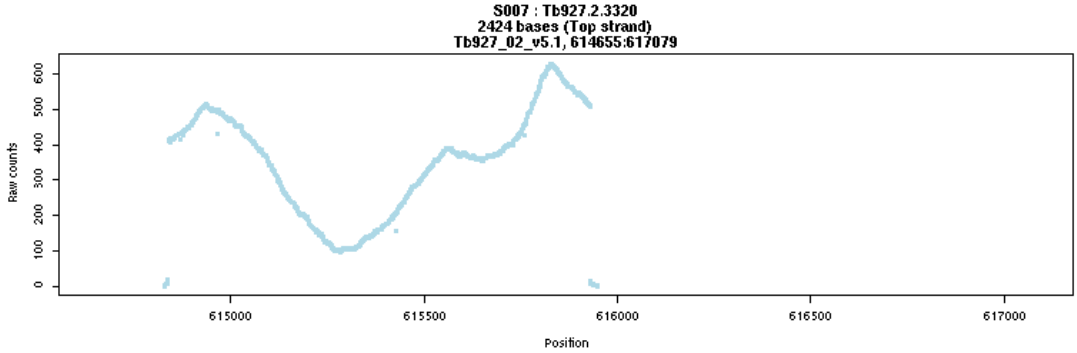

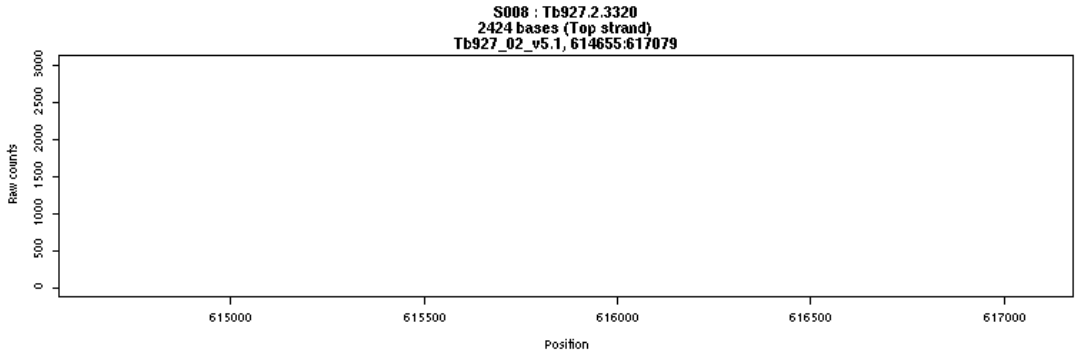

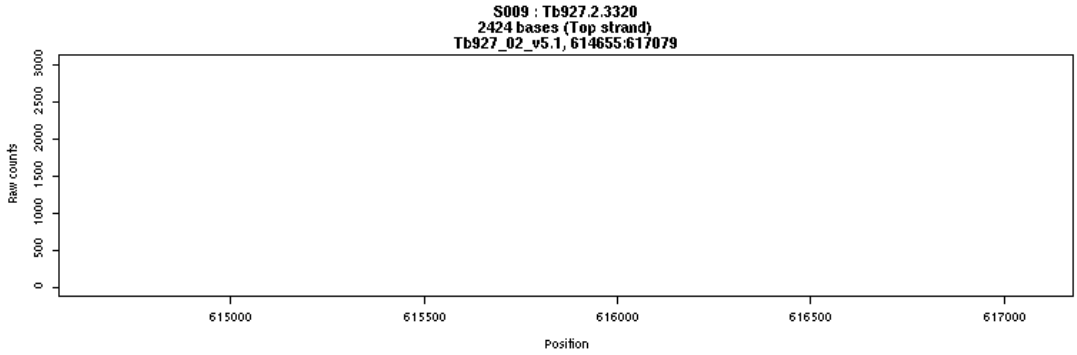

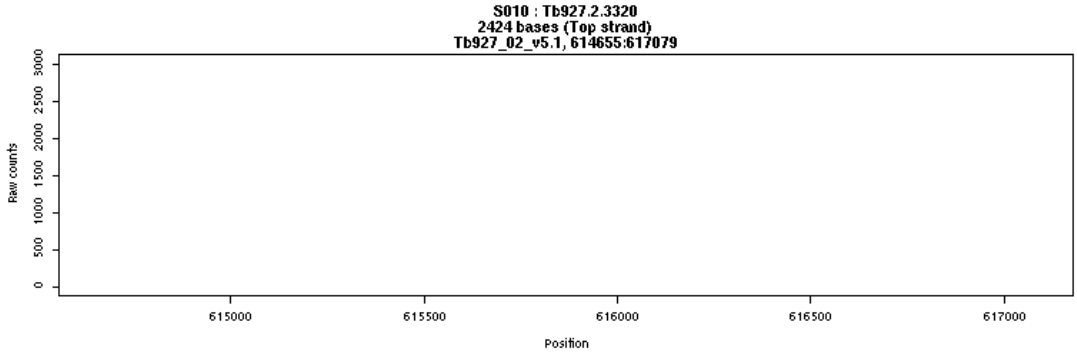

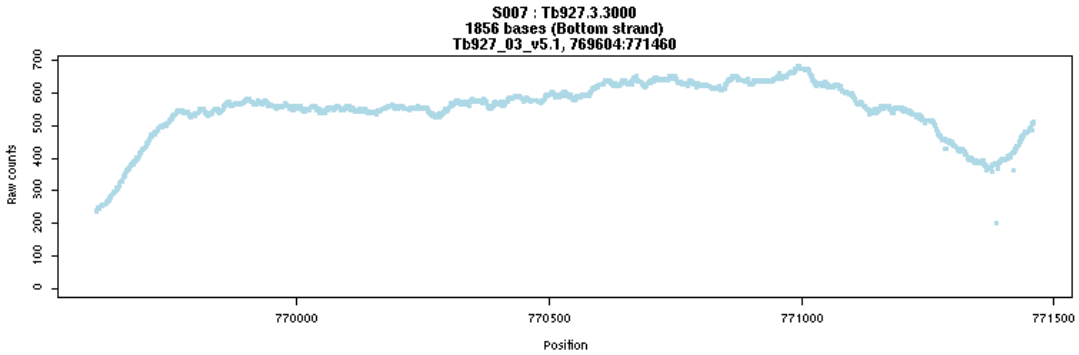
S007 : Tb927.3.3000
1856 bases (Bottom strand)
Tb927_03_v5.1, 769604:771460
Raw counts
0
100
200
300
400
500
600
700
770000
770500
771000
771500
Position

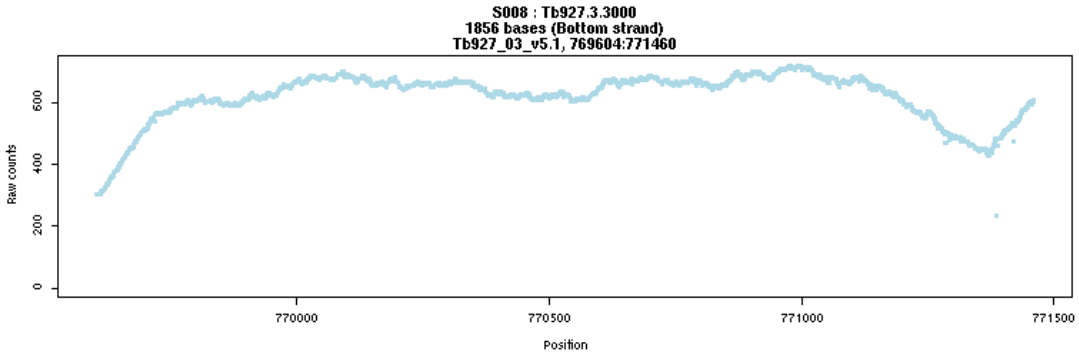
S008 : Tb927.3.3000
1856 bases (Bottom strand)
Tb927_03_v5.1, 769604:771460
Raw counts
0
200
400
600
770000
770500
771000
771500
Position

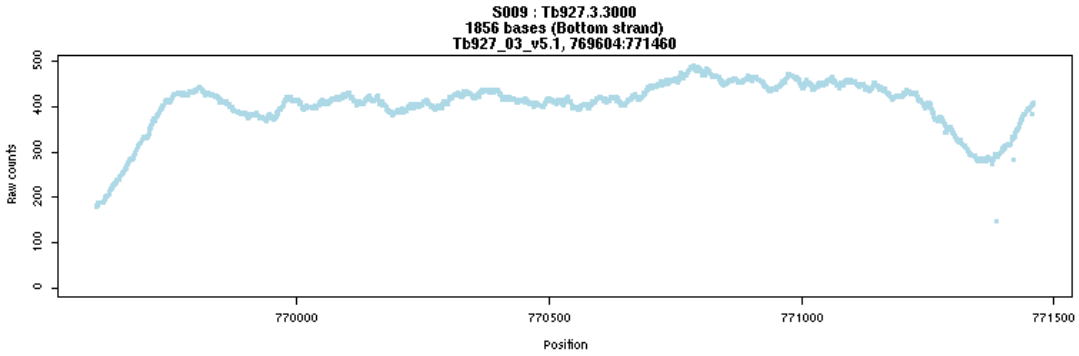
S009 : Tb927.3.3000
1856 bases (Bottom strand)
Tb927_03_v5.1, 769604:771460
Raw counts
0
100
200
300
400
500
770000
770500
771000
771500
Position

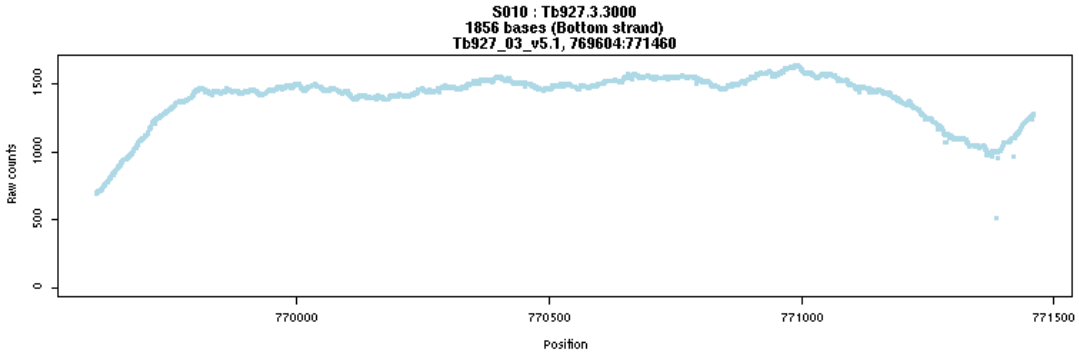
S010 : Tb927.3.3000
1856 bases (Bottom strand)
Tb927_03_v5.1, 769604:771460
Raw counts
0
500
1000
1500
770000
770500
771000
771500
Position

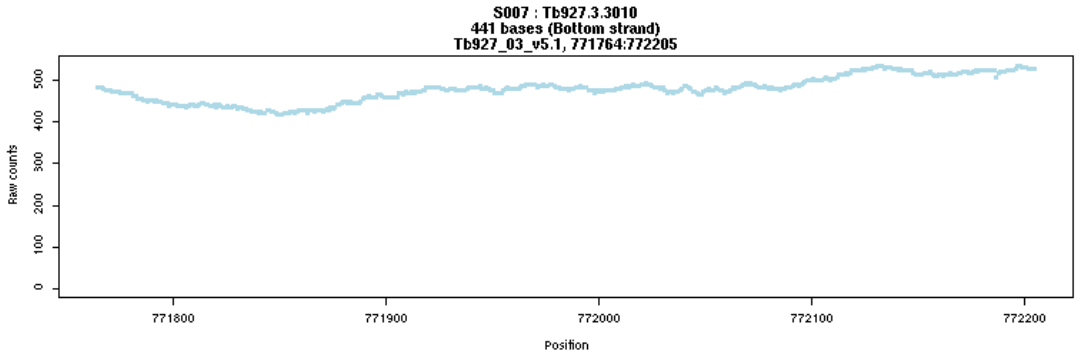
S007 : Tb927.3.3010
441 bases (Bottom strand)
Tb927_03_v5.1, 771764:772205
Raw counts
0
100
200
300
400
500
771800
771900
772000
772100
772200
Position

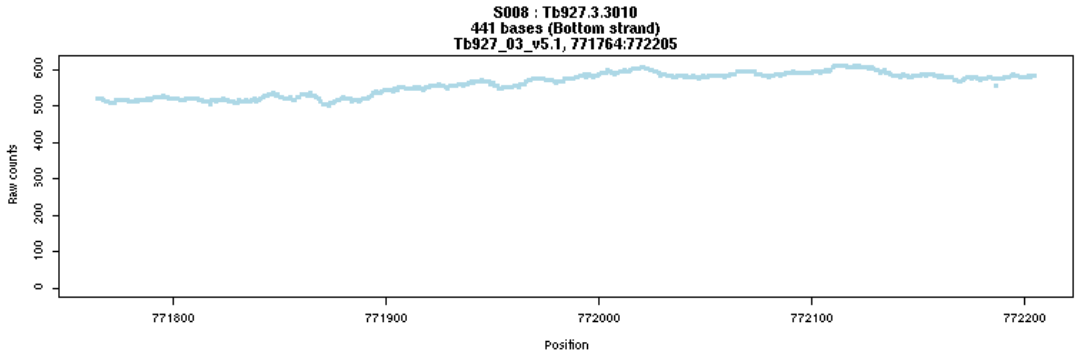
S008 : Tb927.3.3010
441 bases (Bottom strand)
Tb927_03_v5.1, 771764:772205
Raw counts
0
100
200
300
400
500
600
771800
771900
772000
772100
772200
Position

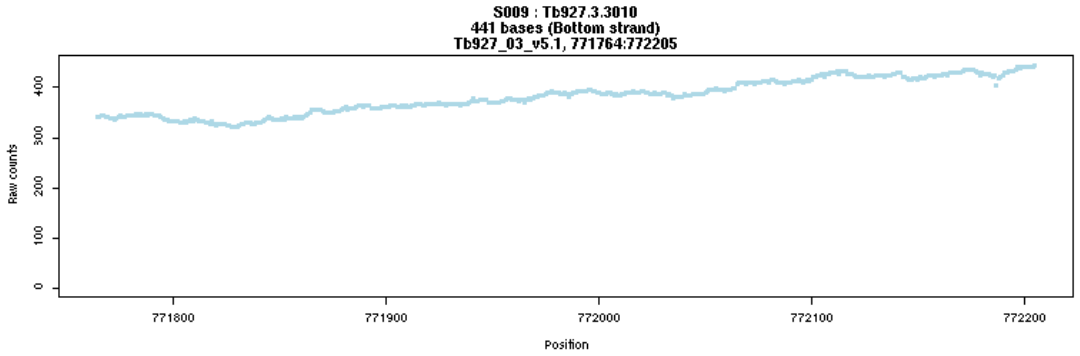
S009 : Tb927.3.3010
441 bases (Bottom strand)
Tb927_03_v5.1, 771764:772205
Raw counts
0
100
200
300
400
771800
771900
772000
772100
772200
Position

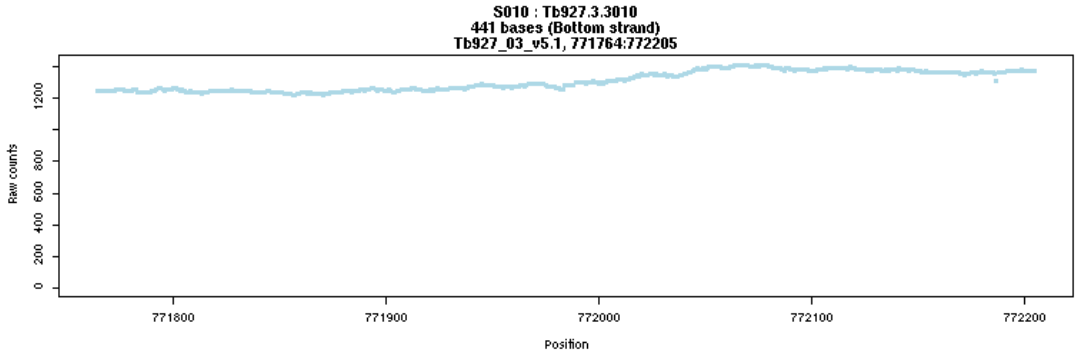
S010 : Tb927.3.3010
441 bases (Bottom strand)
Tb927_03_v5.1, 771764:772205
Raw counts
0
200
400
600
800
1200
771800
771900
772000
772100
772200
Position

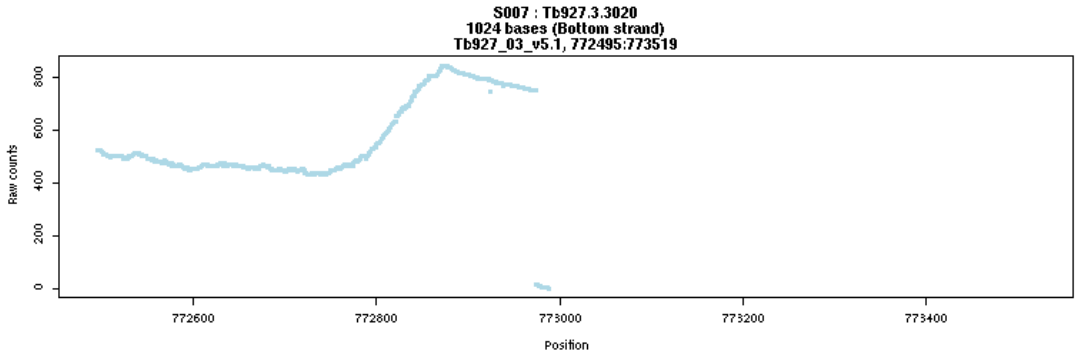
S007 : Tb927.3.3020
1024 bases (Bottom strand)
Tb927_03_v5.1, 772495:773519
Raw counts
0
200
400
600
800
772600
772800
773000
773200
773400
Position

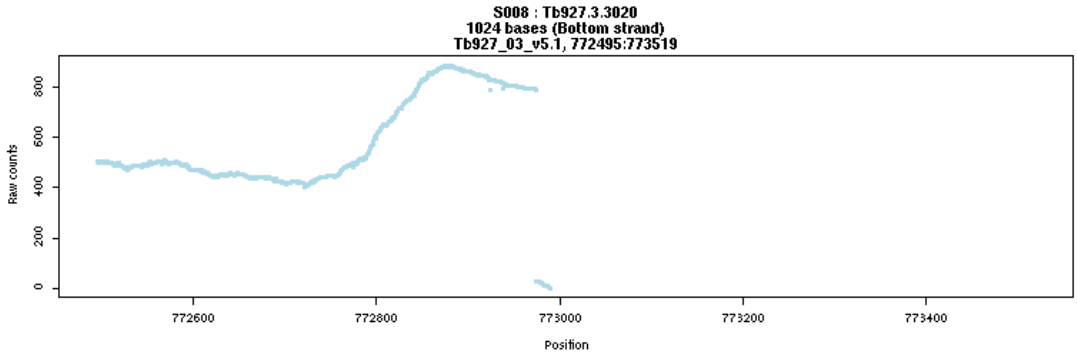
S008 : Tb927.3.3020
1024 bases (Bottom strand)
Tb927_03_v5.1, 772495:773519
Raw counts
0
200
400
600
800
772600
772800
773000
773200
773400
Position

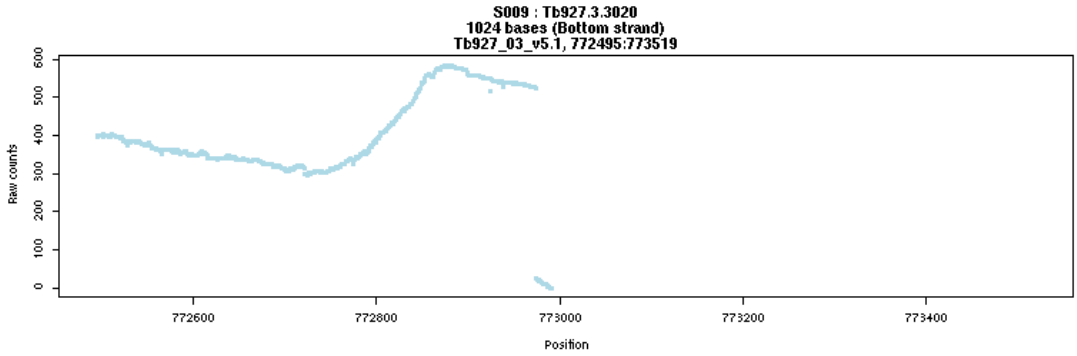
S009 : Tb927.3.3020
1024 bases (Bottom strand)
Tb927_03_v5.1, 772495:773519
Raw counts
0
100
200
300
400
500
600
772600
772800
773000
773200
773400
Position

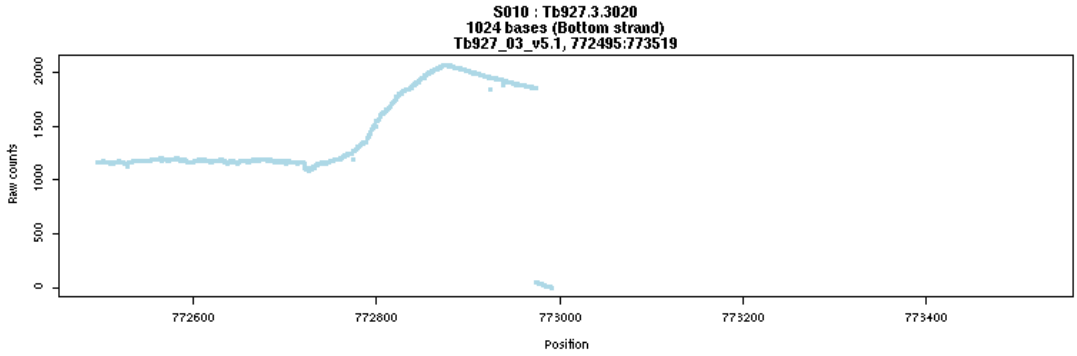
S010 : Tb927.3.3020
1024 bases (Bottom strand)
Tb927_03_v5.1, 772495:773519
Raw counts
0
500
1000
1500
2000
772600
772800
773000
773200
773400
Position

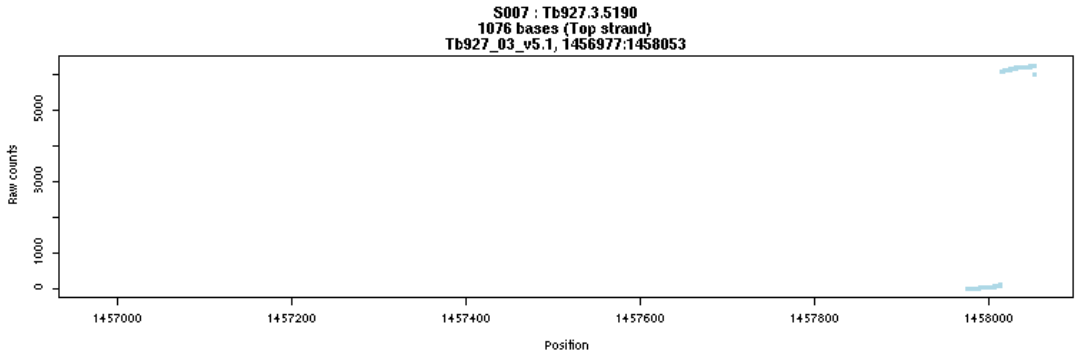
S007 : Tb927.3.5190
1076 bases (Top strand)
Tb927_03_v5.1, 1456977:1458053
Raw counts
0
1000
3000
5000
1457000
1457200
1457400
1457600
1457800
1458000
Position

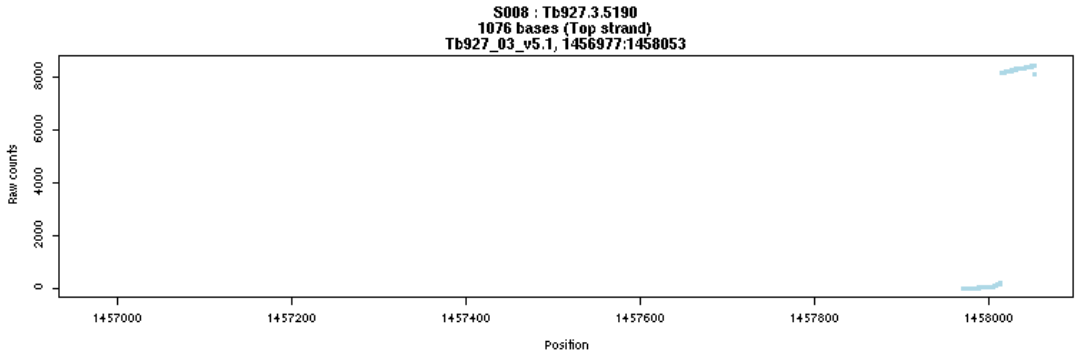
S008 : Tb927.3.5190
1076 bases (Top strand)
Tb927_03_v5.1, 1456977:1458053
Raw counts
0
2000
4000
6000
8000
1457000
1457200
1457400
1457600
1457800
1458000
Position

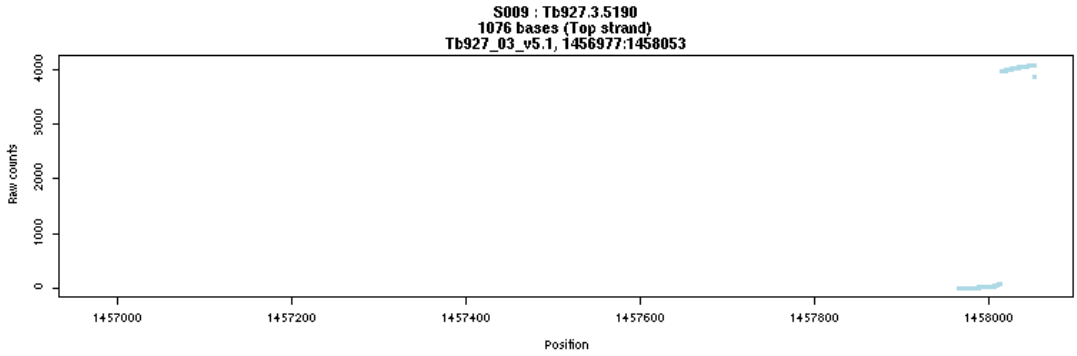
S009 : Tb927.3.5190
1076 bases (Top strand)
Tb927_03_v5.1, 1456977:1458053
Raw counts
0
1000
2000
3000
4000
1457000
1457200
1457400
1457600
1457800
1458000
Position

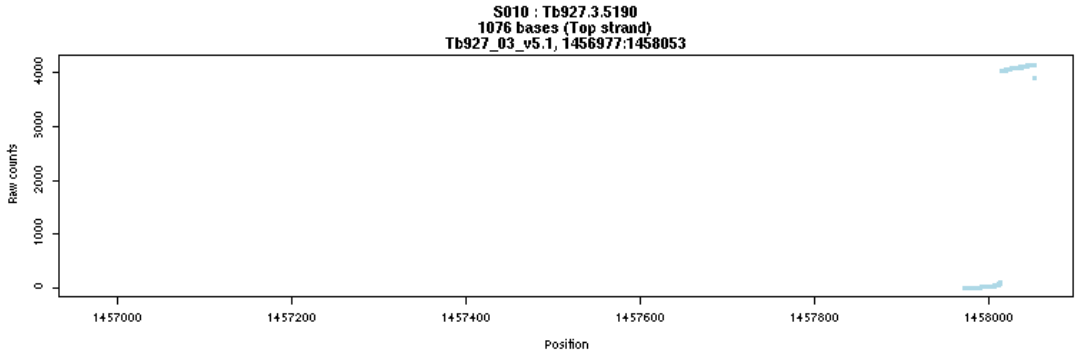
S010 : Tb927.3.5190
1076 bases (Top strand)
Tb927_03_v5.1, 1456977:1458053
Raw counts
0
1000
2000
3000
4000
1457000
1457200
1457400
1457600
1457800
1458000
Position

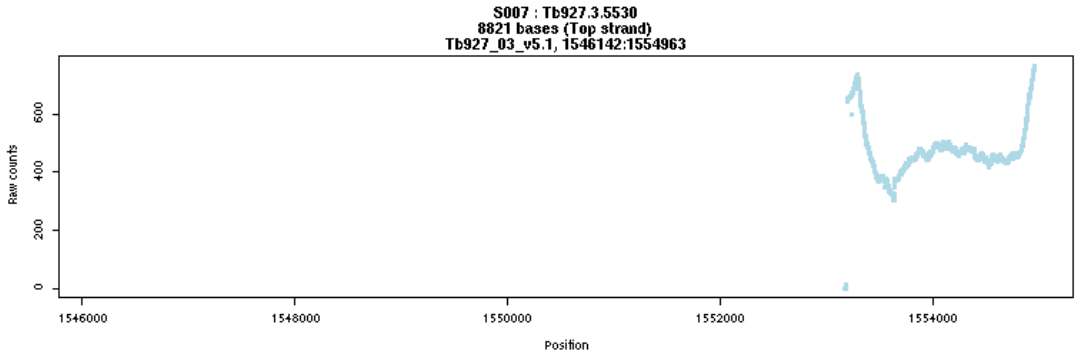
S007 : Tb927.3.5530
8821 bases (Top strand)
Tb927_03_v5.1, 1546142:1554963
Raw counts
0
200
400
600
1546000
1548000
1550000
1552000
1554000
Position

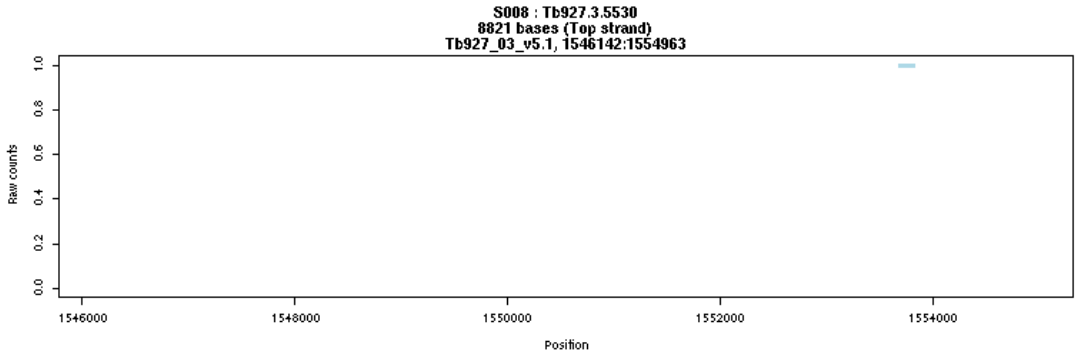
S008 : Tb927.3.5530
8821 bases (Top strand)
Tb927_03_v5.1, 1546142:1554963
Raw counts
0.0
0.2
0.4
0.6
0.8
1.0
1546000
1548000
1550000
1552000
1554000
Position

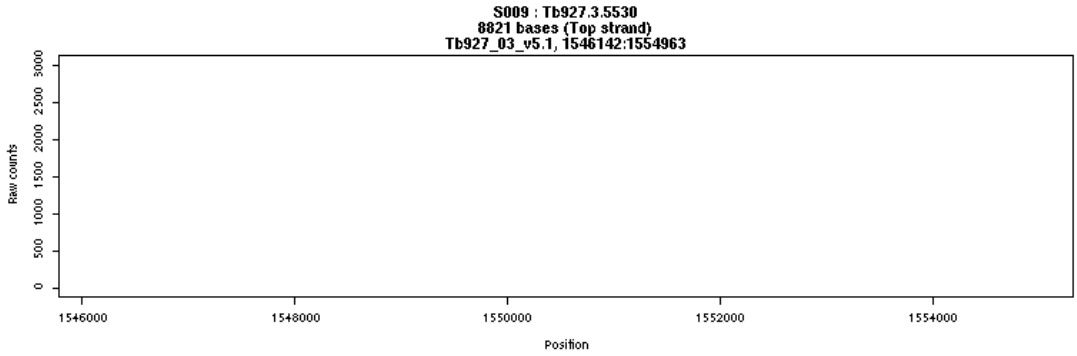
S009 : Tb927.3.5530
8821 bases (Top strand)
Tb927_03_v5.1, 1546142:1554963
Raw counts
0
500
1000
1500
2000
2500
3000
1546000
1548000
1550000
1552000
1554000
Position

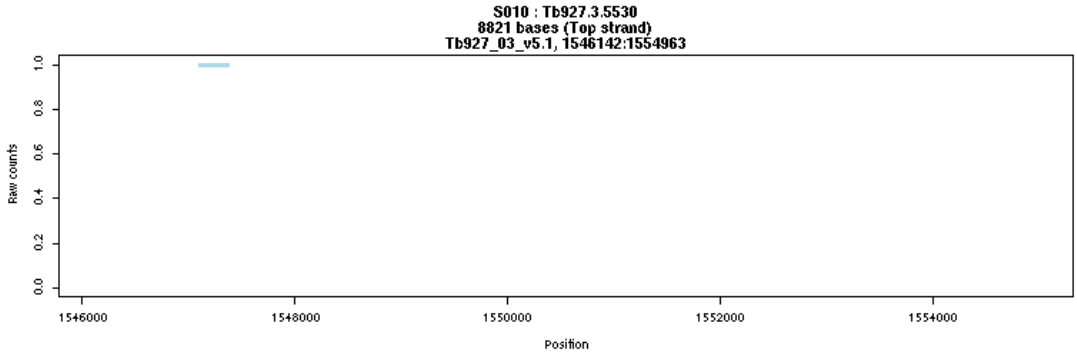
S010 : Tb927.3.5530
8821 bases (Top strand)
Tb927_03_v5.1, 1546142:1554963
Raw counts
0.0
0.2
0.4
0.6
0.8
1.0
1546000
1548000
1550000
1552000
1554000
Position

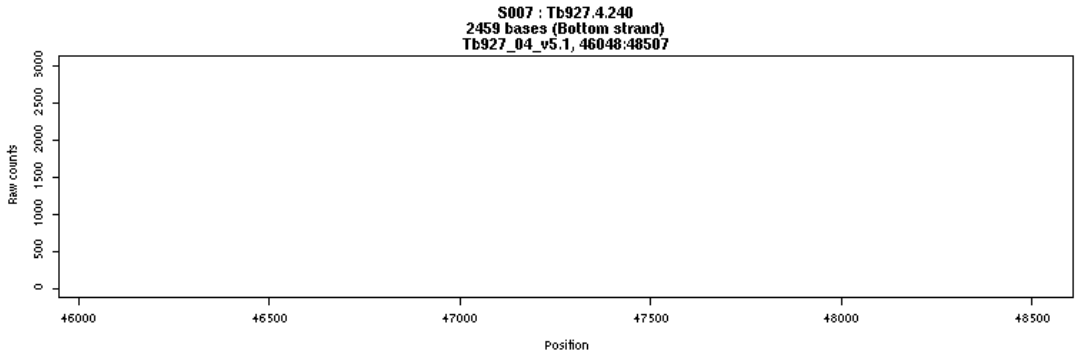
S007 : Tb927.4.240
2459 bases (Bottom strand)
Tb927_04_v5.1, 46048:48507
Raw counts
0
500
1000
1500
2000
2500
3000
46000
46500
47000
47500
48000
48500
Position

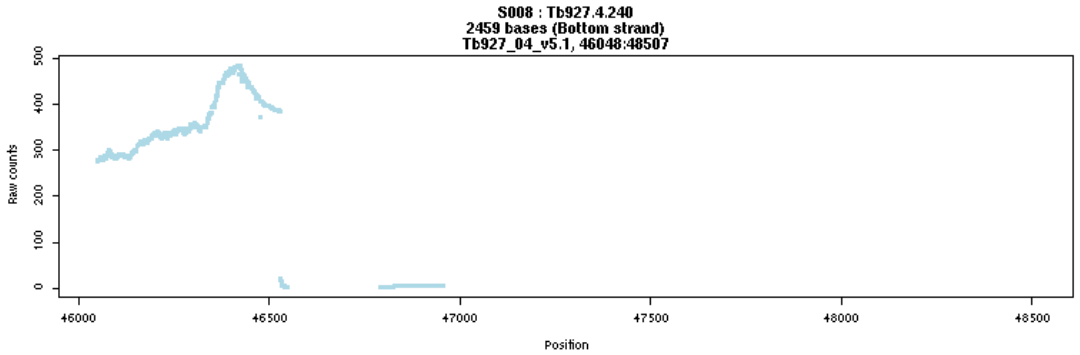
S008 : Tb927.4.240
2459 bases (Bottom strand)
Tb927_04_v5.1, 46048:48507
Raw counts
0
100
200
300
400
500
46000
46500
47000
47500
48000
48500
Position

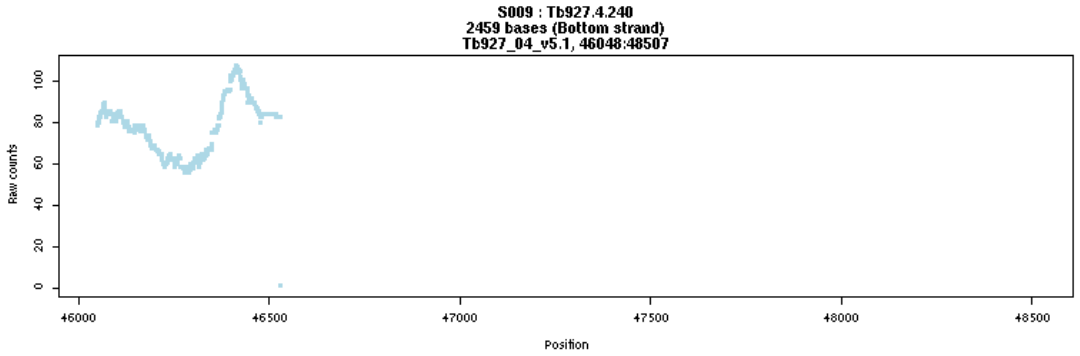
S009 : Tb927.4.240
2459 bases (Bottom strand)
Tb927_04_v5.1, 46048:48507
Raw counts
0
20
40
60
80
100
46000
46500
47000
47500
48000
48500
Position

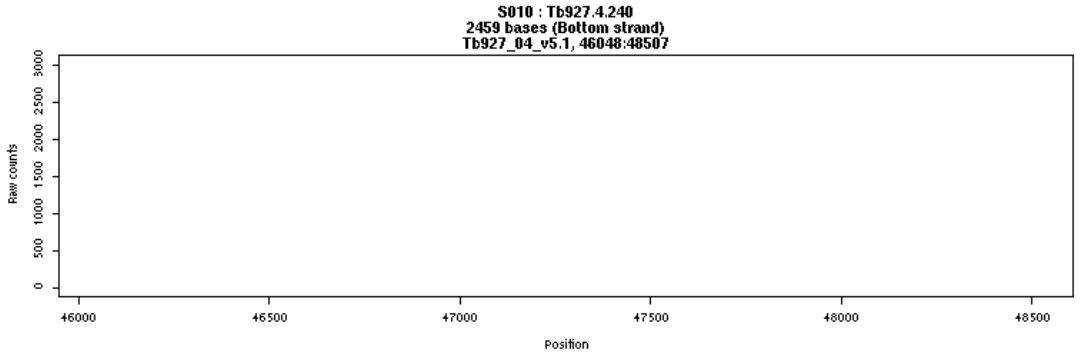
S010 : Tb927.4.240
2459 bases (Bottom strand)
Tb927_04_v5.1, 46048:48507
Raw counts
0
500
1000
1500
2000
2500
3000
46000
46500
47000
47500
48000
48500
Position

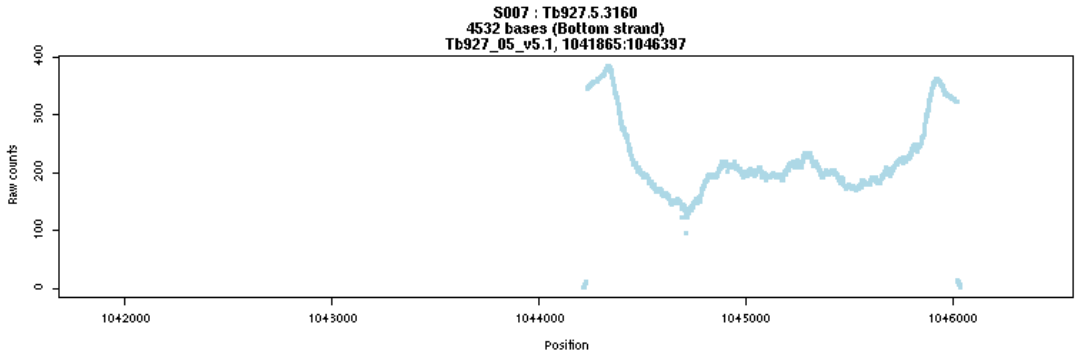
S007 : Tb927.5.3160
4532 bases (Bottom strand)
Tb927_05_v5.1, 1041865:1046397
Raw counts
0
100
200
300
400
1042000
1043000
1044000
1045000
1046000
Position

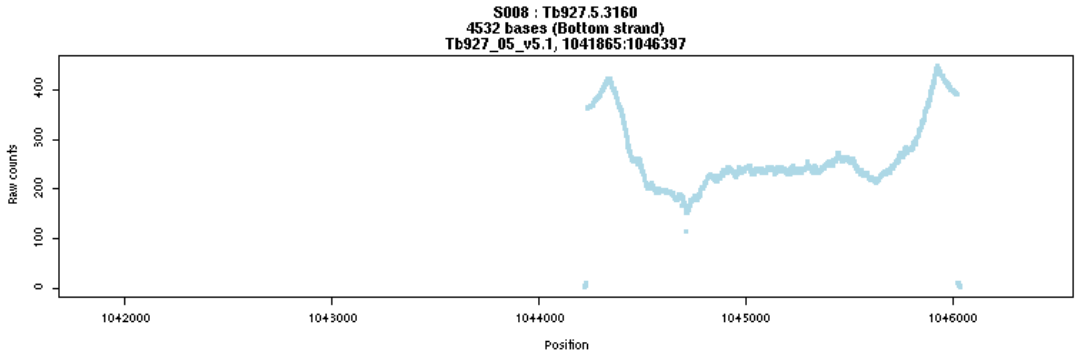
S008 : Tb927.5.3160
4532 bases (Bottom strand)
Tb927_05_v5.1, 1041865:1046397
Raw counts
0
100
200
300
400
1042000
1043000
1044000
1045000
1046000
Position

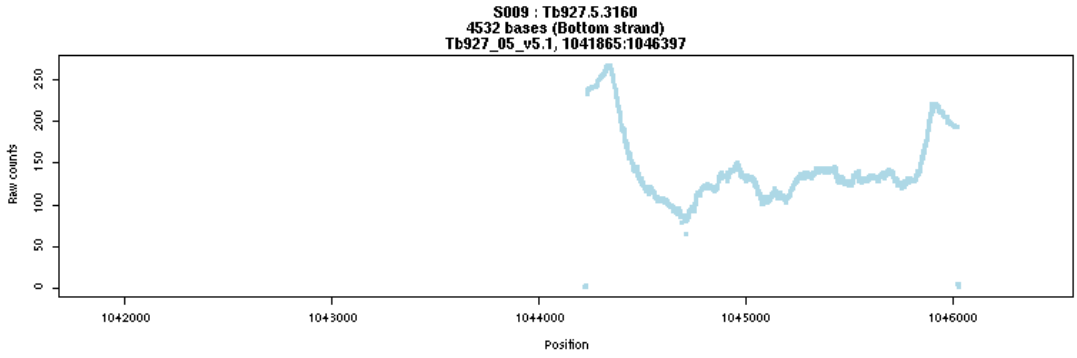
S009 : Tb927.5.3160
4532 bases (Bottom strand)
Tb927_05_v5.1, 1041865:1046397
Raw counts
0
50
100
150
200
250
1042000
1043000
1044000
1045000
1046000
Position

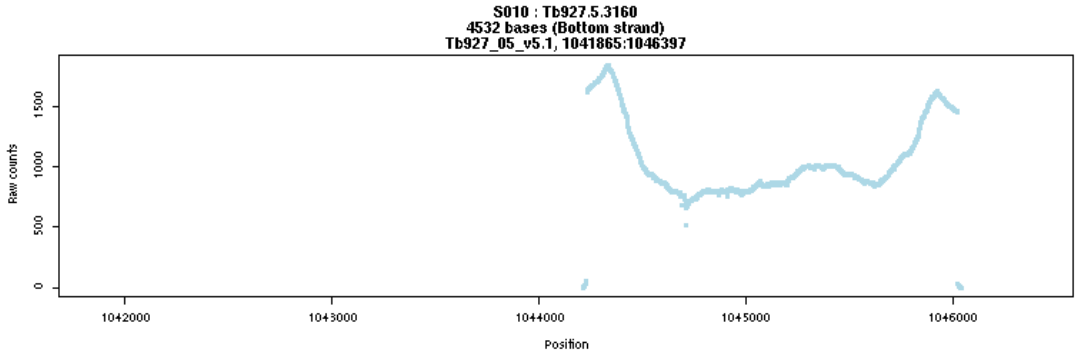
S010 : Tb927.5.3160
4532 bases (Bottom strand)
Tb927_05_v5.1, 1041865:1046397
Raw counts
0
500
1000
1500
1042000
1043000
1044000
1045000
1046000
Position

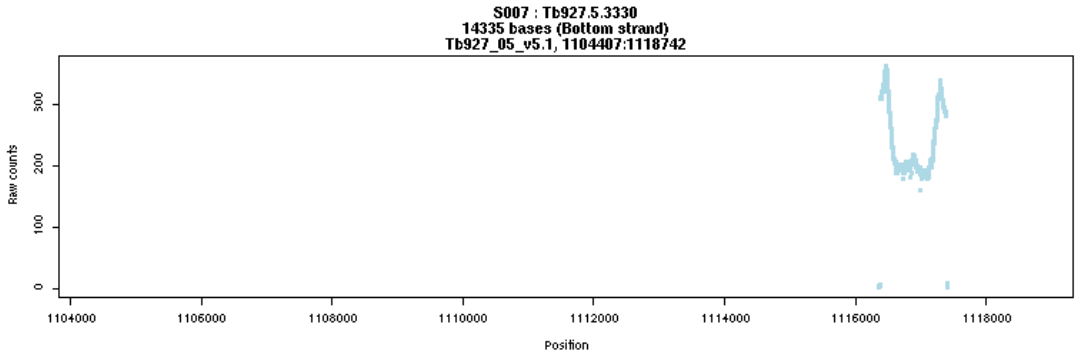
S007 : Tb927.5.3330
14335 bases (Bottom strand)
Tb927_05_v5.1, 1104407:1118742
Raw counts
0
100
200
300
1104000
1106000
1108000
1110000
1112000
1114000
1116000
1118000
Position

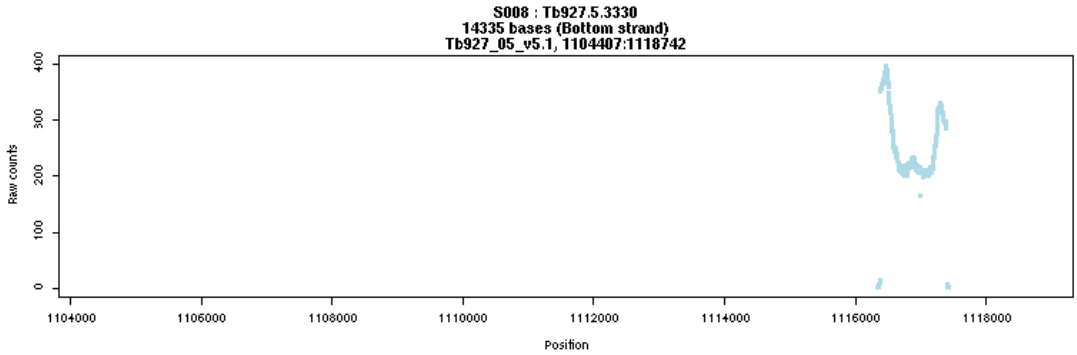
S008 : Tb927.5.3330
14335 bases (Bottom strand)
Tb927_05_v5.1, 1104407:1118742
Raw counts
0
100
200
300
400
1104000
1106000
1108000
1110000
1112000
1114000
1116000
1118000
Position

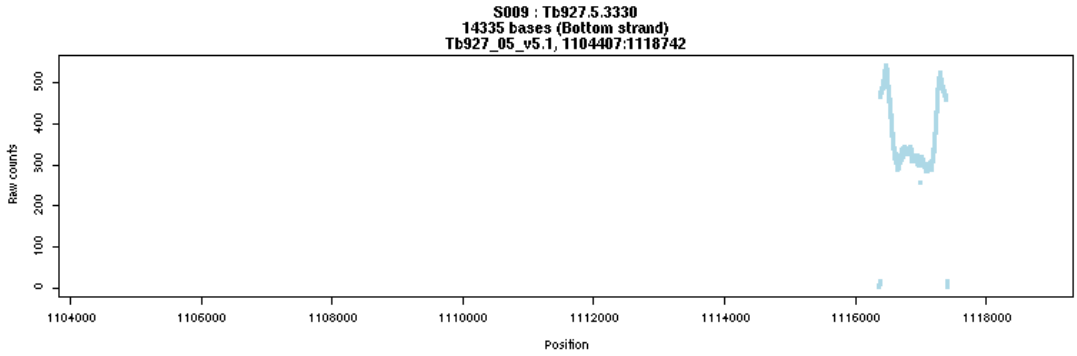
S009 : Tb927.5.3330
14335 bases (Bottom strand)
Tb927_05_v5.1, 1104407:1118742
Raw counts
0
100
200
300
400
500
1104000
1106000
1108000
1110000
1112000
1114000
1116000
1118000
Position

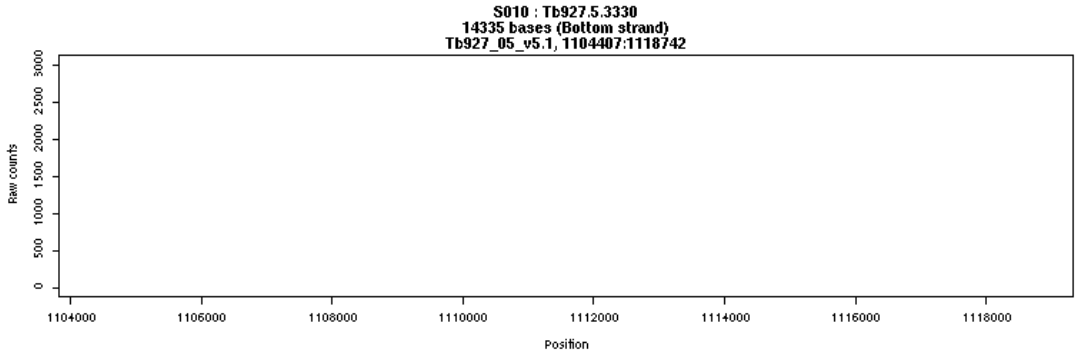
S010 : Tb927.5.3330
14335 bases (Bottom strand)
Tb927_05_v5.1, 1104407:1118742
Raw counts
0
500
1000
1500
2000
2500
3000
1104000
1106000
1108000
1110000
1112000
1114000
1116000
1118000
Position

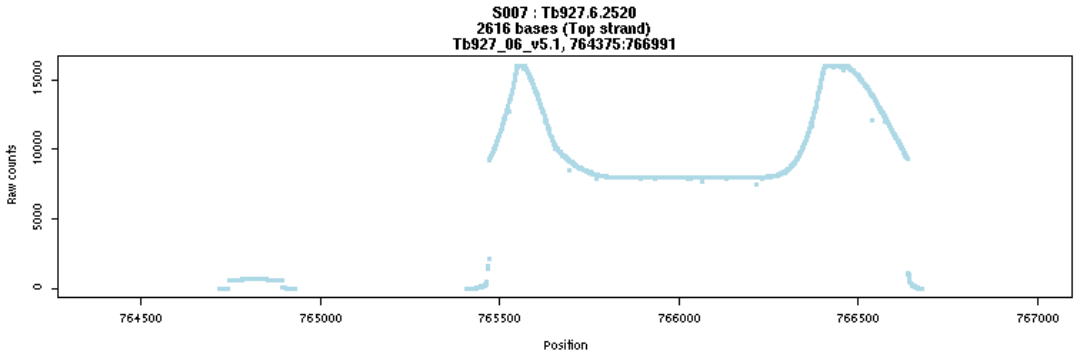
S007 : Tb927.6.2520
2616 bases (Top strand)
Tb927_06_v5.1, 764375:766991
Raw counts
0
5000
10000
15000
764500
765000
765500
766000
766500
767000
Position

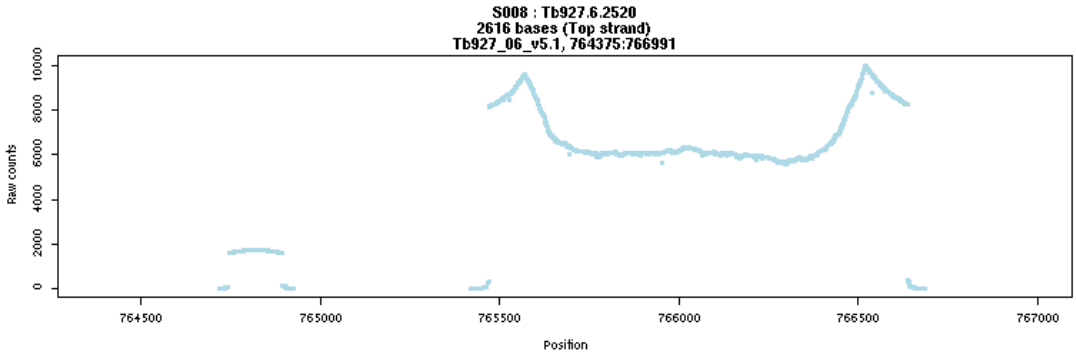
S008 : Tb927.6.2520
2616 bases (Top strand)
Tb927_06_v5.1, 764375:766991
Raw counts
0
2000
4000
6000
8000
10000
764500
765000
765500
766000
766500
767000
Position

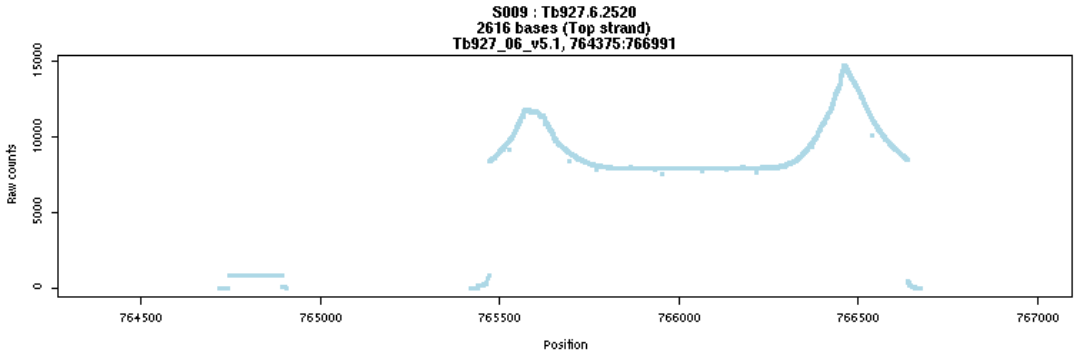
S009 : Tb927.6.2520
2616 bases (Top strand)
Tb927_06_v5.1, 764375:766991
Raw counts
0
5000
10000
15000
764500
765000
765500
766000
766500
767000
Position

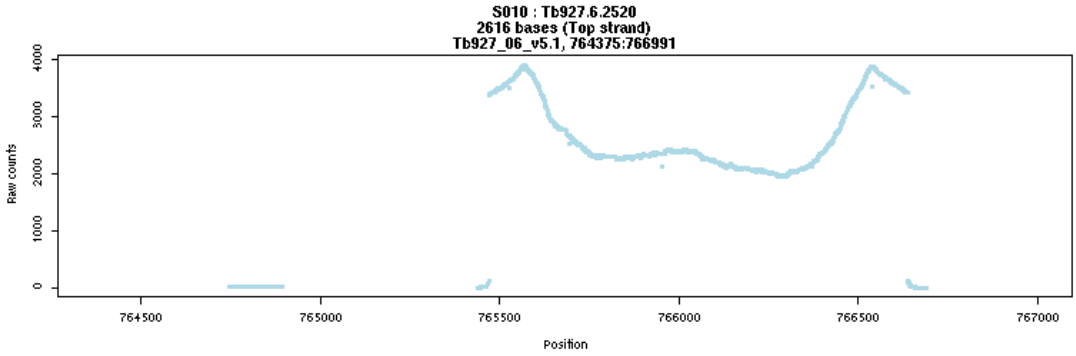
S010 : Tb927.6.2520
2616 bases (Top strand)
Tb927_06_v5.1, 764375:766991
Raw counts
0
1000
2000
3000
4000
764500
765000
765500
766000
766500
767000
Position

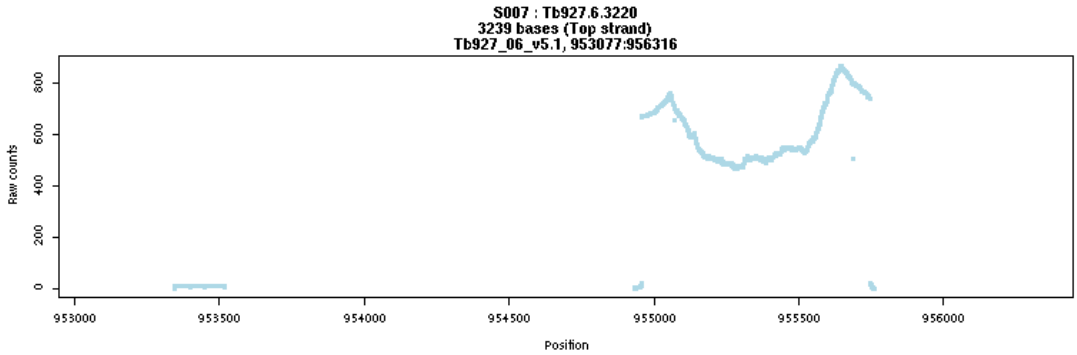
S007 : Tb927.6.3220
3239 bases (Top strand)
Tb927_06_v5.1, 953077:956316
Raw counts
0
200
400
600
800
953000
953500
954000
954500
955000
955500
956000
Position

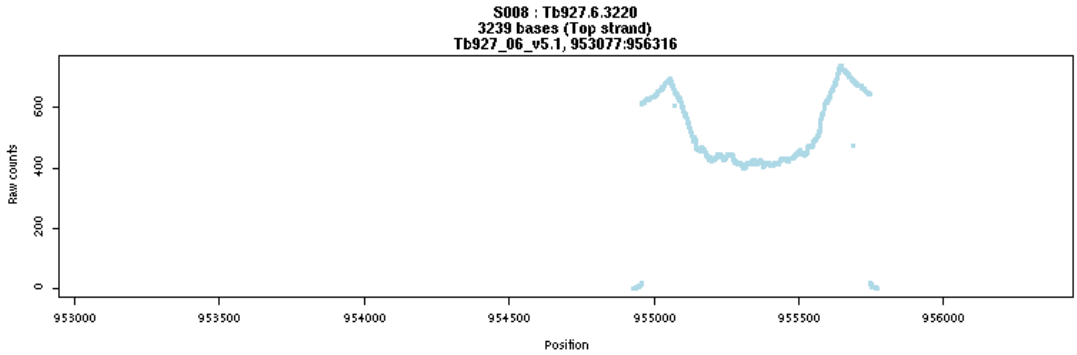
S008 : Tb927.6.3220
3239 bases (Top strand)
Tb927_06_v5.1, 953077:956316
Raw counts
0
200
400
600
953000
953500
954000
954500
955000
955500
956000
Position

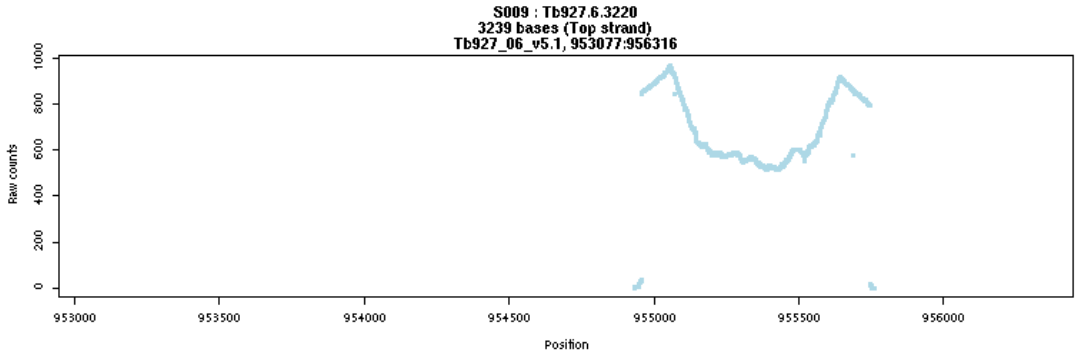
S009 : Tb927.6.3220
3239 bases (Top strand)
Tb927_06_v5.1, 953077:956316
Raw counts
0
200
400
600
800
1000
953000
953500
954000
954500
955000
955500
956000
Position

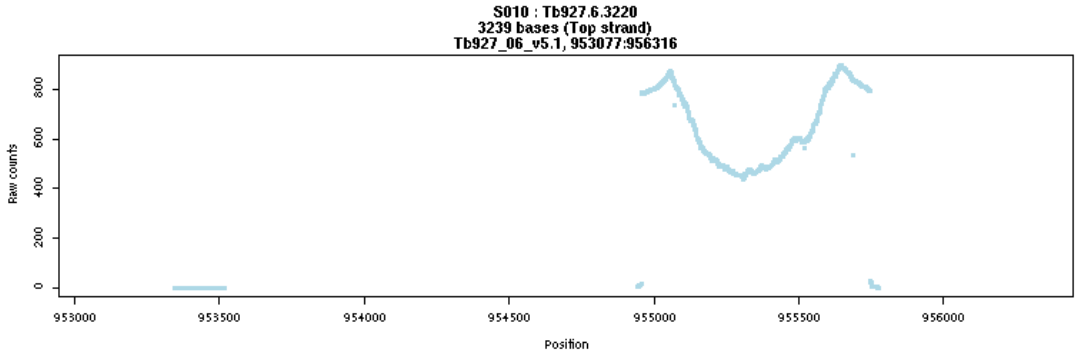
S010 : Tb927.6.3220
3239 bases (Top strand)
Tb927_06_v5.1, 953077:956316
Raw counts
0
200
400
600
800
953000
953500
954000
954500
955000
955500
956000
Position

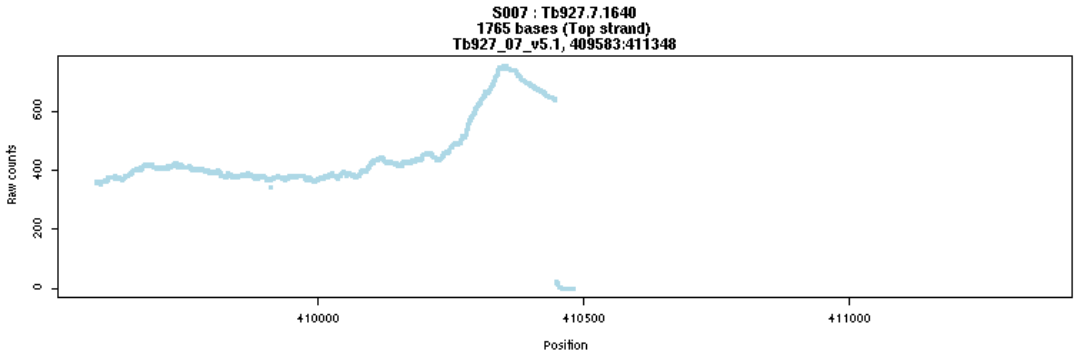
S007 : Tb927.7.1640
1765 bases (Top strand)
Tb927_07_v5.1, 409583:411348
Raw counts
0
200
400
600
410000
410500
411000
Position

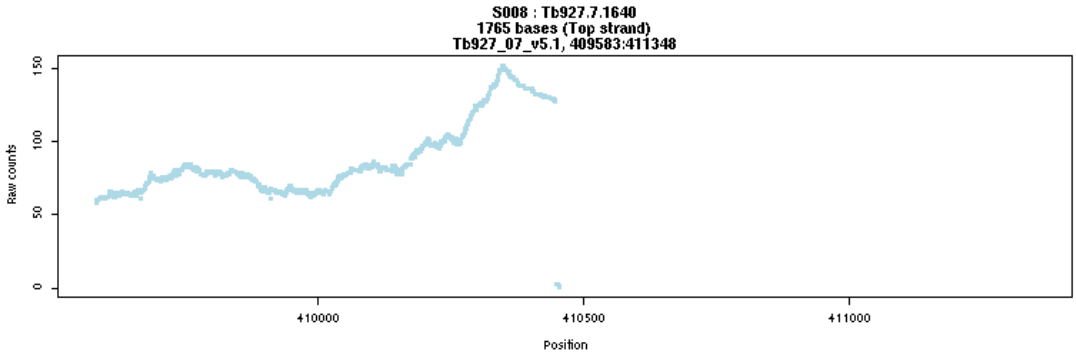
S008 : Tb927.7.1640
1765 bases (Top strand)
Tb927_07_v5.1, 409583:411348
Raw counts
0
50
100
150
410000
410500
411000
Position

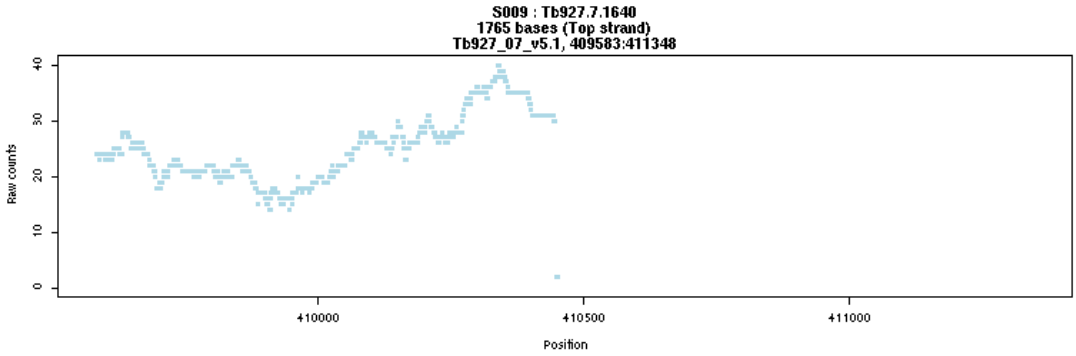
S009 : Tb927.7.1640
1765 bases (Top strand)
Tb927_07_v5.1, 409583:411348
Raw counts
0
10
20
30
40
410000
410500
411000
Position

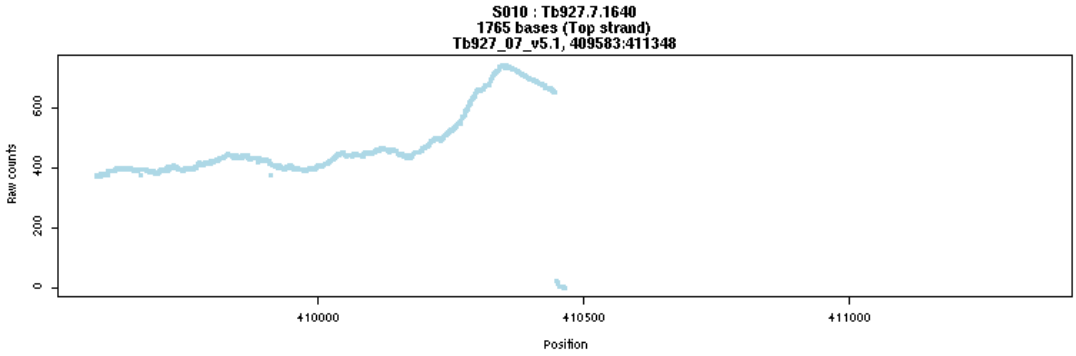
S010 : Tb927.7.1640
1765 bases (Top strand)
Tb927_07_v5.1, 409583:411348
Raw counts
0
200
400
600
410000
410500
411000
Position

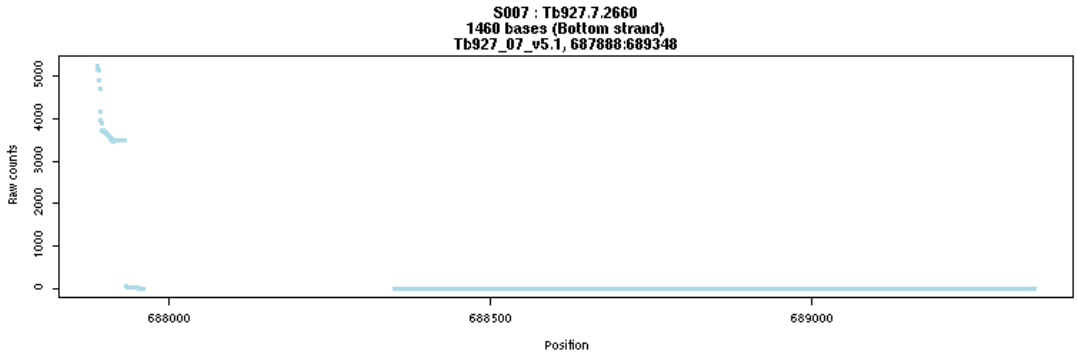
S007 : Tb927.7.2660
1460 bases (Bottom strand)
Tb927_07_v5.1, 687888:689348
Raw counts
0
1000
2000
3000
4000
5000
688000
688500
689000
Position

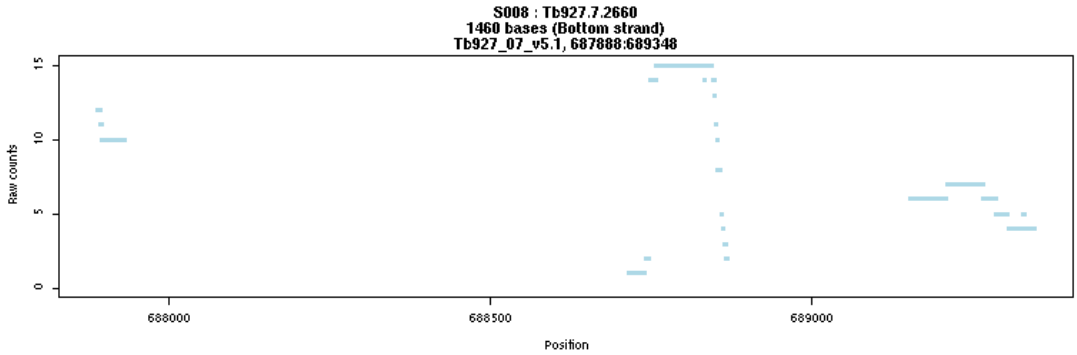
S008 : Tb927.7.2660
1460 bases (Bottom strand)
Tb927_07_v5.1, 687888:689348
Raw counts
0
5
10
15
688000
688500
689000
Position

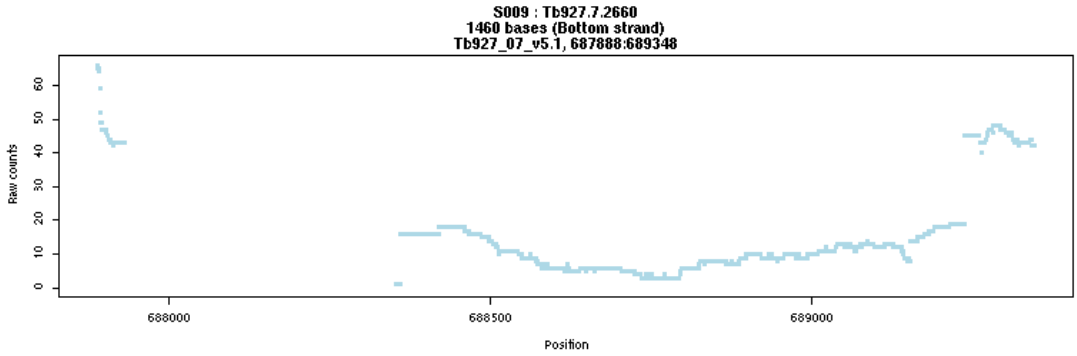
S009 : Tb927.7.2660
1460 bases (Bottom strand)
Tb927_07_v5.1, 687888:689348
Raw counts
0
10
20
30
40
50
60
688000
688500
689000
Position

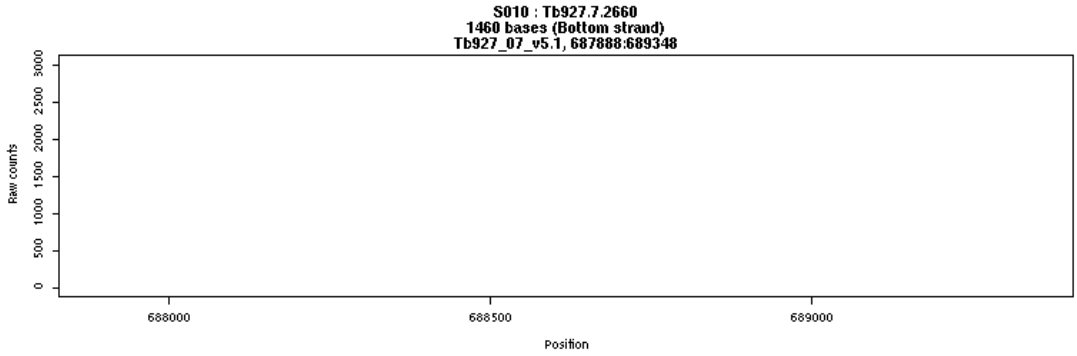
S010 : Tb927.7.2660
1460 bases (Bottom strand)
Tb927_07_v5.1, 687888:689348
Raw counts
0
500
1000
1500
2000
2500
3000
688000
688500
689000
Position

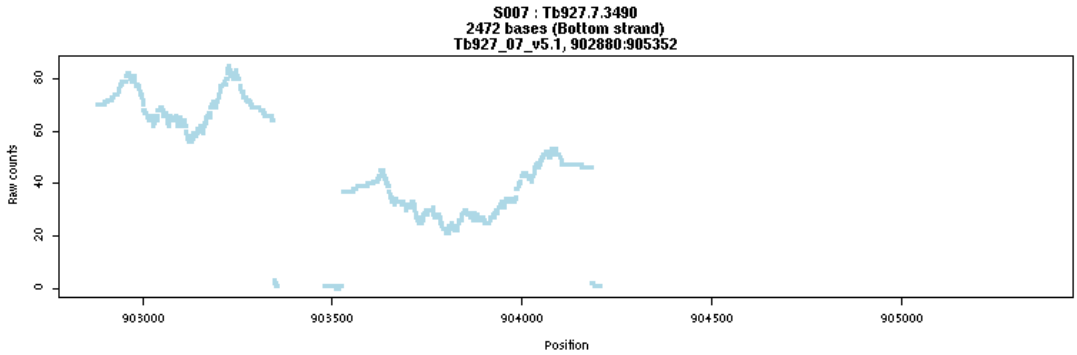
S007 : Tb927.7.3490
2472 bases (Bottom strand)
Tb927_07_v5.1, 902880:905352
Raw counts
0
20
40
60
80
903000
903500
904000
904500
905000
Position

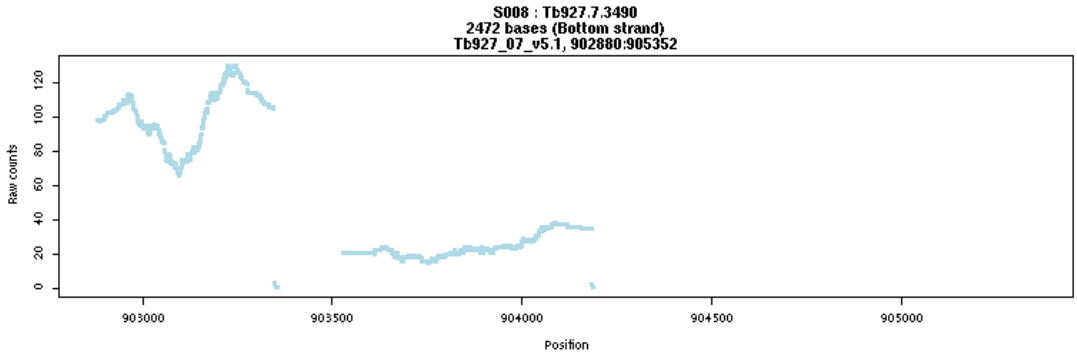
S008 : Tb927.7.3490
2472 bases (Bottom strand)
Tb927_07_v5.1, 902880:905352
Raw counts
0
20
40
60
80
100
120
903000
903500
904000
904500
905000
Position

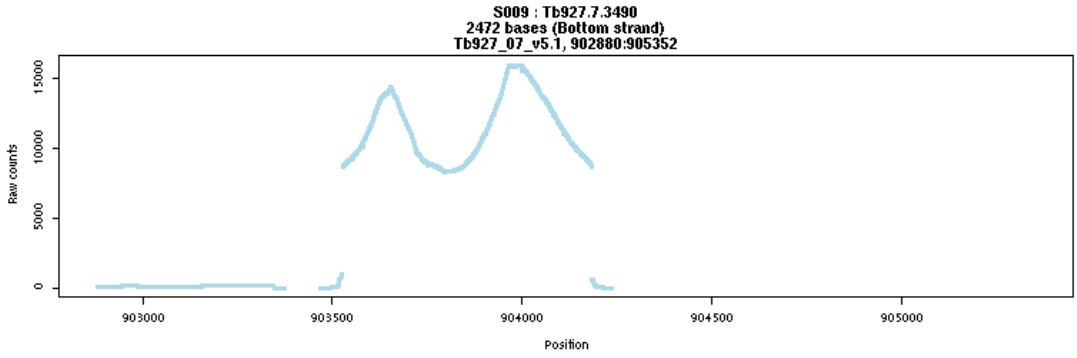
S009 : Tb927.7.3490
2472 bases (Bottom strand)
Tb927_07_v5.1, 902880:905352
Raw counts
0
5000
10000
15000
903000
903500
904000
904500
905000
Position

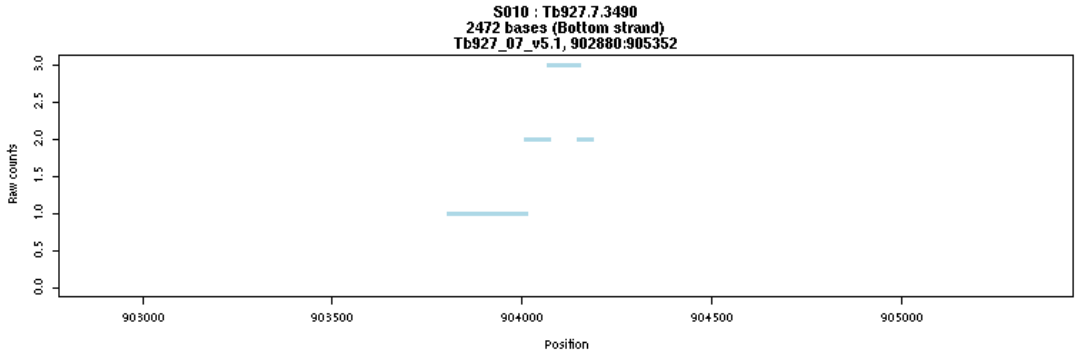
S010 : Tb927.7.3490
2472 bases (Bottom strand)
Tb927_07_v5.1, 902880:905352
Raw counts
0.0
0.5
1.0
1.5
2.0
2.5
3.0
903000
903500
904000
904500
905000
Position

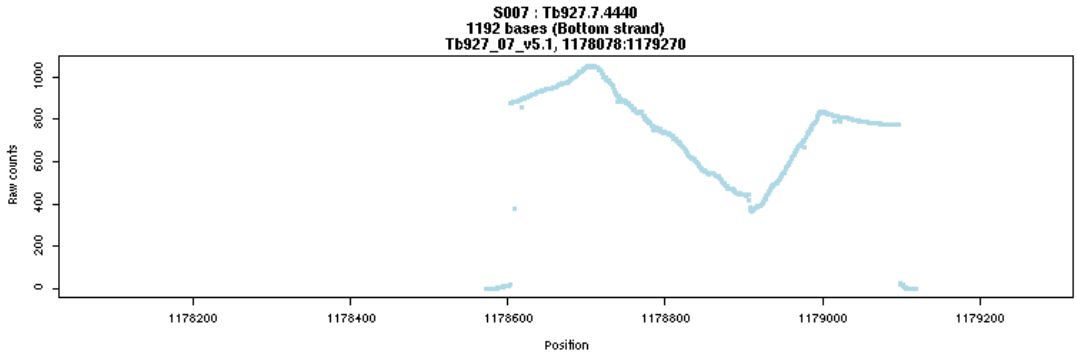
S007 : Tb927.7.4440
1192 bases (Bottom strand)
Tb927_07_v5.1, 1178078:1179270
Raw counts
0
200
400
600
800
1000
1178200
1178400
1178600
1178800
1179000
1179200
Position

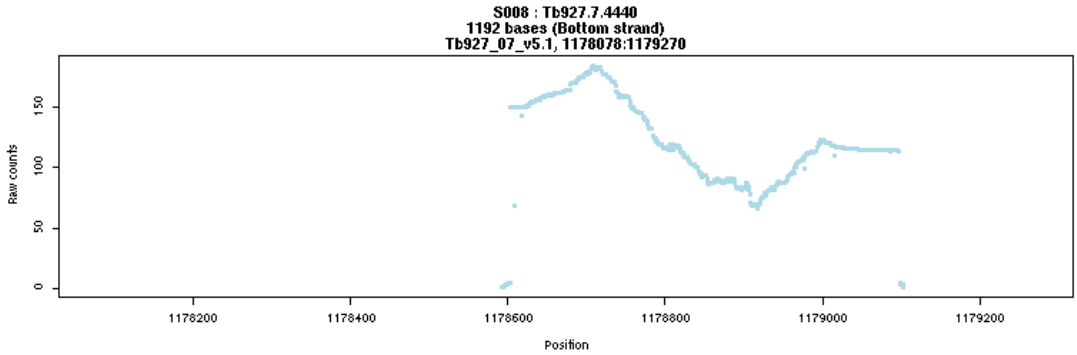
S008 : Tb927.7.4440
1192 bases (Bottom strand)
Tb927_07_v5.1, 1178078:1179270
Raw counts
0
50
100
150
1178200
1178400
1178600
1178800
1179000
1179200
Position

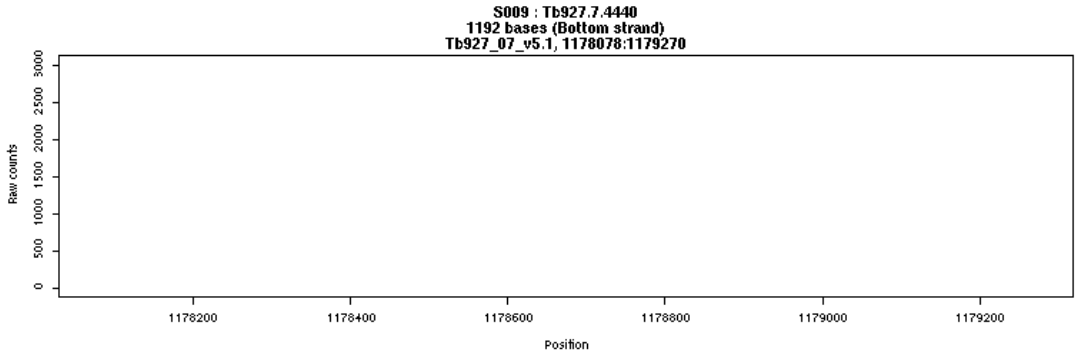
S009 : Tb927.7.4440
1192 bases (Bottom strand)
Tb927_07_v5.1, 1178078:1179270
Raw counts
0
500
1000
1500
2000
2500
3000
1178200
1178400
1178600
1178800
1179000
1179200
Position

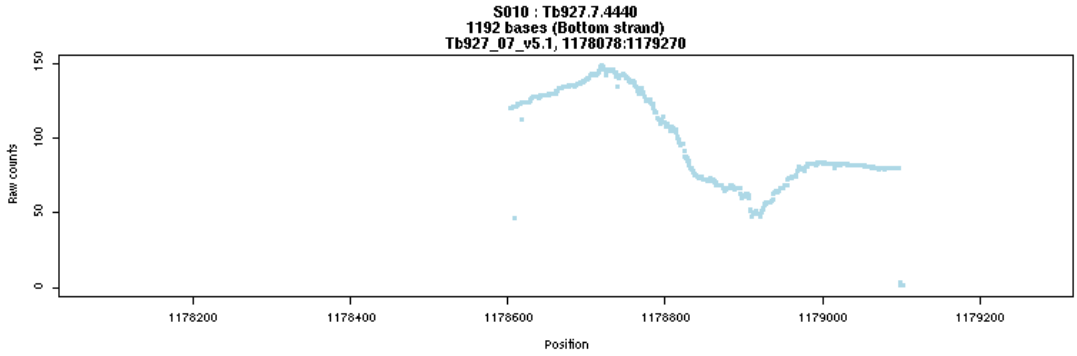
S010 : Tb927.7.4440
1192 bases (Bottom strand)
Tb927_07_v5.1, 1178078:1179270
Raw counts
0
50
100
150
1178200
1178400
1178600
1178800
1179000
1179200
Position

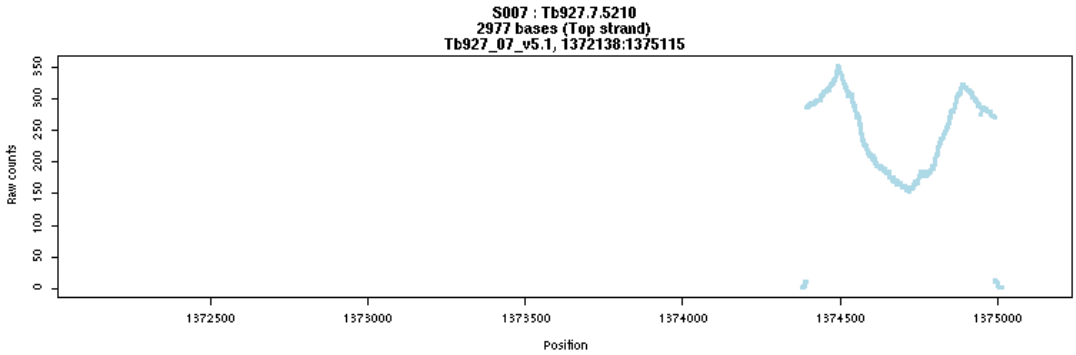
S007 : Tb927.7.5210
2977 bases (Top strand)
Tb927_07_v5.1, 1372138:1375115
Raw counts
0
50
100
150
200
250
300
350
1372500
1373000
1373500
1374000
1374500
1375000
Position

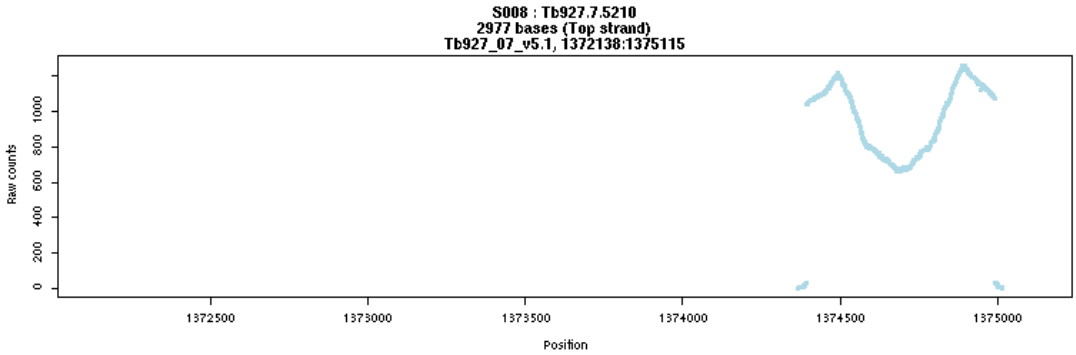
S008 : Tb927.7.5210
2977 bases (Top strand)
Tb927_07_v5.1, 1372138:1375115
Raw counts
0
200
400
600
800
1000
1372500
1373000
1373500
1374000
1374500
1375000
Position

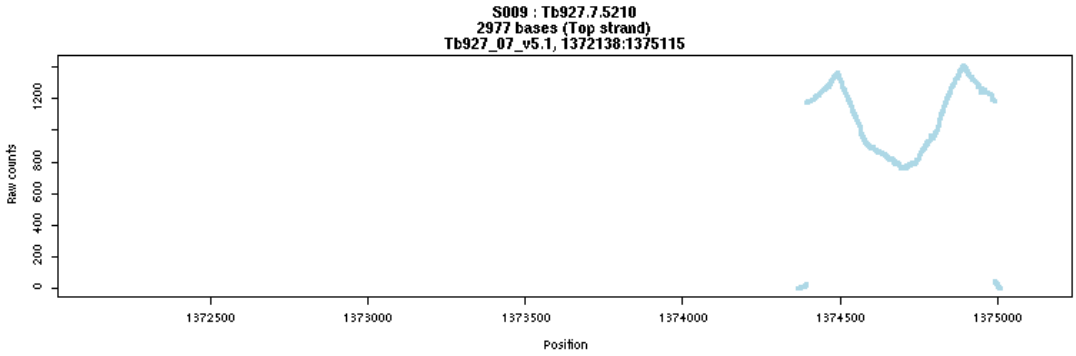
S009 : Tb927.7.5210
2977 bases (Top strand)
Tb927_07_v5.1, 1372138:1375115
Raw counts
0
200
400
600
800
1200
1372500
1373000
1373500
1374000
1374500
1375000
Position

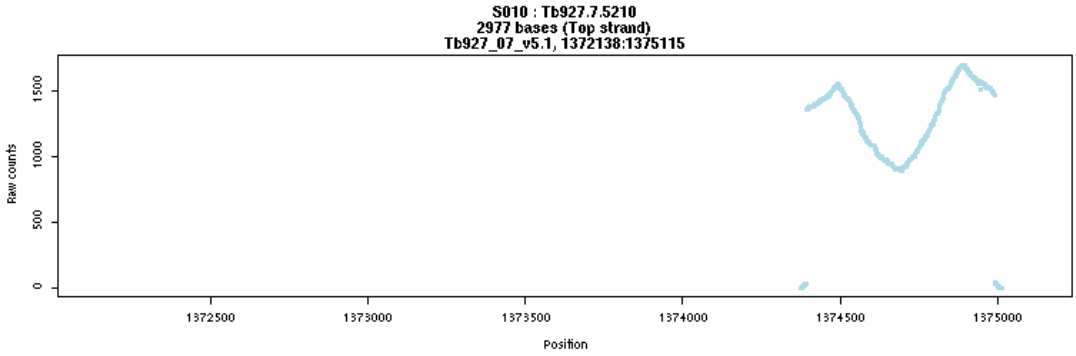
S010 : Tb927.7.5210
2977 bases (Top strand)
Tb927_07_v5.1, 1372138:1375115
Raw counts
0
500
1000
1500
1372500
1373000
1373500
1374000
1374500
1375000
Position

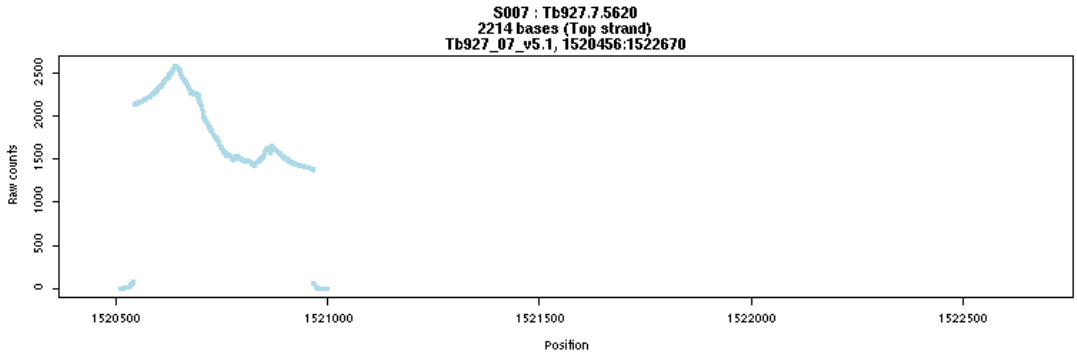
S007 : Tb927.7.5620
2214 bases (Top strand)
Tb927_07_v5.1, 1520456:1522670
Raw counts
0
500
1000
1500
2000
2500
1520500
1521000
1521500
1522000
1522500
Position

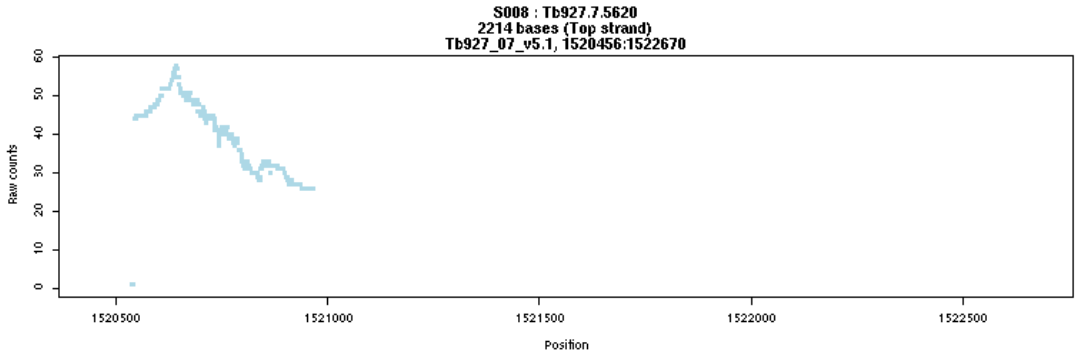
S008 : Tb927.7.5620
2214 bases (Top strand)
Tb927_07_v5.1, 1520456:1522670
Raw counts
0
10
20
30
40
50
60
1520500
1521000
1521500
1522000
1522500
Position

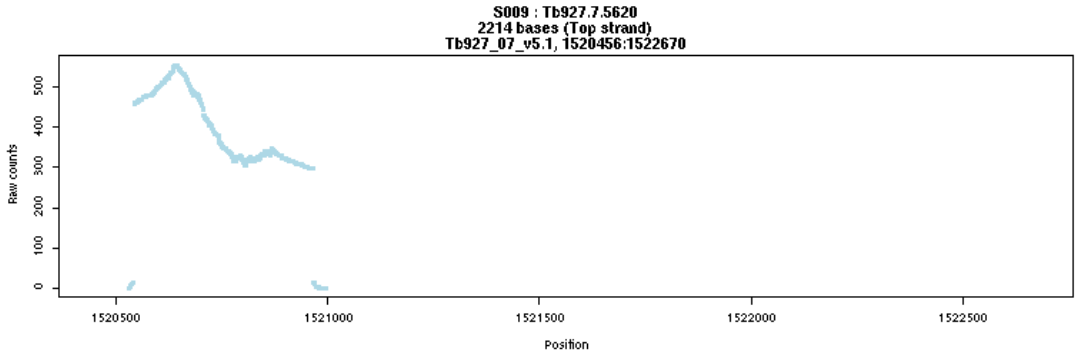
S009 : Tb927.7.5620
2214 bases (Top strand)
Tb927_07_v5.1, 1520456:1522670
Raw counts
0
100
200
300
400
500
1520500
1521000
1521500
1522000
1522500
Position

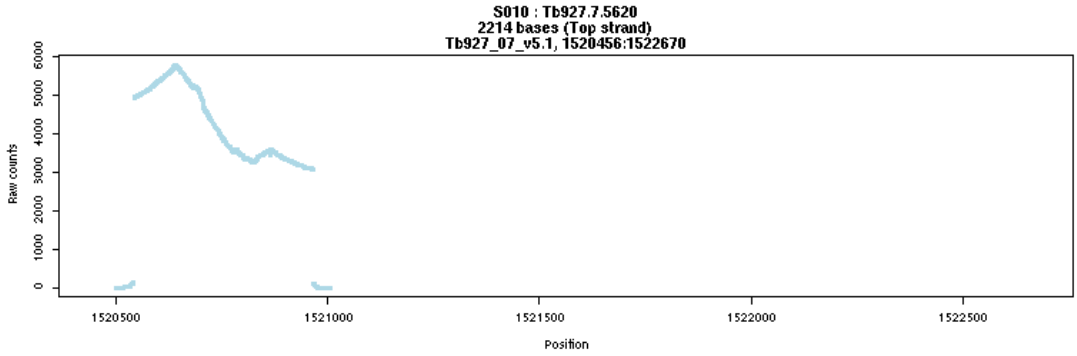
S010 : Tb927.7.5620
2214 bases (Top strand)
Tb927_07_v5.1, 1520456:1522670
Raw counts
0
1000
2000
3000
4000
5000
6000
1520500
1521000
1521500
1522000
1522500
Position

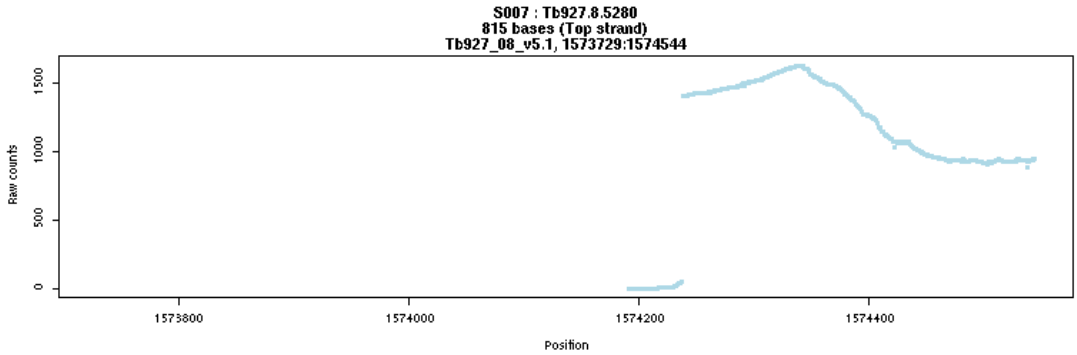
S007 : Tb927.8.5280
815 bases (Top strand)
Tb927_08_v5.1, 1573729:1574544
Raw counts
0
500
1000
1500
1573800
1574000
1574200
1574400
Position

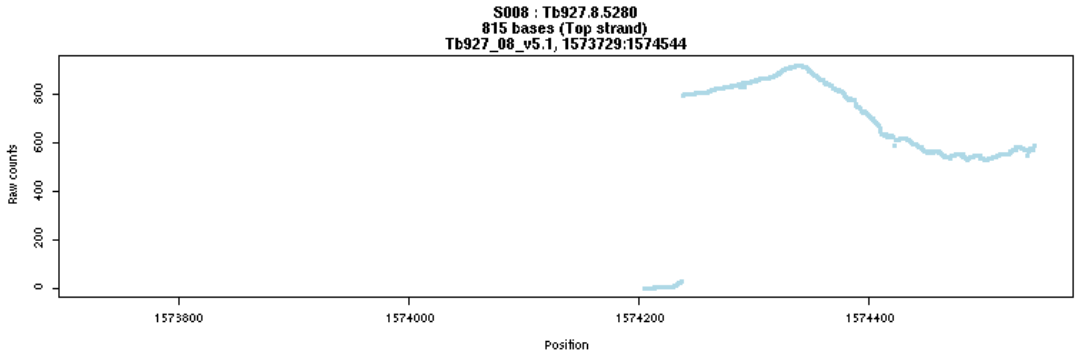
S008 : Tb927.8.5280
815 bases (Top strand)
Tb927_08_v5.1, 1573729:1574544
Raw counts
0
200
400
600
800
1573800
1574000
1574200
1574400
Position

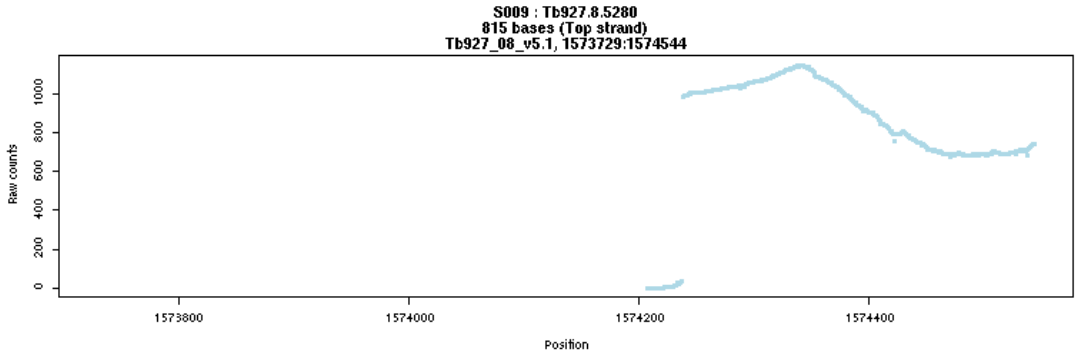
S009 : Tb927.8.5280
815 bases (Top strand)
Tb927_08_v5.1, 1573729:1574544
Raw counts
0
200
400
600
800
1000
1573800
1574000
1574200
1574400
Position

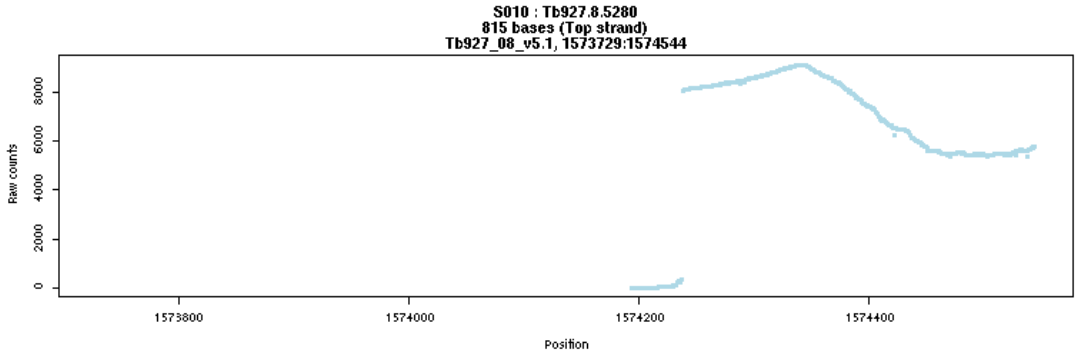
S010 : Tb927.8.5280
815 bases (Top strand)
Tb927_08_v5.1, 1573729:1574544
Raw counts
0
2000
4000
6000
8000
1573800
1574000
1574200
1574400
Position

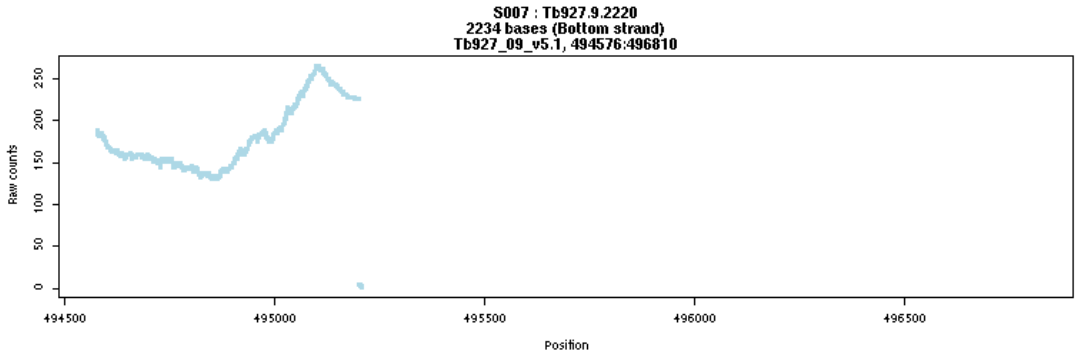
S007 : Tb927.9.2220
2234 bases (Bottom strand)
Tb927_09_v5.1, 494576:496810
Raw counts
0
50
100
150
200
250
494500
495000
495500
496000
496500
Position

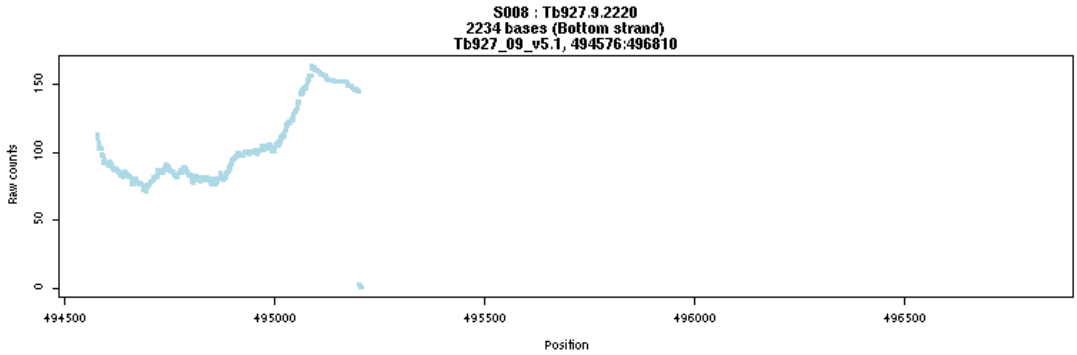
S008 : Tb927.9.2220
2234 bases (Bottom strand)
Tb927_09_v5.1, 494576:496810
Raw counts
0
50
100
150
494500
495000
495500
496000
496500
Position

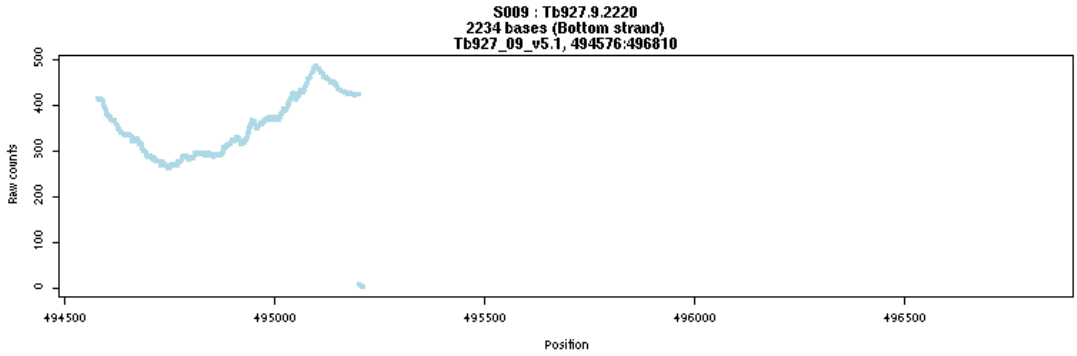
S009 : Tb927.9.2220
2234 bases (Bottom strand)
Tb927_09_v5.1, 494576:496810
Raw counts
0
100
200
300
400
500
494500
495000
495500
496000
496500
Position

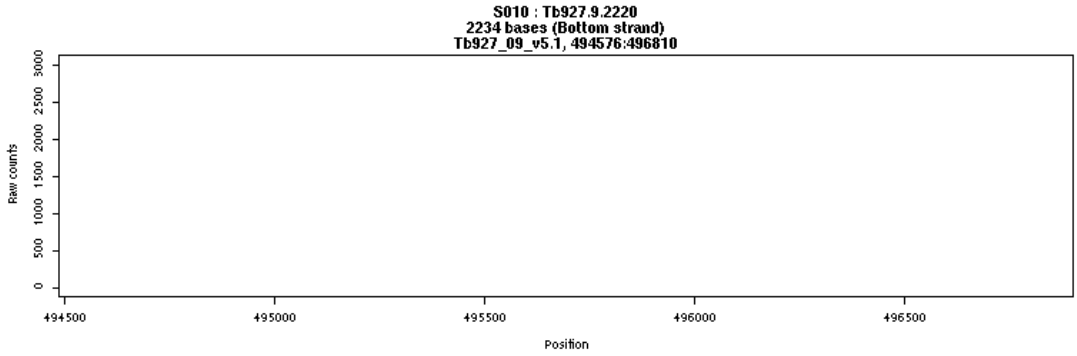
S010 : Tb927.9.2220
2234 bases (Bottom strand)
Tb927_09_v5.1, 494576:496810
Raw counts
0
500
1000
1500
2000
2500
3000
494500
495000
495500
496000
496500
Position

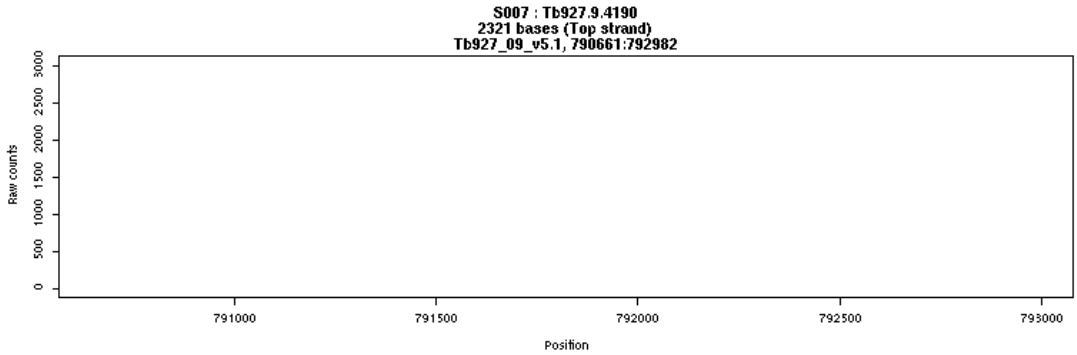
S007 : Tb927.9.4190
2321 bases (Top strand)
Tb927_09_v5.1, 790661:792982
Raw counts
0
500
1000
1500
2000
2500
3000
791000
791500
792000
792500
793000
Position

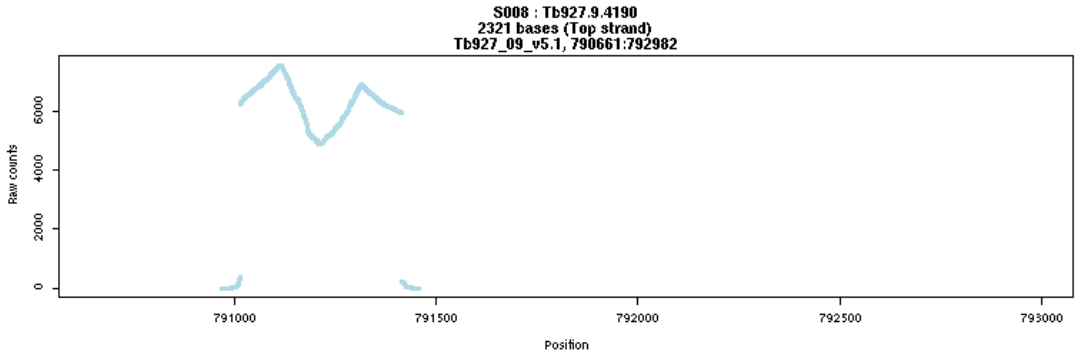
S008 : Tb927.9.4190
2321 bases (Top strand)
Tb927_09_v5.1, 790661:792982
Raw counts
0
2000
4000
6000
791000
791500
792000
792500
793000
Position

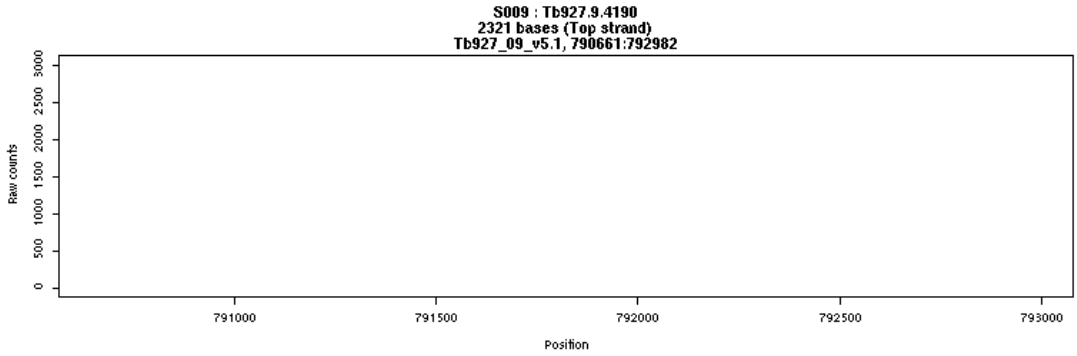
S009 : Tb927.9.4190
2321 bases (Top strand)
Tb927_09_v5.1, 790661:792982
Raw counts
0
500
1000
1500
2000
2500
3000
791000
791500
792000
792500
793000
Position

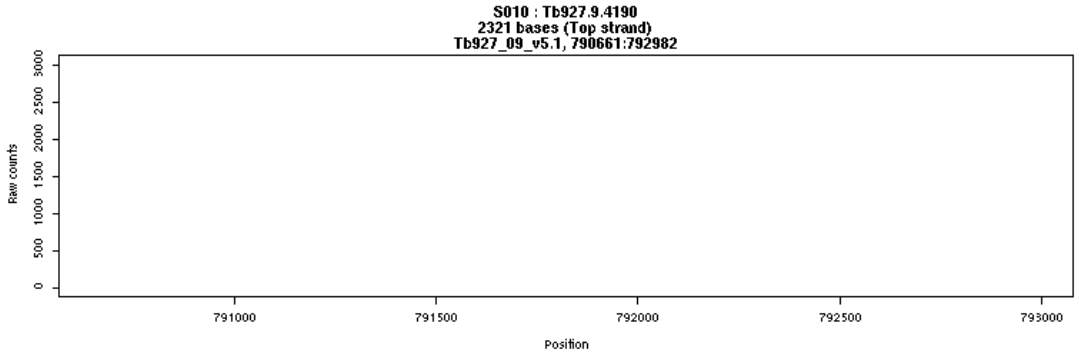
S010 : Tb927.9.4190
2321 bases (Top strand)
Tb927_09_v5.1, 790661:792982
Raw counts
0
500
1000
1500
2000
2500
3000
791000
791500
792000
792500
793000
Position

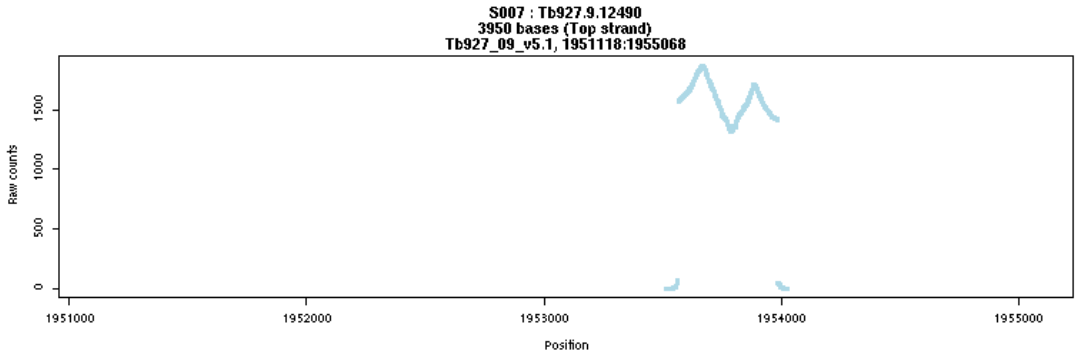
S007 : Tb927.9.12490
3950 bases (Top strand)
Tb927_09_v5.1, 1951118:1955068
Raw counts
0
500
1000
1500
1951000
1952000
1953000
1954000
1955000
Position

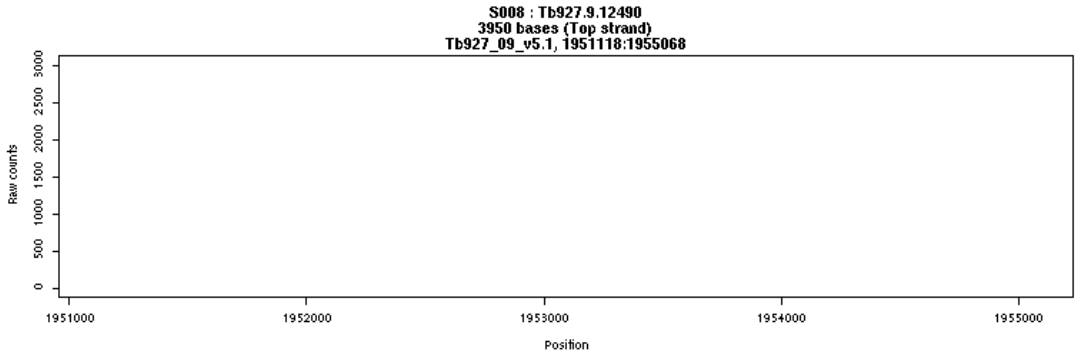
S008 : Tb927.9.12490
3950 bases (Top strand)
Tb927_09_v5.1, 1951118:1955068
Raw counts
0
500
1000
1500
2000
2500
3000
1951000
1952000
1953000
1954000
1955000
Position

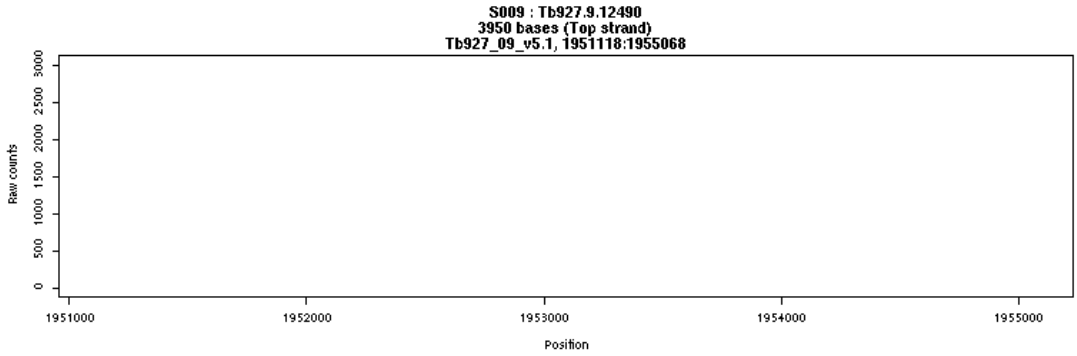
S009 : Tb927.9.12490
3950 bases (Top strand)
Tb927_09_v5.1, 1951118:1955068
Raw counts
0
500
1000
1500
2000
2500
3000
1951000
1952000
1953000
1954000
1955000
Position

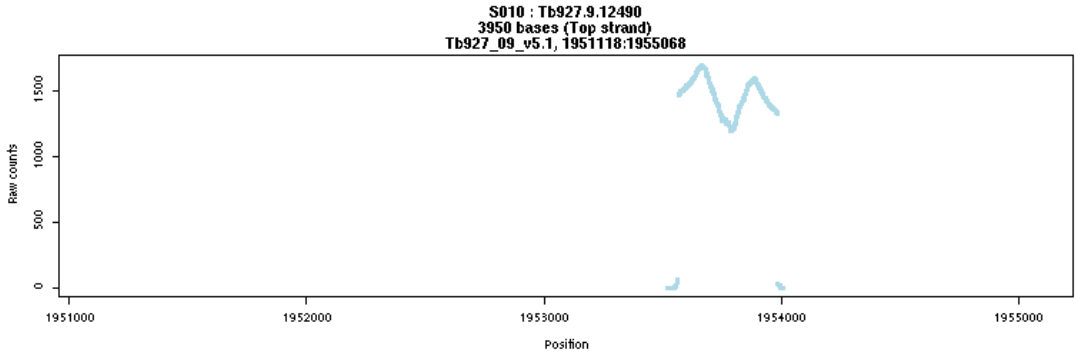
S010 : Tb927.9.12490
3950 bases (Top strand)
Tb927_09_v5.1, 1951118:1955068
Raw counts
0
500
1000
1500
1951000
1952000
1953000
1954000
1955000
Position

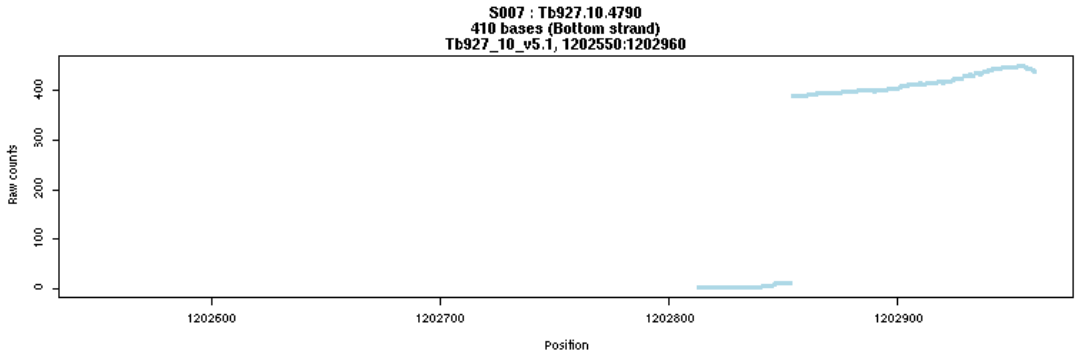
S007 : Tb927.10.4790
410 bases (Bottom strand)
Tb927_10_v5.1, 1202550:1202960
Raw counts
0
100
200
300
400
1202600
1202700
1202800
1202900
Position

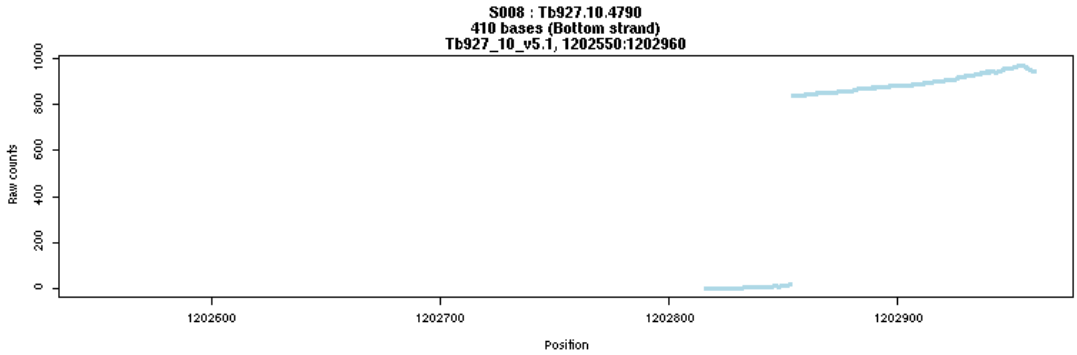
S008 : Tb927.10.4790
410 bases (Bottom strand)
Tb927_10_v5.1, 1202550:1202960
Raw counts
0
200
400
600
800
1000
1202600
1202700
1202800
1202900
Position

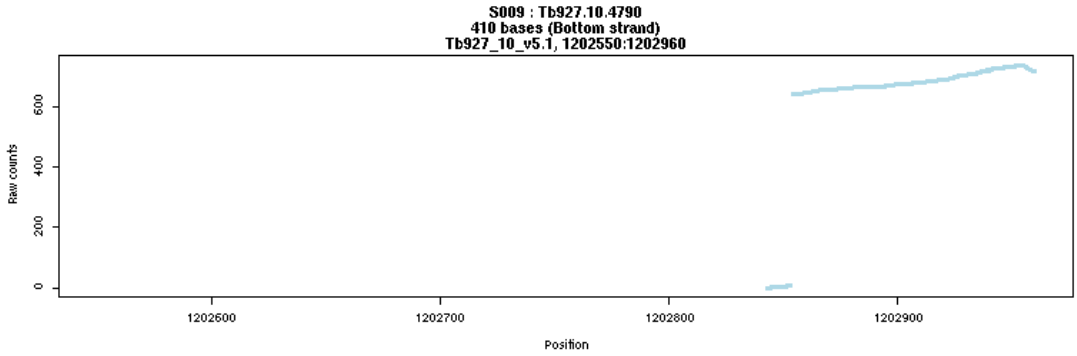
S009 : Tb927.10.4790
410 bases (Bottom strand)
Tb927_10_v5.1, 1202550:1202960
Raw counts
0
200
400
600
1202600
1202700
1202800
1202900
Position

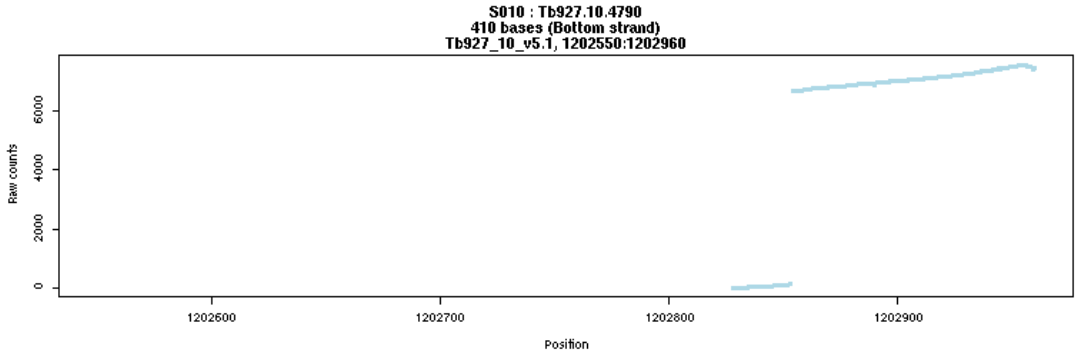
S010 : Tb927.10.4790
410 bases (Bottom strand)
Tb927_10_v5.1, 1202550:1202960
Raw counts
0
2000
4000
6000
1202600
1202700
1202800
1202900
Position

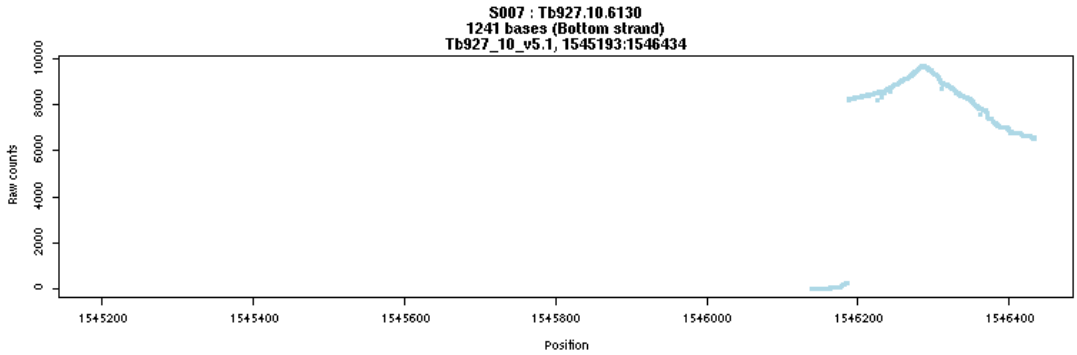
S007 : Tb927.10.6130
1241 bases (Bottom strand)
Tb927_10_v5.1, 1545193:1546434
Raw counts
0
2000
4000
6000
8000
10000
1545200
1545400
1545600
1545800
1546000
1546200
1546400
Position

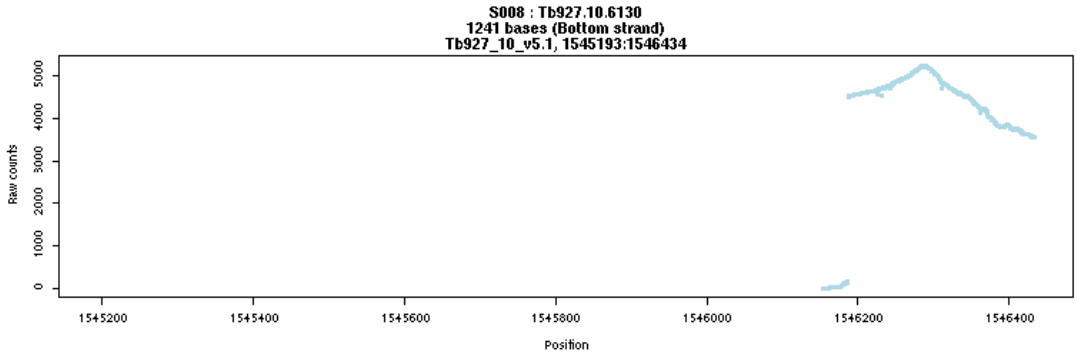
S008 : Tb927.10.6130
1241 bases (Bottom strand)
Tb927_10_v5.1, 1545193:1546434
Raw counts
0
1000
2000
3000
4000
5000
1545200
1545400
1545600
1545800
1546000
1546200
1546400
Position

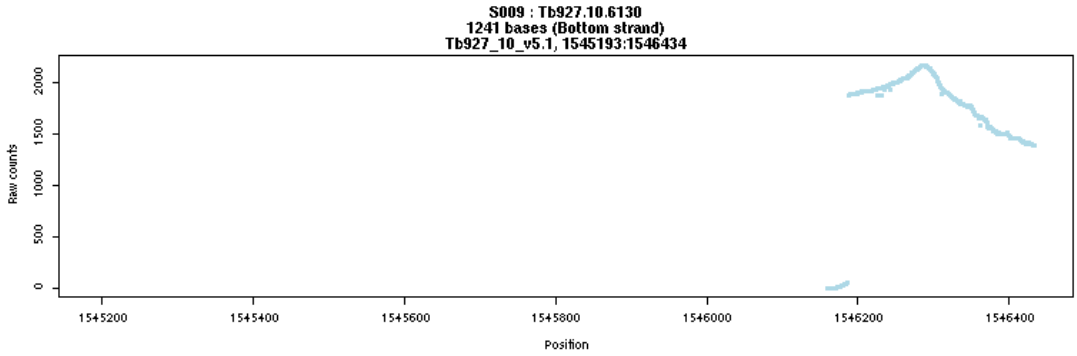
S009 : Tb927.10.6130
1241 bases (Bottom strand)
Tb927_10_v5.1, 1545193:1546434
Raw counts
0
500
1000
1500
2000
1545200
1545400
1545600
1545800
1546000
1546200
1546400
Position

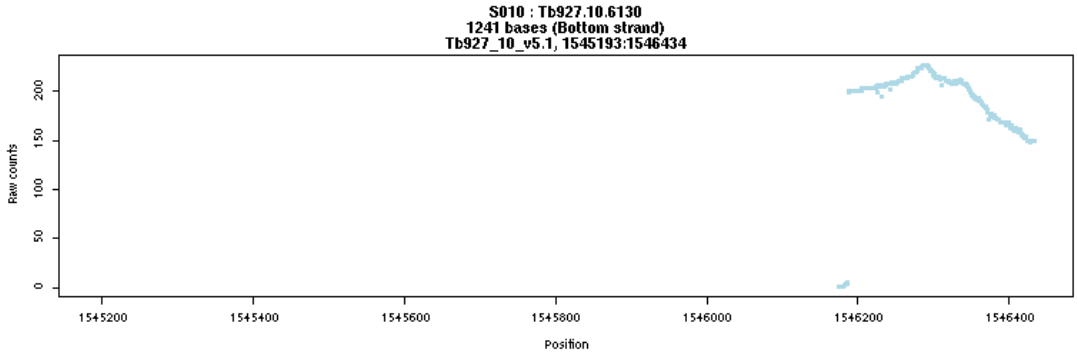
S010 : Tb927.10.6130
1241 bases (Bottom strand)
Tb927_10_v5.1, 1545193:1546434
Raw counts
0
50
100
150
200
1545200
1545400
1545600
1545800
1546000
1546200
1546400
Position

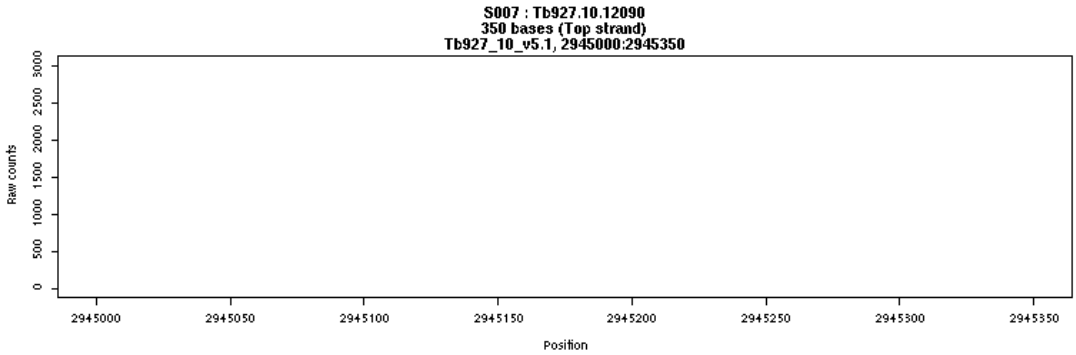
S007 : Tb927.10.12090
350 bases (Top strand)
Tb927_10_v5.1, 2945000:2945350
Raw counts
0
500
1000
1500
2000
2500
3000
2945000
2945050
2945100
2945150
2945200
2945250
2945300
2945350
Position

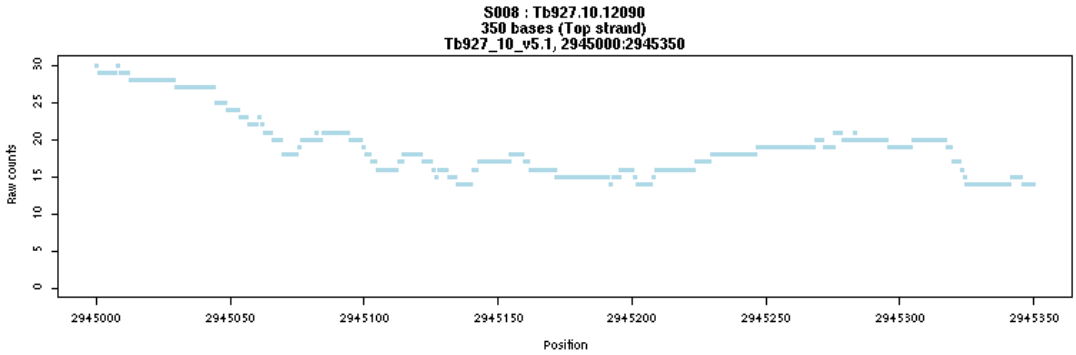
S008 : Tb927.10.12090
350 bases (Top strand)
Tb927_10_v5.1, 2945000:2945350
Raw counts
0
5
10
15
20
25
30
2945000
2945050
2945100
2945150
2945200
2945250
2945300
2945350
Position

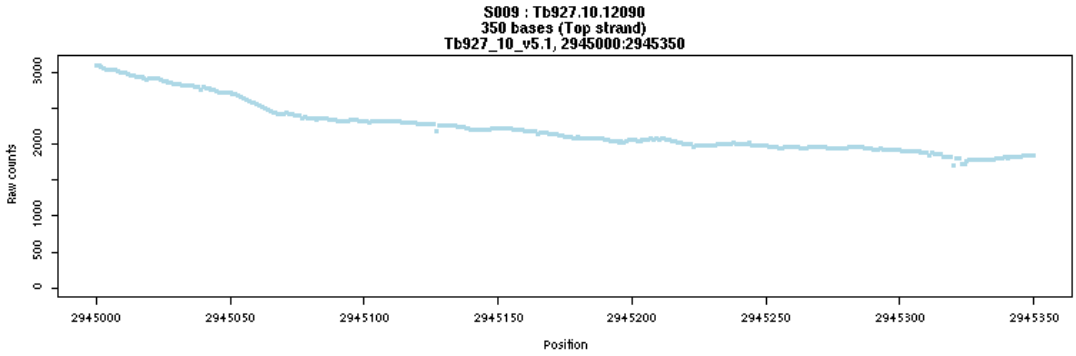
S009 : Tb927.10.12090
350 bases (Top strand)
Tb927_10_v5.1, 2945000:2945350
Raw counts
0
500
1000
2000
3000
2945000
2945050
2945100
2945150
2945200
2945250
2945300
2945350
Position

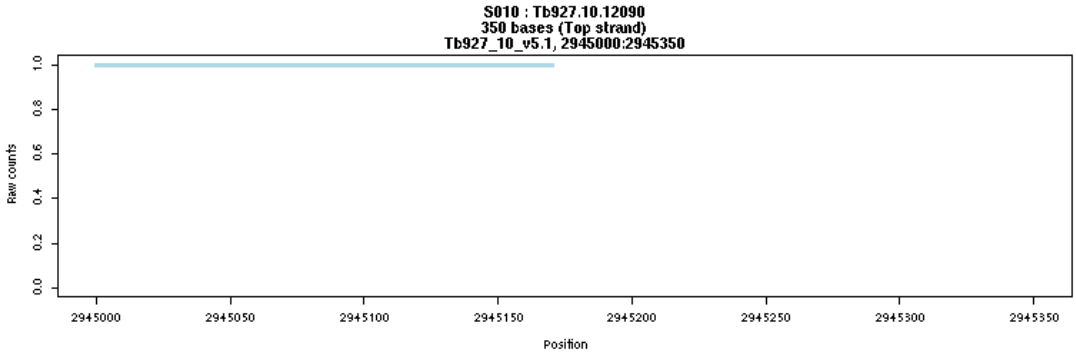
S010 : Tb927.10.12090
350 bases (Top strand)
Tb927_10_v5.1, 2945000:2945350
Raw counts
0.0
0.2
0.4
0.6
0.8
1.0
2945000
2945050
2945100
2945150
2945200
2945250
2945300
2945350
Position

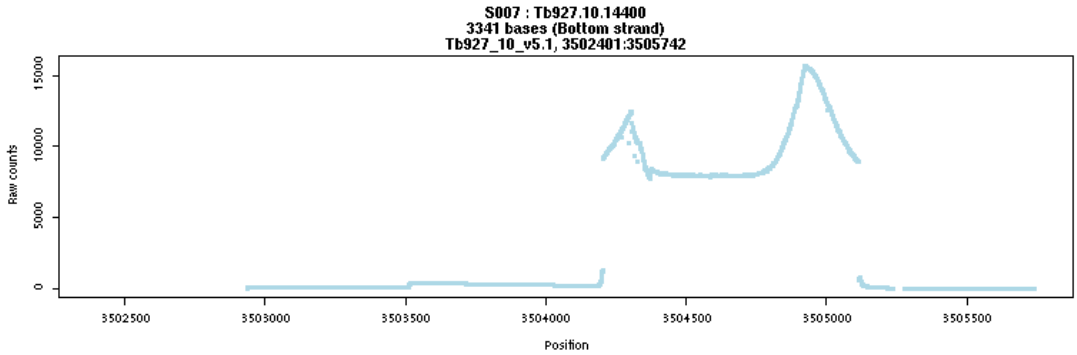
S007 : Tb927.10.14400
3341 bases (Bottom strand)
Tb927_10_v5.1, 3502401:3505742
Raw counts
0
5000
10000
15000
3502500
3503000
3503500
3504000
3504500
3505000
3505500
Position

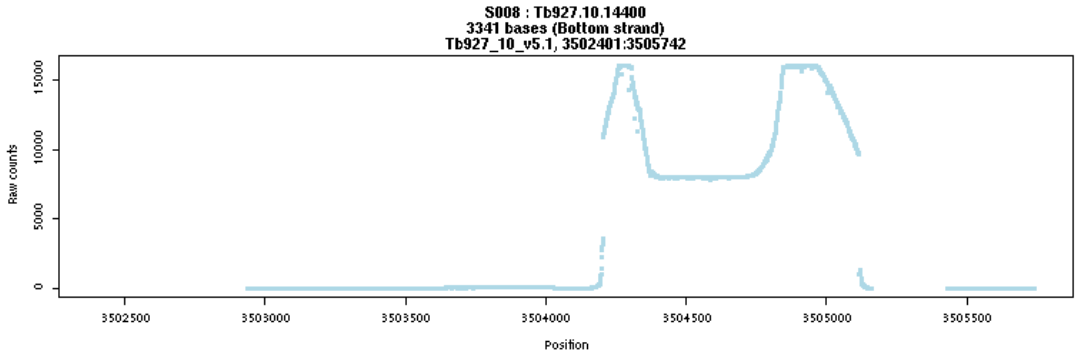
S008 : Tb927.10.14400
3341 bases (Bottom strand)
Tb927_10_v5.1, 3502401:3505742
Raw counts
0
5000
10000
15000
3502500
3503000
3503500
3504000
3504500
3505000
3505500
Position

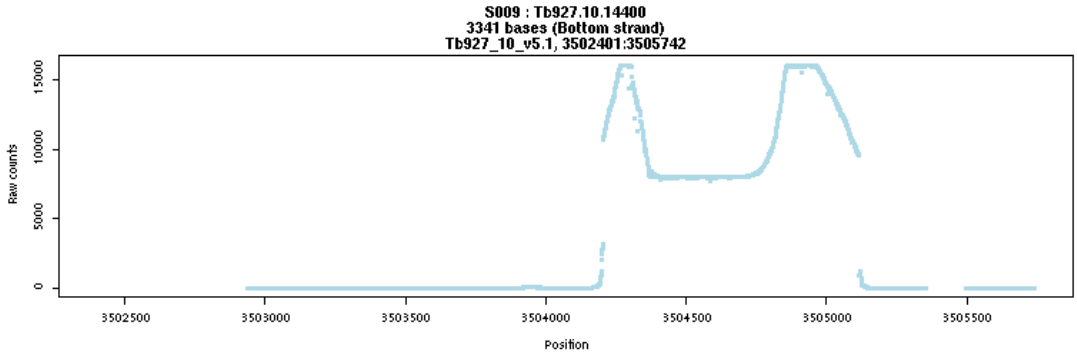
S009 : Tb927.10.14400
3341 bases (Bottom strand)
Tb927_10_v5.1, 3502401:3505742
Raw counts
0
5000
10000
15000
3502500
3503000
3503500
3504000
3504500
3505000
3505500
Position

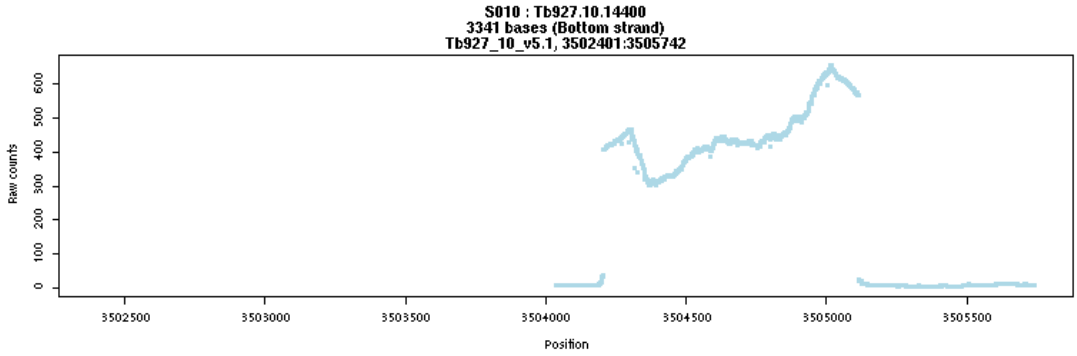
S010 : Tb927.10.14400
3341 bases (Bottom strand)
Tb927_10_v5.1, 3502401:3505742
Raw counts
0
100
200
300
400
500
600
3502500
3503000
3503500
3504000
3504500
3505000
3505500
Position

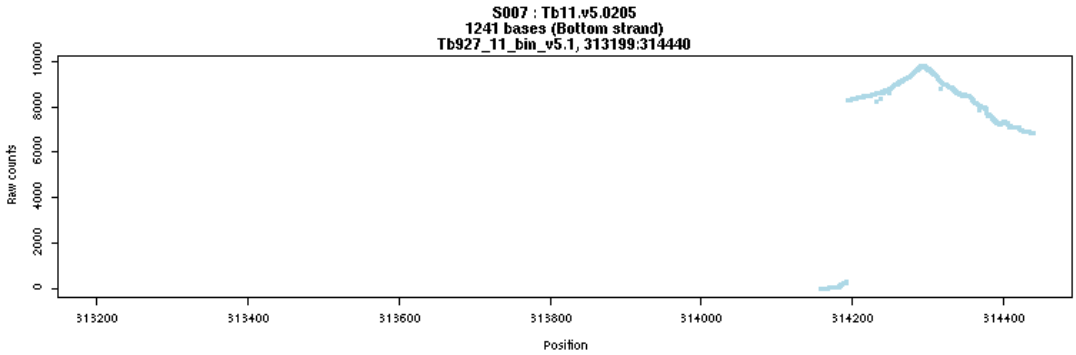
S007 : Tb11.v5.0205
1241 bases (Bottom strand)
Tb927_11_bin_v5.1, 313199:314440
Raw counts
0
2000
4000
6000
8000
10000
313200
313400
313600
313800
314000
314200
314400
Position

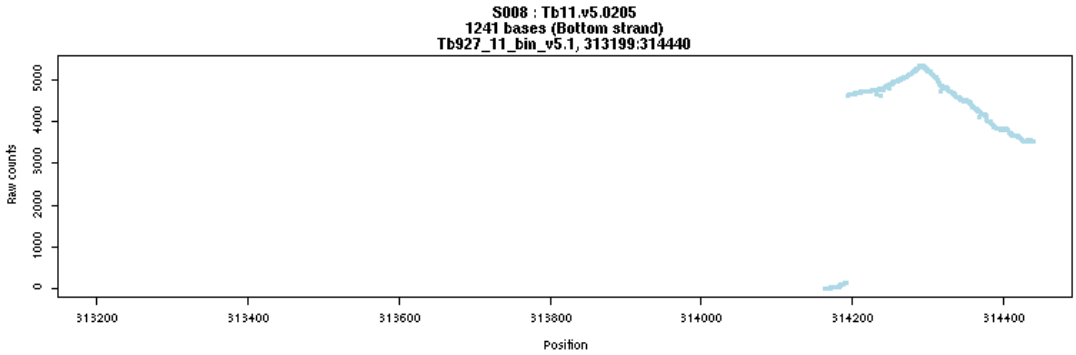
S008 : Tb11.v5.0205
1241 bases (Bottom strand)
Tb927_11_bin_v5.1, 313199:314440
Raw counts
0
1000
2000
3000
4000
5000
313200
313400
313600
313800
314000
314200
314400
Position

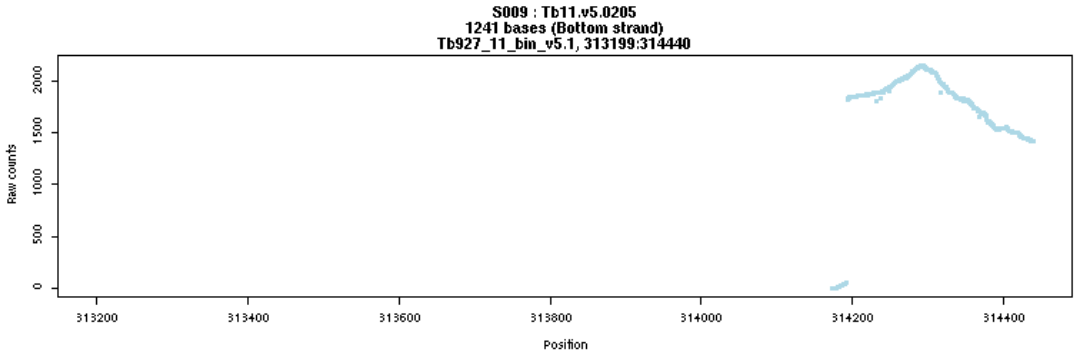
S009 : Tb11.v5.0205
1241 bases (Bottom strand)
Tb927_11_bin_v5.1, 313199:314440
Raw counts
0
500
1000
1500
2000
313200
313400
313600
313800
314000
314200
314400
Position

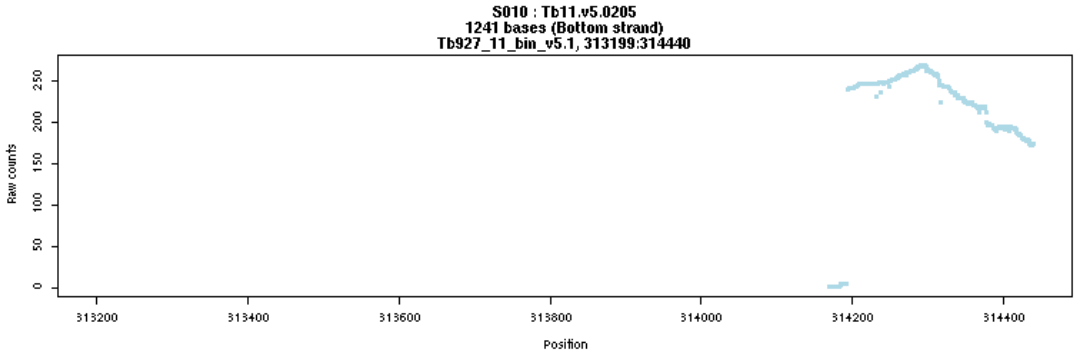
S010 : Tb11.v5.0205
1241 bases (Bottom strand)
Tb927_11_bin_v5.1, 313199:314440
Raw counts
0
50
100
150
200
250
313200
313400
313600
313800
314000
314200
314400
Position

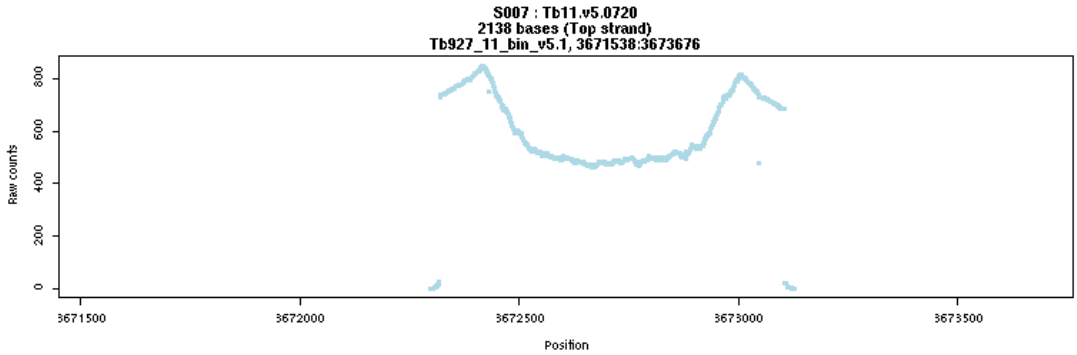
S007 : Tb11.v5.0720
2138 bases (Top strand)
Tb927_11_bin_v5.1, 3671538:3673676
Raw counts
0
200
400
600
800
3671500
3672000
3672500
3673000
3673500
Position

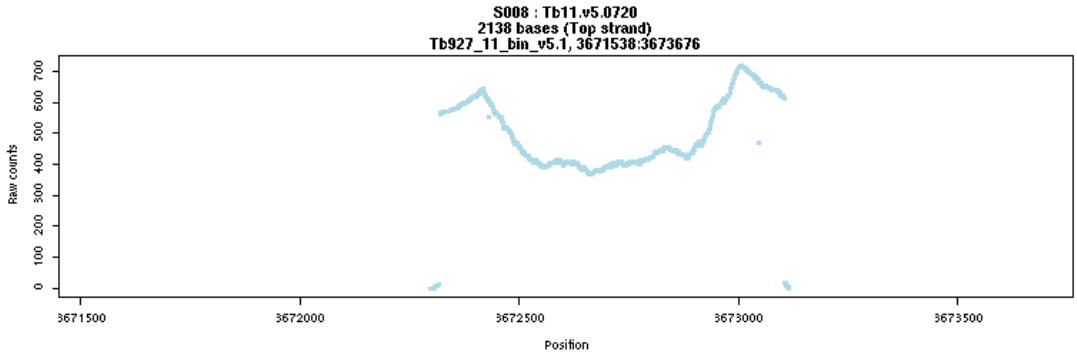
S008 : Tb11.v5.0720
2138 bases (Top strand)
Tb927_11_bin_v5.1, 3671538:3673676
Raw counts
0
100
200
300
400
500
600
700
3671500
3672000
3672500
3673000
3673500
Position

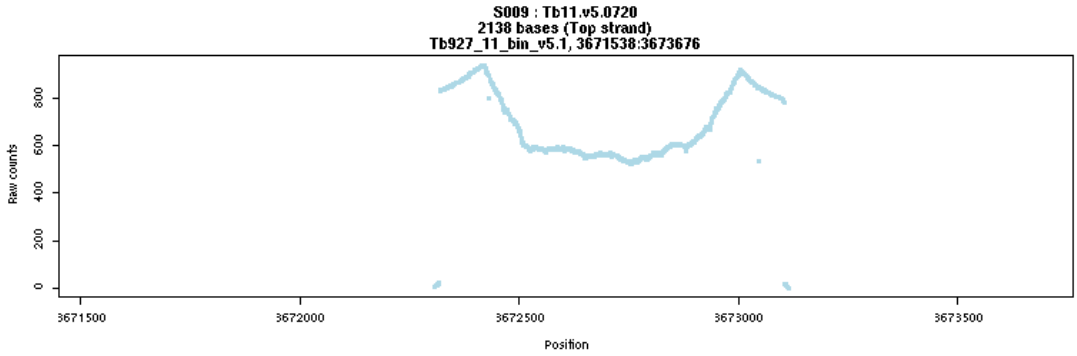
S009 : Tb11.v5.0720
2138 bases (Top strand)
Tb927_11_bin_v5.1, 3671538:3673676
Raw counts
0
200
400
600
800
3671500
3672000
3672500
3673000
3673500
Position

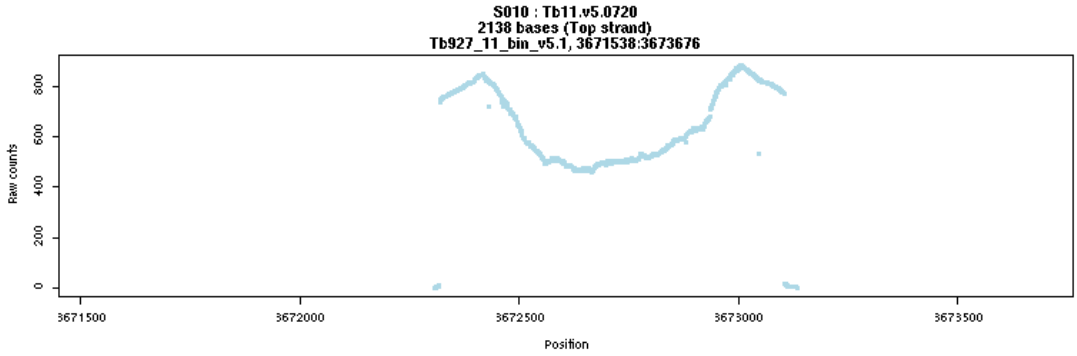
S010 : Tb11.v5.0720
2138 bases (Top strand)
Tb927_11_bin_v5.1, 3671538:3673676
Raw counts
0
200
400
600
800
3671500
3672000
3672500
3673000
3673500
Position

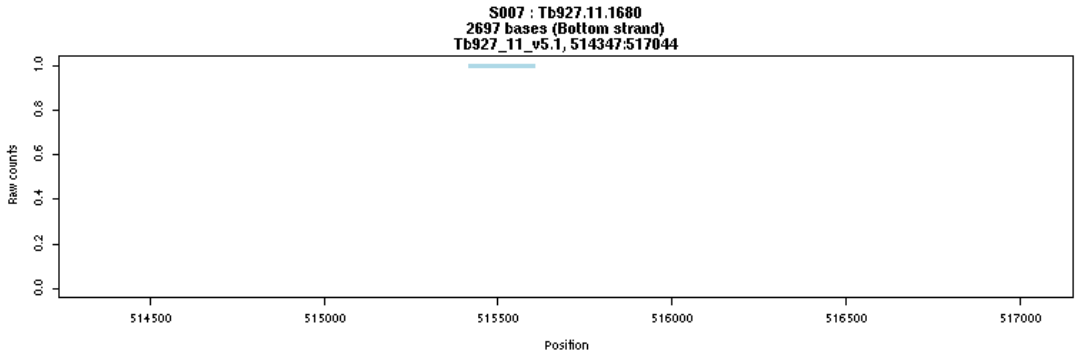
S007 : Tb927.11.1680
2697 bases (Bottom strand)
Tb927_11_v5.1, 514347:517044
Raw counts
0.0
0.2
0.4
0.6
0.8
1.0
514500
515000
515500
516000
516500
517000
Position

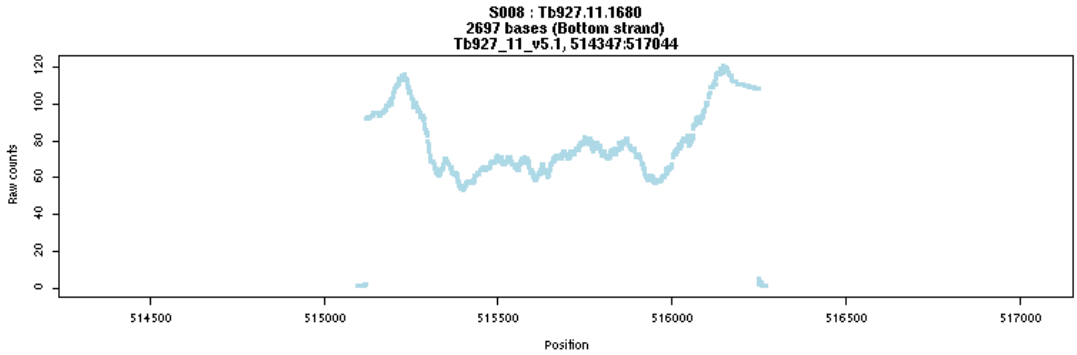
S008 : Tb927.11.1680
2697 bases (Bottom strand)
Tb927_11_v5.1, 514347:517044
Raw counts
0
20
40
60
80
100
120
514500
515000
515500
516000
516500
517000
Position

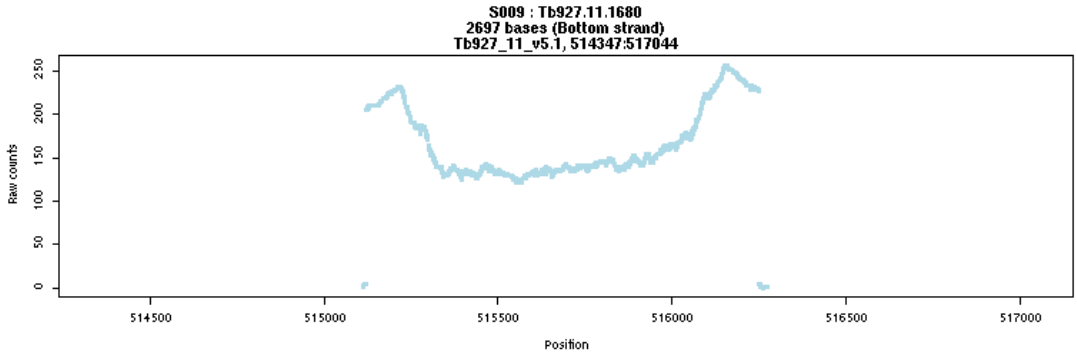
S009 : Tb927.11.1680
2697 bases (Bottom strand)
Tb927_11_v5.1, 514347:517044
Raw counts
0
50
100
150
200
250
514500
515000
515500
516000
516500
517000
Position

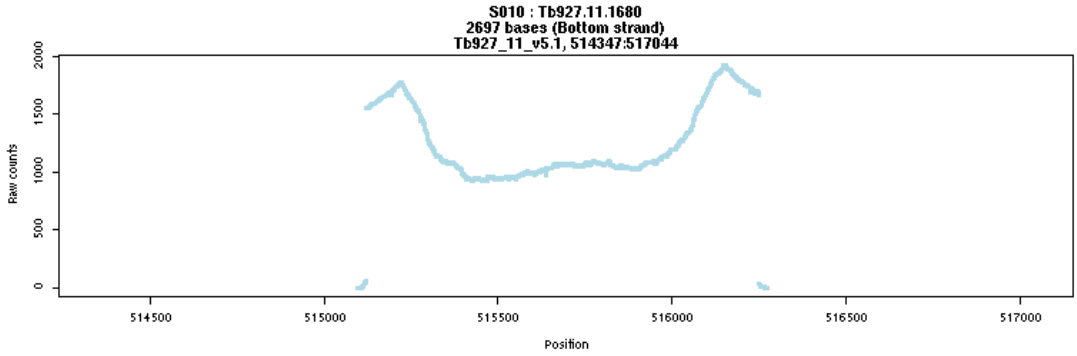
S010 : Tb927.11.1680
2697 bases (Bottom strand)
Tb927_11_v5.1, 514347:517044
Raw counts
0
500
1000
1500
2000
514500
515000
515500
516000
516500
517000
Position

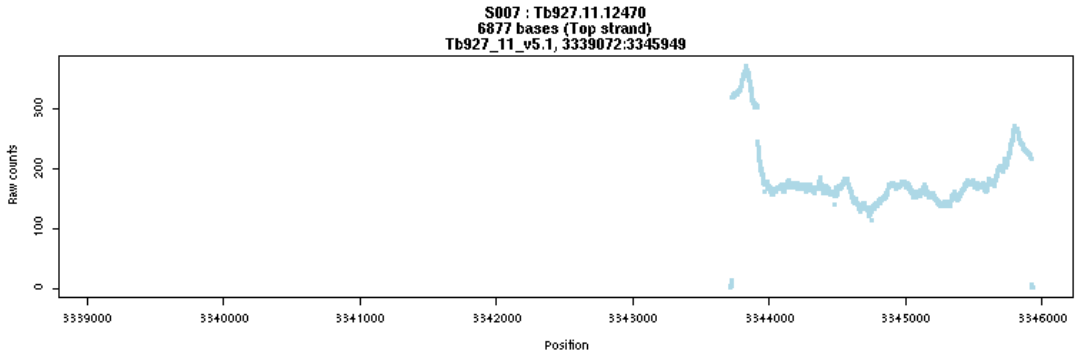
S007 : Tb927.11.12470
6877 bases (Top strand)
Tb927_11_v5.1, 3339072:3345949
Raw counts
0
100
200
300
3339000
3340000
3341000
3342000
3343000
3344000
3345000
3346000
Position

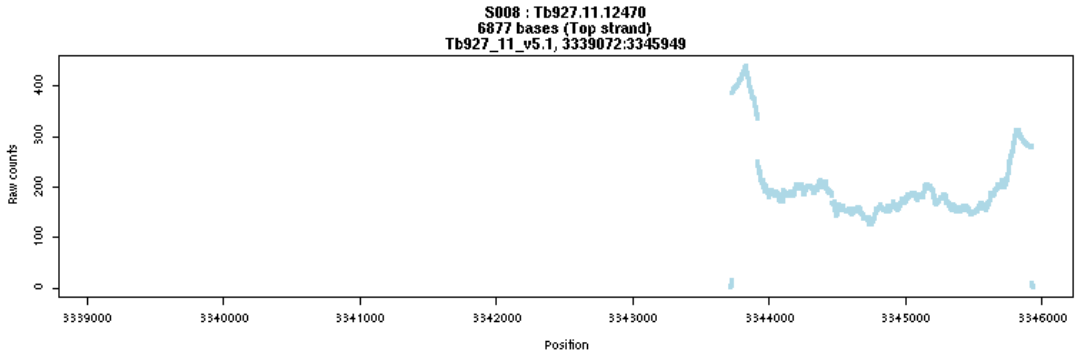
S008 : Tb927.11.12470
6877 bases (Top strand)
Tb927_11_v5.1, 3339072:3345949
Raw counts
0
100
200
300
400
3339000
3340000
3341000
3342000
3343000
3344000
3345000
3346000
Position

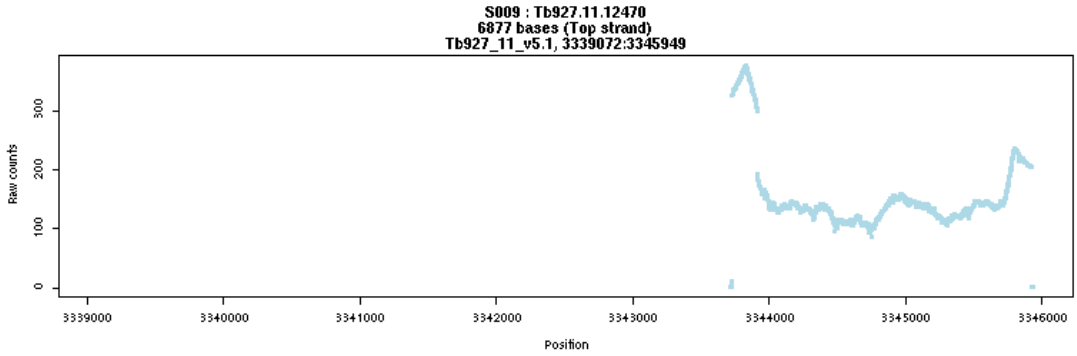
S009 : Tb927.11.12470
6877 bases (Top strand)
Tb927_11_v5.1, 3339072:3345949
Raw counts
0
100
200
300
3339000
3340000
3341000
3342000
3343000
3344000
3345000
3346000
Position

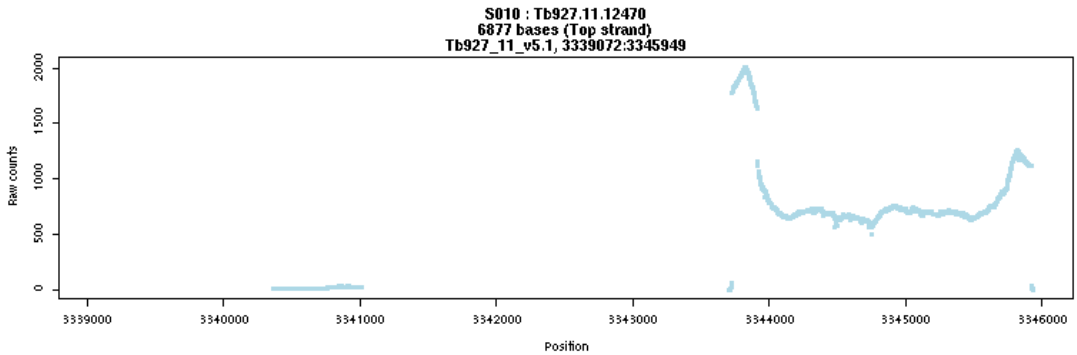
S010 : Tb927.11.12470
6877 bases (Top strand)
Tb927_11_v5.1, 3339072:3345949
Raw counts
0
500
1000
1500
2000
3339000
3340000
3341000
3342000
3343000
3344000
3345000
3346000
Position

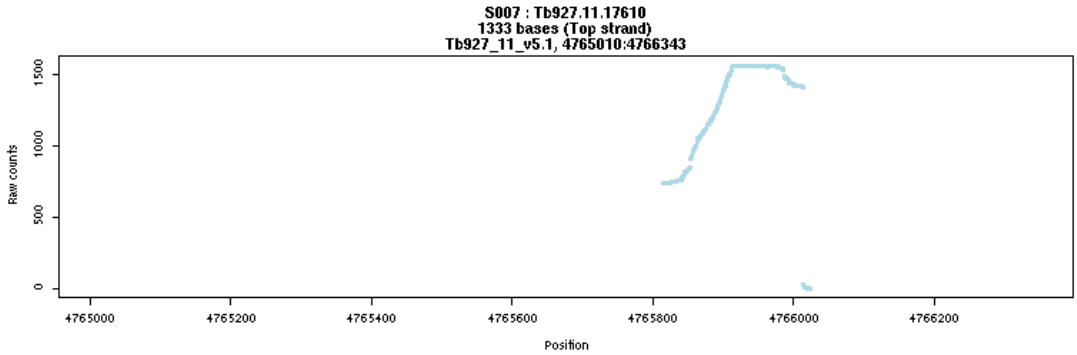
S007 : Tb927.11.17610
1333 bases (Top strand)
Tb927_11_v5.1, 4765010:4766343
Raw counts
0
500
1000
1500
4765000
4765200
4765400
4765600
4765800
4766000
4766200
Position

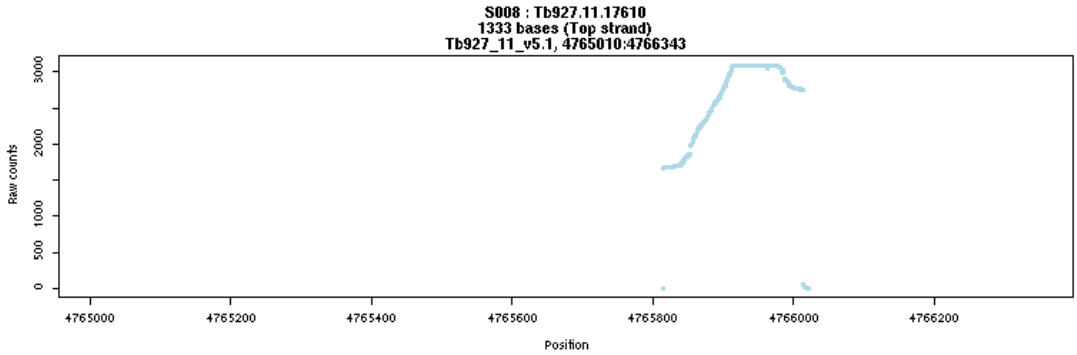
S008 : Tb927.11.17610
1333 bases (Top strand)
Tb927_11_v5.1, 4765010:4766343
Raw counts
0
500
1000
2000
3000
4765000
4765200
4765400
4765600
4765800
4766000
4766200
Position

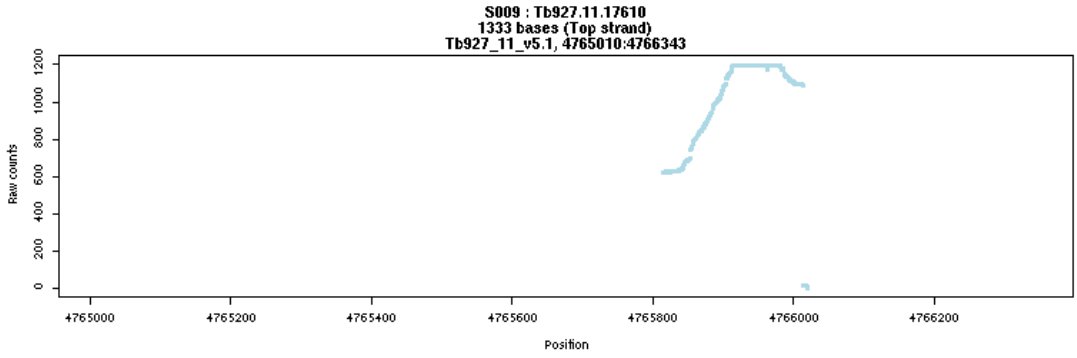
S009 : Tb927.11.17610
1333 bases (Top strand)
Tb927_11_v5.1, 4765010:4766343
Raw counts
0
200
400
600
800
1000
1200
4765000
4765200
4765400
4765600
4765800
4766000
4766200
Position

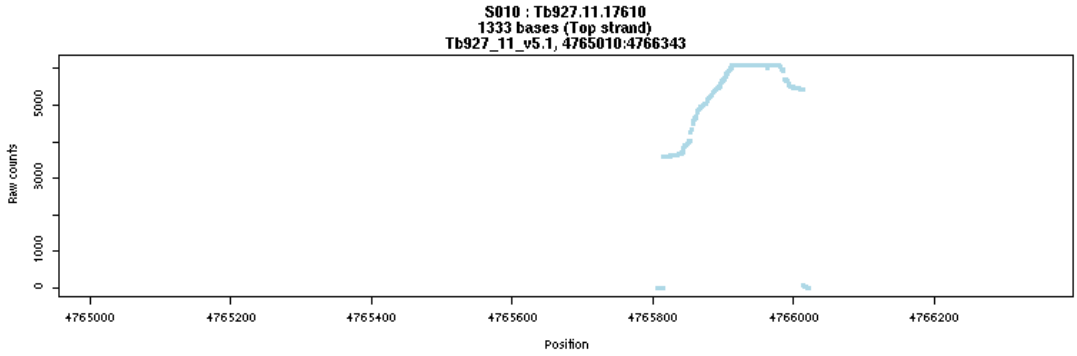
S010 : Tb927.11.17610
1333 bases (Top strand)
Tb927_11_v5.1, 4765010:4766343
Raw counts
0
1000
3000
5000
4765000
4765200
4765400
4765600
4765800
4766000
4766200
Position

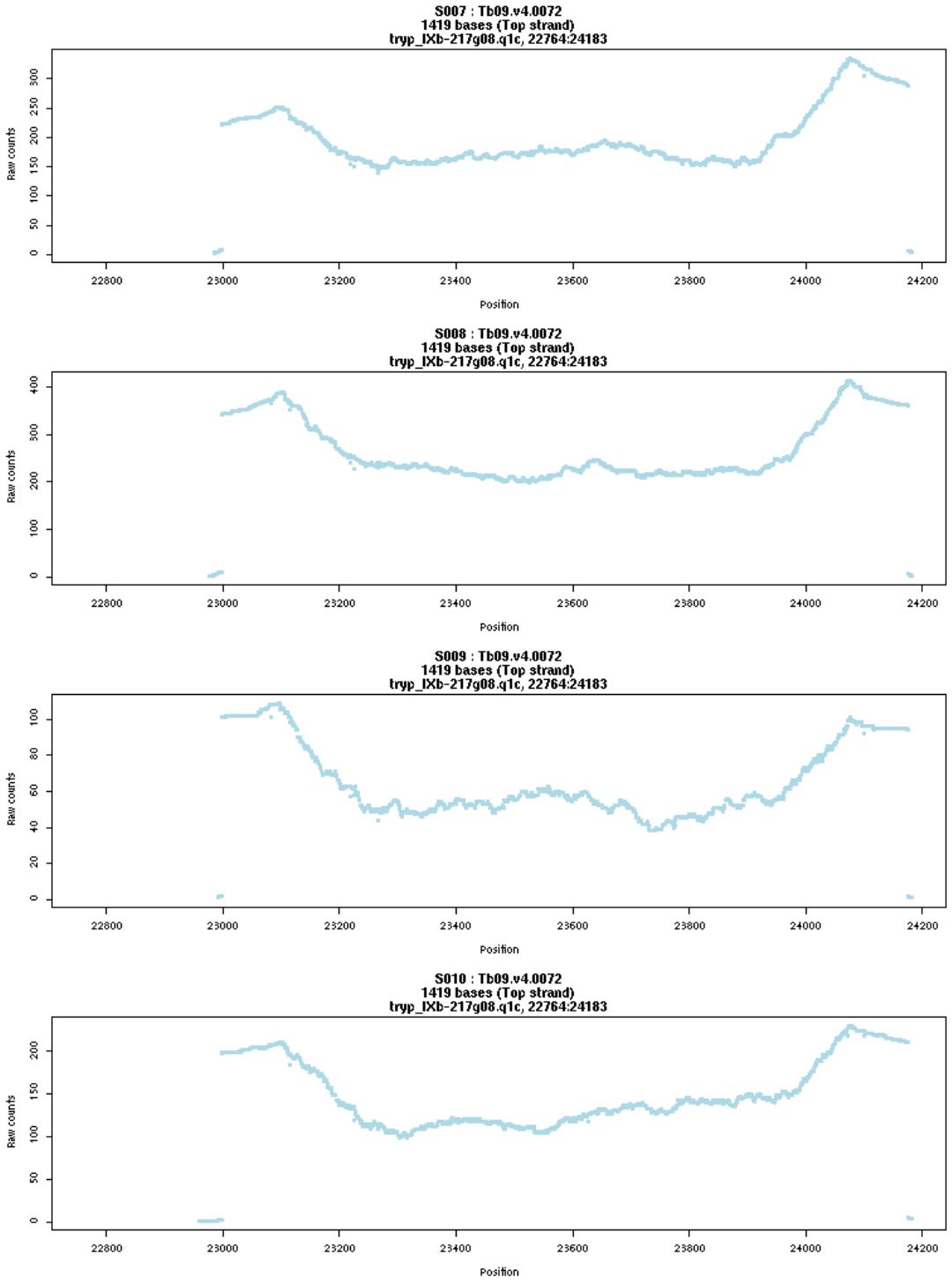

Figure 1 Read densities from Ion Torrent sequencing of RNAi insert specific PCR products aligned to individual genes identified as top hits in the GKI7 RNAi library screen. S007=tet+ R1; S008=tet+ R2; S009=tet+ R4; S010=tet- R1. Top strand graphs show transcription form left to right and bottom strand graphs show transcription from right to left.